

MAPPING ELECTROENCEPHALOGRAPHIC CHANGES IN AMYOTROPHIC LATERAL SCLEROSIS

STEFAN DUKIC



Mapping electroencephalographic changes in amyotrophic lateral sclerosis

Stefan Dukic

Mapping electroencephalographic changes in amyotrophic lateral sclerosis
PhD thesis, University Medical Centre Utrecht, Utrecht University, The Netherlands

© Stefan Dukic, 2023

All rights reserved. No part of this thesis may be reproduced or transmitted in any form or by any means without prior written permission from the author. The copyright of any papers that have been published or accepted for publication has been transferred to the respective journals.

Stichting ALS Nederland funded this work.

Publication of this thesis was financially supported by BioSemi B.V.

ISBN: 978-90-393-7599-0

Cover: In collaboration with Thomas Boerboom and Thomas Heuberger

Printing: ProefschriftMaken | www.proefschriftmaken.nl

Mapping electroencephalographic changes in amyotrophic lateral sclerosis

Het in kaart brengen van elektro-encefalografische veranderingen bij amyotrofische laterale sclerose

(met een samenvatting in het Nederlands)

Proefschrift

ter verkrijging van de graad van doctor aan de
Universiteit Utrecht
op gezag van de
rector magnificus, prof.dr. H.R.B.M. Kummeling,
ingevolge het besluit van het college voor promoties
in het openbaar te verdedigen op

dinsdag 28 november 2023 des ochtends te 10.15 uur

door

Stefan Dukic

geboren op 14 december 1991
te Subotica, Servië

Promotoren:

Prof. dr. L.H. van den Berg

Prof. dr. O. Hardiman

Copromotoren:

Dr. B.T.H.M. Sleutjes

Dr. B. Nasseroleslami

Beoordelingscommissie:

Prof. dr. M.J.N.L. Benders (voorzitter)

Prof. dr. K.P.J. Braun

Prof. dr. R.J. Pasterkamp

Prof. dr. N.F. Ramsey

Prof. dr. C.J. Stam

Contents

Chapter 1	General introduction and thesis outline	7
Chapter 2	Characteristic increases in EEG connectivity correlate with changes of structural MRI in amyotrophic lateral sclerosis	17
Chapter 3	Patterned functional network disruption in amyotrophic lateral sclerosis	65
Chapter 4	β -band oscillations in the sensorimotor network reflect motor symptoms severity in amyotrophic lateral sclerosis	99
Chapter 5	Resting-state EEG reveals four subphenotypes of amyotrophic lateral sclerosis	109
Chapter 6	Localisation of brain networks engaged by the SART provides quantitative markers of executive impairment in amyotrophic lateral sclerosis	143
Chapter 7	EEG network alterations in asymptomatic <i>C9orf72</i> repeat expansion carriers	167
Chapter 8	General discussion and future perspectives	187
Addenda	Summary Summary in Dutch (Nederlandse samenvatting) List of publications Acknowledgments Curriculum vitae	201



Chapter 1

General introduction and thesis outline

Amyotrophic lateral sclerosis

Amyotrophic lateral sclerosis is part of the motor neuron disease (MND) spectrum. It is a neurodegenerative disease that involves progressive motor impairment affecting upper motor neurons (UMNs) and lower motor neurons (LMNs). Typically, symptoms occur focally with deficits spreading contiguously across upper and lower motor neurons.¹ The estimated incidence rate is around 2-3 new cases per 100 000 every year,² which is equivalent to approximately 500 new cases per year in the Netherlands. While ALS can affect people of any age, symptom onset is typically between the ages of 55 and 65.³ Neuromuscular respiratory failure is the most common cause of death in ALS, typically 2-5 years after symptom onset.⁴ To date, no effective treatment is available.

While traditionally considered as a motor disease only, ALS affects extra-motor function as well.⁴ It is now established that there is a substantial overlap between ALS and frontotemporal dementia (FTD), which results from atrophy of the frontal and temporal brain lobes and causes cognitive and behavioural impairments that can vary depending on the affected neural networks. Symptoms of FTD include changes in executive function, language skills, behaviour and personality.⁵ While only around 15% of ALS patients fulfil the criteria for FTD diagnosis,⁶ it is now established that behavioural and/or cognitive symptoms are present in approximately half of ALS patients.⁴

The underlying cause of ALS is unknown in most cases (referred to as 'sporadic ALS'), while inherited 'familial ALS' accounts for approximately 10% of cases.⁷ Mutations linked to ALS are not considered clearly causative and the risk of developing ALS is established to be affected by both genetic and environmental risk factors.^{8,9} While the first ALS-linked genetic mutation was discovered in the *SOD1* gene,¹⁰ the most common and well-established genetic mutation to date is the repeat expansion in the *C9orf72* gene.¹¹ Typically, more than 30 repeats of the *C9orf72* sequence is considered pathogenic, although intermediate repeat numbers (24-30) are also significantly prevalent in ALS patients.¹² This mutation has also been identified to cause FTD.^{13,14}

Undoubtedly, ALS research has made significant progress over the years, albeit many important questions remain unanswered. Perhaps most importantly, the link between risk genes and risk factors that can lead to the manifestation of multiple phenotypes and their early detection and prognosis are yet to be determined. A better understanding of ALS pathogenesis can aid the identification of therapeutic targets, earlier treatment strategies and improved clinical trial designs.

Biomarkers in amyotrophic lateral sclerosis

Biomarkers are quantifiable changes in an individual's biology that can be used to identify the presence or characteristics of a disease. Namely, they can be used for diagnosis (to identify that a disease is present) or prognosis (to measure how a disease will progress).

Diagnosis of ALS remains predominantly contingent on the expertise of experienced neurologists, causing a diagnostic delay of approximately 10–16 months.¹⁵ Currently, diagnosis of ALS is primarily based on patient’s history and clinical examination of lower motor neuron (LMN) degeneration (such as atrophy and weakness) and upper motor neuron (UMN) degeneration (such as abnormal reflexes). In addition, further evidence of LMN degeneration (such as muscle fasciculations) captured by invasive needle electromyography (EMG), can be used to confirm diagnosis of ALS. Nevertheless, an objective, quantifiable biomarker of UMN degeneration remains to be identified and is urgently required given that LMN signs can obscure the clinical identification of UMN signs¹⁶ and that there is a considerable variability in the appreciation of UMN signs among physicians.¹⁷

Patient prognosis in ALS can be highly variable and unpredictable, although advancements in prediction models based on patients’ characteristics are made.¹⁸ While these predictions can be useful for clinical trials, they are limited in ability to demonstrate therapeutic effects of drug candidates. Currently, clinical trials use outcome measures that are based primarily on survival and on semi-quantitative tools, such as ALSFRS-R (ALS functional rating scale revised) scores. The subjective nature of ALSFRS-R scoring and its specificity primarily to LMN disease progression, however, limits the sensitivity of this approach to capture all aspects of disease progression sufficiently. As a result, it can be challenging to identify significant therapeutic effects on patients amidst disease heterogeneity within and between treatment groups. To mitigate this effect in clinical trials, current attempts are based on reducing variation in patient cohorts through use of restrictive recruitment criteria. This approach, nevertheless, substantially limits the number of patients eligible for clinical trials and does not account for potential heterogeneity across patients with differential brain network impairments.

These issues could be solved by development of objective, quantitative biomarkers of ALS that capture UMN dysfunction and extra-motor changes. Moreover, biomarker research improves our disease understanding, which can lead to new therapeutic targets and strategies, and better prediction of individual disease trajectories. Structural magnetic resonance imaging (MRI) and diffusion tensor imaging (DTI) can point to precise locations of atrophy along the neural axis. The tissue atrophy, however, is likely to occur after an earlier stage of pre-clinical molecular, cellular and functional pathology. This highlights the potential application of electrophysiology in the development of biomarkers. Electroencephalography (EEG) refers to the non-invasive recording of electrical brain activity above the scalp, which approximates the firing frequencies of neurons. Using EEG, we thus directly obtain real-time information transmission throughout the whole brain on a millisecond timescale. This is in contrast to other modalities that rely on secondary measures (such as blood oxygenation changes in functional MRI) and modalities that can assess only a restricted section of the brain (such as magnetic resonance spectroscopy). Unlike these neuroimaging modalities, EEG is also relatively inexpensive and mobile. While EEG sessions are often considered repetitive, they are organised in short blocks of several minutes and they do not require participants to lie flat for a single continuous period without moving (which

would be unsustainable for many ALS patients with respiratory system decline or excess salivation).

Electroencephalography

Electrical brain activity captured by EEG reflects the communication between populations of neurons, as practically all signals travelling through the nervous system are transmitted electrically. A large neuron can receive inputs from other neurons via a densely covered network of 10^{4-5} synapses.¹⁹ These inputs can generate either an excitatory postsynaptic potential or an inhibitory postsynaptic potential: the former makes it easier for the target neuron to fire an action potential, while the latter acts in the opposite manner. Big pyramidal neurons within the grey matter (i.e., the outer layer of the brain) and the postsynaptic potentials are believed to be the primary generators of the electric potentials captured by EEG (Fig. 1A). This, however, is only possible when at least tens of thousands of neurons (equivalent to a brain patch of a few cm^2) are arranged in parallel and entrained at the same time, which then results in a potential of a few microvolts at the scalp surface.²⁰

The brain produces electrical rhythms in multiple frequencies, which can be isolated from the raw EEG signal (Fig. 1B). Different psychological processes are linked to different frequencies, which are often grouped into bands: delta (0.5-4 Hz), theta (4-8 Hz), alpha (8-12 Hz), beta (13-30 Hz) and gamma (lower gamma 30-50Hz; upper gamma >50 Hz). This allows for an investigation of brain activity in terms of the power of oscillations at different frequency bands. In addition, band-specific communication between brain areas can be assessed using functional connectivity (which can be phase- or amplitude-based).²¹ These EEG measures are often applied when examining activity of the brain while at rest, a so-called 'resting-state' paradigm.

Brain signals can be recorded as well during experimental tasks that activate specific networks, such as those engaged in sensory, motor or cognitive processing. The corresponding neural signatures are observed in EEG as 'event-related potentials' (ERPs; Fig. 1C). These potentials are estimated by averaging many EEG signals, which are time-locked to a task stimulus or to a response. This approach assumes that only relevant signals occur consistently and will, therefore, be maintained after averaging. The sequential activations of brain processes implicated in the task can be individually quantified by characterising different peaks within the ERP (e.g., average peak amplitude or its timing). These peaks are often termed as, for instance, N200 (or N2; negative deflection around 200 ms post-stimulus) or P300 (or P3; positive deflection around 300 ms post-stimulus). Here, it is important to note that one peak is not necessarily equivalent to an activation of one brain area. Namely, a summation of multiple simultaneously or sequentially activated brain areas can be observed as one peak. It is, therefore, said that EEG has low spatial resolution. Nevertheless, these two traditional approaches (i.e., the resting-state and the ERP analysis) allow us to study brain function and can be combined to provide a well-rounded insight into the effects of disease pathology on brain network function.

Source localisation

While EEG has many advantages, they have been often negated by its poor spatial resolution, which limits the ability to attribute sensor-space activations to specific cortical regions. This limitation can, however, be mitigated with the use of source localisation algorithms, which are based on mathematical models and physiological assumptions. As there is no a unique solution that determines which cortical brain areas can give rise to the electrical activity recorded by EEG, there are various algorithms, such as minimum-norm (e.g., LORETA)²² and beamforming (e.g., LCMV).²³ Regardless of the source localisation method used, either an MRI²⁴/DTI²⁵ template or an individualised scan is needed (Fig. 1D). The scans are used to build a source model, which outlines the location and number of brain sources, and a head model, which describes the geometry of the head and electrical conductivities of the composite tissues (Fig. 1E). Using this information together with EEG electrode positions, a ‘forward model’ is determined, which estimates the activity across the electrodes given activity in each location of the source model. A source localisation method is then applied on the forward model and the recorded EEG signals to estimate cortical activity pattern (Fig. 1F). This ameliorates spatial resolution of EEG data and enables us to interrogate activity emerging from specific cortical sources (also referred to as the source-space analysis).

Electroencephalography in ALS

Electroencephalography research in ALS is still scarce and to date, there are no robust EEG biomarkers for diagnosis or prognosis. While some studies have used the task-based approach to assess specifically either motor or cognitive functioning, other studies have used the resting-state paradigm to capture brain changes more generally.

Studies analysing movement-related oscillations reported decreased pre-movement β -band desynchronisation,^{26,27} and decreased²⁸ or asymmetrical²⁶ post-movement β -band synchronisation. A study assessing the motor network using the ‘readiness potential’ (which indicates motor preparation) did not observe statistically significant difference, but it showed that more severe signs of spasticity are associated with diminished amplitudes of the potential.²⁹ A similar study, however, showed that patients do have a significantly lower amplitude of the readiness potential.³⁰ These two studies suggest that the impairment of the motor network, encompassing the supplementary motor area, middle cingulate gyri and the motor cortex, can be detected using EEG.

Studies assessing cognitive networks in ALS, focused primarily on analysing the N2a (a negative peak at approximately 200 ms post-stimulus) and P3 (a positive peak at around 200-500 ms) ERPs during an oddball paradigm. While there are many variations of this paradigm, each of them consists of a ‘standard’ stimulus and an occasionally occurring ‘deviant’ stimulus, and they are used to study covert (captured by the N2a) or overt (captured by the P3 peak) attention. While one study using the ‘mismatch negativity’ paradigm (which elicits the N2a) showed no difference in amplitude and timing of N2a,³¹ a recent study showed increased average delay of MMN that

correlated with response-inhibition task performance.³² Finally, studies assessing P3 ERP showed increase in its latency^{31,33} and decrease in its amplitude.^{31,34}

Resting-state EEG studies also identified changes in the sensorimotor cortex, as exemplified by the presence of decreased α -band power.^{26,35-39} In terms of brain connectivity, previous studies have shown altered patterns, such as increased connectivity in the frontoparietal network across a broad spectrum of frequencies,⁴⁰⁻⁴² but also decreased widespread connectivity and network impairment implicating α -band⁴³ and β -band.^{43,44}

Most of these studies are explorative, with low number of patients and lacking reproducibility. Namely, task-based studies are largely non-overlapping in terms of paradigms being used, while the resting-state studies often diverge in their analysis approach. In fact, all these studies rarely exploit the advances in signal processing by using the existing source reconstruction approaches and high-density EEG montages to gain better insight into the brain dysfunction. Finally, identification of ALS subgroups and assessment of the presymptomatic stages of ALS using EEG are still unexplored.

Thesis outline

The overarching aim of this thesis is to provide better understanding of ALS through EEG. Namely, the thesis tackles how high-density EEG can be used in ALS for identifying network dysfunction, patient subgrouping and early detection of the disease. The following four chapters are capitalising on the resting-state paradigm. In **chapter 2**, we evaluate the performance of resting-state paradigm to differentiate ALS patients from healthy controls by capturing aberrant EEG activity and connectivity patterns in sensor-space. In **chapter 3**, we expand these findings by means of source localisation, which demonstrates the ability of source-space analysis to identify specific brain networks that are altered in ALS. In **chapter 4**, we focus on EEG biomarker assessment by exploring the role of β -band spectral power as a biomarker of disease severity. In **chapter 5**, we apply a robust clustering approach to determine whether we can identify specific subphenotypes of ALS patients based on the resting-state network dysfunction. The last two chapters exploit a task-based paradigm that assesses sustained attention. In **chapter 6**, we introduce which brain networks are affected in ALS during this task, whilst in **chapter 7**, we shift our focus to the presymptomatic EEG changes in *C9orf72* carriers during the same task. At last, in **chapter 8**, we discuss the key findings of this thesis and give directions for future research.

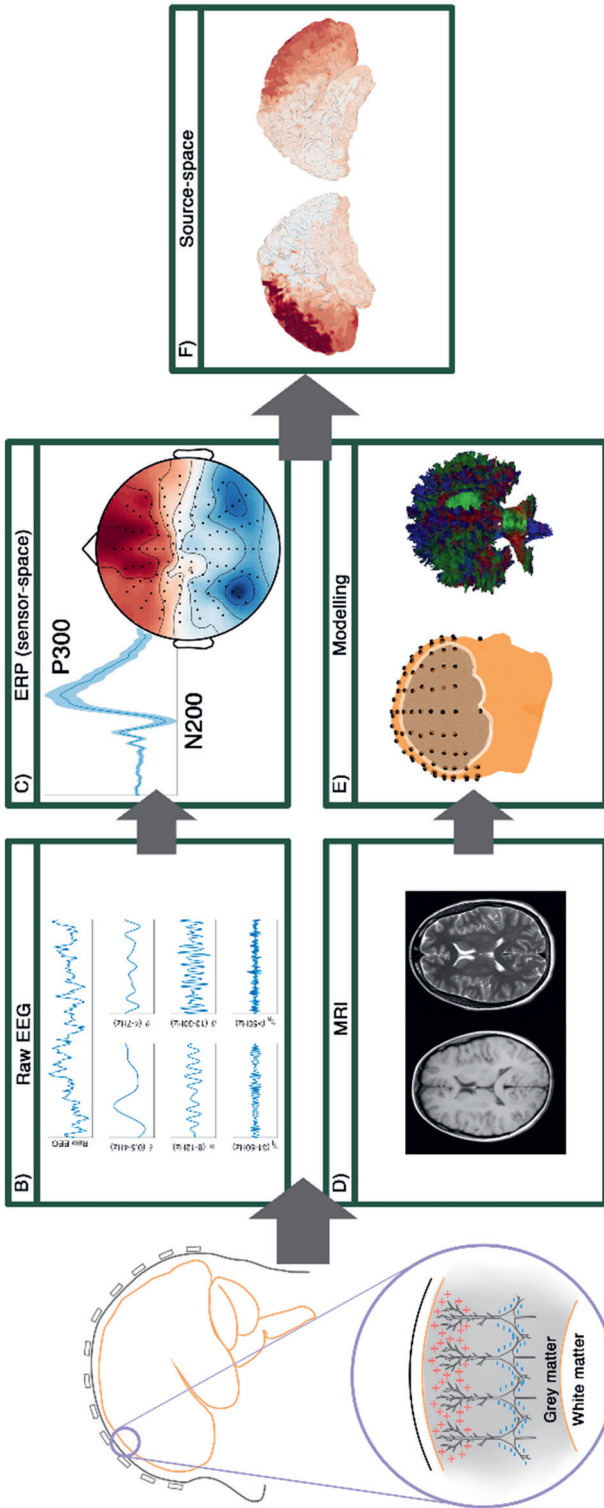
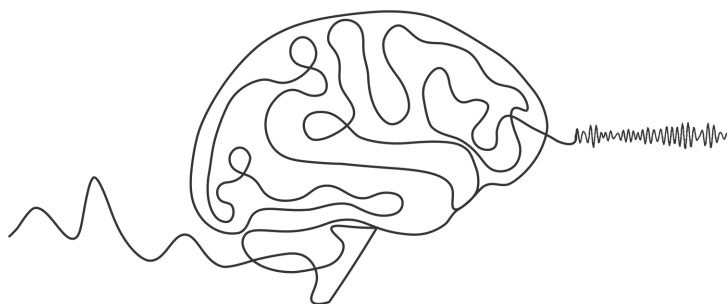


Figure 1. Schematic overview of EEG data origins and analysis. (A) Big pyramidal neurons within the grey matter of the cortex and the postsynaptic potentials are believed to be the primary generators of the electric potentials captured by EEG. This is, however, only possible when at least tens of thousands of neurons (equivalent to a cortical patch of a few cm²) are arranged in parallel and entrained at the same time, which then results in a potential of a few microvolts at the scalp surface; (B) The brain produces rhythms in multiple frequencies, which can be isolated from the raw EEG signal and grouped into bands; (C) Electrical signals can be recorded during tasks that activate specific networks and result in neural signatures called event-related potentials; (D) Source localisation methods require either an MRI/DTI templates or individual's MRI/DTI scans; (E) These MRI/DTI scans are used for building head models and tissue conductivity estimation; (F) By applying source reconstruction methods on EEG data we go from sensor- to source-space analysis.

References

1. Ravits, J. M. & La Spada, A. R. ALS motor phenotype heterogeneity, focality, and spread. *Neurology* **73**, 805–811 (2009).
2. Huisman, M. H. B. *et al.* Population based epidemiology of amyotrophic lateral sclerosis using capture–recapture methodology. *J Neurol Neurosurg Psychiatry* **82**, 1165–1170 (2011).
3. de Jongh, A. D. *et al.* Incidence, Prevalence, and Geographical Clustering of Motor Neuron Disease in the Netherlands. *Neurology* **96**, e1227–e1236 (2021).
4. van Es, M. A. *et al.* Amyotrophic lateral sclerosis. *The Lancet* **390**, 2084–2098 (2017).
5. Strong, M. J., Lomen-Hoerth, C., Caselli, R. J., Bigio, E. H. & Yang, W. Cognitive impairment, frontotemporal dementia, and the motor neuron diseases. *Ann Neurol* **54**, S20–S23 (2003).
6. Phukan, J. *et al.* The syndrome of cognitive impairment in amyotrophic lateral sclerosis: a population-based study. *J Neurol Neurosurg Psychiatry* **83**, 102–108 (2012).
7. Al-Chalabi, A., Van Den Berg, L. H. & Veldink, J. Gene discovery in amyotrophic lateral sclerosis: Implications for clinical management. *Nature Reviews Neurology* vol. 13 96–104 (2017).
8. Wang, M. D., Little, J., Gomes, J., Cashman, N. R. & Krewski, D. Identification of risk factors associated with onset and progression of amyotrophic lateral sclerosis using systematic review and meta-analysis. *Neurotoxicology* **61**, 101–130 (2017).
9. Al-Chalabi, A. & Hardiman, O. The epidemiology of ALS: a conspiracy of genes, environment and time. *Nat Rev Neurol* **9**, 617–628 (2013).
10. Rosen, D. R. *et al.* Mutations in Cu/Zn superoxide dismutase gene are associated with familial amyotrophic lateral sclerosis. *Nature* **1993** 362:6415 **362**, 59–62 (1993).
11. Renton, A. E., Chiò, A. & Traynor, B. J. State of play in amyotrophic lateral sclerosis genetics. *Nature Neuroscience* **2013** **17**:1 **17**, 17–23 (2013).
12. Iacoangeli, A. *et al.* C9orf72 intermediate expansions of 24–30 repeats are associated with ALS. *Acta Neuropathol Commun* **7**, 115 (2019).
13. DeJesus-Hernandez, M. *et al.* Expanded GGGGCC Hexanucleotide Repeat in Noncoding Region of C9ORF72 Causes Chromosome 9p-Linked FTD and ALS. *Neuron* **72**, 245–256 (2011).
14. Renton, A. E. *et al.* A Hexanucleotide Repeat Expansion in C9ORF72 Is the Cause of Chromosome 9p21-Linked ALS-FTD. *Neuron* **72**, 257–268 (2011).
15. Richards, D., Morren, J. A. & Pioro, E. P. Time to diagnosis and factors affecting diagnostic delay in amyotrophic lateral sclerosis. *J Neurol Sci* **417**, 117054 (2020).
16. Swash, M. Why are upper motor neuron signs difficult to elicit in amyotrophic lateral sclerosis? *J Neurol Neurosurg Psychiatry* **83**, 659–662 (2012).
17. Thaller, M. & Hughes, T. Inter-rater agreement of observable and elicitable neurological signs. *Clinical Medicine* **14**, 264–267 (2014).
18. Westeneng, H. J. *et al.* Prognosis for patients with amyotrophic lateral sclerosis: development and validation of a personalised prediction model. *Lancet Neurol* **17**, 423–433 (2018).
19. Nunez, P. L. & Srinivasan, R. *Electric Fields of the Brain: The neurophysics of EEG 2nd ed. Electric Fields of the Brain: The neurophysics of EEG* (Oxford University Press, 2006).
20. Goldenholz, D. M. *et al.* Mapping the signal-to-noise-ratios of cortical sources in magnetoencephalography and electroencephalography. *Hum Brain Mapp* **30**, 1077–1086 (2009).
21. Siegel, M., Donner, T. H. & Engel, A. K. Spectral fingerprints of large-scale neuronal interactions. *Nat Rev Neurosci* **13**, 121–34 (2012).
22. Pascual-Marqui, R. D. Discrete, 3D distributed, linear imaging methods of electric neuronal activity. Part 1: exact, zero error localization. *Linas* (2007).
23. Van Veen, B. D., Van Drongelen, W., Yuchtman, M. & Suzuki, A. Localization of brain electrical activity via linearly constrained minimum variance spatial filtering. *IEEE Trans Biomed Eng* **44**, 867–80 (1997).
24. Fonov, V., Evans, A., McKinstry, R., Almlí, C. & Collins, D. Unbiased nonlinear average age-appropriate brain templates from birth to adulthood. *Neuroimage* **47**, S102 (2009).
25. Mori, S. *et al.* Stereotaxic white matter atlas based on diffusion tensor imaging in an

- ICBM template. *Neuroimage* **40**, 570–582 (2008).
26. Bizovičar, N., Dreo, J., Koritnik, B. & Zidar, J. Decreased movement-related beta desynchronization and impaired post-movement beta rebound in amyotrophic lateral sclerosis. *Clinical Neurophysiology* **125**, 1689–99 (2014).
 27. Kasahara, T. *et al.* The correlation between motor impairments and event-related desynchronization during motor imagery in ALS patients. *BMC Neurosci* **13**, 1–10 (2012).
 28. Riva, N. *et al.* Cortical activation to voluntary movement in amyotrophic lateral sclerosis is related to corticospinal damage: Electrophysiological evidence. *Clinical Neurophysiology* **123**, 1586–92 (2012).
 29. Westphal, K. P. *et al.* Bereitschaftspotential in amyotrophic lateral sclerosis (ALS): lower amplitudes in patients with hyperreflexia (spasticity). *Acta Neurol Scand* **98**, 15–21 (1998).
 30. Thorns, J. *et al.* Movement initiation and inhibition are impaired in amyotrophic lateral sclerosis. *Exp Neurol* **224**, 389–394 (2010).
 31. Hanagasi, H. A. *et al.* Cognitive impairment in amyotrophic lateral sclerosis: evidence from neuropsychological investigation and event-related potentials. *Cognitive Brain Research* **14**, 234–244 (2002).
 32. Iyer, P. M. *et al.* Mismatch Negativity as an Indicator of Cognitive Sub-Domain Dysfunction in Amyotrophic Lateral Sclerosis. *Front Neurol* **8**, 395 (2017).
 33. Paulus, K. S. *et al.* Visual and auditory event-related potentials in sporadic amyotrophic lateral sclerosis. *Clinical Neurophysiology* **113**, 853–861 (2002).
 34. Portet, F., Cadilhac, C., Touchon, J. & Camu, W. Cognitive impairment in motor neuron disease with bulbar onset. *Amyotroph Lateral Scler Other Motor Neuron Disord.* **2**, 23–29 (2001).
 35. Mai, R., Facchetti, D., Micheli, A. & Poloni, M. Quantitative electroencephalography in amyotrophic lateral sclerosis. *Electroencephalogr Clin Neurophysiol* **106**, 383–386 (1998).
 36. Maruyama, Y. *et al.* Electroencephalography of completely locked-in state patients with amyotrophic lateral sclerosis. *Neurosci Res* **162**, 45–51 (2021).
 37. Jayaram, V. *et al.* Brain-computer interfacing in amyotrophic lateral sclerosis: Implications of a resting-state EEG analysis. in *2015 37th Annual International Conference of the IEEE Engineering in Medicine and Biology Society (EMBC)* 6979–82 (IEEE, 2015).
 38. Santhosh, J., Bhatia, M., Sahu, S. & Anand, S. Decreased electroencephalogram alpha band [8–13 Hz] power in amyotrophic lateral sclerosis patients: A study of alpha activity in an awake relaxed state. *Neurol India* **53**, 99 (2005).
 39. Khalili-Ardali, M., Wu, S., Tonin, A., Birbaumer, N. & Chaudhary, U. Neurophysiological aspects of the completely locked-in syndrome in patients with advanced amyotrophic lateral sclerosis. *Clinical Neurophysiology* **132**, 1064–1076 (2021).
 40. Blain-Moraes, S., Mashour, G. A., Lee, H., Huggins, J. E. & Lee, U. Altered cortical communication in amyotrophic lateral sclerosis. *Neurosci Lett* **543**, 172–6 (2013).
 41. Iyer, P. M. *et al.* Functional Connectivity Changes in Resting-State EEG as Potential Biomarker for Amyotrophic Lateral Sclerosis. *PLoS One* **10**, e0128682 (2015).
 42. Govaarts, R. *et al.* Cortical and subcortical changes in resting-state neuronal activity and connectivity in early symptomatic ALS and advanced frontotemporal dementia. *Neuroimage Clin* **34**, 102965 (2022).
 43. Fraschini, M. *et al.* Functional brain connectivity analysis in amyotrophic lateral sclerosis: An EEG source-space study. *Biomed Phys Eng Express* **4**, 037004 (2018).
 44. Fraschini, M. *et al.* EEG functional network topology is associated with disability in patients with amyotrophic lateral sclerosis. *Sci Rep* **6**, 1–7 (2016).



Chapter 2

Characteristic increases in EEG connectivity correlate with changes of structural MRI in amyotrophic lateral sclerosis

Bahman Nasserouleslami, Stefan Dukic, Michael Broderick, Kieran Mohr, Christina Schuster, Brighid Gavin, Russell McLaughlin, Mark Heverin, Alice Vajda, Parameswaran M. Iyer, Niall Pender, Peter Bede, Edmund C. Lalor[†], Orla Hardiman[†]

[†] Joint senior authors



Abstract

Amyotrophic lateral sclerosis (ALS) is a terminal progressive adult-onset neurodegeneration of the motor system. Although originally considered a pure motor degeneration, there is increasing evidence of disease heterogeneity with varying degrees of extra-motor involvement. How the combined motor and non-motor degeneration occurs in the context of broader disruption in neural communication across brain networks has not been well characterized. Here, we have performed high-density cross-sectional and longitudinal resting-state EEG recordings on 100 ALS patients and 34 matched controls, and have identified characteristic patterns of altered EEG connectivity that have persisted in longitudinal analyses. These include strongly increased EEG coherence between parietal-frontal scalp regions (in γ -band) and between bilateral regions over motor areas (in θ -band). Correlation with structural MRI from the same patients shows that disease-specific structural degeneration in motor areas and corticospinal tracts parallels a decrease in neural activity over scalp motor areas, while the EEG over the scalp regions associated with less extensively involved extra-motor regions on MRI exhibit significantly increased neural communication. Our findings demonstrate that EEG-based connectivity mapping can provide novel insights into progressive network decline in ALS. These data pave the way for development of validated cost-effective spectral EEG-based biomarkers that parallel changes in structural imaging.

Introduction

Amyotrophic lateral sclerosis (ALS) is a heterogeneous neurodegenerative disease characterized primarily by degeneration of upper and lower motor neurons¹ with variable degrees of extra motor involvement. Clinical manifestations of ALS dichotomize into those associated with apparently pure motor system degeneration involving disruption in motor cortex, corticospinal tracts and motor networks;^{2,3} and degeneration of extra-motor regions, associated with clinical features of cognitive decline, ranging from mild executive impairment through to behavioural variant frontotemporal dementia (bvFTD).^{4,5}

While there is an urgent need for non-invasive biomarkers that address disease heterogeneity, the majority of imaging² and electrophysiological⁶ studies to date have focussed primarily on quantification of the selective structural degeneration and functional deficiencies of motor pathways. The increasing involvement of broader motor and non-motor regions and networks suggests that a more extensive assessment of large-scale brain connectivity is indicated.

Previous electro-/magneto-encephalography (EEG/MEG) and functional MRI (fMRI) studies have reported abnormal functional connectivity patterns in neuropsychiatric diseases,^{7,8} Alzheimer's disease,^{9,10} Parkinson's disease,¹¹ and fronto-temporal dementia, FTD.¹² In ALS, fMRI shows increased functional connectivity in the left motor cortex of ALS patients¹³ and a previous EEG study has reported increased parietal-to-frontal connectivity.¹⁴ These changes in connectivity have been confirmed by our group¹⁵ in a small sample size ($n = 18$) of ALS patients. We have shown that graph-theoretic measures of connectivity (e.g. degree values, clustering coefficient and assortativity) demonstrate increased connectivity in the θ (central and frontal) and in α and γ bands (widespread). Notwithstanding these findings, the nature of ALS-specific alteration in cortical connectivity (e.g. the brain regions and frequency bands) has not been fully evaluated in the context of disease heterogeneity with broader motor and extra-motor involvement,^{1,16} and the extent by which connectivity changes persist or evolve as the disease progresses is not known. Furthermore, the underlying reasons for disease-specific changes are unclear, and it remains to be determined whether such alterations in connectivity are due to local structural degeneration in motor regions, widespread structural decline, or compensatory neural communication. Resolution of these challenges will provide translational opportunities in ALS whereby the diagnosis, sub-phenotyping and targeted therapeutics can be based on the underlying changes in specific neural networks.

In this study, we have used high-density EEG to investigate the altered cortical connectivity patterns in a large ALS cohort (comprising 100 patients including 78 spinal-onset, 15 bulbar-onset and 7 ALS-FTD, including 12 probands carrying the pathogenic hexanucleotide repeat expansion in *C9orf72*) and 8 patients with bvFTD who had no clinical evidence of motor degeneration. 34 healthy age-matched controls were included in the study for comparative purposes.

We have identified disease-specific patterns that are significantly different in resting-state recordings between ALS patients and controls. These changes persist on repeated longitudinal assessment, and correlate with structural and diffusion tensor imaging (DTI) MRI measurements from the same patients. Our findings, that the effects of focal disease-specific and broader structural degeneration can be reproducibly characterized using spectral EEG, provide an exciting prospect for the development of novel non-invasive biomarkers in ALS and related neurodegenerative conditions.

Methods

Ethical approval

This study was approved by the ethics committee of Beaumont Hospital, Dublin, Ireland (REC reference: 13/102) and the Tallaght Hospital / St. James's Hospital Joint Research Ethics Committee (REC) (REC reference: 2014 Chairman's Action 7, CRFSJ 0046) for St James's Hospital, Dublin, Ireland. The experimental procedure conformed with the Declaration of Helsinki. All participants, including the patients and healthy controls, provided written informed consent before taking part in the experiments.

Experimental design

The study sought to find spectral power and connectivity signatures that distinguish ALS patients from healthy controls, using EEG recordings from both groups. No randomisation or blinding was applied, as the potential differences between the groups were not known and could not affect the experiment and data acquisition. Power analysis was performed post-hoc.

Participants

Patient recruitment

Recruitment was undertaken from ALS patients attending the National ALS specialty clinic in Beaumont Hospital. Healthy controls were recruited from neurologically-normal spouses of ALS patients, and from neurologically-normal age-matched individuals recruited as part of an existing cohort study of cognition in ALS.

Inclusion criteria

The recruited patients, included individuals above 18 years of age diagnosed with ALS, ALS-FTD or FTD. In the ALS and ALS-FTD groups, patients were within the first 18 months since diagnosis and fulfilled the El Escorial diagnostic criteria for Possible, Probable or Definite ALS. In the FTD group, patients (including behavioural variant, semantic dementia and progressive aphasia) who fulfilled the revised diagnostic criteria for FTD⁷ were included.

Exclusion criteria

Patients diagnosed with Primary Lateral Sclerosis (PLS), Progressive Muscular Atrophy (PMA), Flail Arm/Leg, Transient Ischemic Attack (TIA), Multiple Sclerosis (MS), stroke, epilepsy, seizure disorder, brain tumours, structural brain diseases, other degenerative brain diseases and other comorbidities (e.g. human immunodeficiency virus) were excluded.

Demographics of patients and controls

A total of 100 patients with ALS (f/m: 30/70; age: 60.2 ± 11.1 years in the range 29-82), 8 patients with FTD (f/m: 5/3; age 66.8 ± 8.1 in the range 57-81) and 34 healthy controls (f/m: 19/15; age: 58.1 ± 13.9 in the range 30-78) were recruited (Table 1). The FTD patients were recruited as part of a parallel study on FTD and the subsequent data analysis for the FTD group was performed separately from the ALS group.

Medical profile

Within the ALS group (excluding ALS-FTD patients), 78 patients had spinal onset, 15 bulbar onset, and 7 ALS-FTD (4 spinal onset and 3 bulbar onset), as listed in Table 1. For 93 patients, the ALS functional rating scale revised, ALSFRS-R,¹⁸ was carried out ± 1 month of EEG data acquisition (not biased to before or after recording, $p > 0.1$, Wilcoxon's Signed Rank test, $n = 100$) and ranged from 13 to 48, with a mean (\pm SD) of 36.0 ± 7.8 (Table 1). Twelve of 83 patients tested for hexanucleotide repeat expansion in *C9orf72* had positive results (Table 1). From 93 patients with available family history, 18 had a known family history of at least one first or second degree relative with ALS.¹⁹ From 95 patients with known history of taking riluzole at the time of EEG recording, 12 patients were off riluzole and 83 were on riluzole with 69.0 ± 63.0 days (median \pm IQR) past since starting the medication.

Experiment

Experimental paradigm

The experimental paradigm was resting-state with the eyes open, which was undertaken in 3 blocks of 2 minutes for both the patient and control groups. Subjects sat in a comfortable chair and were required to fixate at the letter X (6x8 cm) on an A4-sized piece of paper, which was located at a distance of about 1m in front of them. They were asked to be relaxed and minimise unnecessary eye movements during the EEG acquisition.

Data acquisition

EEG recordings were conducted in dedicated laboratories in the University of Dublin and St. James's Hospital, Dublin using a BioSemi® ActiveTwo system with 128 active sintered Ag-AgCl electrodes and headcaps (BioSemi B.V., Amsterdam, The Netherlands). For spectral power, the 18 recordings performed in hospital were significantly lower (Mann-Whitney U-test, $P = 0.0055$, $AUC = 0.72$, $n_1 = 18$, $n_2 = 82$), therefore these

recordings were excluded from the comparisons of spectral power. Each subject was fitted with an appropriately sized EEG cap. The EEG data were filtered online over the range 0-134 Hz, and digitized at 512 Hz. Longitudinal study, included 4 subsequent recording sessions (T2-T5) scheduled every 4-months after the first recording session (T1), in which 57, 36, 25, and 17 subjects attended, respectively.

Table 1. Age, gender, diagnosis status and ALSFR-R of the participants.

Group	n	Male	Female	Age (y)*	Dx-EEG T1† (days)*	ALSFRS-R
Control	34	15	19	58.1 ± 13.9	-	-
ALS	All	100	70	60.2 ± 11.1	283 ± 357	36.0 ± 7.8 (n = 93)
	Spinal	78	57	59.8 ± 11.2	292 ± 379	35.8 ± 7.1 (n = 72)
	Bulbar	15	9	57.1 ± 9.6	234 ± 262	35.4 ± 11.1 (n = 14)
	ALS-FTD	7	4	71.5 ± 6.9	289 ± 301	38.9 ± 7.1 (n = 7)
	C9orf72+	12	5	60.9 ± 8.6	366 ± 313	37.9 ± 8.8 (n = 11)
C9orf72-	71	55	61.3 ± 11.5	298 ± 395	35.2 ± 8.0 (n = 68)	
FTD	8	3	5	66.8 ± 8.1	-	-

† Dx-EEG T1 is the time interval between diagnosis and the T1 EEG recording.

* Numbers show mean ± standard deviation. The Spinal and Bulbar groups exclude ALS-FTD patients.

Data analysis

EEG preprocessing

After the quality checks by visual inspection (EyeBallGUI),²⁰ we used an automatic artefact rejection method²¹ based on statistical thresholding²² and verified the efficacy of the procedure by visual inspection in 16 subjects. See the Supplementary material for details.

EEG processing

Bipolar channels (n = 125) were formed by subtracting adjacent electrodes to estimate the superficial cortical brain activity and minimise the effects of volume conduction and deeper brain sources, as well as to reduce the effects of unrejected artefacts such as EMG.²³ The EEG signals were high-pass filtered with cut-off frequency of 1 Hz. To calculate the spectral power, coherency function and coherence,²⁴ the signal was epoched into 1s segments and multiplied by a Hann window function and then the auto- and cross-spectra were estimated by taking the median of complex frequency domain values across all the data epochs.²¹ The epoch length did not have a significant effect on results as the findings with 10s epochs were the same. The band-specific real, imaginary and absolute values of the cortico-cortical coherency function were estimated in the δ (2-4 Hz), θ (5-7 Hz), α (α_l : 8-10 Hz, α_h : 11-13 Hz), β (β_l : 14-20 Hz, β_h : 21-30Hz), and γ (γ_l : 31-47Hz, γ_h : 53-97 Hz) frequency bands between all 125 bipolar

channel combinations (performed in sensor-space). These frequency bands were selected according to the frequency ranges that change in motor tasks,²⁵⁻²⁸ as well as resting-state studies in ALS⁵ and in healthy subjects.²⁹ All the signal analysis was performed in MATLAB (Mathworks Inc., Natick, MA, USA), using scripts coded for this study (See the Supplementary material for details).

Measures of spectral power and connectivity

The log-scale spectral power, $\log_{10}(1 + F_{xx}(f))$, where $F_{xx}(f)$ represents the auto-spectrum of the signal $x(t)$ at frequency f , was calculated for each bipolar channel in each frequency band as a measure of spectral power. The real and absolute values of the complex coherency function $C_{xy}(f) = F_{xy}(f) / \sqrt{F_{xx}(f)F_{yy}(f)}$ (where $F_{xx}(f)$ and $F_{yy}(f)$ are the auto-spectra and $F_{xy}(f)$ the cross-spectrum of the signals $x(t)$ and $y(t)$ pertaining to two bipolar EEG channels), were calculated for all channel pairs, in each frequency band. For each electrode, the median of the real coherence quantified the oscillation synchrony (real coherence corresponds to zero-lag no-delay synchrony), and the median absolute coherence quantified the (average) connectivity of the node (with arbitrary phase differences); which were calculated between each node and all other 124 bipolar channels. The average connectivity or synchrony at each electrode was represented by median coherence with all other electrodes, as the change in the value of the median can indicate the overall shift of the group of coherence values. As pre-whitening the EEG signals⁷ had negligible effect on the results, it was not used for the final analysis. These spectral power, synchrony and connectivity measures were analysed as groups of multivariate variables. Additionally, to perform univariate statistics, each measure of spectral power and connectivity was averaged across all bipolar electrodes and additionally assessed in ALS patients versus controls. For verification and validation of these connectivity measures, please see the Supplementary material.

Point-to-point analysis of connectivity

The potential point-to-point pattern of the altered connectivity was assessed using 2 approaches. First, the changes in the average connectivity were further inspected by choosing reference or 'seeding points'. Second, we found the discriminant eigen-connectivities³⁰ to extract more explicitly point-to-point patterns (see Supplementary material).

Linear discriminant analysis

Fisher's linear discriminant analysis (LDA)^{31,32} was applied separately on the 4 EEG and 9 MRI measures to find the most discriminant linear combination of measures based on the eigenvectors of $S_w^{-1}S_b$ (S_b and S_w : between-group and within-group covariance matrices). Additionally, a regularised ($\lambda = 0.05$) LDA was performed on high-dimensional EEG measures [8 frequency bands x 3 measures (power, connectivity, synchrony) x 125 channels = 3000 variables]. For EEG measures (but not for MRI), the first discriminant component was the dominant (accounting for more than 90% of discriminatory variance).

Correlates with MRI scores

Fifty-nine of the spinal- and bulbar-onset ALS patients (including 5 *C9orf72+* and 38 *C9orf72-* patients) participated in a parallel MRI study,³ as described in the Supplementary material. We sought to include measures that were maximally different between the controls and patients^{2,3,33} and to find potential relations between the alterations in EEG and affected regions as defined by MRI. We have previously shown that in spinal onset ALS there is a predominant involvement of posterior internal capsule and medial corona radiata pathology, and that the main motor-related degeneration is the selective involvement of corticospinal and corticobulbar fibres.³ We also included regions (primarily white matter tracts) that are found to contribute to generation of EEG oscillations.^{27,34,35} Consequently, 9 structural and DTI measures were chosen for correlation analyses on this basis in advance (a priori) of the analysis: Grey matter thickness in the left and right motor areas (separately averaged across precentral gyrus, central sulcus, and superior precentral sulcus), average fractional anisotropy (FA) of the left and right thalamo-cortical pathways, average FA of the left and right superior corona radiata, average FA of the left and right corticospinal tracts in the internal capsules and cerebral peduncles, and average FA of corpus callosum. These regions were defined by atlas-based segmentation, and were selected due to their known degeneration in ALS,³ or their potential contribution to oscillatory EEG signatures – for thalamo-cortical projections.²⁷ As there was a high level of correlation between these 9 MRI measures of degeneration, principal component analysis, PCA,³⁶ was used to extract the principal directions of neurodegeneration, as ‘degeneration modes’. Before PCA, the MRI and EEG scores were transformed to standard normal distributions (see Supplementary material). The scores corresponding to each degeneration mode were then correlated with measures of spectral power, synchrony and connectivity. As a control, the age-dependent degeneration (found by the correlation vector of the patients’ age with structural MRI scores in each mode) was calculated and the percent variance of each degeneration mode explained by age was found. As limiting the analyses to the *C9orf72-* patients showed negligible confounding effect of the *C9orf72* genotype on imaging measures,³⁷ the MRI-EEG analyses were performed on the entire cohort of 59 patients.

Statistical analysis

For statistical analysis, we first used frequentist statistics to discard the unaffected measures and to find the potentially interesting effects due to ALS; next, we used Empirical Bayesian Inference (EBI) to more accurately infer the disease-specific effects in the presence of complex high-dimensional correlations in the data (difficult to address with frequentist methods), but more importantly to estimate the statistical power and Bayesian posterior probabilities.

Frequentist statistics

The between-group comparisons of spectral power and connectivity measures were performed using the p-values of the Mann-Whitey U-test and the area under the curve (AUC) for the receiver operating characteristics curve.³⁸ The pairwise comparisons

(e.g. for longitudinal data) were performed using Wilcoxon's Signed Rank test. For comparison of several groups (ALS phenotypes), the Kruskal-Wallis non-parametric 1-way analysis of variance test was employed. Analysis of correlations was performed using Spearman's rank correlation coefficients. The frequency measures were assessed within the 8 defined frequency bands. To account for multiple comparisons, rejection of null hypotheses was performed by adaptive false discovery rate (aFDR) at $q = 0.05$.^{39,40} For each measure and frequency-band, the FDR was applied on the bipolar channels being compared ($n = 125$), i.e. across channels but not across measures or frequency bands. This procedure served as a screening method for potentially significant differences between the groups. A similar procedure was used to assess the significance of individual connections when seeding from one channel at a specific frequency band at $q = 0.10$.

To assess the statistical significance of the eigen vectors from PCA and LDA for EEG and MRI measures, a null and non-null bootstrapping resampling approach was used to calculate the standard deviations, p -values and statistical power (see Supplementary material).

Empirical Bayesian inference

EBI^{41,42} is a statistical approach for inferring statistical significance and finding effects in individual variables of high-dimensional observations. It uses a test statistic in each variable to quantify the level of effect in/between the groups. The test statistic values for all variables using the original observations, as well as the null-permuted data are used to estimate the probability density function of the data and the null, respectively. Subsequently, the prior and posterior probabilities are estimated from the density functions; which are used to estimate the FDR and statistical power for each threshold level of the posterior probabilities. The EBI was applied on the AUC³⁸ as the test statistic, for statistical analysis of the spectral power and connectivity measures between ALS and controls. For each measure, data from the 8 frequency bands and 125 bipolar channels were analysed together (1000 variables).

Results

Analysis of differences in neural activity and connectivity between the ALS cohort and controls in the characteristic EEG frequency bands showed significant differences after aFDR corrections (Supplementary Fig. 2-4). Additional analyses based on the statistical power and Bayesian posterior probabilities further confirmed the findings (Supplementary Fig. 2 and 3, rows 4):

Decreased spectral power

We detected a significant decrease in the low-frequency (θ -band) spectral power in ALS patients (excluding pure FTD patients) versus healthy controls (Fig. 1). This decrease of θ -band power in ALS patients was significant over bilateral motor areas of scalp, and spread to other scalp locations and the adjacent frequency bands (δ - and α_1 -bands) (Supplementary Fig. 2).

Increased average connectivity

We detected widespread and significant increases in average connectivity in ALS patients compared to healthy controls (Fig. 1). The most notable changes were detected over bilateral motor regions of scalp for θ -band and over parietal and frontal scalp regions for γ -band (Supplementary Fig. 3). This strong effect also spread to adjacent locations and frequency bands.

Alterations in average synchronous EEG oscillations were also captured (Supplementary Fig. 4). In ALS patients, the γ -band average synchrony was significantly reduced above bilateral primary motor areas of scalp (with additional but lesser involvement of parietal-occipital scalp regions), suggesting that altered neural activity in motor cortical areas was a function of structural change.

The identified increases in the average connectivity were further inspected to determine whether they originated from specific increases in point-to-point connectivity. For this purpose, overall connectivity across regions was inspected in the corresponding frequency bands. The lateral-central C_4 and midline-parietal P_z channels (representing bilateral motor, and parietal scalp regions) were chosen as reference or 'seeding points' (Fig. 2), as these regions showed significant ALS-specific changes in the average connectivity. This analysis showed that increased connectivity in the θ frequency band originated from increased connectivity between left and right motor areas of scalp (Fig. 2). Similarly, increased connections in γ frequency band were found within parietal scalp areas and between parietal-frontal scalp regions.

Analysis of changes in the point-to-point connectivity (without reference to average connectivity) also showed significant differences between controls and ALS patient group (Supplementary Fig. 5). The major effects were the increased coherence in θ -band between the scalp regions over the 2 motor areas, and pattern of the increased coherence in γ -band between the parietal-frontal scalp regions. The main eigen-connectivities (Fig. 2, bottom row) show the dominance of these patterns more explicitly.

These 4 spectral power and connectivity measures that showed significant changes in ALS (θ -band spectral power, θ -band connectivity, γ -band connectivity and γ -band synchrony), were used as 4 average (across all electrodes) measures to further study the changes in the ALS group.

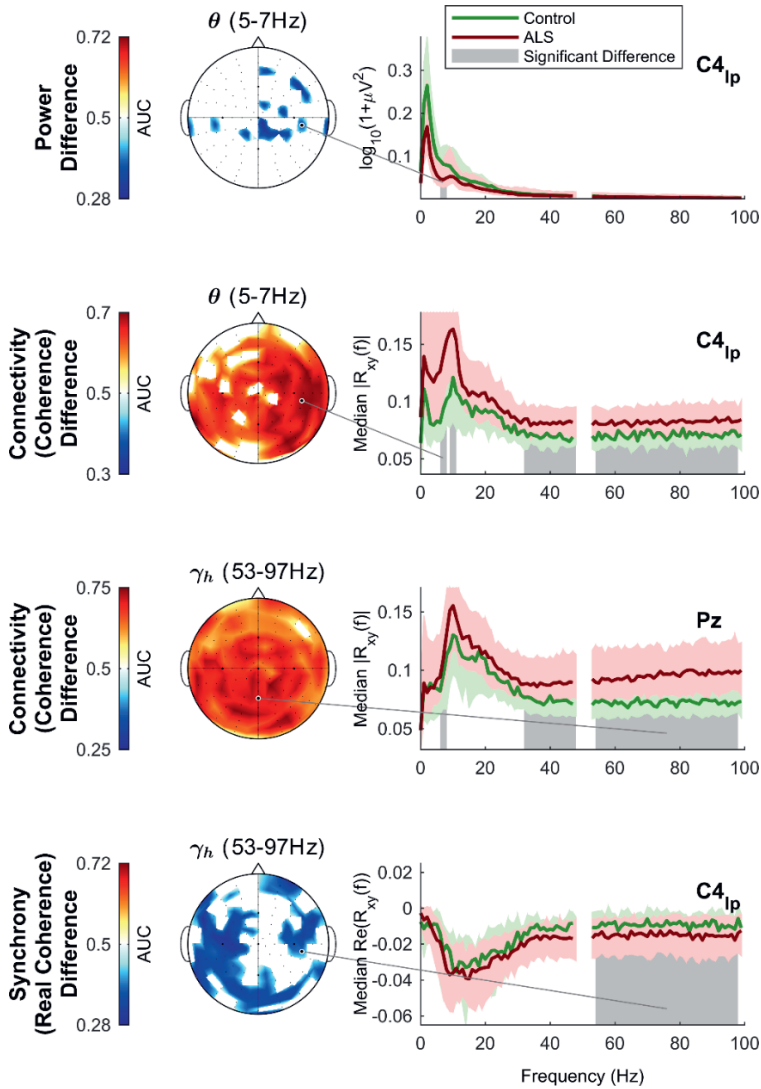


Figure 1. In ALS patients, spectral EEG power is significantly decreased in θ -band over the bilateral motor regions of scalp, while the median coherence is significantly increased in θ -band over motor areas and in γ -band over parietal and frontal scalp regions. The spectral power and median coherence are shown in 2 representative electrodes $C4_{Ip}$ (right motor region) and Pz (parietal region) over scalp as a function of frequency. The spatial spread of the altered features is shown topographically in the θ - and γ_h -frequency bands. Significant difference between the healthy controls ($n = 34$) and ALS patients ($n = 100$) was assessed in the 8 defined frequency bands using Man-Whitney U-test and adaptive false discovery rate (FDR), as elaborated on in Supplementary Fig. 2 and 3. Notice the extension of changes to adjacent frequency bands (from γ to β_h). AUC: Area under the receiver operating characteristics curve.

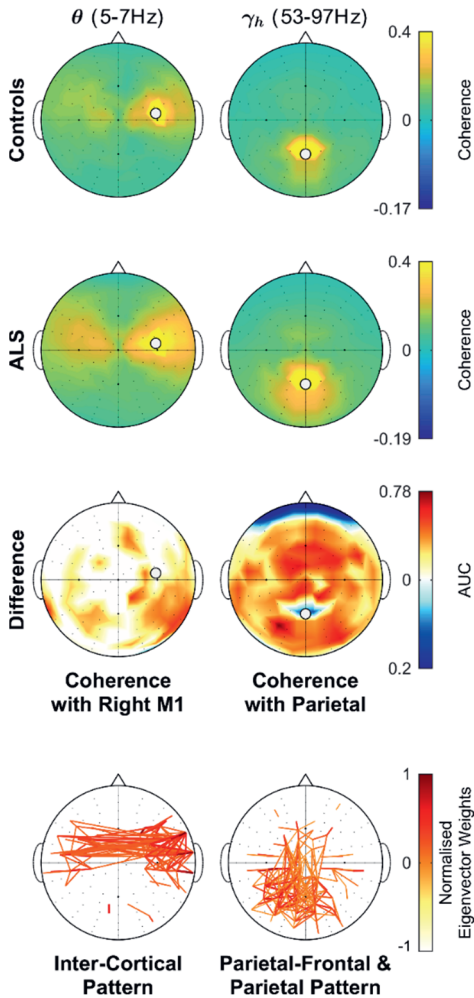


Figure 2. The dominant changes in EEG connectivity include increased θ -band inter-cortical and γ -band fronto-parietal coherence over scalp. The average values in controls and ALS groups, as well as between-group (ALS-Control) differences in coherence is shown with reference to (i.e. taken as connectivity seeds) the areas with dominant change in median connectivity: **Left:** Change in θ -band median coherence over scalp motor areas (see Supplementary Fig. 3) expanded by seeding from right M1 (location C_3). Notice the higher connectivity between \circ (right) and the left motor areas over scalp. **Right:** Changes in γ -band median absolute coherence in parietal and frontal scalp areas (see Supplementary Fig. 3), expanded by seeding from parietal area (location P_2). Notice the higher connectivity between \circ and both parietal and frontal scalp areas. Only the statistically significant connections (adaptive FDR, $q = 0.1$) are shown. AUC: Area under the receiver operating characteristics curve. **Bottom Row:** Point-to-point connectivity patterns from discriminant eigen-connectivity analysis (see Supplementary material), confirming the increase in θ -band inter-cortical and γ -band frontoparietal coherence.

ALS can be discriminated from controls using spectral EEG-based mapping

A comparison between ALS and controls was performed in individual channels (topographic maps), as well as on average across all bi-polar electrodes in the affected frequency bands using the linear discrimination combination of 4 spectral power and connectivity measures (Fig. 3). The findings closely resembled the individual patterns of change in both average quantitative measures and topographic maps, confirming that the detected changes are not only valid detections, but also key discriminants between ALS and controls.

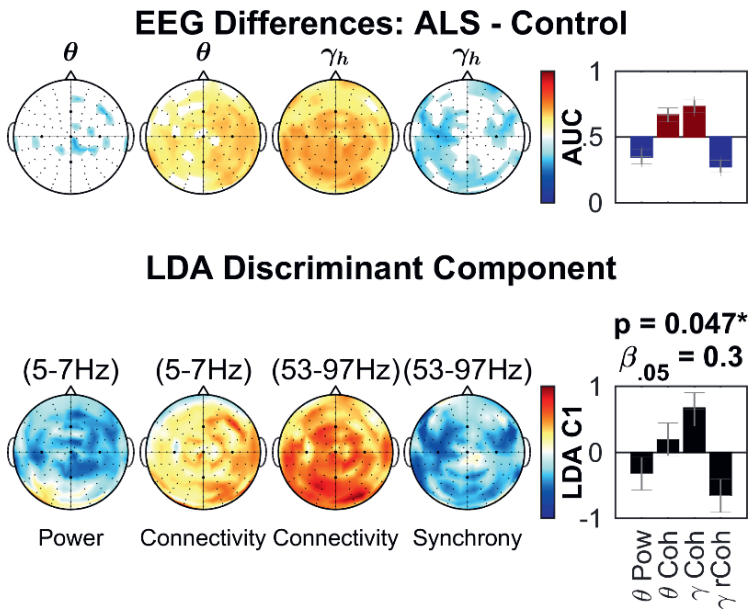


Figure 3. The linear discriminant analysis (LDA) direction for spectral EEG power and connectivity measures is similar to the differences of individual measures between ALS and controls, both for topographic maps and individual measures. The 4 EEG measures include the θ -band spectral power (θ Pow), θ -band median coherence (θ Coh), γ_h -band median coherence (γ Coh), and γ_h -band median real coherence (γ rCoh), all averaged across all electrodes, as in Fig. 3. **Bar plots (right):** The individual measures are compared on top, while the eigenvector of LDA is shown on the bottom. AUC: Area under the receiver operating characteristics curve. The p-value and $\beta_{.05}$ correspond to the shape (and not the presence of) of the LDA eigen vector. **Topographic maps (left):** comparison of individual electrodes for each measure between controls and ALS patients is shown on top, while the 1st eigen-vector (LDA C1) of high-dimensional regularised LDA (125 channels \times 3 measures \times 8 frequency bands = 3000) is shown on the bottom (only $4 \times 125 = 500$ relevant variables of the vectors are shown in the topographic map). See text for methods and statistics. Error bars: standard deviations.

EEG differences between ALS patients and controls do not discriminate between ALS subgroups

Connectivity measures that discriminated between ALS patients and controls were used to measure differences between traditionally-defined ALS subgroups (bulbar onset, spinal onset, ALS-FTD, FTD and the presence or absence of the *C9orf72* variant) (Fig. 4). While these measures were different between ALS and controls, there was no difference between ALS subgroups (Supplementary Fig. 6), although increased parietal-frontal connectivity was strongly present in FTD patients without ALS, and the median γ_h connectivity measure (Fig. 4) was significantly higher for FTD compared to the control group (Mann-Whitney U-test, $p = 0.0073$, $AUC=0.83$, $1-\beta_{0.05}=0.87$, $n_1 = 34$, $n_2 = 8$) but was not higher than the ALS group.

Degeneration in structural MRI shows discriminatory power comparable to EEG features, but with a complex pattern

To validate the findings of altered connectivity as markers of selective networks disruption, we sought to determine the relationship of our observed neurophysiologic signatures with ALS-specific MRI changes in 59 ALS patients who had undergone contemporaneous scans.^{3,33} The focus was on nine regions of interests (including both grey and white matter) that show maximal degeneration and/or contribute to EEG oscillations which were selected from MRI data. The AUC values for these MRI measures (Fig. 5, top) were comparable to the EEG measures (Fig. 3, top) in terms of discriminatory power. The maximally discriminant MRI (Cortico-Spinal Tract's Fractional Anisotropy) and EEG (γ -band median connectivity) measures had similar AUC of 0.73, while the average of the AUC values for the 4 EEG measures (0.69) was higher than the one for 9 MRI measures (0.66). See Supplementary Table 1.

Linear discriminant components are shown in Figure 5. While all of the MRI measures decreased in ALS, the discriminant components were not symmetric. We found that the discriminant vectors did not resemble the average changes in MRI individual measures (Figure 5, top). Rather, the average changes in MRI measures were due to the combined effect of several sub-components (in contrast to the EEG where the main discriminant component resembled the average changes in individual measures). These data suggest that the relationship between MRI changes and EEG changes in ALS is complex (a multi-parameter relationship/correlation that cannot be explained by a simple one-to-one relationship). Because it was not possible to infer the overall differences by inspection, we used a combination of PCA and several low and high-dimensional correlations to further study the complex relationship between MRI and EEG findings.

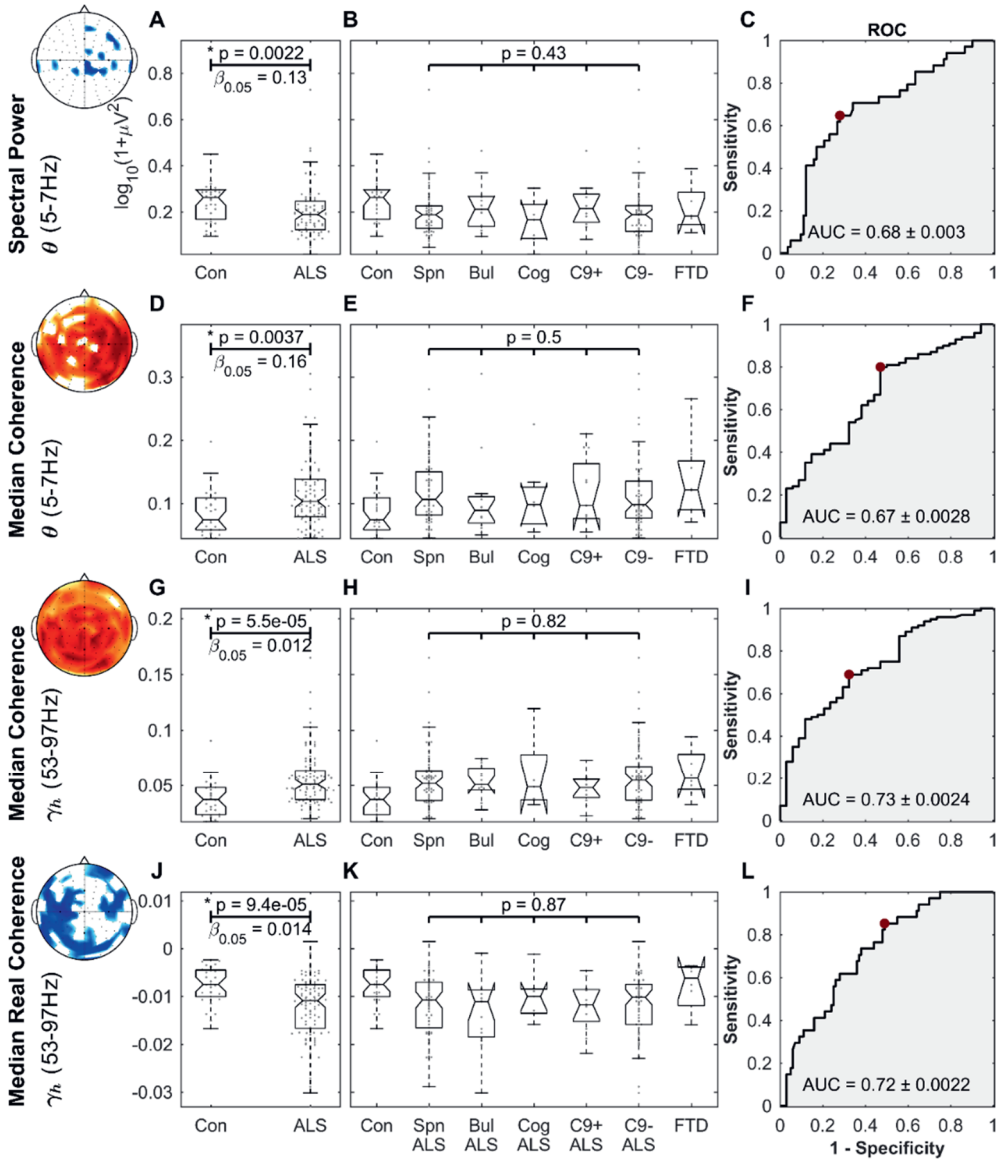


Figure 4. The spectral EEG power and connectivity measures are different between ALS and controls, but not between ALS subgroups. A, D, G & J: Comparison between healthy controls and all ALS patients. B, E, H & K: Comparison between ALS subgroups. ‘Con’, ‘Spn’, ‘Bul’, ‘Cog’, ‘C9+’ and ‘C9-’ stand for Control, Spinal, Bulbar, ALF-FTD, *C9orf72*-positive and *C9orf72*-negative subgroups, respectively. C, F, I & L: Receiver operating curve (ROC), comparing the discriminatory power, the optimal level of sensitivity-specificity (red dot), as well as the area under the curve (AUC), achieved for linear discrimination of controls and ALS patients using each measure. For each measure and frequency band, the average of all bipolar electrodes is used. See text for methods and statistics.

2

Changes in EEG power and coherence correlate with changes in structural MRI measures

As there was a high level of correlation between the MRI indices, PCA was used to extract the principal modes of neurodegeneration. The scores corresponding to each degeneration mode were correlated with measures of spectral power, synchrony and connectivity using the spectral EEG datasets, while recognizing that the MRI degeneration modes were combinations of changes in both grey and white matter.

The PCA-extracted modes of degeneration included 3 principal components that accounted for 57.3, 20.4, and 8.4 percent of normalised variance. The first 3 degeneration modes accounted for variances larger than (or comparable to) those of age and the direction of their eigenvectors were statistically consistent (Fig. 6). The first of these, involved wide-spread general degeneration in all regions of interest (consistency: $p = 0.0001$, $\beta_{0.05} = 1e-6$), which resembled the variability modes in healthy controls and age-related degeneration, albeit accounting for more than 4 times the variance than was explained by age. This mode was correlated with median cortico-cortical coherence in θ -band (and in γ -band), as well as the spectral power in θ -band. The overall correlation of the scores of this mode with the EEG scores along the individual EEG-MRI correlation vector was $r = 0.28 \pm 0.096$ ($p = 0.043$, $\beta_{0.05} = 0.25$). The second degeneration mode was formed primarily by the differential degeneration of corticospinal tracts and motor cortex, thus representing a motor-related disease-specific degeneration (consistency: $p = 0.00033$, $\beta_{0.05} = 0.00033$). This emphasised the differential degeneration of white and grey matters in motor cortical regions and tracts. Importantly, this mode was strongly correlated with θ -band spectral power (and γ -band synchrony). The overall correlation with EEG scores along the individual EEG-MRI correlation vector was $r = 0.42 \pm 0.1$ ($p = 0.0094$, $\beta_{0.05} = 0.041$). The third degeneration mode did not show any notable correlations with the EEG measures. The topographic maps of these correlations were similar to the topographic maps of the significant changes in ALS vs. controls. (See Supplementary Fig. 7 and 8 for the detailed topographic maps of EEG correlations with MRI scores and the corresponding statistical inference.)

Taken together, these data showed increased connectivity and reduced synchrony and spectral power measures in ALS patients which correlated to the MRI scores of structural neurodegeneration in the regions extensively or moderately affected in ALS (see the correlation data in Fig 7, top). The scalp regions with increased EEG connectivity extended beyond the regions over motor areas affected in ALS, which is an indication of both direct and indirect effects of neurodegeneration on spectral EEG measures.

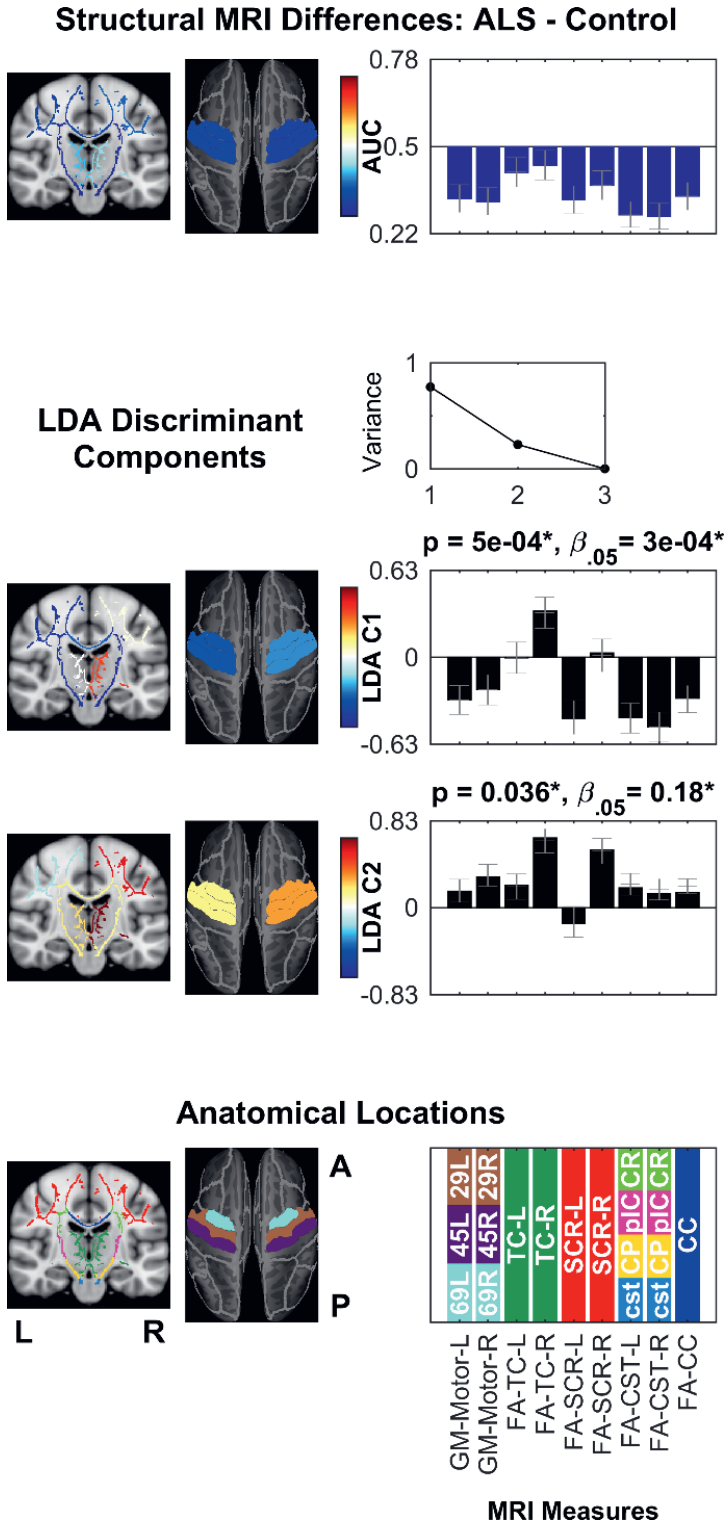


Figure 5. The linear discriminant analysis (LDA) directions for MRI measures is more complex than the differences of individual measures between ALS and controls. The 9 MRI measures include Grey Matter Thickness⁴³ in left and right motor cortices (GM-Motor-L & GM-Motor-R), Fractional Anisotropy⁴⁴ in left and right Thalamo-cortical pathways/loops (FA-TC-L & FA-TC-R), Superior Corona Radiata (FA-SCR-L & FA-SCR-R), Corticospinal Tracts (FA-CST-R & FA-CST-L), as well as Corpus Callosum (FA-CC). See Schuster et al.³ and the original references^{43,44} for the details. **Bar plots (right):** The individual measures are compared on top, while the eigenvectors of LDA are shown in the middle. AUC: Area under the receiver operating characteristics curve. The p-value and $\beta_{.05}$ correspond to the shape of the LDA eigenvectors. **MRI maps (left):** Comparison of individual measures between controls and ALS patients is shown on top, while the 1st and 2nd eigenvectors (LDA C1 & C2) of LDA are shown in the middle. AUC: Area under the receiver operating characteristics curve. See text for methods and statistics. A/P/L/R: Anterior/Posterior/Left/Right. Error bars: standard deviations.

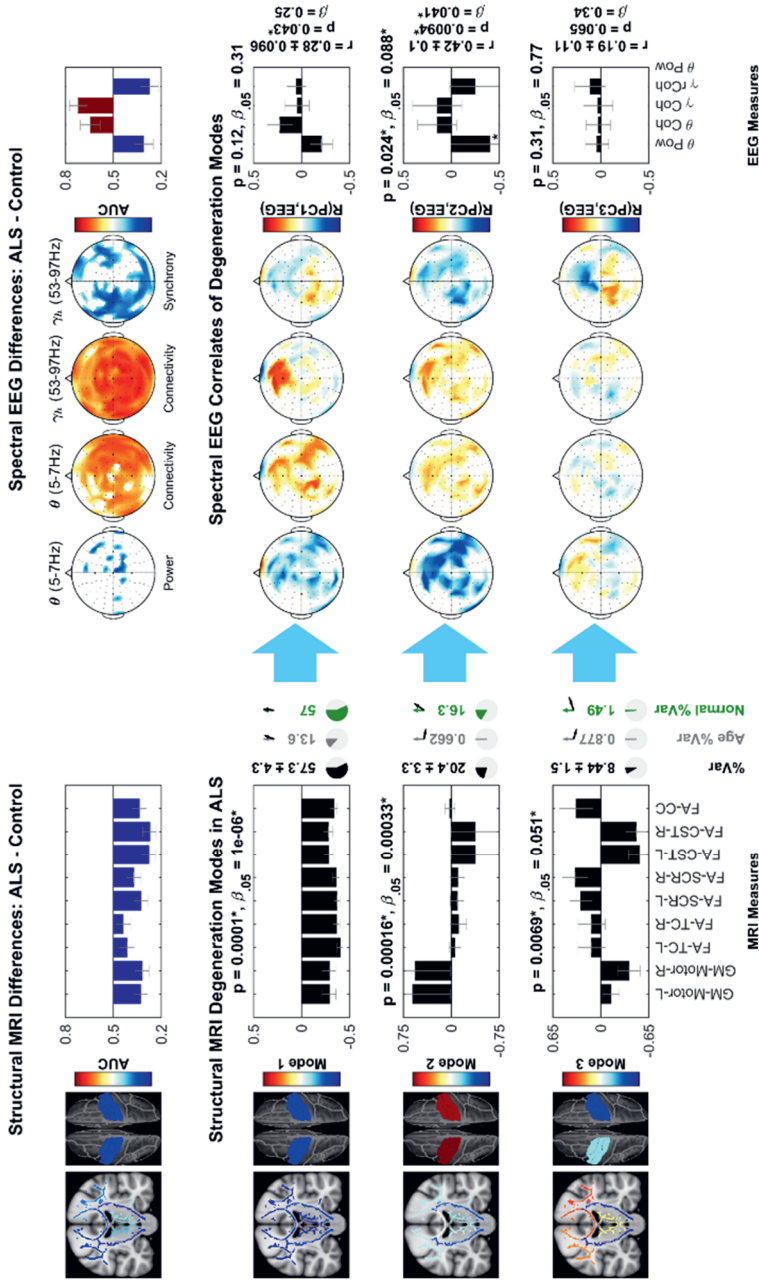


Figure 6. The MRI degeneration mode pertaining to motor-specific decline in ALS is significantly correlated with the decreased spectral power and oscillation synchrony, while the general uniform degeneration mode is additionally correlated with the increased coherence. The top row shows the ALS-specific changes in MRI (left) and EEG (right), side by side (see Fig. 4 & Fig. 5). Rows 2-4 show the first 3 modes of degeneration in structural MRI found by PCA (left), as well as their correlations with EEG measures (right). The percent of the variance explained by each mode, the parts explained by age, or along the structural covariance modes in healthy controls, as well as the angle of mode's direction with age or normal covariance are shown with black, grey, and green pie plots and vectors. The p-value and $\beta_{0.05}$ above the bar plots correspond to the shape of the eigenvectors or degeneration vectors. The error bars and \pm show standard deviations calculated from non-null bootstrapping. '+': significance at $p < 0.05$, '*': aFDR significance at $q = 0.05$. The r, p-value and $\beta_{0.05}$ to the right of correlation vectors correspond to the correlation of the overall EEG measures along the correlation vector direction with MRI.

Longitudinal study of EEG measures shows progressive increase in connectivity

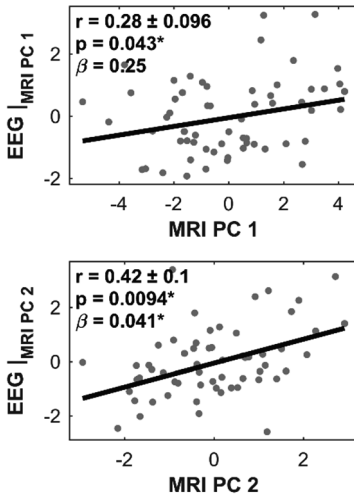
We examined the longitudinal changes in spectral EEG at 4 subsequent recording sessions (T₂-T₅) scheduled every 4-months after the initial recording session (T₁) for each patient. Significant progressive changes were noted in connectivity, when the average quantitative measures were examined as univariate measures (Fig. 7). These changes were all consistent in direction as the disease progressed, showing an accentuation of the signatures. However, when the multivariate topographic maps were tested for significant changes (corrected for multiple testing), only the θ - and γ -band coherences exhibited a significant increase in specific scalp locations (Supplementary Fig. 9).

Gender, age and medication effects on EEG measures

To ensure that the observed effects were not affected by other confounding factors (e.g. the effect of medications including the anti-glutamate drug riluzole) and to evaluate the effect of age, gender and clinical disability, additional confirmatory tests were performed.

There was no effect of age or gender in the controls for EEG spectral power or connectivity measures. Neither was there any effect of age, gender, or disease-duration in the ALS patients for any of the EEG measures. More importantly, none of the major EEG indices (as shown in Fig. 4) was different between patients on riluzole and those not on riluzole ALS therapy ($p > 0.10$, Mann-Whitney U-test, $n_1 = 83$, $n_2 = 12$). Spearman's rank correlation did not show any significant relationship ($p > 0.1$, $n = 83$) between the EEG measures and the time duration that patients had been on riluzole at the time of EEG recordings. Similar analysis found no correlations of the EEG measures with time-since-diagnosis or the clinical disability scale (ALSFRS-R scores, sub-scores, nor fine/gross motor factor-scores).¹⁸ Therefore, the identified EEG signatures were not directly related to motor disability, but rather reflected key patterns of disease-specific network alterations. Finally, potential changes in the peak frequency, a commonly inspected spectral measure, were analysed. There were no significant shifts in the peak frequency for spectral power or median coherence in any of the 125 EEG channels (Mann-Whitney U-test, $n_1 = 34$, $n_2 = 100$, $n_{\text{comparisons}} = 125$, $q_{\text{FDR}} = 0.1$).

Correlation of MRI Degeneration Modes with Spectral EEG Measures



Longitudinal Changes of Spectral EEG Measures

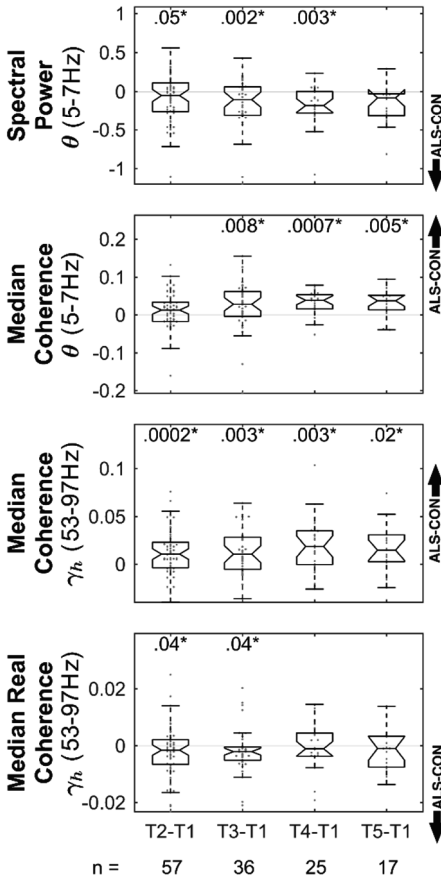


Figure 7. TOP: The MRI and EEG scores show the correlation of the degeneration modes 1 (general uniform degeneration) and 2 (motor-specific decline) with the altered EEG measures. The scores and the linear regression lines correspond to the rows 2 and 3 in Fig. 6. BOTTOM: The Longitudinal spectral EEG power and connectivity measures continue to change in a 16-month follow-up, in the same direction as ALS versus healthy controls. The bar plots show the pairwise differences of the 4 EEG measures (used in Fig. 3, Fig. 4 and Fig. 6) in follow-up sessions T2, T3, T4, and T5 against the first recording T1. The numbers above the box-plots show the aFDR-corrected significant p-values of the Wilcoxon's Signed Rank test. The arrows on the right show the direction of change of the measures in ALS (T1) versus healthy controls (see Fig. 4).

Discussion

Our data demonstrate that high-density spectral EEG mapping is a potentially robust tool in the assessment of selective changes in neural connectivity in ALS. Notably, spectral power (decrease in θ -band over motor scalp areas), oscillation synchrony (decrease in median real coherence in γ -band) and functional connectivity (higher median coherence in θ -band between bilateral scalp regions over motor areas, and in γ -bands between parietal and frontal scalp regions) are reliable characteristic discriminating factors between ALS patients and healthy controls. Furthermore, changes in spectral power and EEG coherence correlate with structural changes in key brain regions (Fig. 6). Our findings therefore point to a novel, network-wise characterisation of neurodegeneration in ALS, which is based on altered connectivity patterns with a specific signature of increased θ -band coherence between the motor regions of scalp and increased γ -band parietal-frontal coherence.

These changes are unlikely to originate from artefacts, as the location of electrodes that show maximal connectivity increase are not the expected locations for eye-movement (frontal electrodes) or EMG (peripheral electrodes) artefacts. This was additionally confirmed using ICA pre-processing for further artefact removal (see Supplementary material). Moreover, the seeding patterns (Fig. 2 and S5) show that the patterns of increased connectivity are maximal over 2 scalp regions (parietal and frontal; left and right) and not only in a single large region. Additionally, the increased connectivity due to an increased activity in a focal source (a single neural brain source or an artefactual component), would simultaneously lead to increased spectral power, while we observed unchanged or decreased spectral power in ALS. Furthermore, the phase values for a notable number of coherence values are distant from 0 or $\pm\pi$ (values expected due to point-spread or single artefactual components). Finally, the attempt to map the changes in cross-spectra to focal sources failed, as it led to distributed sources across the brain regions (Supplementary material). Taken together, the observed increased connectivity is not likely to be due to artefacts or a single deep source. (See also Supplementary material for the extended methods and results on the verification of the connectivity measures.)

Inference from high-dimensional data

Previously, high-dimensional analyses of connectivity patterns have been challenging due to multiple comparison problem and lack of reproducibility, especially for fMRI studies.⁴⁵ Our study implemented several approaches to avoid false discoveries. These included a large sample size and the use of a frequentist method (adaptive false discovery rate, aFDR) to limit the false discoveries. We also used Empirical Bayesian inference (EBI) to validate the achieved false discovery rate and importantly estimate the Bayesian posterior probability. We estimated statistical power for low-dimensional and high-dimensional data to validate the reproducibility of findings and relied on inference from average values rather than hand-picked measures. The longitudinal follow-up data show similar patterns of changes in the course of the disease and act as re-tests.

Potential mechanisms of changes in EEG

The distinct correlations between MRI metrics and EEG measures indicate the involvement of corresponding structural regions which provides the anatomical substrate of the EEG alterations detected. Specifically, the decreased spectral power in θ -band (and adjacent frequency bands) and the altered γ -band synchrony in bilateral motor regions of scalp are paralleled by structural degeneration in motor cortex and corticospinal tracts in ALS. This interpretation is supported by our data: firstly, both the power and synchrony changes are concentrated above motor regions (about C₃ and C₄ locations) where the disease-specific degeneration is maximal; secondly, the 2nd degeneration mode represents ALS-specific degeneration (including the differential white-grey-matter degeneration) with strong correlation with θ -band spectral power. Finally, although the changes in the spectral power were not as strong as changes in coherences, the spectral power showed a stronger correlation with motor-related disease-specific degeneration.

Segregation of variability in our MRI data into degeneration modes also yielded a widespread pattern of degeneration (resembling the normal covariance in controls) that included areas known to be severely affected in ALS (grey matter motor regions and corticospinal tracts); moderately affected in ALS (superior corona radiata and corpus callosum) and areas that are clinically less apparent (Thalamocortical pathways). EEG correlates of this degeneration mode are a decline in spectral power, with a concomitant increase in functional communication (θ -band intercortical coherence and γ -band parietal-frontal coherence over scalp). These changes can be interpreted based on the existing knowledge on the neuropathology of the condition. In typical ALS, progression is thought to involve initial primary degeneration within the motor system (especially the upper and lower motor neurons),^{46,47} with spread to other regions as the disease progresses.^{33,48} Therefore, the spectral power decrease in θ -band which is maximal above the motor regions of scalp and maximally correlated with motor-related degeneration modes, mainly reflects the primary motor aspect of the disease. On the other hand, the connectivity increases (especially the γ -band increase between parietal and frontal scalp regions; also strongly present in FTD) that shows considerable longitudinal progression, reflect mostly the spread of the disease to other regions. Further validation of this explanation is warranted in future studies.

In a situation where the baseline neural activity and communication is constant, degeneration in white matter is expected to attenuate communication and connectivity. The observation of increased coherence is therefore likely to reflect extra compensatory activity within and outside areas associated with white matter degeneration. This change may be a signature of network over-activity and a reflection of the disease severity. Our data therefore indicate that coherence, which quantifies neural communication in the brain, can also indirectly reflect structural degeneration, and can be potentially harnessed to characterise progressive neurodegeneration. Future studies using computational neural modelling would be of utility in assessing this perspective, as invasive neurophysiological recordings in human disease would be precluded by ethical considerations.

The underlying mechanisms for ALS are not yet fully understood and are most likely heterogeneous.⁴⁹ One possibility is that early neurodegeneration of interneurons interrupts the balance between excitatory and inhibitory network activity.⁵⁰ Another possibility is that pathological changes in excito-inhibitory networks are driven by a combination of 'dying-forward' and 'dying-back' of individual groups of neurons, and that neuronal death occurs as a function of excessive excitotoxicity.⁵¹ There is preliminary evidence for both possibilities, and while the structural neurodegeneration is reflected in the MRI measures and the unbalanced excito-inhibitory network activity reflected in EEG measures, the causality between the changes in the EEG and MRI measures remains to be determined.

In this study, we used the real part of the cortico-cortical coherence measure to index frequency-specific synchronous oscillations (i.e., oscillations with zero lag), as has been previously described for the time domain using pre-whitened cross-correlations in MEG.^{7,8} These synchronous oscillations were interpreted as originating from structural neural pathways such as thalamo-cortical pathways (loops) that lead to simultaneous zero-lag propagation of oscillatory brain activity.⁸ Consequently, the observed patterns of synchrony alteration (Fig. 3), is an indication of structural separation and isolation of motor cortex from more frontal and parietal regions in the brain. This measure was specifically included as the zero-lag synchronous neural oscillations and has been shown previously to discriminate between healthy individuals and neuropsychiatric patients.⁷ The utility of this measure was afforded by the bipolar spatial filters applied that attenuate the field-spread effects of deeper sources, hence, allowing the *bona fide* zero-lag synchrony be aggregated between superficial sources. The correlation with motor-specific degeneration in MRI and concentration over bilateral M1 areas support the validity of this measure.

Utility of EEG for studying and diagnosing neurodegeneration

The observed EEG signatures provide additional and important insights into ALS pathogenesis, which are beyond the scope of current structural MRI and clinical evaluation. Despite the traditional view that ALS is a focal structural degeneration of motor neurons, these data point to major changes that occur at the network level (found by EEG measures of neural activity and connectivity) which correlate in a complex manner with structural degeneration. Furthermore, these changes are related (though through a complex mechanism with direct and indirect effects) to the structural degeneration. The absence of a correlation with clinical phenotypes, while not intuitive, suggests that the patterned changes that we observed in both cross-sectional and longitudinal datasets are consistent markers of the disease process, regardless of the clinical disability profile. This is an important observation, indicating that spectral EEG has potential for development as a novel biomarker of network degeneration. The correlation with MRI findings, and the progression of observed changes over time support the potential clinical utility of spectral EEG as a disease biomarker, and refinement of these combined measures could form a new basis for novel definition of disease classification.¹⁶ Moreover, this spectral and connectivity-based characterisation is also

applicable in cognate neurodegenerative diseases, particularly FTD. The increased Frontal-Parietal connectivity changes identified in ALS are also strongly present in the FTD cohort, supporting the notion that it is a neural signature indicative of frontal dysfunction in FTD. Overall, the connectivity-based characterisation informs of the altered functions of the network and paves the way for future network-based characterisation and mapping of the neurodegenerative diseases.

While the primary goal of this study was to elucidate disease specific changes and their underlying mechanisms, these measures also have potential as future targets for diagnosis and prognosis of specific aspects of the disease. Our data provide a robust proof of concept for the use of spectral EEG for patient stratification based on network-based pathology in the neurodegenerative disorders. Such an approach has significant advantages over other imaging and diagnostic modalities (e.g. MRI). Given the relative differences between EEG and MRI in terms of cost and accessibility, it is noteworthy that the discriminatory power of EEG coherence measures (based on AUC values) was actually comparable or higher than individual MRI measures (see Supplementary Table 1). EEG closely reflects the real-time neural activity with excellent temporal resolution, is widely accessible, portable and inexpensive. Spectral EEG recordings can be performed comfortably in extended ranges of patients with neurological impairments within existing clinical settings. We have shown that the potential diagnostic utility can be further enhanced using previously reported pattern analysis techniques^{7,52} and/or neuroelectric source imaging.^{53,54} Future studies using task-based paradigms, including motor⁵⁵ and cognitive tasks,⁵⁶ carry additional potential in deconstructing sensory or motor aspects of neuro-pathology, including those that are specifically captured by these resting-state measures.

Limitations

The identified changes in spectral power and cortico-cortical connectivity have been assessed in the sensor-space corresponding to scalp locations that provide relatively low spatial resolution. Using source analysis^{29,57,58} to identify the corresponding brain regions that give rise to the reported findings has the potential to further enhance our understanding of the underlying disease pathophysiology in future studies. While challenging and requiring special considerations due to the potential confounding factors of neurodegeneration and the resulting structural changes in the brain, the potential benefits would be considerable.

Additionally, investigation of the effects of mimic disease conditions and other neurological diseases (other than the ALS-FTD range) on the identified EEG signatures will be required to establish the specificity of this technology for adjunct diagnostic purposes.

Conclusion

This is the first study of its kind to demonstrate the validity of spectral EEG as a measure of structural degeneration in ALS. Correlations between EEG measures and contemporaneous changes in structural MRI indicate that changes in neural activity in

motor areas mirror focal disease-specific structural changes in amyotrophic lateral sclerosis. Moreover, the increased connectivity (cortico-cortical coherences) reflects network over-activity in affected motor regions (inter-cortical θ -band) and less degenerated regions such as parietal and frontal areas (γ -band), and likely represents an indirect potentially compensatory effect of degeneration.

Our data confirm that spectral EEG is a novel and potentially sensitive methodology by which the neurodegeneration in ALS and related conditions can be characterised in terms of specific disruptions in neural communication. This technology can be harnessed as an inexpensive and clinically useful disease biomarker in assessing the efficacy of targeted drug therapies for neurodegeneration.

References

1. Hardiman, O., Van Den Berg, L. H. & Kiernan, M. C. Clinical diagnosis and management of amyotrophic lateral sclerosis. *Nat Rev Neurol* **7**, 639–49 (2011).
2. Bede, P. & Hardiman, O. Lessons of ALS imaging: Pitfalls and future directions - A critical review. *NeuroImage: Clinical* vol. 4 436–443 (2014).
3. Schuster, C., Elamin, M., Hardiman, O. & Bede, P. The segmental diffusivity profile of amyotrophic lateral sclerosis associated white matter degeneration. *Eur J Neurol* **23**, 1361–1371 (2016).
4. Byrne, S. *et al.* Aggregation of neurologic and neuropsychiatric disease in amyotrophic lateral sclerosis kindreds: a population-based case-control cohort study of familial and sporadic amyotrophic lateral sclerosis. *Ann Neurol* **74**, 699–708 (2013).
5. Elamin, M. *et al.* Identifying behavioural changes in ALS: Validation of the Beaumont Behavioural Inventory (BBI). *Amyotroph Lateral Scler Frontotemporal Degener* **18**, 68–73 (2017).
6. de Carvalho, M. *et al.* Neurophysiological measures in amyotrophic lateral sclerosis: Markers of progression in clinical trials. **6**, 17–28 (2009).
7. Georgopoulos, A. P. *et al.* Synchronous neural interactions assessed by magnetoencephalography: a functional biomarker for brain disorders. *J Neural Eng* **4**, 349–355 (2007).
8. Langheim, F. J. P., Leuthold, A. C. & Georgopoulos, A. P. Synchronous dynamic brain networks revealed by magnetoencephalography. *Proc Natl Acad Sci US A* **103**, 455–459 (2006).
9. Vecchio, F. *et al.* Resting state cortical EEG rhythms in Alzheimer's disease: toward EEG markers for clinical applications: a review. *Suppl Clin Neurophysiol* **62**, 223–236 (2013).
10. Stam, C. J. *et al.* Magnetoencephalographic evaluation of resting-state functional connectivity in Alzheimer's disease. *Neuroimage* **32**, 1335–1344 (2006).
11. Stoffers, D. *et al.* Increased cortico-cortical functional connectivity in early-stage Parkinson's disease: an MEG study. *Neuroimage* **41**, 212–222 (2008).
12. Pievani, M., de Haan, W., Wu, T., Seeley, W. W. & Frisoni, G. B. Functional network disruption in the degenerative dementias. *Lancet Neurol* **10**, 829–843 (2011).
13. Agosta, F. *et al.* Sensorimotor Functional Connectivity Changes in Amyotrophic Lateral Sclerosis. *Cerebral Cortex* **21**, 2291–2298 (2011).
14. Blain-Moraes, S., Mashour, G. A., Lee, H., Huggins, J. E. & Lee, U. Altered cortical communication in amyotrophic lateral sclerosis. *Neurosci Lett* **543**, 172–6 (2013).
15. Iyer, P. M. *et al.* Functional Connectivity Changes in Resting-State EEG as Potential Biomarker for Amyotrophic Lateral Sclerosis. *PLoS One* **10**, e0128682 (2015).
16. Al-Chalabi, A. *et al.* Amyotrophic lateral sclerosis: moving towards a new classification system. *Lancet Neurol* **15**, 1182–94 (2016).
17. Rascovsky, K. *et al.* Sensitivity of revised diagnostic criteria for the behavioural variant of frontotemporal dementia. *Brain* **134**, 2456–2477 (2011).
18. Cedarbaum, J. M. *et al.* The ALSFRS-R: a revised ALS functional rating scale that incorporates assessments of respiratory function. *J Neurol Sci* **169**, 13–21 (1999).
19. Byrne, S., Elamin, M., Bede, P. & Hardiman, O. Absence of consensus in diagnostic criteria for familial neurodegenerative diseases. *J Neurol Neurosurg Psychiatry* **83**, 365–367 (2012).
20. Mohr, K. S., Nasserolleslami, B., Iyer, P. M., Hardiman, O. & Lalor, E. C. EyeBallGUI: A Tool for Visual Inspection and Binary Marking of Multi-channel Bio-signals. *bioRxiv* 129437 (2017).
21. Dukic, S. *et al.* Estimation of coherence using the median is robust against EEG artefacts. in *Proceedings of the Annual International Conference of the IEEE Engineering in Medicine and Biology Society, EMBS* (2017).
22. Nolan, H., Whelan, R. & Reilly, R. B. FASTER: Fully Automated Statistical Thresholding for EEG artifact Rejection. *J Neurosci Methods* **192**, 152–62 (2010).
23. Muthukumaraswamy, S. D. High-frequency brain activity and muscle artifacts in MEG/EEG: a review and recommendations. *Front Hum Neurosci* **7**, (2013).
24. Halliday, D. M. *et al.* A framework for the analysis of mixed time series/point process data—theory and application to the study of physiological tremor, single

- motor unit discharges and electromyograms. *Prog Biophys Mol Biol* **64**, 237–278 (1995).
25. Nasserleslami, B., Lakany, H. & Conway, B. A. Identification of time–frequency EEG features modulated by force direction in arm isometric exertions. *2011 5th International IEEE/EMBS Conference on Neural Engineering, NER 2011* 422–425 (2011).
 26. Nasserleslami, B., Lakany, H. & Conway, B. A. EEG signatures of arm isometric exertions in preparation, planning and execution. *Neuroimage* **90**, 1–14 (2014).
 27. Pfurtscheller, G. & Lopes Da Silva, F. H. Event-related EEG/MEG synchronization and desynchronization: Basic principles. *Clinical Neurophysiology* **110**, 1842–1857 (1999).
 28. Vuckovic, A. *et al.* The influence of central neuropathic pain in paraplegic patients on performance of a motor imagery based Brain Computer Interface. *Clin Neurophysiol* **126**, 2170–2180 (2015).
 29. Muthuraman, M. *et al.* EEG-MEG Integration Enhances the Characterization of Functional and Effective Connectivity in the Resting State Network. *PLoS One* **10**, (2015).
 30. Leonardi, N. *et al.* Principal components of functional connectivity: a new approach to study dynamic brain connectivity during rest. *Neuroimage* **83**, 937–950 (2013).
 31. Recognition, P. *et al.* *Manual Solutions Fukunaga*. (1990).
 32. Izenman, A. J. *Modern Multivariate Statistical Techniques*. (2008).
 33. Bede, P. *et al.* The selective anatomical vulnerability of ALS: ‘disease-defining’ and ‘disease-defying’ brain regions. *Amyotroph Lateral Scler Frontotemporal Degener* **17**, 561–570 (2016).
 34. Vuckovic, A. *et al.* Dynamic oscillatory signatures of central neuropathic pain in spinal cord injury. *J Pain* **15**, 645–655 (2014).
 35. Xu, R. *et al.* Movement-related cortical potentials in paraplegic patients: abnormal patterns and considerations for BCI-rehabilitation. *Front Neuroeng* **7**, (2014).
 36. Principal Component Analysis for Special Types of Data. in *Principal Component Analysis* (ed. Jolliffe, I. T.) 338–372 (Springer New York, 2002).
 37. Bede, P. *et al.* Multiparametric MRI study of ALS stratified for the C9orf72 genotype. *Neurology* **81**, 361–369 (2013).
 38. Zhou, X.-H., McClish, D. & Obuchowski, N. *Statistical Methods in Diagnostic Medicine*. *Wiley Series in Probability and Statistics*. (Wiley, 2011).
 39. Benjamini, Y. & Hochberg, Y. Controlling the False Discovery Rate: A Practical and Powerful Approach to Multiple Testing. *Journal of the Royal Statistical Society. Series B (Methodological)* vol. 57 289–300 (1995).
 40. Benjamini, Y., Krieger, A. M. & Yekutieli, D. Adaptive linear step-up procedures that control the false discovery rate. *Biometrika* **93**, 491–507 (2006).
 41. Efron, B., Tibshirani, R., Storey, J. D. & Tusher, V. Empirical Bayes Analysis of a Microarray Experiment. *J Am Stat Assoc* **96**, 1151–60 (2001).
 42. Efron, B. Size, power and false discovery rates. *The Annals of Statistics* **35**, 1351–77 (2007).
 43. Destrieux, C., Fischl, B., Dale, A. & Halgren, E. Automatic parcellation of human cortical gyri and sulci using standard anatomical nomenclature. *Neuroimage* **53**, 1–15 (2010).
 44. Oishi, K. *et al.* Human brain white matter atlas: identification and assignment of common anatomical structures in superficial white matter. *Neuroimage* **43**, 447–457 (2008).
 45. Eklund, A., Nichols, T. E. & Knutsson, H. Cluster failure: Why fMRI inferences for spatial extent have inflated false-positive rates. *Proc Natl Acad Sci U S A* **113**, 7900–7905 (2016).
 46. Huynh, W. *et al.* Assessment of the upper motor neuron in amyotrophic lateral sclerosis. *Clin Neurophysiol* **127**, 2643–2660 (2016).
 47. de Carvalho, M. & Swash, M. Lower motor neuron dysfunction in ALS. *Clin Neurophysiol* **127**, 2670–2681 (2016).
 48. Burke, T. *et al.* A Cross-sectional population-based investigation into behavioral change in amyotrophic lateral sclerosis: subphenotypes, staging, cognitive predictors, and survival. *Ann Clin Transl Neurol* **4**, 305–317 (2017).
 49. Al-Chalabi, A. & Hardiman, O. The epidemiology of ALS: a conspiracy of genes, environment and time. *Nat Rev Neurol* **9**, 617–628 (2013).
 50. Turner, M. R. & Kiernan, M. C. Does inter-neuronal dysfunction contribute to neurodegeneration in amyotrophic lateral sclerosis? *Amyotrophic Lateral Sclerosis* **13**, 245–250 (2012).
 51. Kiernan, M. C. *et al.* Amyotrophic lateral sclerosis. *The Lancet* **377**, 942–955 (2011).

52. Herman, P., Prasad, G., McGinnity, T. M. & Coyle, D. Comparative analysis of spectral approaches to feature extraction for EEG-based motor imagery classification. *IEEE Trans Neural Syst Rehabil Eng* **16**, 317–326 (2008).
53. Lei, X., Wu, T. & Valdes-Sosa, P. A. Incorporating priors for EEG source imaging and connectivity analysis. *Front Neurosci* **9**, (2015).
54. Muthuraman *et al.* Beamformer source analysis and connectivity on concurrent EEG and MEG data during voluntary movements. *PLoS One* **9**, (2014).
55. Fisher, K. M., Zaaimi, B., Williams, T. L., Baker, S. N. & Baker, M. R. Beta-band intermuscular coherence: a novel biomarker of upper motor neuron dysfunction in motor neuron disease. *Brain* **135**, 2849–2864 (2012).
56. Iyer, P. M. *et al.* Mismatch Negativity as an Indicator of Cognitive Sub-Domain Dysfunction in Amyotrophic Lateral Sclerosis. *Front Neurol* **8**, 395 (2017).
57. Ramírez, R. R., Wipf, D. & Baillet, S. Neuroelectromagnetic Source Imaging of Brain Dynamics. in *Computational Neuroscience* (eds. Chaovalitwongse, W., Pardalos, P. M. & Xanthopoulos, P.) 127–155 (Springer New York, 2010).
58. Khan, S. *et al.* Somatosensory cortex functional connectivity abnormalities in autism show opposite trends, depending on direction and spatial scale. *Brain* **138**, 1394–1409 (2015).

Supplementary material

Supplementary methods

EEG preprocessing

After the quality of the acquired datasets from controls and patients were checked by visual inspection (EyeBallGUI, <http://eyeballgui.sf.net>),¹ we used an automated artefact rejection method, based on a verified statistical thresholding approach FASTER,² which accounts for major types of artefacts and provides high sensitivity and specificity. Contaminated epochs were detected using 4 statistical features (amplitude range, mean shift, variance, and mean spectral power in 0-2 Hz and 20-40 Hz frequency bands) of the data at Z-scores threshold of ± 3.5 separately on each channel, each epoch (containing all the channels), mean channel and mean epoch. The contaminated epochs and channels, detected with the set thresholds were removed from the analysis. The details of the preprocessing method has been published elsewhere.³ To make sure of the efficacy of the preprocessing, the rejections by the preprocessing routine was visually inspected in 8 random controls and 8 random patients to verify the success in exclusion of contamination by eye movements, movement artefacts, and facial EMG. The data rejection rates in the controls and patients were 9.3 ± 2.7 % (range: 3-14 %) in controls and 11.4 ± 6.4 % (range: 3.4-50.5 %) in patients.

EEG processing

Bipolar channels were formed by subtracting adjacent electrodes along the tangential directions (See Supplementary Fig. 1) to estimate the superficial cortical brain activity and minimise the effects of volume conduction and deeper brain sources. Additionally, the use of spatial filters considerably reduces the effects of artefacts such as EMG,⁴ that may not have been fully excluded from the analysis. Simple bipolar spatial filter was preferred over surface Laplacian,⁵ as it relies on two monopolar channels rather five; hence providing more independent pairwise coherence connectivity values that do not share common (surrounding) reference electrodes. Using a tangential pattern (and the corresponding directions as in Supplementary Fig. 1) for forming bipolar channels did not affect the nature of the results. In separate analyses, similar results were obtained when radial pattern and directions were used for forming bipolar channels. This referencing method provided 125 bipolar channels from 128 monopolar recordings. The EEG signals were high-pass filtered by a dual-pass 5-th order Butterworth filter with cut-off frequency of 1 Hz. To calculate the spectral power, coherency function and coherence,⁶ the signal was epoched into 1s segments and multiplied by a Hann window function and then the auto- and cross-spectra were estimated. The epoch length did not have a significant effect on results as the findings with 10s epochs were the same. The band-specific real, imaginary and absolute values of the coherency function were estimated in the δ (2-4 Hz), θ (5-7 Hz), α (α_1 : 8-10 Hz, α_2 : 11-13 Hz), β (β_1 : 14-20 Hz, β_2 : 21-30 Hz), and γ (γ_1 : 31-47 Hz, γ_2 : 53-97 Hz) frequency bands between all 125 bipolar channel combinations (performed in sensor-space). These frequency bands were selected according to the frequency ranges that change in motor tasks,^{7,8} as well

as resting-state studies in ALS⁹ and in healthy subjects.¹⁰ The elements of cross-spectral matrices (used for calculation of spectral power, coherency function and coherence) were estimated by taking the median (as opposed to the conventional mean) of complex frequency domain values across all the data epochs. The use of median for coherence and power suppresses the effect of outlier and artefactual data,³ especially should their nature be different in controls versus patients. All the signal analysis was performed in MATLAB (Mathworks Inc., Natick, MA, USA), using scripts coded for this study.

Transformation to normal for correlation analysis

MRI and EEG measures were transformed to standard normal distributions, by first rank-transforming the data, and subsequently replacing the rank data k with $iCDF_{normal(0,1)} = (2k - 1/2n)$, where $iCDF$ is the inverse cumulative distribution function and n the number of data points.¹¹

Discriminant eigen-connectivities for point-to-point analysis

First, the 125×125 connectivity matrix was thresholded at $p < 0.025$ to reduce the dimensions by selecting the point-to-point connections that afford higher levels of discrimination. Next, regularised ($\lambda = 0.001$) Fisher's linear discriminant analysis (LDA)^{12,13} was applied to the significantly different point-to-point variables. The point-to-point variables constituting the largest 10% of the vector components in the first dominant principal discriminant vector were selected as the representatives for the dominant difference pattern in the corresponding frequency. The thresholding values ($p < 0.025$ and 10%) had negligible effects on the nature of outcome and was therefore chosen to provide visually informative number of connections.

Summary of MRI data acquisition methods

A 3T Achieva system (Philips, Amsterdam, The Netherlands) was used to acquire the MR data (gradient strength: 80 mT/m, slew rate: 200 T/m/s, 8-channel receive-only head coil) for the T₁-weighted images (FOV = 256 × 256 × 160 mm, spatial resolution: 1 mm³) and DTI images (FOV = 245 × 245 × 150 mm, spatial resolution: 0.5 mm³). Diffusion Tensor Imaging (DTI) datasets underwent corrections for eddy current, motion and brain-tissue extraction using FSL.¹⁴ Subsequent extraction of grey and white matter data for regions of interest were extracted from existing atlases.^{15,16} See Schuster *et al.*¹⁷ for full details.

Statistics for MRI and EEG principal components using bootstrapping

To assess the statistical significance of the eigen vectors from PCA and LDA for EEG and MRI measures the following null and nonnull bootstrapping resampling approach was used: In 10,000 random null resampling (with replacement) where the group labels for controls and ALS were not respected, as well as in 10,000 nonnull bootstraps with replacement where the data was resampled from the same group, the absolute dot-product of the eigenvectors by the original eigen-vector was used to form the null

and nonnull distributions. The p-value was taken as the average empirical quantile of 250 randomly selected nonnull values against the null data, while the empirical probability density function for null and nonnull distributions were used to calculate the power by numerical integration at $\alpha = 0.05$. The eigenvectors generated from bootstrap re-sampling were used to estimate the standard deviation for the components of the eigen-vectors, and when required to estimate the distribution and standard deviation of the correlation and correlation-vectors with EEG measures.

Verification of the estimated connectivity

To investigate if the estimated coherence patterns and the observed changes reflect an underlying neural connectivity, three additional analyses were performed.

Eigen-spectrum of the cross-spectral matrices: The eigen-spectrum of the cross-spectral matrices can reveal the potentially spurious or nonglobal dynamics (extreme unbalanced large/small values or almost equal values), and was therefore found in individual frequency bands for each healthy control and ALS patient. To assess the significance of eigen-spectrum of the cross-spectral matrix, parallel-analysis,¹⁸ together with FDR was employed. This was followed by estimation of both the magnitude and phase of the coherence matrices in controls and patients in individual frequency bands.

Testing for a neural or artefactual focal source underlying the estimated connectivity: A general 3-layer head model based on an MRI template (27),¹⁹ was used to find an average lead field matrix for the 128-channel EEG montage, using the FieldTrip Toolbox.²⁰ Following the calculation of the bipolar lead field matrix, the observed ALS-Control pattern of change in the cross-spectral matrix was mapped to the source-space, under the (null) hypothesis that the changes originate from changes in minimum/limited number of focal active sources. This null condition was realised by calculation of the inverse lead-field matrix under the constraint of minimum number of active (nonzero) sources.

Re-calculation of connectivity with ICA-based preprocessing: To ensure that the potentially unrejected artefacts in the γ -band, especially the high-frequency frontal components due to ocular EMG and micro-saccades, or other high-frequency spikes or EMG components²¹ did not influence the findings, we used independent component analysis (ICA),²² a blind source separation method²³ for artefact removal. After the application of the previously explained artefact rejection by statistical thresholding, ICA (FastICA)²⁴ was used on the remaining data to extract the independent components. The artefactual components were subsequently rejected by visual inspection. All the subsequent steps for signal analysis were similarly applied on the ICA-cleaned data.

Supplementary results

Verification of neural connectivity

Eigen-spectrum of the cross-spectral matrices: The cross-spectra matrices for individual frequency bands in the controls and ALS patients show that the cross-spectral patterns are nonuniform (including low and high values) and depend on electrode

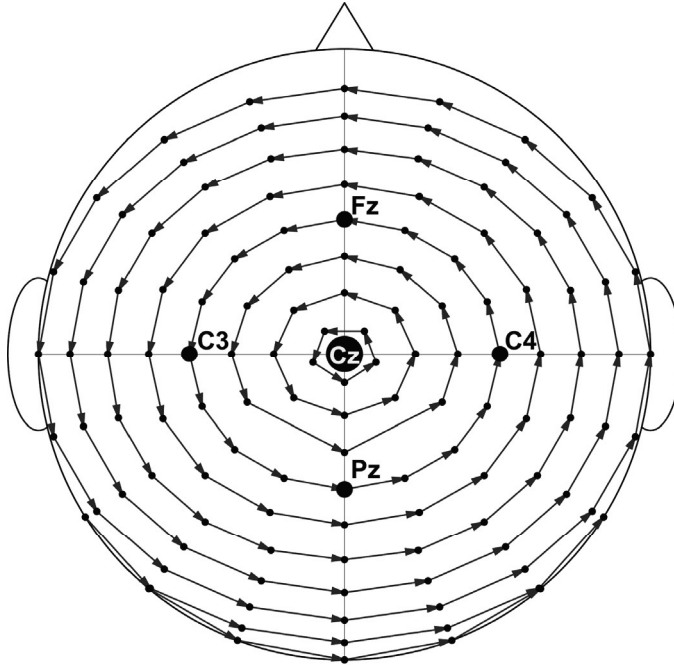
combinations and frequencies (Supplementary Fig. 10). This suggests that the bipolar coherences reflect multiple complex patterns (between the parietal, frontal and left/right sensorimotor scalp areas) that are not local effects or global effects coming from simple single origins. Importantly, the eigen-spectra for all of the cross-spectral matrices show more than 6 significant eigen values, indicating a complex dynamic that cannot be explained by a simple underlying source. Notably, the majority of phase values for the corresponding coherence matrices and a notable number of values with significant between-group differences (Supplementary Fig. 11) had nonzero phase values (distant from 0 or $\pm\pi$), which cannot be due to volume conduction effect of limited focal (deep) sources.

Distributed source underlying the estimated connectivity: Supplementary Fig. 12 shows that in the attempt to map the observed changes in the cross-spectra to a few focal sources (either neural or artefactual), the results still point to several wide-spread underlying brain sources. This suggests that the observed changes in coherence measures are unlikely to originate from limited focal brain sources or a few artefactual components in the periphery; hence, confirming that they represent the changes in the neural connectivity between the different regions of the brain.

Effect of ICA preprocessing: The results with and without ICA preprocessing were very similar for both the θ -band and γ -band changes in the connectivity. Supplementary Fig. 13 shows the γ -band average connectivity measure (that could potentially be more prone to contamination by high-frequency artefacts) and its changes in the ALS patients against healthy controls. It is shown that the difference between controls and ALS patients is present with a similar level of significance, regardless of performing the preprocessing with or without ICA. ICA led to increased levels of connectivity in both group (equally for controls and patients), which implies the lack of major contamination without ICA preprocessing. The θ -band connectivity pattern was similarly unaffected by ICA.

In addition to these findings, the observed connectivity patterns were reproducible when we changed the epoch length from 1s to 10s. In summary, these results suggest that the estimated coherence measures reflect the neural connectivity between distinct brain regions; therefore, the observed differences between the controls and patients reflect a pathological change in connectivity which cannot be explained by focal neural or artefactual sources or by other known types of artefacts.

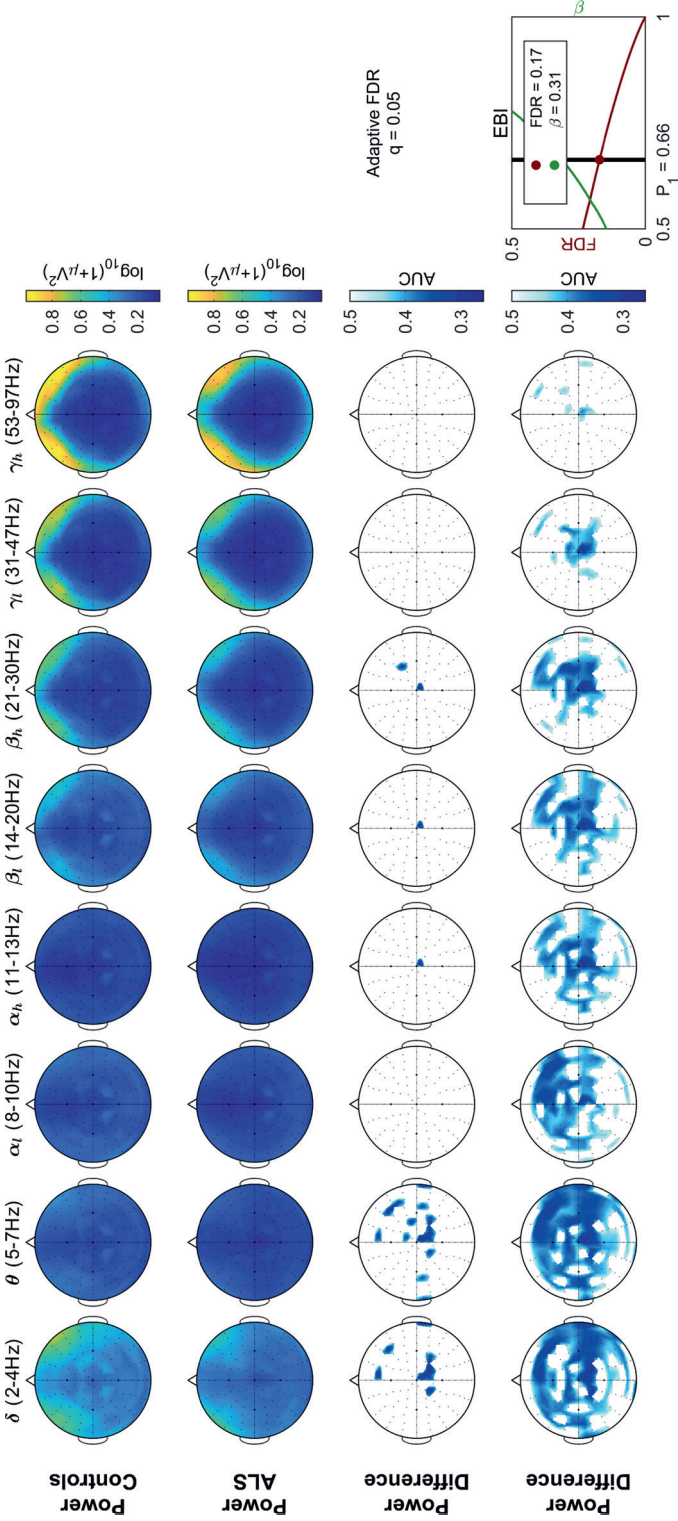
Supplementary figures and tables



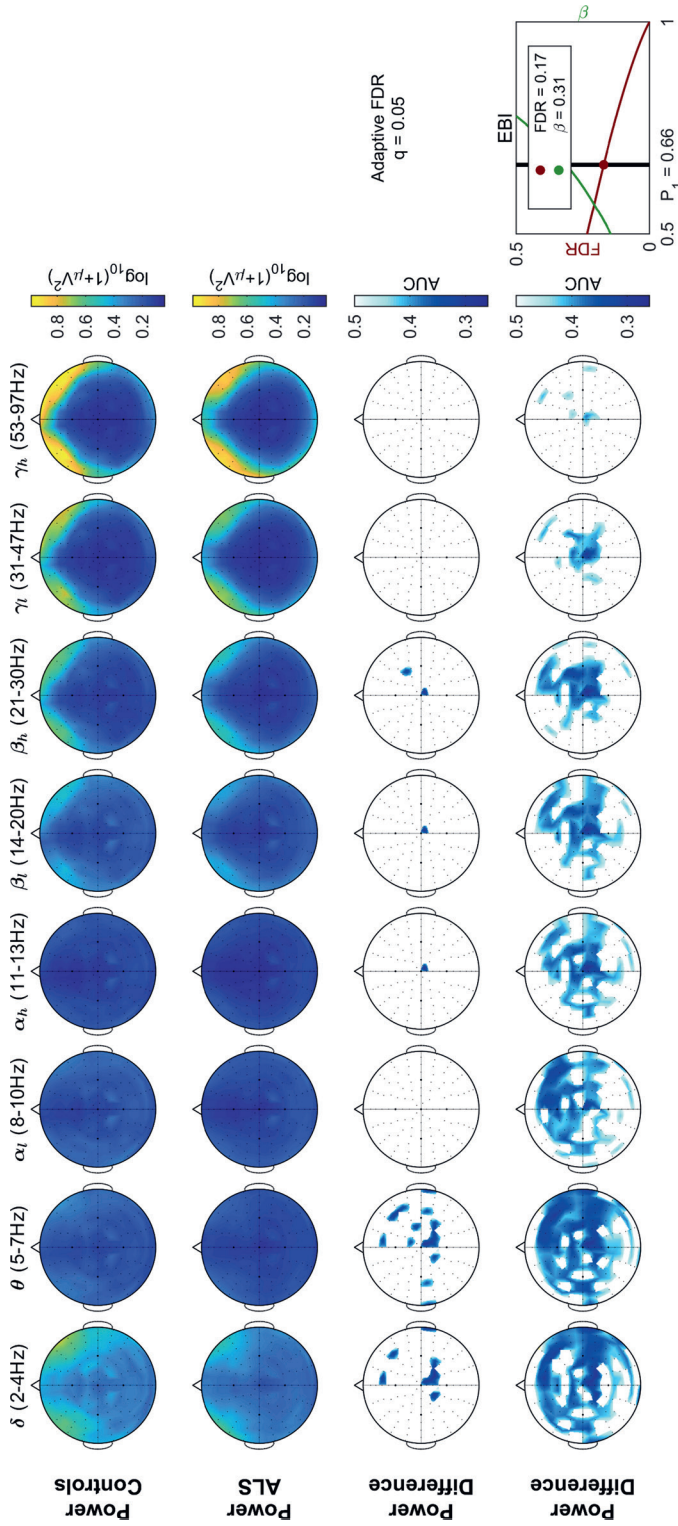
2

Formation of Bipolar Channels

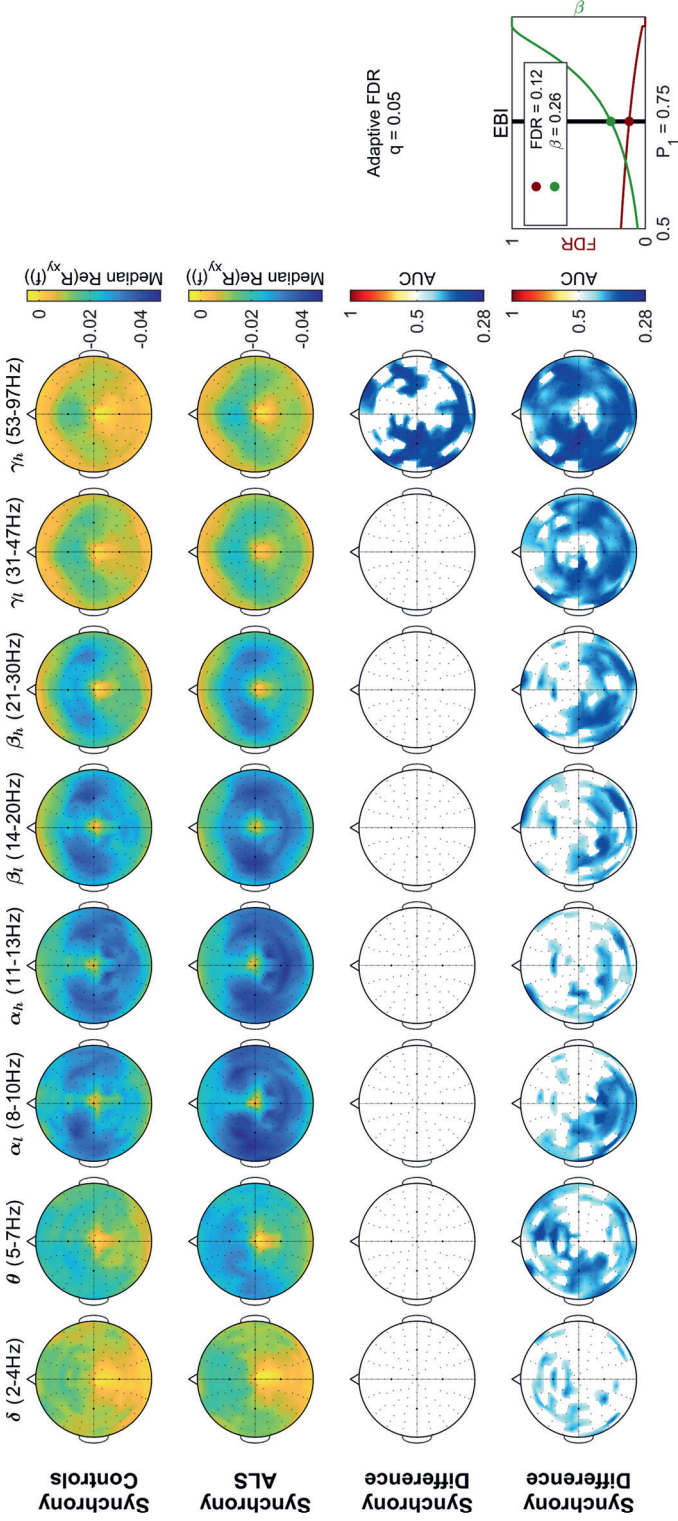
Supplementary Figure 1. Bipolar channels are formed from unipolar EEG recordings. Each arrow represents a bipolar channel, where the electrode at the tip is subtracted from the electrode at the end.



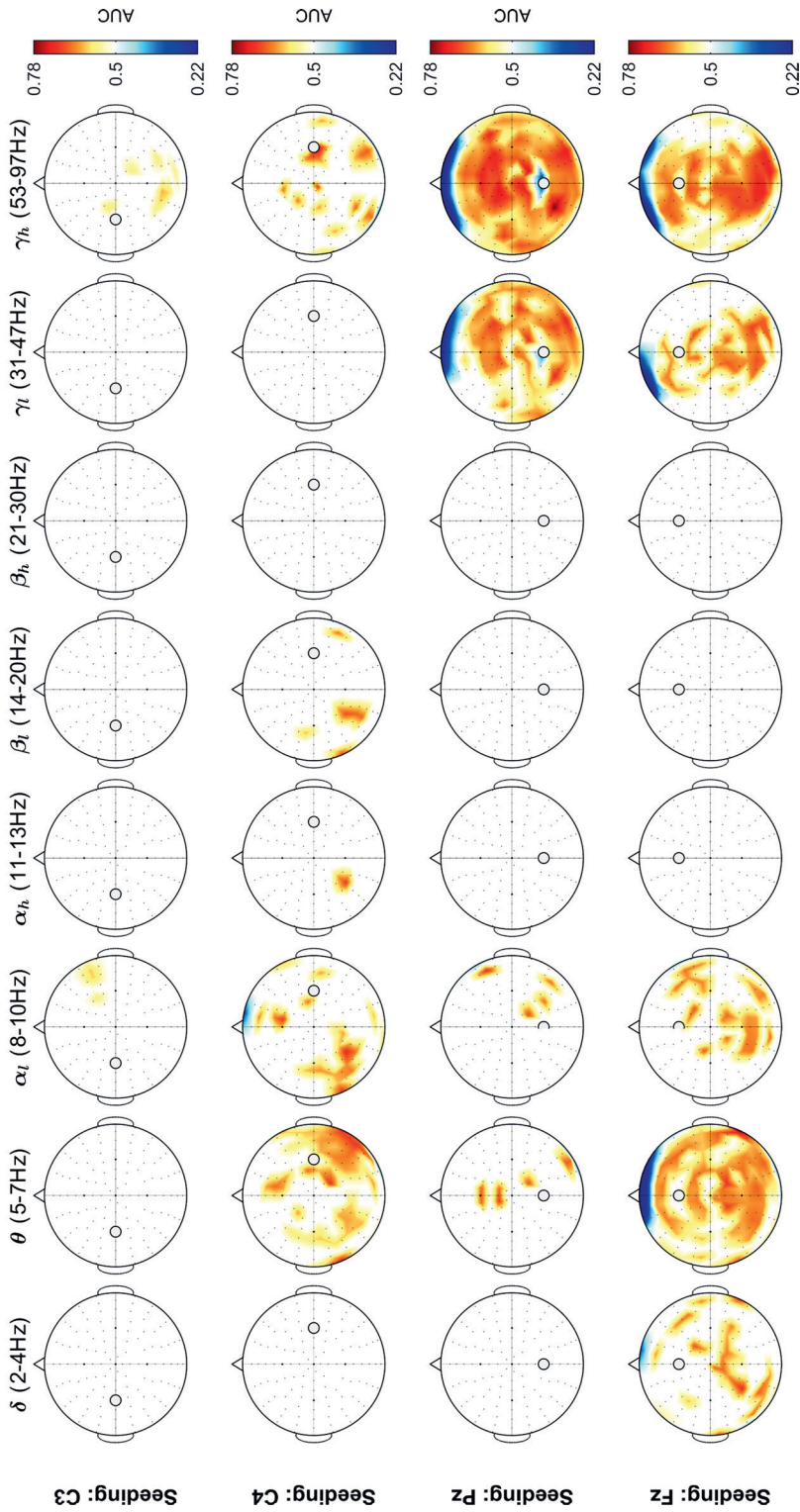
Supplementary Figure 2. Spectral EEG power is significantly decreased in ALS patients, especially in θ -band over the motor areas of scalp. Spectral power of bipolar EEG channels, $\log_{10}(1+\mu V^2)$, in healthy controls ($n = 34$), ALS patients ($n = 100$), and their statistically significant difference, as assessed by adaptive false discovery rate (aFDR) and Empirical Bayesian Inference (EBI). The estimated ratio of channels with between-group effects ($p_t = 0.42$), was used to find the corresponding threshold for the posterior probability of effect $P_t = 0.66$. This threshold yielded FDR of 0.17 and statistical power ($1-\beta$) of 0.69. AUC: Area under the receiver operating characteristics curve.



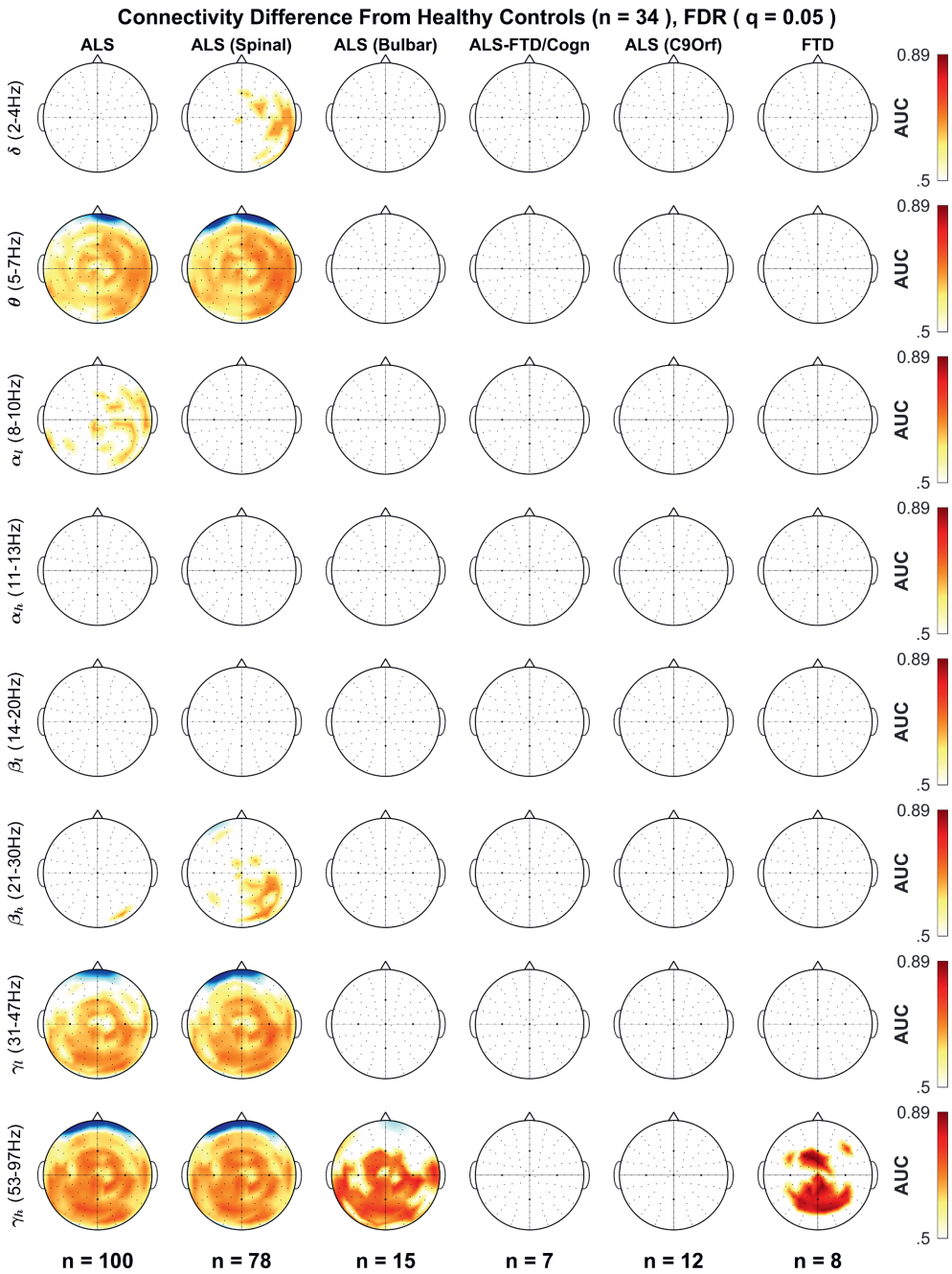
Supplementary Figure 2. Spectral EEG power is significantly decreased in ALS patients, especially in θ -band over the motor areas of scalp. Spectral power of bipolar EEG channels, $\log_{10}(1+\mu V^2)$, in healthy controls ($n = 34$), ALS patients ($n = 100$), and their statistically significant difference, as assessed by adaptive false discovery rate (aFDR) and Empirical Bayesian Inference (EBI). The estimated ratio of channels with between-group effects ($p_i = 0.42$), was used to find the corresponding threshold for the posterior probability of effect $P_i = 0.66$. This threshold yielded FDR of 0.17 and statistical power ($1-\beta$) of 0.69. AUC: Area under the receiver operating characteristics curve.



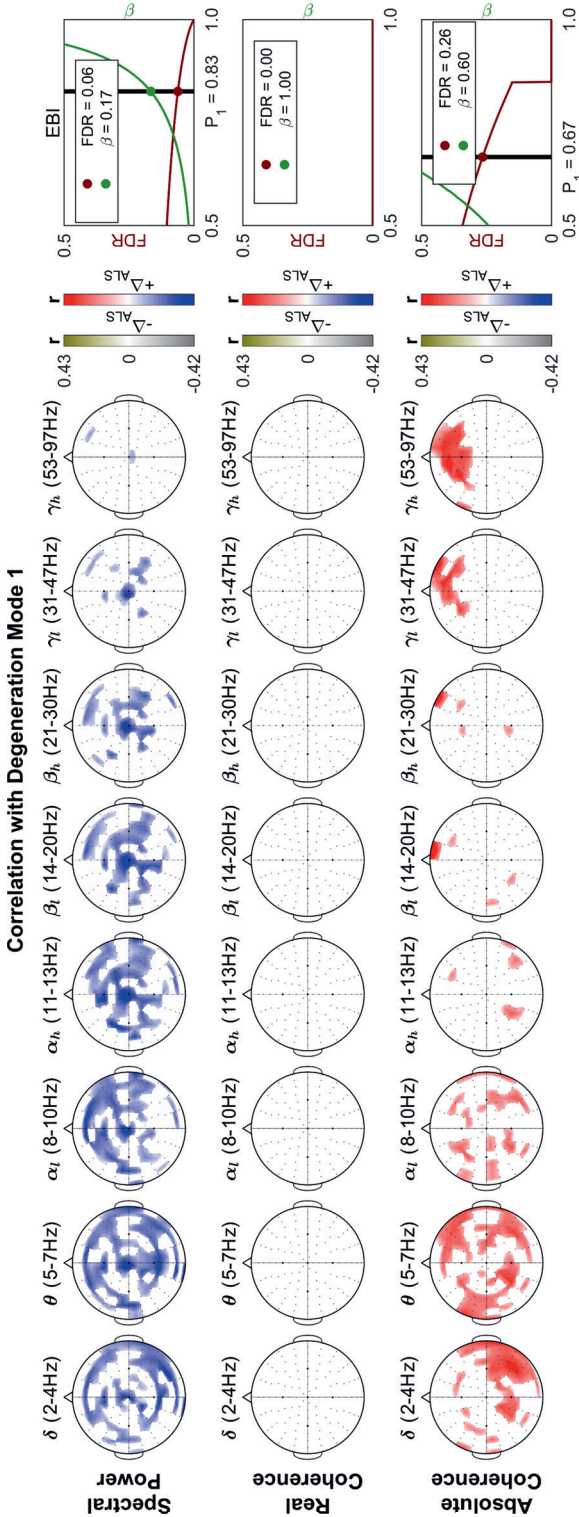
Supplementary Figure 4. Synchronous EEG oscillations are significantly changed in high γ -band above bilateral primary motor and parietal scalp areas in ALS patients. Median real coherence between bipolar EEG channels, in healthy controls ($n = 34$), ALS patients ($n = 100$), and their statistically significant difference, as assessed by adaptive false discovery rate (aFDR) and Empirical Bayesian Inference (EBI). The estimated ratio of channels with between-group effects ($p_1 = 0.54$), was used to find the corresponding threshold for the posterior probability of effect $P_1 = 0.75$. This threshold yielded FDR of 0.12 and statistical power $(1-\beta)$ of 0.74. AUC: Area under the receiver operating characteristics curve.



Supplementary Figure 5. Seeding from selected electrodes explains the 2 significant altered connectivity measure: the increased θ -band coherence has an inter-cortical pattern over scalp and the increased γ -band coherence is between the parietal-frontal regions of scalp. The seeding aimed to include parietal (Pz), frontal (Fz), and right motor (C₃) scalp areas and show the differences between healthy controls (n = 34) and ALS patients (n = 100) in coherence between bipolar EEG channels. Statistically significant differences with reference to healthy controls, as assessed by adaptive false discovery rate (aFDR) at $q = 0.1$.

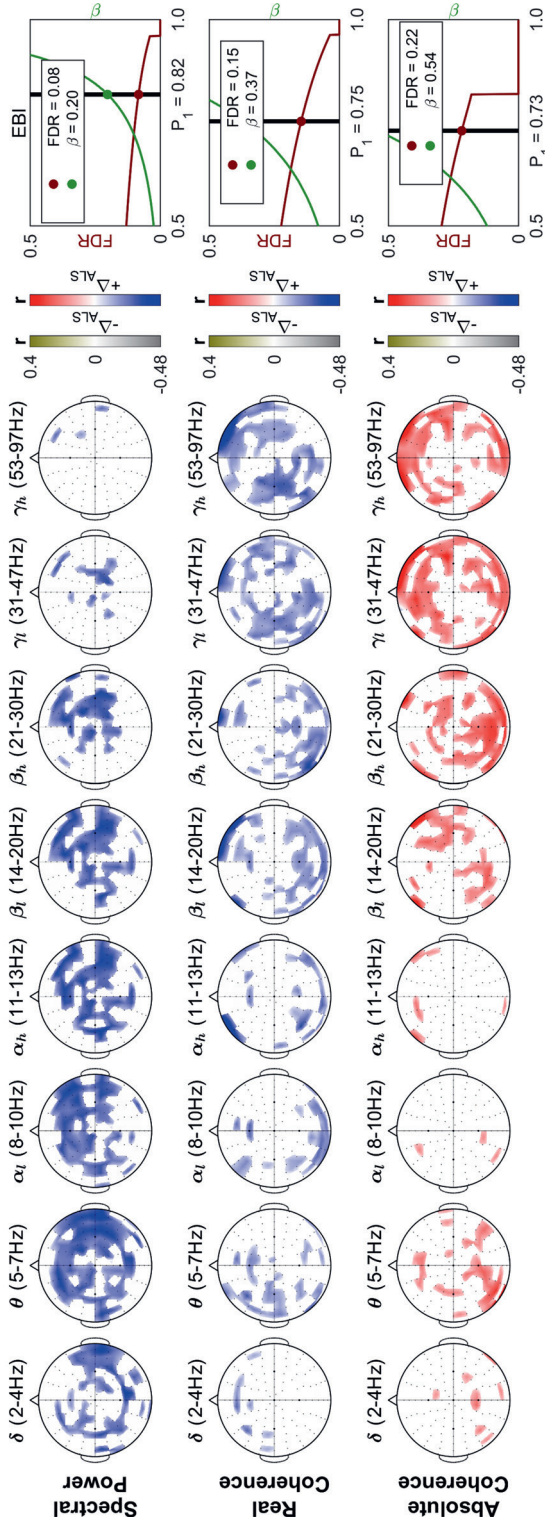


Supplementary Figure 6. High γ -band increase in average connectivity in ALS is also strongly present in FTD. The difference between healthy controls (n = 34) and ALS/FTD patient subgroups in median coherence between bipolar EEG channels. Statistically significant differences with reference to healthy controls, as assessed by adaptive false discovery rate (aFDR) at $q = 0.05$.

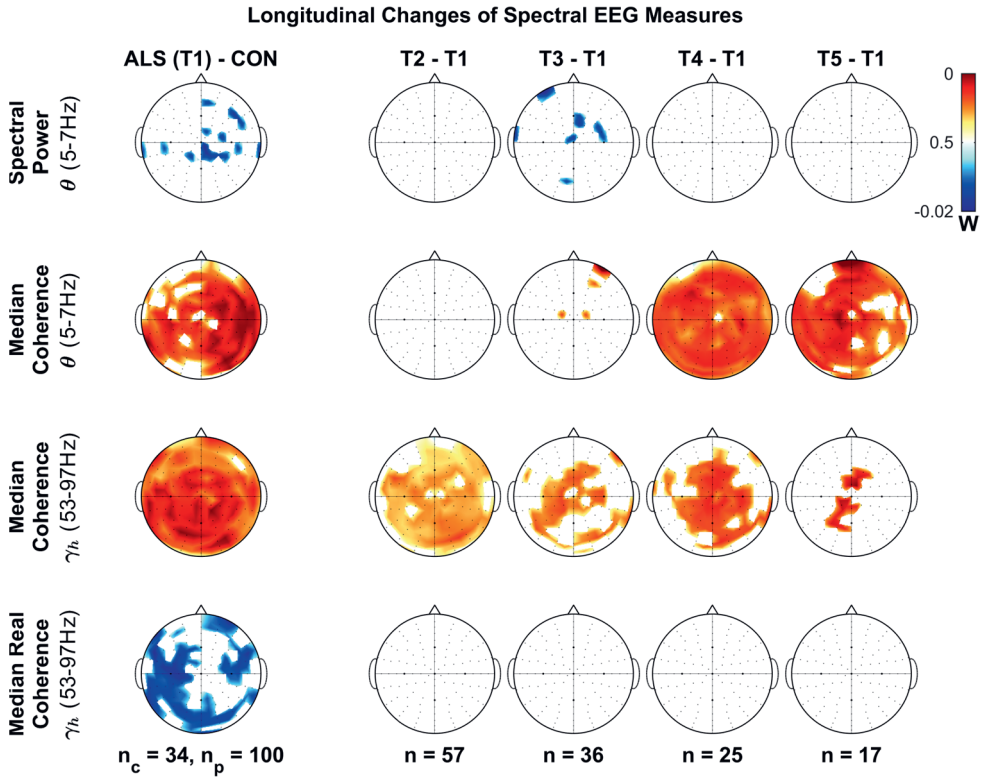


Supplementary Figure 7. The 1st MRI degeneration mode, widespread uniform degeneration, correlates with the increased connectivity (mainly in θ - and γ -bands), as well as the decrease in spectral power (maximal in θ -band). The correlation coefficient (r) between the scores of the 1st MRI degeneration mode (1-dimensional) and high-dimensional EEG measures in 59 ALS patients. The 125 channels \times 8 frequency bands \times 3 measures of power, connectivity (median absolute coherence) and synchrony (median real coherence) constitute 3000 EEG variables. The statistically significant correlations were found by Empirical Bayesian Inference (EBI) in each measure using the estimated ratio of channels with significant correlations as the threshold, with subsequent calculation of the posterior probability of effect (P), FDR, and statistical power ($1-\beta$). **Colours: The colour maps use grey/blue ($r < 0$) where higher structural degeneration corresponds to lower corresponding EEG values and olive/red ($r > 0$) where higher structural degeneration corresponds to higher corresponding EEG values. The blue-red colour-map is used where the direction of changes in EEG values due to degeneration (correlation direction) is in the same direction as ALS-specific changes ($+\Delta_{ALS}$), and the grey-olive colour-map is used where the direction of changes is in the opposite direction of ALS-specific changes ($-\Delta_{ALS}$). Only the significant values are shown.**

Correlation with Degeneration Mode 2

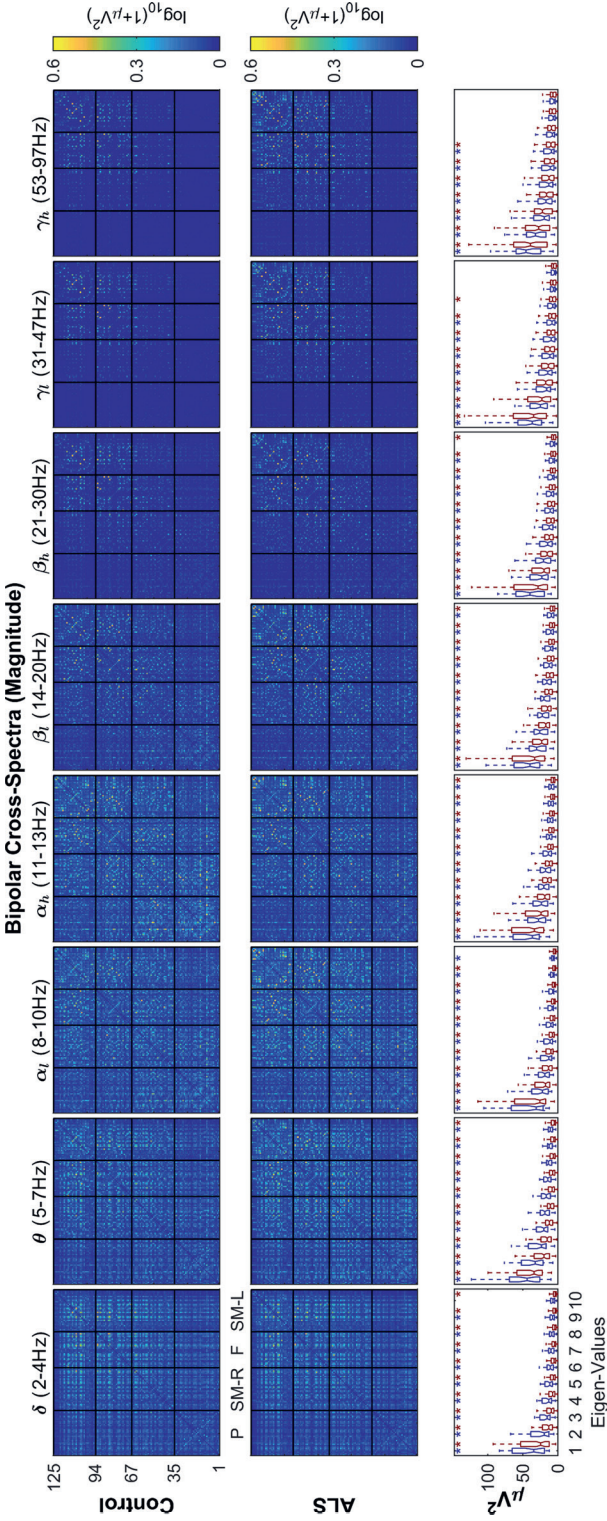


Supplementary Figure 8. The 2nd Degeneration Mode, differential white-grey matter motor-cortical degeneration (motor-specific decline in ALS), correlates with the decrease in spectral power (maximal in θ -band) and the decreased synchrony (maximal in γ -band over bilateral motor regions of scalp), as well as the increased connectivity (γ -band). See Supplementary Fig. 7 for details.

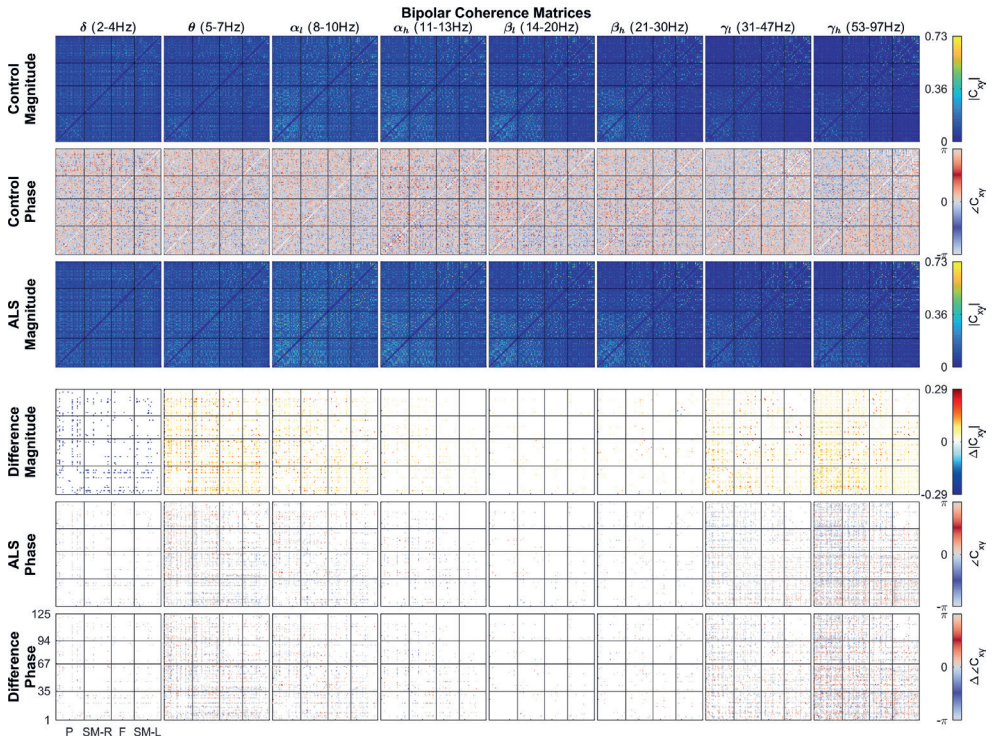


2

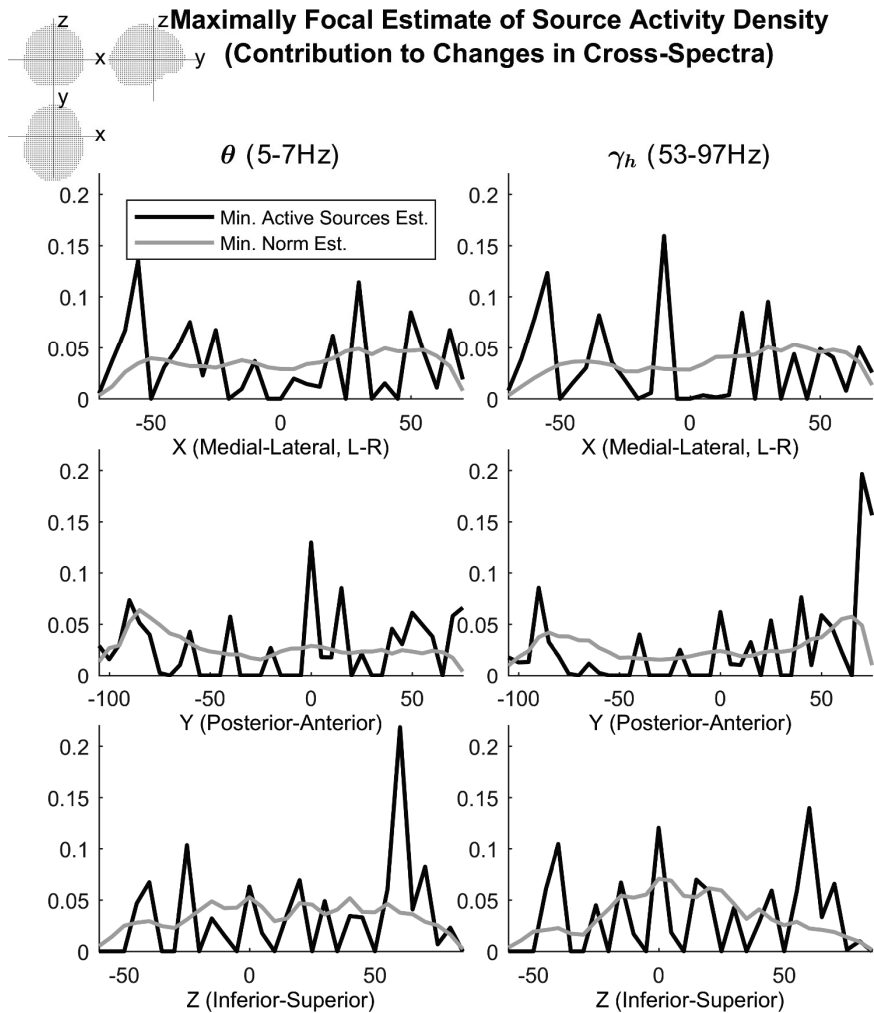
Supplementary Figure 9. The longitudinal spectral EEG power and connectivity measures continue to change in a 16-month follow-up, where the 2 average connectivity measures show maximum changes but at different rates. The topographic maps show the statistically significant pairwise differences of the 4 EEG measures (used in Fig. 3, 4 and 6) in follow-up sessions T2, T3, T4, and T5 against the first recording T1. The significance was inferred from the null-permutations in Empirical Bayesian Inference analysis of pairwise changes in individual electrodes in times T2-T5 versus T1 (n 's show the number of subjects in follow-up recording sessions). The significance threshold W is the normalised Wilcoxon's Signed Rank test-statistic where 1 shows maximum increase, 0, maximum decrease and 0.5 no change. The topographic maps for the ALS- CON differences (left column) are provided for comparison.



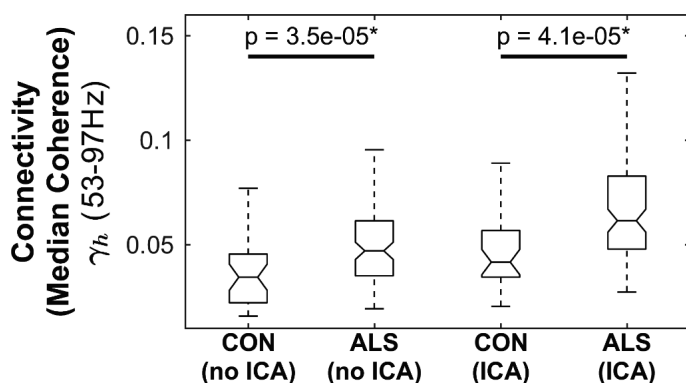
Supplementary Figure 10. The cross spectra matrices and their eigen-spectra show complex location- and frequency-dependent dynamics that is picked-up by the coherence analysis in controls and patients, which is unlikely to originate from spurious connectivity or nonglobal dynamic. The bipolar cross-spectral matrices for individual frequency bands (see Text) and their significant eigen-values (found using parallel-analysis at $q = 0.05$) show that there are 6 or more main components that constitute the complex network dynamics in each frequency band in both controls and patients.



Supplementary Figure 11. The coherence matrices show nonzero phase differences, unlikely to be due to field-spread of single focal (deep) sources or artefacts. The magnitude ($||$) and phase values (\angle) of the complex coherency matrices (C_{xy}) in individual frequency bands show location- and frequency-dependent patterns in controls, ALS patients and in their difference (Δ). A notable proportion of the high-coherence connections in the coherence matrix (row 1) have nonzero (different from 0 or $\pm\pi$) phase values in controls (row 2, highlighted by blue/red). The coherence values in ALS (row 3) include both similar and different patterns compared to controls. The significant effects in CON-ALS differences (highlighted in row 4, aFDR $q = 0.1$) similarly show nonzero phase values in ALS (row 5) and nonzero differences between controls and ALS patients (row 6). Notice especially the stronger effects in the θ - and γ_2 -bands, where the main connectivity changes were found (see Supplementary Fig. 3). This is unlikely to be due to field-spread of single focal (deep) source or artefactual components.



Supplementary Figure 12. The attempt to deliberately associate the observed average changes in the cross-spectra between CON-ALS to only a few focal active sources failed, yielding distributed sources across brain. The changes in the bipolar cross spectral matrices (which includes both power and coherence information) in the θ and γ_h frequency bands (where maximum ALS-related change was observed) were mapped to the brain sources ($n = 16,008$). The source activity density in 3 anatomical directions for changes in each frequency bands are shown. Notice that the mapping under the constraint of minimum active (nonzero) number of sources, failed to find limited focal activities. The commonly-used minimum-norm estimate (MNE) results are provided for comparison only.



Supplementary Figure 13. ICA-preprocessing does not affect the observed differences of connectivity between ALS and controls. The median γ_h -band connectivity (the measure most prone to high-frequency artefacts) is significantly higher in ALS versus controls with and without ICA-preprocessing; even though the ICA effect in general was to increase the connectivity (equally for both controls and patients).

2

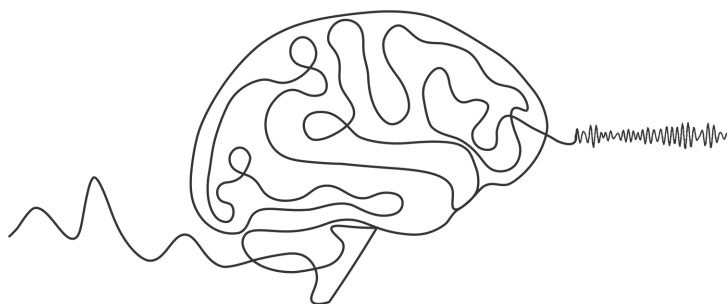
Supplementary Table 1. The discriminatory power of the EEG vs. MRI measures

MRI Measure	AUC \pm SD	EEG Measure	AUC \pm SD
GM-Motor-L	0.67 \pm 0.002	FA-CC	0.65 \pm 0.003
GM-Motor-R	0.68 \pm 0.002	FA-CC	0.67 \pm 0.0028
FA-TC-L	0.58 \pm 0.0023	FA-CC	0.73 \pm 0.0024
FA-TC-R	0.56 \pm 0.0023	FA-CC	0.72 \pm 0.0022
FA-SCR-L	0.67 \pm 0.002		
FA-SCR-R	0.63 \pm 0.0022		
FA-CST-L	0.72 \pm 0.0018		
FA-CST-R	0.73 \pm 0.0018		
FA-CC	0.66 \pm 0.002		

For MRI measures, the area under the curve (AUC) values for the receiver operating characteristic curve were found from MRI data of 59 ALS patients and 69 healthy controls. For EEG Measures, the AUC values were found from 100 ALS patients and 34 healthy controls.

References

1. Mohr, K. S., Nasseroleslami, B., Iyer, P. M., Hardiman, O. & Lalor, E. C. EyeBallGUI: A Tool for Visual Inspection and Binary Marking of Multi-channel Bio-signals. *bioRxiv* 129437 (2017).
2. Nolan, H., Whelan, R. & Reilly, R. B. FASTER: Fully Automated Statistical Thresholding for EEG artifact Rejection. *J Neurosci Methods* **192**, 152–62 (2010).
3. Dukic, S. *et al.* Estimation of coherence using the median is robust against EEG artefacts. in *Proceedings of the Annual International Conference of the IEEE Engineering in Medicine and Biology Society, EMBS* (2017).
4. Muthukumaraswamy, S. D. High-frequency brain activity and muscle artifacts in MEG/EEG: a review and recommendations. *Front Hum Neurosci* **7**, (2013).
5. Hjorth, B. Principles for transformation of scalp EEG from potential field into source distribution. *J Clin Neurophysiol* **8**, 391–396 (1991).
6. Halliday, D. M. *et al.* A framework for the analysis of mixed time series/point process data—theory and application to the study of physiological tremor, single motor unit discharges and electromyograms. *Prog Biophys Mol Biol* **64**, 237–278 (1995).
7. Pfurtscheller, G. & Lopes Da Silva, F. H. Event-related EEG/MEG synchronization and desynchronization: Basic principles. *Clinical Neurophysiology* **110**, 1842–1857 (1999).
8. Nasseroleslami, B., Lakany, H. & Conway, B. A. EEG signatures of arm isometric exertions in preparation, planning and execution. *Neuroimage* **90**, 1–14 (2014).
9. Iyer, P. M. *et al.* Functional Connectivity Changes in Resting-State EEG as Potential Biomarker for Amyotrophic Lateral Sclerosis. *PLoS One* **10**, e0128682 (2015).
10. Muthuraman, M. *et al.* EEG-MEG Integration Enhances the Characterization of Functional and Effective Connectivity in the Resting State Network. *PLoS One* **10**, (2015).
11. Efron, B. Size, power and false discovery rates. *The Annals of Statistics* **35**, 1351–77 (2007).
12. Fukunaga, K. *Introduction to statistical pattern recognition 2nd ed.* (Academic Press Professional, Inc., 1990).
13. Izenman, A. J. *Modern Multivariate Statistical Techniques.* (2008).
14. Smith, S. M. *et al.* Tract-based spatial statistics: voxelwise analysis of multi-subject diffusion data. *Neuroimage* **31**, 1487–1505 (2006).
15. Oishi, K. *et al.* Human brain white matter atlas: identification and assignment of common anatomical structures in superficial white matter. *Neuroimage* **43**, 447–457 (2008).
16. Destrieux, C., Fischl, B., Dale, A. & Halgren, E. Automatic parcellation of human cortical gyri and sulci using standard anatomical nomenclature. *Neuroimage* **53**, 1–15 (2010).
17. Schuster, C., Elamin, M., Hardiman, O. & Bede, P. The segmental diffusivity profile of amyotrophic lateral sclerosis associated white matter degeneration. *Eur J Neurol* **23**, 1361–1371 (2016).
18. Franklin, S. B., Gibson, D. J., Robertson, P. A., Pohlmann, J. T. & Fralish, J. S. Parallel Analysis: a method for determining significant principal components. *Journal of Vegetation Science* **6**, 99–106 (1995).
19. Holmes, C. J. *et al.* Enhancement of MR Images Using Registration for Signal Averaging. *J Comput Assist Tomogr* **22**, (1998).
20. Oostenveld, R., Fries, P., Maris, E. & Schoffelen, J.-M. FieldTrip: Open source software for advanced analysis of MEG, EEG, and invasive electrophysiological data. *Comput Intell Neurosci* **2011**, 156869 (2011).
21. Hipp, J. F. & Siegel, M. Dissociating neuronal gamma-band activity from cranial and ocular muscle activity in EEG. *Front Hum Neurosci* **7**, 338 (2013).
22. Makeig, S., Bell, A., Jung, T.-P. & Sejnowski, T. J. Independent Component Analysis of Electroencephalographic Data. in *Advances in Neural Information Processing Systems* vol. 8 (1995).
23. Héroult, J., Jutten, C. & Ans, B. Détection de grands primitives dans un message composite par une architecture de calcul neuromimétique en apprentissage non supervisé. *Actes du Xe colloque GRETSI* **2**, (1985).
24. Hyvärinen, A. Fast and robust fixed-point algorithms for independent component analysis. *IEEE Trans Neural Netw* **10**, 626–634 (1999).



Chapter 3

Patterned functional network disruption in amyotrophic lateral sclerosis

Stefan Dukic, Roisin McMackin, Teresa Buxo, Antonio Fasano, Rangariroyashe Chipika, Marta Pinto-Grau, Emmet Costello, Christina Schuster, Michaela Hammond, Mark Heverin, Amina Coffey, Michael Broderick, Parameswaran M. Iyer, Kieran Mohr, Brighid Gavin, Niall Pender, Peter Bede, Muthuraman Muthuraman, Edmund C. Lalor, Orla Hardiman[†], Bahman Nasserolelami[†]

[†] Joint senior authors



Abstract

Amyotrophic lateral sclerosis (ALS) is a progressive neurodegenerative disease primarily affecting motor function, with additional evidence of extensive non-motor involvement. Despite increasing recognition of the disease as a multi-system network disorder characterised by impaired connectivity, the precise neuroelectric characteristics of impaired cortical communication remain to be fully elucidated. Here, we characterise changes in functional connectivity using beamformer source analysis on resting-state electroencephalography recordings from 74 ALS patients and 47 age-matched healthy controls. Spatio-spectral characteristics of network changes in the ALS patient group were quantified by spectral power, amplitude envelope correlation (co-modulation) and imaginary coherence (synchrony). We show patterns of decreased spectral power in the occipital and temporal (δ - to β -band), lateral/orbitofrontal (δ - to θ -band) and sensorimotor (β -band) regions of the brain in patients with ALS. Furthermore, we show increased co-modulation of neural oscillations in the central and posterior (δ -, θ - and γ_1 -band) and frontal (δ - and γ_1 -band) regions, as well as decreased synchrony in the temporal and frontal (δ - to β -band) and sensorimotor (β -band) regions. Factorisation of these complex connectivity patterns reveals a distinct disruption of both motor and non-motor networks. The observed changes in connectivity correlated with structural MRI changes, functional motor scores and cognitive scores. Characteristic patterned changes of cortical function in ALS signify widespread disease-associated network disruption, pointing to extensive dysfunction of both motor and cognitive networks. These statistically-robust findings, that correlate with clinical scores, provide a strong rationale for further development as biomarkers of network disruption for future clinical trials.

Introduction

Amyotrophic lateral sclerosis (ALS) is a neurodegenerative disease of upper and lower motor neurons resulting in progressive loss of bulbar and limb function.¹ Although originally considered a disease exclusively of the motor system,² widespread non-motor³ and subcortical⁴ structural changes are now recognised.⁵ Clinical and neuroimaging evidence confirms extensive involvement of motor⁵⁻⁷ and cognitive^{8,9} pathways and networks. These network impairments manifest as measurable changes in cortical connectivity, informing altered dynamics within different networks, which may lead to widespread changes in neural signalling beyond the regions of direct disease pathology.

Functional magnetic resonance imaging (fMRI) studies have identified increased connectivity in the sensorimotor networks of ALS patients^{5,10} based on BOLD (blood oxygen-level dependent) signal. However, network impairment can also be interrogated using neuroelectric signals captured with electroencephalography (EEG). These signals appear in varying frequency bands and can differ substantially across networks.¹¹ This variability is due to the complex hierarchical organisation of projections between different granular layers forming connections between different areas,^{12,13} which oscillate at either lower or higher frequencies.¹⁴ These spectral signatures of connectivity require high temporal resolution and cannot be captured by fMRI.^{15,16}

Previous EEG studies have shown altered patterns, such as increased frontal-to-parietal connectivity in ALS.^{6,8,17} To date however, there have been limited attempts to localise abnormal EEG patterns to specific brain regions. A recent magnetoencephalography study in ALS has focussed on slow/broadband fMRI-like activity, and has demonstrated widespread changes within the posterior brain regions.¹⁸ However, because network interactions are often marked by narrow band cortical oscillations,¹⁹ it has not been possible to address the spectral aspects of ALS-specific changes in brain networks using broadband signals. Moreover, although source-space studies that use frequency-specific analysis have also been performed in ALS,^{20,21} the phase- and amplitude-based connectivity profiles of specific brain networks affected by ALS remain to be established.

The majority of the commonly used EEG connectivity measures falls into two categories: amplitude-based and phase-based indices. Within a given frequency-band, these two different groups of measures reflect two conceptually different aspects of the cortical communication. Amplitude-based measures are predominantly used to quantify co-modulation of the oscillatory activity in distinct brain areas at infra-slow rates (<0.1 Hz), which are shown to resemble slow co-modulations observed in resting-state fMRI.^{22,23} These fluctuations seem to emerge from the regulation and coordination of the network activity for an (upcoming) functionally distinct task in the brain at larger temporal and spatial scales; therefore, reflecting the functional organisation of the brain networks.^{11,24,25} Phase-based coupling likely informs on facilitation and regulation of communication between distinct brain areas on faster timescales.^{11,26} In principle, these two measures are independent of one another.²⁷ For instance, the activity in two brain regions can strongly co-vary, albeit their phase values being randomly

distributed. These two types of measures and their corresponding underlying mechanisms seem to interact and work together; with the amplitude-based coupling indicating the priming of the activation of brain areas needed for an upcoming task, and the phase-based coupling indicating the instantaneous synchronous influences in the networks.²⁶ Nevertheless, exploring brain dynamics exclusively using either amplitude- or phase-based connectivity measure provides limited insights into the underlying functional changes and ALS pathophysiology in general.

To date, evidence of correlation between the brain network impairments in ALS observed from neuroelectric signals and clinical scores of motor and cognitive function has been limited. In addition to this, the observed changes have not discriminated between the traditionally-defined clinical ALS subgroups (e.g. bulbar- versus spinal-onset ALS or ALS with presence or absence of the pathologic hexanucleotide expansion in *C9orf72*).^{6,28}

Here, we have reconstructed resting-state brain activity and performed functional connectivity analysis using both amplitude- and phase-based measures in a large group of ALS patients and healthy controls. Our findings correlate with clinical measures, providing robust evidence that measurement of functional connectivity can be used as a complementary investigative tool to interrogate ALS-associated changes in brain networks.

Methods

Ethical approval

Approval was obtained from the ethics committee of Beaumont Hospital, Dublin, Ireland (REC reference: 13/102) and the Tallaght Hospital / St. James's Hospital Joint Research Ethics Committee (REC) (REC reference: 2014 Chairman's Action 7, CRFSJ 0046) for St James's Hospital, Dublin, Ireland. The experimental procedure conformed to the Declaration of Helsinki. All participants provided written informed consent before taking part in the experiments.

Participants

Patient recruitment

Patients with ALS were recruited from the National ALS clinic in Beaumont Hospital Dublin. Healthy controls were recruited from an existing control cohort of a neuropsychology study in ALS.²⁹

Inclusion criteria

All ALS patients were within the first 18 months of their diagnosis and fulfilled the revised El Escorial diagnostic criteria for Possible, Probable or Definite ALS.³⁰

Exclusion criteria

Patients diagnosed with primary lateral sclerosis, progressive muscular atrophy, flail arm/leg syndromes, prior transient ischemic attacks, multiple sclerosis, stroke, epilepsy, seizure disorder, brain tumours, structural brain abnormalities, other neurodegenerative conditions and other medical morbidities, such as human immunodeficiency virus, were excluded.

The demographic profile of patients and controls

A total of 56 ALS patients with spinal onset (m/f: 41/15; mean age: 57.9 ± 12.2 years), 15 patients with bulbar onset (m/f: 10/5; age: 59.0 ± 8.4 years) and three patients with respiratory onset (m/f: 2/1; age: 62.0 ± 5.3 years) were recruited, along with 47 healthy controls (m/f: 15/32; age: 58.4 ± 12.3) (see Table 1). Patients and controls were matched for age (Mann-Whitney U-test, $p = 0.87$). The post-hoc 2-way ANOVA analysis of gender-imbalance (Chi-Square test, $p < 0.001$) showed no significant interaction effects on the main findings (Supplementary Fig. 1).

Genetic profile

Seven (m/f: 4/3; age: 61.0 ± 7.4) of 73 genetically tested patients had the hexanucleotide repeat expansion in *C9orf72* (see Table 1).

Experiment

Experimental paradigm

The experiment was resting-state with eyes open, divided into three 2-minute recording blocks, allowing for rest between blocks. Subjects were seated in a comfortable chair, asked to relax and let their mind wander, while they fixate their gaze at the letter X (6 cm × 8 cm) printed on an A4 sheet of paper placed approximately 1 m in front of them.

EEG acquisition

EEG data with 128 channels were collected using the BioSemi® Active Two system (BioSemi B.V., Amsterdam, The Netherlands) and sampled at 512 Hz after a low-pass anti-aliasing filter (0–104 Hz) which was applied by the acquisition hardware. Recordings were conducted in dedicated laboratories in the University of Dublin and St. James's Hospital, Dublin.

MRI data

Magnetic resonance data were available for 37 ALS patients.³¹ Structural T1-weighted MRI data were acquired on a 3 Tesla Philips Achieva system with a gradient strength of 80 mT/m and slew rate of 200 T/m/s using an 8-channel receive-only head coil. They were obtained using a three-dimensional inversion recovery prepared spoiled gradient recalled echo (IR-SPGR) sequence with Field-of-view = $256 \times 256 \times 160$ mm, spatial resolution = 1 mm^3 .^{31,32} MRI scans were individually screened for the presence

of vascular alterations on FLAIR and DWI sequences and patients with co-morbid vascular white matter lesions were not included.³³

Table 1. Breakdown of demographics.

Group	N	Male	Female	Age (years) [†]	Disease duration (days) [†]	EEG delay (days) [†]	ALSFRS-R [†]
Controls	47	15 [‡]	32 [‡]	58.4±12.3			
ALS							
ALL	74	53 [‡]	21 [‡]	58.3±11.3	694±623	221±327	37.5±6.5 (n = 61)
Spinal	56	41	15	57.9±12.2	736±688	239±370	37.4±6.2 (n = 47)
Bulbar	15	10	5	59.0±8.4	497±225	185±100	38.5±8.4 (n = 11)
Thoracic	3	2	1	62.0±5.3	890±617	79±46	35.0±5.6 (n = 3)
<i>C9orf72</i> ⁺	7	4	3	61.0±7.4	908±917	385±408	34.8±9.5 (n = 6)
<i>C9orf72</i> ⁻	66	49	17	58.4±11.2	673±593	204±318	37.8±6.3 (n = 54)

[†] Numbers show mean ± standard deviation

[‡] Effects of gender imbalance were found insignificant

· Disease duration is the time interval between the estimated symptom onset and the EEG recording

· EEG Delay is the time interval between the date of diagnosis and the EEG recording

· ALSFRS-R = Amyotrophic lateral sclerosis functional rating scale revised

· *C9orf72*[±] = Presence/Absence of the repeat expansion in the chromosome 9 open reading frame 72

Disease severity and neuropsychology data

The ALS functional rating scale revised (ALSFRS-R) scores³⁴ from 61 patients, and contemporaneous scores from a standardised neuropsychological battery^{35,36} from 34 patients were obtained for clinico-neurophysiological correlations. The scores from the neuropsychological battery were standardised into z-scores, adjusting for age and education from a sample of 100 healthy controls.

Data analysis

EEG data preprocessing

An automatic artefact rejection method³⁷ based on statistical thresholding was used to discard data contaminated by noise (Controls: mean 10%, range 2-19%; ALS: mean 11%, range 4-24%). After visual inspection, channels with higher levels of noise (Controls: mean 2, range 0-7; ALS: mean 3.8, range 0-10) were removed and then

interpolated from the rest of the electrodes using spherical spline interpolation.³⁸ Data were band-pass (1-97 Hz) and notch (50 Hz) filtered, and referenced to common average.

EEG source localisation

EEG data were source-reconstructed using the linearly constrained minimum variance (LCMV) beamformer³⁹ to obtain time-varying signals originating from the brain. An atlas-based approach was applied to estimate signals from 90 brain regions. The included regions of interest (ROI) were from the automated anatomical labelling (AAL) atlas,⁴⁰ excluding the cerebellum and including the subcortical regions (see Supplementary Fig. 2).

Estimating spectral power

For each ROI, spectral power was calculated using the auto-spectrum:

$$S_x = |FT\{x(t)\}|^2$$

where $x(t)$ is a time-domain signal corresponding to brain region and $FT\{\cdot\}$ is a Fourier transformation. Spectral power was estimated in six frequency bands, as the sum of the auto-spectrum values within each frequency band.

Estimating functional connectivity

For each pair of ROI, functional connectivity was calculated from two different perspectives to inform on different aspects of connectivity between brain regions.

An amplitude-based measure, the ‘amplitude envelope correlation’ (AEC),²³ measures the correlation between the power envelopes of two oscillatory time-series. It reflects the simultaneous presence and co-modulation of the intensity of the oscillatory activity in two regions. The phase synchrony of the oscillations in the two ROI is not reflected in AEC. This amplitude-based measure was chosen because of its capability to mirror the functional networks obtained in fMRI studies.⁴¹

A phase-based measure, the ‘imaginary coherence’ (iCoh),⁴² captures the extent to which two signals have a constant relative non-zero phase. This measure reflects the neuronal communication between the brain regions that contribute to synchronous neural oscillations, even though the intensity of the activities in the two ROI may behave differently.

Estimating the functional connectivity in source-space requires caution, since signals beamformed at spatially separate cortical locations are not necessarily independent.⁴³ This signal leakage can lead to spurious zero-lagged connectivity between reconstructed signals.⁴⁴ Hence, removing instantaneous relationships between pairs of projected signals would mitigate the problem, albeit at the expense of removing true instantaneous interactions between them. The implementation of the connectivity measures in this study corrects for this zero-lag leakage.

Amplitude envelope correlation

To mitigate the problem of spurious connectivity caused by source localisation methods, we performed time-domain orthogonalisation of the reconstructed time-series⁴⁵ between each pair of the ROI before estimating the power envelopes, as following:

$$p_x = |HT\{x(t)\}|$$

$$p_y = |HT\{y(t)\}|$$

where $x(t)$ and $y(t)$ are time-domain signals representing two brain regions and filtered to a specific frequency band, and $HT\{\cdot\}$ is a Hilbert transformation. Estimated power envelopes were then down-sampled to 0.5 Hz. As a measure of association, an absolute value of Pearson's correlation was used on the entire log-transformed power time-series, as following:

$$AEC = |corr(\log(p_x), \log(p_y))|$$

Imaginary coherence

Unlike AEC, iCoh is not affected by the limitation of source localisation methods.⁴⁴ It is defined as following:

$$iCoh(f) = |\mathcal{I}m\{S_{xy}(f)\}| / \sqrt{S_x(f)S_y(f)}$$

where $\mathcal{I}m\{S_{xy}\}$ denotes the imaginary part of cross-spectral density between the signal $x(t)$ and $y(t)$, whereas S_x and S_y are the auto-spectral densities calculated for those signals. Imaginary coherence was estimated from 2 s long epochs.

These two measures were calculated for all possible pairs of estimated ROI signals, resulting in two symmetric 90×90 connectivity matrices for each subject. This was carried out for six separate frequency bands: δ (2-4 Hz), θ (5-7 Hz), α (8-13 Hz), β (14-30 Hz) and γ (γ_l : 31-47 Hz, γ_h : 53-97 Hz). Frequencies of 48-52 Hz were excluded from the analysis due to the potential power-line noise. This resulted in 12 connectivity matrices per subject which are referred to as 'Point-to-point connectivity'. These matrices can be seen as weighted network matrices with elements representing link weights between network nodes. Additionally, each matrix was averaged using algebraic mean across ROI to estimate the average connectivity of each brain region. This resulted in one value per ROI, representing mean node strength (average link weight), from each connectivity matrix.

Connectivity modules

To extract and compare the connectivity modules/networks affected in ALS, we used non-negative matrix factorisation (NMF).⁴⁶ This method factorises a given matrix V , such that $V_{n \times m} \approx W_{n \times k} \cdot H_{k \times m}$, where matrices W (weight vectors) and H (basis vectors) are non-negative and n , k and m denote the number of subjects, number of basis vectors and number of all possible brain connections, respectively. The non-negativity

constraint makes the NMF purely additive and therefore, suitable for the decomposition of complex connectivity patterns ($V_{n \times m}$) into k basis vectors (that is, connectivity modules or networks) represented as a positive connectivity matrix ($H_{k \times m}$). Additionally, weight matrix ($W_{n \times k}$) informs us of the level of activation of each network per subject.

Factorisation of concatenated connectivity data from both healthy controls and ALS patients was used to reveal latent discriminant networks that are altered in ALS. To identify the networks that are affected in ALS, we applied NMF on all point-to-point connections that reached significant difference (Mann-Whitney U-test, $p < 0.05$) between healthy controls and ALS patients. Factorisation was applied on a data matrix containing an equal number ($n = 47$) of healthy controls and ALS patients (selected at random) to avoid any bias towards one of the groups. The random sampling of ALS patients was repeated 250 times and the matrices W and H were averaged over the outcomes. At each run, to avoid the local minimum problem during the numerical solutions, multiple random starting values ($n = 100$) for W and H matrices were used. The number of modules to be extracted from the connectivity matrices was determined as the value that minimised the Bayesian information criterion.⁴⁷

Correlates of EEG with MRI, neuropsychology and disease severity

We correlated the signal analysis findings with the structural MRI data, motor disease severity (ALSFRS-R) and cognitive scores derived from a neuropsychological battery.

MRI studies have consistently shown motor and extra-motor grey matter atrophy^{48,49} and correlation between motor system pathology with ALSFRS-R.^{3,50-52} Consequently, we first sought to correlate the alterations in connectivity within motor and frontal networks (algebraic mean of the network connectivity matrix) with the cortical volume of those networks; where both motor and frontal networks are represented by several ROI (see section 'Network definitions for correlation analysis' in the Supplementary material).

Subsequently, the algebraic mean of the motor network connectivity matrix was correlated with the ALSFRS-R scores. In addition, the scores from the neuropsychological battery were correlated with the alterations in frontoparietal and frontotemporal networks as captured by the weights corresponding to these networks from the NMF analysis. More specifically, we used the composite of summed executive function scores for the correlation with the alterations in frontoparietal network, and the composite of summed language function scores for the correlation with the alterations in frontotemporal network. The executive composite score included the following tests: Verbal fluency,⁵³ Backward Digit span,⁵³ D-KEFS Sorting Test,⁵⁴ D-KEFS Colour-Word Interference Test,⁵⁴ Reading the Mind in the Eyes⁵⁵ and Conflicting Emotional Prosody from the Florida Affect Battery.⁵⁶ The language composite score included: the PALPA (Auditory Lexical Decision, Visual Lexical Decision, Word Spelling, Word Reading, and Auditory Sentence-Picture Matching and Written Sentence-Picture Matching subtests)⁵⁷ and the Boston Naming test.⁵⁸

In all cases, except in correlations with cognitive scores, the Spearman's partial correlation was used to test the presence of the hypotheses, and at the same time to correct for the age of patients. In the case of correlations with cognitive scores, the Spearman's correlation was used, since the cognitive scores were z-scored, already accounting for age.

Statistical analysis

Statistical analysis of high-dimensional measures suffers from high rates of false positive findings, which necessitates the use of advanced statistics to mitigate the problem. To determine the statistical significance of the observed differences in each of the three high-dimensional measures (spectral power, AEC and iCoh), we used frequentist statistics together with an implementation of the Empirical Bayesian inference (EBI)^{59,60} suited to neuroelectric signal analysis.⁶¹ EBI provides major benefits, such as reliable estimation of FDR, calculation of statistical power and the posterior Bayesian probability, which are not afforded by alternative methods.

We used the area under the curve (AUC) of the receiver operating characteristics curve to make the between-group comparisons.⁶² To further infer statistical significance in a high-dimensional space, EBI is applied on the test statistics (i.e. AUC), which exploits both the original (non-null) observations and null-permuted data to estimate the probability density function of the data and null, respectively. We then estimated the posterior probability (P_1) and the statistical power ($1-\beta$). The statistical analysis was performed separately for each of the three measures and for each frequency band in the case of point-to-point connectivity, while in the case of spectral power and average connectivity the analysis was done on the concatenated data across frequencies. False discovery rate (FDR) was set to 10%. This selection was based on careful inspection of curves that explain the relationship between FDR and power (or between Type I and Type II errors) as a function of thresholds.⁶¹

To assess the statistical significance and statistical power of the connectivity modules from the NMF analysis and the correlations between EEG connectivity and other measures, a null and non-null bootstrapping resampling ($n = 10000$) approach was applied.^{6,61} In the former case, the resampling was applied on the NMF weights, whereas in the latter case, it was applied on the data used in the correlation analysis. Here, to control for multiple comparisons, rejection of null hypothesis was additionally checked using adaptive FDR (aFDR)⁶³ set to 5%.

In the analysis of ALS subgroups 2-way ANOVA was applied on all three EEG measures (spectral power, AEC and iCoh) in two frequency bands that showed the most prominent changes in ALS patients compared to healthy controls. The analysis was performed on each measure and frequency band separately, with the *C9orf72* status (presence/absence of the gene mutation) and the site of symptom onset (bulbar/spinal) chosen as independent variables. Data used were averaged from selected brain regions that had the highest discriminatory power between healthy controls and ALS patients in each measure and frequency band separately. Prior to the ANOVA analysis, data were transformed to standard normal distributions using the inverse normal transformation.^{60,64}

The analyses were carried out in MATLAB (v2018a Mathworks Inc., Natick, MA, USA) using the FieldTrip toolbox,⁶⁵ EBI toolbox,⁶¹ and custom written scripts.

Results

Spectral power revealed similar decrease across low- and mid-frequency bands

Spectral power in ALS was significantly decreased and widespread from δ - to β -band (Fig. 1). The most notable changes were found in the occipital and temporal (from δ - to β -band), lateral/orbitofrontal (δ - and θ -band) and sensorimotor (β -band) regions.

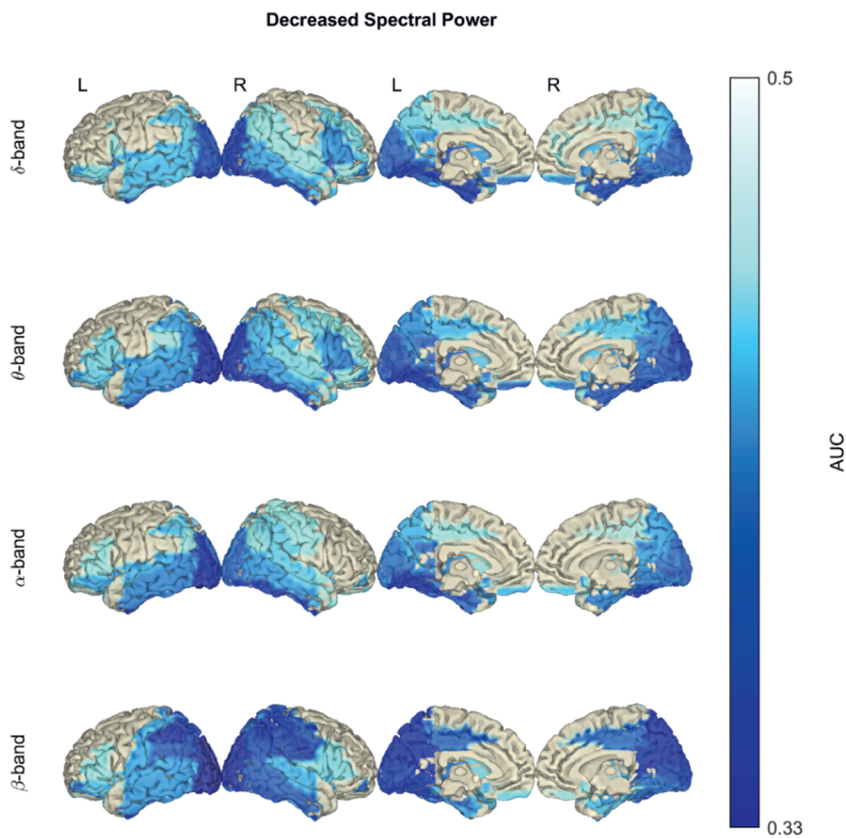


Figure 1. In ALS, spectral power is significantly decreased between δ and β frequency bands. Notice the dominant decrease in the posterior and temporal regions. Statistical difference between healthy controls ($n = 47$) and ALS patients ($n = 74$) was assessed in the six defined frequency bands using EBI. FDR was set to 10%, yielding an estimated statistical power of $1 - \beta = 0.82$ and posterior probability of $P_1 = 0.64$ (across all frequency bands). AUC: Area under the receiver operating characteristic curve. No changes were detected in the γ frequency bands; therefore, they are not shown. Frequency bands: δ (2-4 Hz), θ (5-7 Hz), α (8-13 Hz) and β (14-30 Hz).

Average connectivity reflects frequency-dependent changes in co-modulation and synchrony

Changes in the amplitude envelope correlation revealed increased co-modulation at δ , θ & γ_1 bands

ALS patients showed a significant and widespread increase in AEC connectivity compared to healthy controls (Fig. 2), with most notable changes in the central and posterior (δ -, θ - and γ_1 -band), and frontal (δ - and γ_1 -band) regions.

Changes in imaginary coherence revealed decreased synchrony at δ & β -bands

ALS patients showed significant decrease in iCoh connectivity across multiple frequency bands compared with healthy controls (Fig. 3). The changes were observed in temporal and frontal lobes from δ - to β -band, while in β -band the decreased connectivity was additionally observed in the sensorimotor cortex. For an overview of results from the statistical analysis of spectral power, and average co-modulation and synchrony, see Supplementary Fig. 3.

Changes in point-to-point connectivity patterns are widespread

Significant widespread increase in the point-to-point co-modulation of the neural activity was found in ALS patients compared with healthy controls in θ - and γ_1 -band (Fig. 4, upper). The θ -band co-modulation was observed within the regions encompassing the central, parietal and occipital lobe, as well as between these regions and the remainder of the brain; whereas the γ_1 -band co-modulation was present in the whole brain, but to a lesser extent within the frontal, between frontal and subcortical, and within and between temporal and subcortical regions.

Conversely, we detected significant decreases in the point-to-point synchrony in ALS patients compared with healthy controls in δ - and β -band (Fig. 4, lower). As it was the case for co-modulation, the changes in synchrony were widespread – the δ -band synchrony was decreased within the frontal regions, between the frontal and the occipital, temporal and subcortical regions, as well as between and within the temporal and subcortical regions; the β -band synchrony was primarily decreased between and within the central and parietal regions and the rest of the brain (except the frontal region), and to a lesser extent within the occipital and subcortical regions.

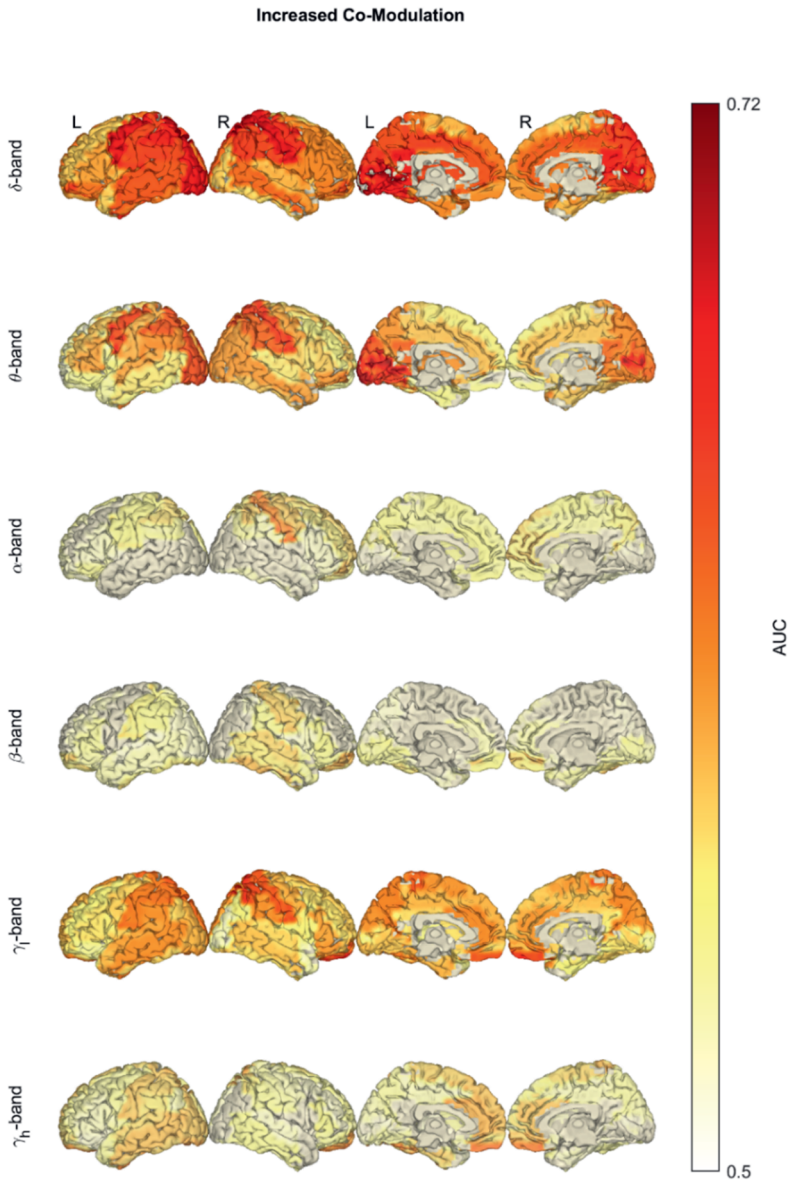


Figure 2. In ALS, the average co-modulation is significantly increased in the δ , θ & γ frequency bands. Notice the increase of amplitude envelope correlation (AEC) in the central and posterior regions (δ -, θ - and γ_1 -band) and frontal regions (δ - and γ_1 -band). Statistical difference between healthy controls ($n = 47$) and ALS patients ($n = 74$) was assessed in the six defined frequency bands using EBI. FDR was set to 10%, yielding an estimated statistical power of $1 - \beta = 0.93$ and posterior probability of $P_i = 0.71$ (across all frequency bands). AUC: Area under the receiver operating characteristic curve. Frequency bands: δ (2-4 Hz), θ (5-7 Hz), α (8-13 Hz), β (14-30 Hz) and γ (γ_1 : 31-47 Hz, γ_h : 53-97 Hz).

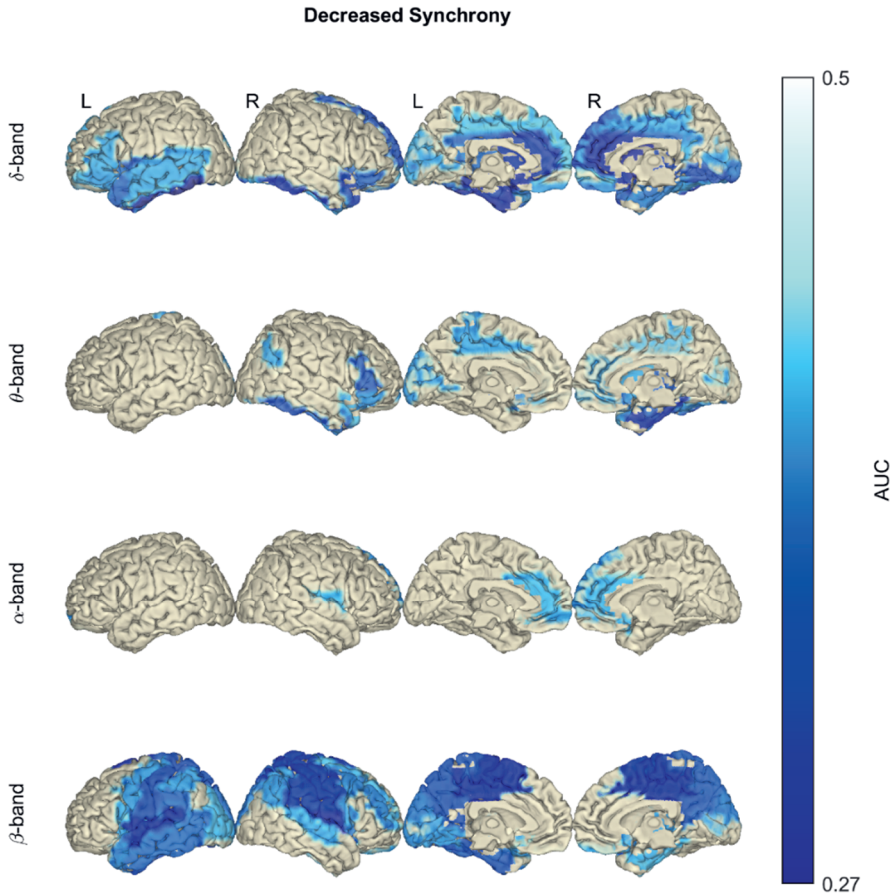


Figure 3. In ALS, the average synchrony is significantly decreased in the δ & β frequency bands. Notice the decrease of imaginary coherence (iCoh) in temporal and frontal lobes (δ -, θ - and α -band), and in the sensorimotor cortex (β -band). Statistical difference between healthy controls ($n = 47$) and ALS patients ($n = 74$) was assessed in the six defined frequency bands using EBI. FDR was set to 10%, yielding an estimated statistical power of $1 - \beta = 0.55$ and posterior probability of $P_i = 0.77$ (across all frequency bands). AUC: Area under the receiver operating characteristic curve. No changes were detected in the γ frequency bands; therefore, they are not shown. Frequency bands: δ (2-4 Hz), θ (5-7 Hz), α (8-13 Hz) and β (14-30 Hz).

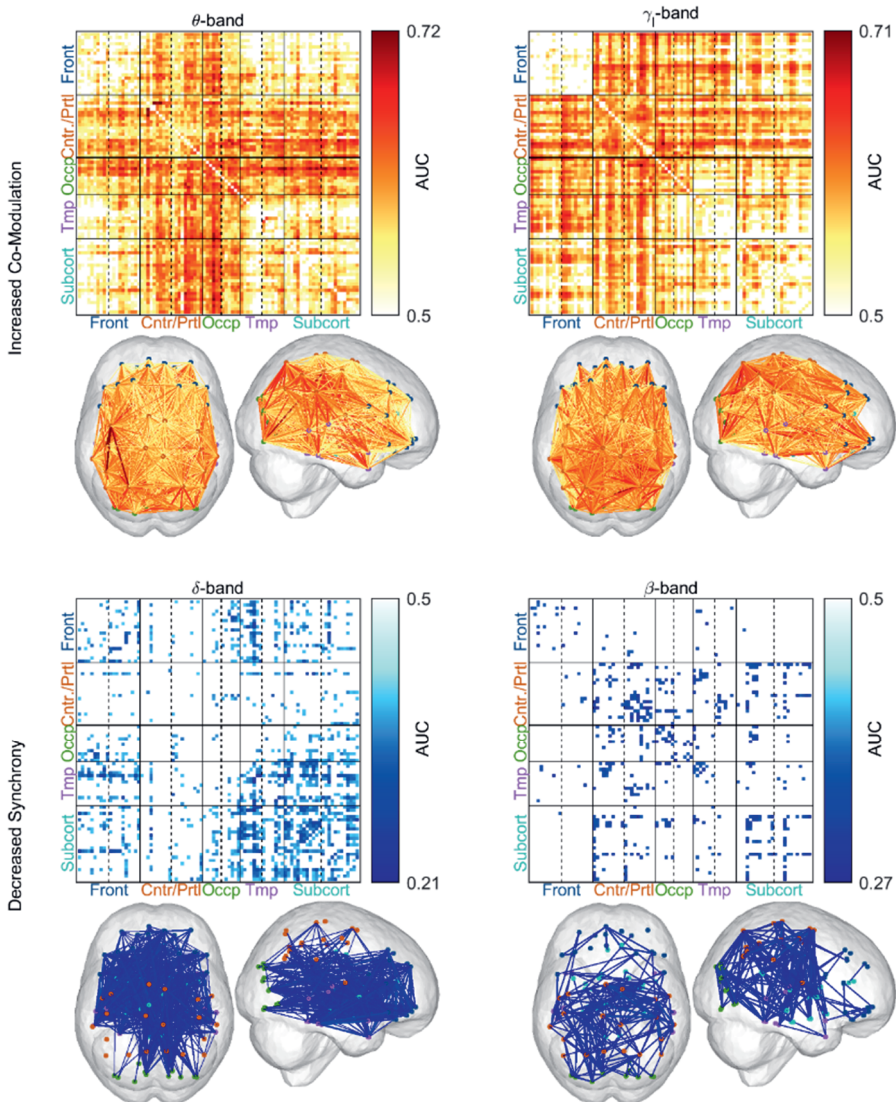


Figure 4. The increase of point-to-point co-modulation and the decrease of point-to-point synchrony have a widespread pattern in ALS patients. Note that the widespread patterns of increased co-modulation (AEC) are predominantly in the θ - and γ -bands, while synchrony (iCoh) patterns were predominantly in the δ - and β -bands. Statistical difference between healthy controls ($n = 47$) and ALS patients ($n = 74$) was assessed separately in the six defined frequency bands using EBI. FDR was set to 10% (in each frequency band), yielding an estimated statistical power of $1 - \beta = 0.96$ and posterior probability of $P_1 = 0.56$ in the θ -band AEC and an estimated statistical power of $1 - \beta = 0.89$ and posterior probability of $P_1 = 0.7$ in the γ -band AEC. For synchrony measures, the 10% FDR threshold yielded an estimated statistical power of $1 - \beta = 0.39$ and posterior probability of $P_1 = 0.8$ in the δ -band iCoh and an estimated statistical power of $1 - \beta = 0.16$ and posterior probability of $P_1 = 0.83$ in the β -band iCoh. AUC: Area under the receiver operating characteristic curve. No changes were detected in the other frequency bands; therefore, they are not shown. The abbreviations 'Front', 'Cntr/Prtl', 'Occp', 'Tmp', 'Subcort' stand for Frontal, Central/Parietal, Occipital, Temporal and Subcortical, respectively. For the order of ROI used in the connectivity matrix, see Supplementary Fig. 2. Frequency bands: δ (2-4 Hz), θ (5-7 Hz), β (14-30 Hz) and γ (31-47 Hz).

The connectivity modules describe the (sub-)networks affected in ALS

Considering the non-specific widespread connectivity patterns identified in point-to-point analysis, we sought to further analyse the complex patterns into distinct networks. The Bayesian information criterion determined the preferred number of connectivity modules (M) to be one or two in each frequency band and measure. The factorised networks (i.e. the basis vectors extracted by NMF) resemble the occipital network (θ -AEC M_1 ; Fig. 5A), motor-loops of basal ganglia and/or thalamus (γ_1 -AEC M_1 ; Fig. 5B), frontal network (δ -iCoh M_1 ; Fig. 5C), sensorimotor network (β -iCoh M_1 ; Fig. 5D), frontoparietal network (θ -AEC M_2 ; Fig. 5E), frontotemporal network (γ_1 -AEC M_2 ; Fig. 5F) and combined occipitofrontal and uncinate fasciculus (δ -iCoh M_2 ; Fig. 5G).

Statistical analysis of the weights corresponding to both modules of AEC and iCoh showed the networks that were significantly different in the ALS patient group. Namely, weights corresponding to θ -AEC M_1 ($p < 0.001$; $1-\beta_{0.05} = 0.99$) and M_2 ($p < 0.001$; $1-\beta_{0.05} = 1$) and γ_1 -AEC M_1 ($p < 0.001$; $1-\beta_{0.05} = 0.97$) and M_2 ($p = 0.001$; $1-\beta_{0.05} = 0.89$) were significantly higher in ALS patients. Conversely, weights corresponding to δ -iCoh M_1 ($p < 0.001$; $1-\beta_{0.05} = 0.9$) and M_2 ($p = 0.014$; $1-\beta_{0.05} = 0.65$) and β -iCoh M_1 ($p < 0.001$; $1-\beta_{0.05} = 0.99$) were significantly lower in ALS patients. In all cases, the statistical significance and statistical power of the connectivity modules were estimated using a bootstrapping method and controlled for false positives with an α FDR set to 5%. Figure 5 points to the increased or decreased activity of each network in ALS, where all the network connections in a module were pooled, normalised to the range between 0 and 1, and then each network was multiplied with the sign of the AUC value (centred around zero). The AUC value for each network corresponds to NMF weights of both groups.

EEG differences between ALS patients and controls do not discriminate between ALS subgroups

To assess the differences between ALS subgroups based on site of onset (spinal, bulbar) and presence or absence of the pathologic hexanucleotide expansion in *C9orf72*, we used EEG measures that discriminated between ALS patients and healthy controls (Fig. 6). Brain regions that reached the highest AUC values between ALS patients and healthy controls in each of the following measures include: spectral power in θ -band (L/R occipital gyri) and β -band (L/R post-central gyri and precuneus); co-modulation in δ -band (L/R postcentral and superior parietal gyri) and θ -band (L/R calcarine fissure and lingual gyri); synchrony in δ -band (L/R anterior cingulate gyri) and β -band (L/R pre- and post-central gyri). Although these measures showed difference between ALS patients and healthy controls, they did not discriminate between subgroups based on site of onset (p_1) or genomic status (p_2) in any of the measures (i.e. spectral power in θ -band ($p_1 = 0.471$; $p_2 = 0.218$) and β -band ($p_1 = 0.484$; $p_2 = 0.301$); co-modulation in δ -band ($p_1 = 0.554$; $p_2 = 0.445$) and θ -band ($p_1 = 0.708$; $p_2 = 0.267$); synchrony in δ -band ($p_1 = 0.826$; $p_2 = 0.35$) and β -band ($p_1 = 0.409$; $p_2 = 0.717$)).

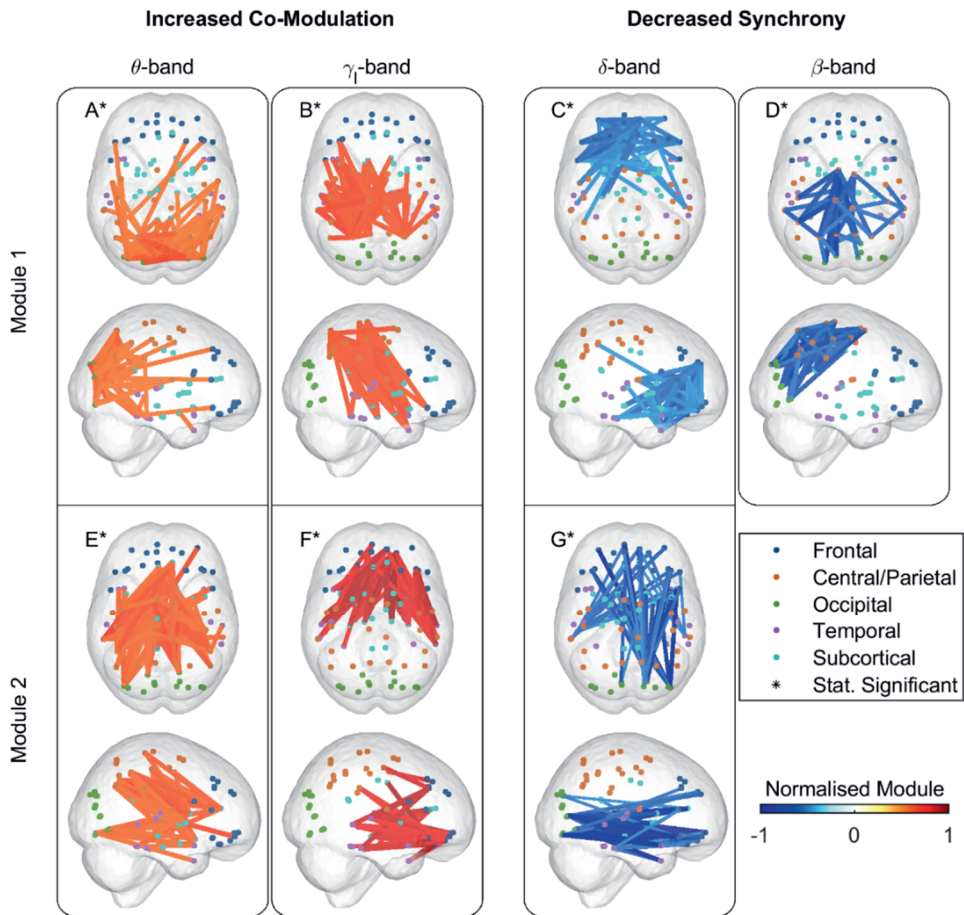


Figure 5. The connectivity modules reveal the (sub-)network with frequency-specific increase of co-modulation and decrease of synchrony in ALS. The factorised (sub-)networks resemble the occipital network (A), motor-loops of basal ganglia and/or thalamus (B), frontal network (C), sensorimotor network (D), frontoparietal network (E), frontotemporal network (F) and combined occipitofrontal and uncinate fasciculus (G). The connectivity modules from NMF analysis of the affected co-modulation or synchrony in ALS reveal the altered brain networks, while the changes in module's weights show the increase or decrease in the activity of these networks. Statistical analysis between ALS patients and healthy controls ($n_c = 47$ & $n_p = 47$) of the weights corresponding to the connectivity modules reached significance in all cases (marked with asterisk) as controlled by aFDR at $q = 0.05$. Frequency bands: δ (2-4 Hz), θ (5-7 Hz), β (14-30 Hz) and γ_1 (31-47 Hz).

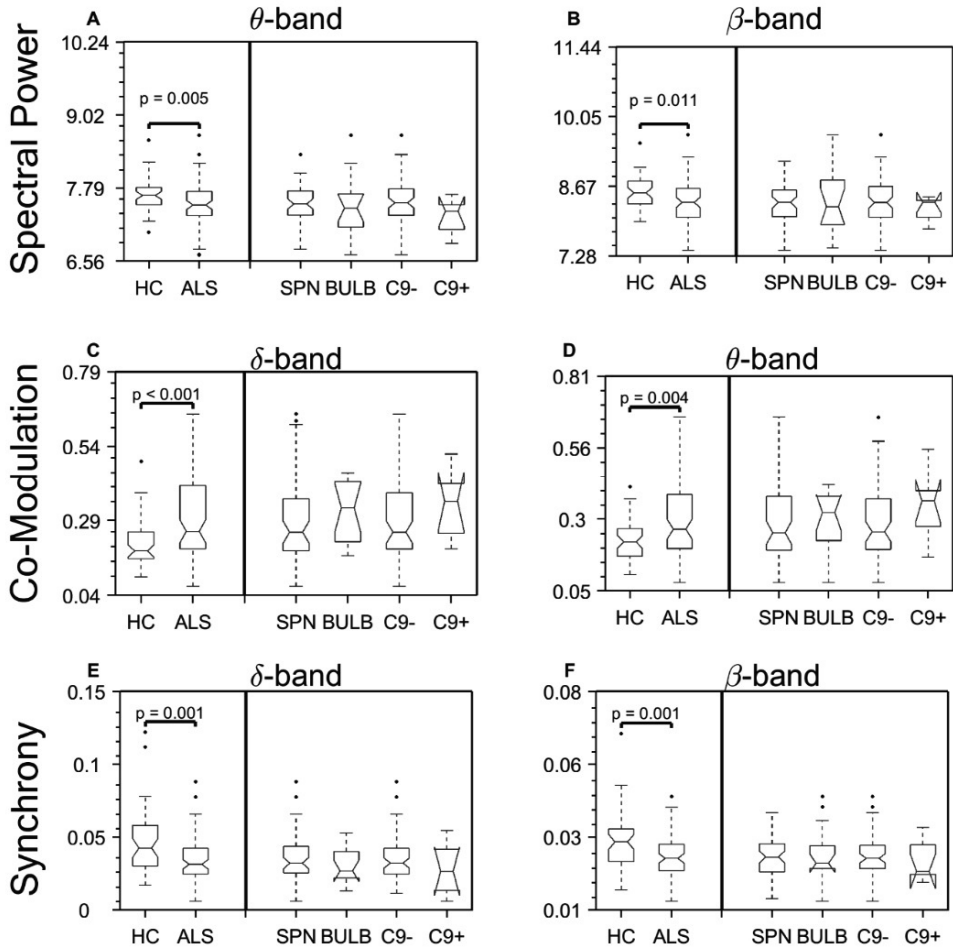


Figure 6. The observed EEG spectral power and connectivity changes are not different between ALS subgroups. The comparison shows the differences between healthy controls and ALS subgroups. Statistical difference between healthy controls and pooled ALS patients was assessed using Mann-Whitney U-test, whereas statistical difference between patient subgroups was assessed using 2-way ANOVA in all three measures, each in two frequency bands with the most prominent changes (see Fig. 1-3). None of the measures showed statistically significant difference among ALS subgroups. Spectral power data were log-transformed for plotting purposes. The abbreviations ‘HC’, ‘SPN’, ‘BULB’, ‘C9-’, ‘C9+’ stand for Healthy controls, Spinal, Bulbar, *C9orf72*-negative and *C9orf72*-positive, respectively. The number of ALS patients in each subgroup are $n = 55, 15, 63$ and 7 , respectively. There are six *C9orf72*-positive patients in the spinal and one in the bulbar subgroup. Frequency bands: δ (2-4 Hz), θ (5-7 Hz) and β (14-30 Hz).

The EEG measures of connectivity change reflect the neurodegeneration and functional impairment in both motor and cognitive domains

The changes in cortico-cortical EEG connectivity were correlated with the changes captured by other modalities in both cognitive and motor domain; namely, the identified discriminant measures correlated with structural degeneration as captured by MRI, as well as the functional scores (ALSFRS-R for motor function and neuropsychological battery scores for cognitive function). Figure 7 shows the significant correlations in each domain and for functional and structural measures.

For EEG-MRI (Fig. 7A-B), these correlations were between the altered connectivity of motor and frontal networks with the grey matter volume of those networks. In the case of the motor network, the average motor network β -band iCoh was correlated with the average cortical volume (Fig. 7A), whereas in the case of the frontal network, the average δ -band iCoh connectivity was correlated with average cortical volume (Fig. 7B). We also found correlations between altered EEG connectivity and functional scores (Fig. 7C-E). In the motor domain, the correlation was between the ALSFRS-R scores with the average β -band iCoh connectivity changes in the motor network (Fig. 7C). In the cognitive domain, we found correlations between the neuropsychological battery scores and the alterations in the frontoparietal and frontotemporal networks (Fig. 7D-E); Namely, between the composite of executive function scores and the θ -band AEC NMF weights (frontoparietal network), as well as between the composite of language function scores and the γ -band AEC NMF weights (frontotemporal network).

These correlations (Fig. 7) were significant between the changes in connectivity and grey matter volume in the motor network ($r = 0.34$; $p = 0.032$; $1-\beta_{0.05} = 0.55$) and frontal network ($r = 0.47$; $p = 0.006$; $1-\beta_{0.05} = 0.82$); changes in connectivity of the motor network and ALSFRS-R ($r = 0.27$; $p = 0.029$; $1-\beta_{0.05} = 0.57$); changes in frontoparietal network with the executive function scores from the neuropsychological battery ($r = -0.34$; $p = 0.033$; $1-\beta_{0.05} = 0.54$); and changes in frontotemporal network with the language scores from the neuropsychological battery ($r = -0.38$; $p = 0.034$; $1-\beta_{0.05} = 0.59$).

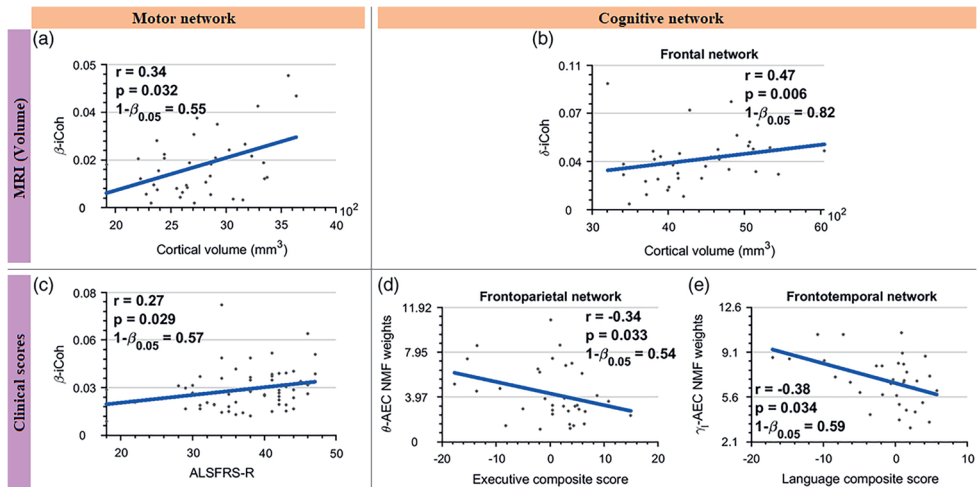


Figure 7. The changes in EEG connectivity correlate with the structural atrophy in MRI in the motor (A) and cognitive (B) networks, as well as measures of functional motor impairment (C. ALSFRS-R), functional cognitive impairment (D. and E. Standardised neuropsychological battery scores). The values of r and p correspond to Spearman's partial correlation corrected for age (A-C) and Spearman's correlation (D and E), whereas $1-\beta_{0.05}$ represents statistical power at 0.05. The number of ALS patients used in the analyses are $n = 37, 37, 61, 34$ and 34 , respectively. The shown p -values are aFDR-corrected at $q = 0.05$. Frequency bands: δ (2-4 Hz), θ (5-7 Hz), β (14-30 Hz) and γ_1 (31-47 Hz).

Discussion

This study demonstrates that neuroelectric signal analysis can capture and quantify important changes that occur in functional networks in ALS. Using spectral power and two conceptually different measures of connectivity that reflect co-modulation (AEC) and synchrony (iCoh) we have demonstrated statistically-robust neurophysiological evidence of a multisystem disruption of networks in ALS patients. These disruptions correlate with functional impairment as detected using ALSFRS-R and neuropsychological assessment, as well as with structural changes captured by MRI.

Spectral power changes in ALS disease

The observed changes in spectral power are consistent with previously described θ - and α -band power decrease above the sensorimotor network.^{6,66} Other studies in ALS have similarly identified decreased post-movement β -band power above motor cortices,^{67,68} which is considered a reflection of idling and/or an active inhibition of the motor network.⁶⁹

Different frequency bands are mediated by complex neurochemistry and oscillations of frequencies 12-80 Hz are linked to pyramidal neurons, regulated by GABA_A inhibitory interneurons.⁷⁰ Loss of GABAergic interneurons, together with pyramidal neurons, has been observed in both motor and non-motor areas in ALS;⁷¹ consequently, the decrease in the lower frequency spectral power can be attributed to structural degeneration of pyramidal cells and/or loss of interneurons that entrain them. These changes in spectral power observed beyond motor network^{4,6,9} across multiple

frequency bands, support the evolving recognition of significant involvement of non-motor networks in ALS.

Correlating connectivity changes in networks affected by ALS with structural MRI and clinical scores

Our AEC connectivity findings are consistent with resting-state fMRI findings of increased connectivity changes in the cingulate^{5,10} and parietal cortices,⁷² and prefrontal,⁵ temporal and parahippocampal^{73,74} regions in ALS patients. Factorised AEC networks from NMF analysis, showing increased connectivity in the θ - and γ_1 -band, resemble the frontoparietal and frontotemporal networks, respectively.

The frontoparietal network is required for active maintenance of information relevant for successful performance in working memory.⁷⁵ Functional connectivity within this network,^{6,8,17} as well as the white matter volumes of association fibres within the frontal brain regions and cingulum are known to be affected in ALS; while the latter changes show correlation with memory impairments in ALS patients.⁷⁶ In addition, degeneration of neurons in frontal and temporal regions³ and associated tracts⁷⁶ is linked to language impairment⁷⁷ in ALS. We have identified significant correlations between our observed neurophysiological changes in the frontoparietal and frontotemporal network and composite scores of executive and language function, respectively. The observed negative correlation supports the role of such network dysfunction in cognitive impairment. These observations confirm the validity of neuroelectric signalling as a measure of clinically relevant network disruption in ALS.

Analysis of the iCoh networks using NMF showed that the most prominent changes are in the δ -band frontal and β -band sensorimotor networks, further demonstrating impaired connectivity in ALS patients. The identified positive correlation with structural MRI indicates that functional abnormalities we have detected are due to the loss of cortical atrophy in these regions. Taken together with a positive correlation between the average β -band iCoh in the motor network and the ALSFRS-R, these data support the use of advanced neurophysiological tools to characterise motor network decline.

Spectral EEG measures as a marker of ALS disease

Numerous studies in neurodegenerative diseases, particularly in dementias, have identified the potential of EEG resting-state measures as biomarkers for differential diagnosis and clinical trial outcome measures (see the review by McMackin et al.⁷⁸). By definition, ALS is a clinical diagnosis. The El Escorial criteria³⁰ often used in clinical practice, allows for supportive evidence of both upper and lower motor neuron degeneration, the latter based on clinical neurophysiological studies. Diagnosis relies on physicians' expertise in marking specific set of symptoms corroborated by objective findings from laboratory, neurophysiological and neurological examination. Current clinical trial outcome measures similarly rely on semi-quantitative tools, such as the ALSFRS-R scale, a 48-point clinical measure of motor, bulbar and respiratory decline. To date, there have been no reliable objective measures of cognitive/behavioural change suited for use as outcomes in clinical trials.

Quantitative EEG has the potential to capture upper motor system changes in ALS. Transcranial magnetic stimulation (TMS) studies have already demonstrated the utility of quantitative upper motor neuron biomarkers that distinguish ALS from mimic disorders.⁷⁹ These TMS measures do not capture the broader, non-motor degeneration established in ALS, such as that in cognitive networks. Conversely, EEG can capture both motor and non-motor disruption. This is especially desirable from the clinical trial design perspective, where not only the severity of the disease, but specific (sub)phenotypes of disease that can be characterised by differential change in brain network architecture, are likely to be important in the evolution of a precision medicine approach towards treatments.⁸⁰ Our observed alterations in functional connectivity correlate with structural degeneration, and functional motor and cognitive measures. These changes confirm that neuroelectric signal analysis has a potential to be developed as a novel marker of ALS that reflects additional and previously uncharacterised dimensions of the disease, regardless of the site of onset. The high level of AUC values for the co-modulation (0.72) and synchrony measures (0.27 or 0.73), show that these read-outs can be used to develop quantitative biomarkers after further analysis of the sensitivity-specificity characteristics, establishing normative values, and further validation steps.

Conclusions

This study is the first to simultaneously interrogate power activity, co-modulation and synchrony of brain networks in ALS to decipher the nature of change in network function caused by the disease using standard 128-channel EEG recordings. In doing so, we have identified increased co-modulation and decreased synchrony in both motor and non-motor networks. Taken together, these data provide a compelling argument for the development of quantitative EEG, a non-invasive and inexpensive technology, as a robust data-driven tool for measuring network disruption in ALS.

References

1. Hardiman, O., Van Den Berg, L. H. & Kiernan, M. C. Clinical diagnosis and management of amyotrophic lateral sclerosis. *Nat Rev Neurol* **7**, 639–49 (2011).
2. Achi, E. Y. & Rudnicki, S. A. ALS and Frontotemporal Dysfunction: A Review. *Neurol Res Int* **2012**, 806306 (2012).
3. Bede, P. *et al.* Grey matter correlates of clinical variables in amyotrophic lateral sclerosis (ALS): a neuroimaging study of ALS motor phenotype heterogeneity and cortical focality. *J Neurol Neurosurg Psychiatry* **84**, 766–73 (2013).
4. Bede, P. *et al.* Connectivity-based characterisation of subcortical grey matter pathology in frontotemporal dementia and ALS: a multimodal neuroimaging study. *Brain Imaging Behav* **12**, 1696–1707 (2018).
5. Douaud, G., Filippini, N., Knight, S., Talbot, K. & Turner, M. R. Integration of structural and functional magnetic resonance imaging in amyotrophic lateral sclerosis. *Brain* **134**, 3470–9 (2011).
6. Nasserouleslami, B. *et al.* Characteristic Increases in EEG Connectivity Correlate With Changes of Structural MRI in Amyotrophic Lateral Sclerosis. *Cereb Cortex* **29**, 27–41 (2019).
7. Proudfoot, M. *et al.* Impaired corticomuscular and interhemispheric cortical beta oscillation coupling in amyotrophic lateral sclerosis. *Clinical Neurophysiology* **129**, 1479–1489 (2018).
8. Iyer, P. M. *et al.* Functional Connectivity Changes in Resting-State EEG as Potential Biomarker for Amyotrophic Lateral Sclerosis. *PLoS One* **10**, e0128682 (2015).
9. McMackin, R. *et al.* Dysfunction of attention switching networks in amyotrophic lateral sclerosis. *Neuroimage Clin* **22**, 101707 (2019).
10. Agosta, F. *et al.* Sensorimotor Functional Connectivity Changes in Amyotrophic Lateral Sclerosis. *Cerebral Cortex* **21**, 2291–2298 (2011).
11. Siegel, M., Donner, T. H. & Engel, A. K. Spectral fingerprints of large-scale neuronal interactions. *Nat Rev Neurosci* **13**, 121–34 (2012).
12. Kopell, N., Kramer, M. A., Malerba, P. & Whittington, M. A. Are Different Rhythms Good for Different Functions? *Front Hum Neurosci* **4**, 187 (2010).
13. Barbas, H. General Cortical and Special Prefrontal Connections: Principles from Structure to Function. *Annu Rev Neurosci* **38**, 269–289 (2015).
14. Jensen, O., Bonnefond, M., Marshall, T. R. & Tiesinga, P. Oscillatory mechanisms of feedforward and feedback visual processing. *Trends Neurosci* **38**, 192–4 (2015).
15. Laufs, H. Endogenous brain oscillations and related networks detected by surface EEG-combined fMRI. *Hum Brain Mapp* **29**, 762–9 (2008).
16. Hipp, J. F., Hawellek, D. J., Corbetta, M., Siegel, M. & Engel, A. K. Large-scale cortical correlation structure of spontaneous oscillatory activity. *Nat Neurosci* **15**, 884–90 (2012).
17. Blain-Moraes, S., Mashour, G. A., Lee, H., Huggins, J. E. & Lee, U. Altered cortical communication in amyotrophic lateral sclerosis. *Neurosci Lett* **543**, 172–6 (2013).
18. Proudfoot, M. *et al.* Increased cerebral functional connectivity in ALS: A resting-state magnetoencephalography study. *Neurology* **90**, e1418–e1424 (2018).
19. Buzsáki, G. & Draguhn, A. Neuronal oscillations in cortical networks. *Science* **304**, 1926–9 (2004).
20. Fraschini, M. *et al.* Functional brain connectivity analysis in amyotrophic lateral sclerosis: An EEG source-space study. *Biomed Phys Eng Express* **4**, 037004 (2018).
21. Sorrentino, P. *et al.* Brain functional networks become more connected as amyotrophic lateral sclerosis progresses: a source level magnetoencephalographic study. *Neuroimage Clin* **20**, 564–71 (2018).
22. Tagliazucchi, E., von Wegner, F., Morzelewski, A., Brodbeck, V. & Laufs, H. Dynamic BOLD functional connectivity in humans and its electrophysiological correlates. *Front Hum Neurosci* **6**, 339 (2012).
23. Brookes, M. J. *et al.* Measuring functional connectivity using MEG: Methodology and comparison with fMRI. *Neuroimage* **56**, 1082–1104 (2011).
24. Leopold, D. A., Murayama, Y. & Logothetis, N. K. Very Slow Activity Fluctuations in Monkey Visual Cortex: Implications for Functional Brain Imaging. *Cerebral Cortex* **13**, 422–33 (2003).
25. Munk, M. H., Roelfsema, P. R., König, P., Engel, A. K. & Singer, W. Role of reticular activation in the modulation of

- intracortical synchronization. *Science* **272**, 271–4 (1996).
26. Engel, A. K., Gerloff, C., Hülsmann, C. C. & Nolte, G. Intrinsic Coupling Modes: Multiscale Interactions in Ongoing Brain Activity. *Neuron* **80**, 867–86 (2013).
 27. Bruns, A., Eckhorn, R., Jokeit, H. & Ebner, A. Amplitude envelope correlation detects coupling among incoherent brain signals. *Neuroreport* **11**, 1509–14 (2000).
 28. Iyer, P. M. *et al.* Mismatch Negativity as an Indicator of Cognitive Sub-Domain Dysfunction in Amyotrophic Lateral Sclerosis. *Front Neurol* **8**, 395 (2017).
 29. Burke, T. *et al.* A Cross-sectional population-based investigation into behavioral change in amyotrophic lateral sclerosis: subphenotypes, staging, cognitive predictors, and survival. *Ann Clin Transl Neurol* **4**, 305–17 (2017).
 30. Ludolph, A. *et al.* A revision of the El Escorial criteria - 2015. *Amyotroph Lateral Scler Frontotemporal Degener* **16**, 291–2 (2015).
 31. Schuster, C., Elamin, M., Hardiman, O. & Bede, P. The segmental diffusivity profile of amyotrophic lateral sclerosis associated white matter degeneration. *Eur J Neurol* **23**, 1361–1371 (2016).
 32. Schuster, C., Hardiman, O. & Bede, P. Survival prediction in Amyotrophic lateral sclerosis based on MRI measures and clinical characteristics. *BMC Neurol* **17**, 73 (2017).
 33. Bede, P., Iyer, P. M., Finegan, E., Omer, T. & Hardiman, O. Virtual brain biopsies in amyotrophic lateral sclerosis: Diagnostic classification based on in vivo pathological patterns. *Neuroimage Clin* **15**, 653–658 (2017).
 34. Cedarbaum, J. M. *et al.* The ALSFRS-R: a revised ALS functional rating scale that incorporates assessments of respiratory function. *J Neurol Sci* **169**, 13–21 (1999).
 35. Abrahams, S., Newton, J., Niven, E., Foley, J. & Bak, T. H. Screening for cognition and behaviour changes in ALS. *Amyotroph Lateral Scler Frontotemporal Degener* **15**, 9–14 (2014).
 36. Pinto-Grau, M. *et al.* Screening for cognitive dysfunction in ALS: validation of the Edinburgh Cognitive and Behavioural ALS Screen (ECAS) using age and education adjusted normative data. *Amyotroph Lateral Scler Frontotemporal Degener* **18**, 99–106 (2017).
 37. Dukic, S. *et al.* Estimation of coherence using the median is robust against EEG artefacts. in *2017 39th Annual International Conference of the IEEE Engineering in Medicine and Biology Society (EMBC)* 3949–3952 (IEEE, 2017).
 38. Perrin, F., Pernier, J., Bertrand, O. & Echallier, J. F. Spherical splines for scalp potential and current density mapping. *Electroencephalogr Clin Neurophysiol* **72**, 184–7 (1989).
 39. Van Veen, B. D., Van Drongelen, W., Yuchtman, M. & Suzuki, A. Localization of brain electrical activity via linearly constrained minimum variance spatial filtering. *IEEE Trans Biomed Eng* **44**, 867–80 (1997).
 40. Tzourio-Mazoyer, N. *et al.* Automated Anatomical Labeling of Activations in SPM Using a Macroscopic Anatomical Parcellation of the MNI MRI Single-Subject Brain. *Neuroimage* **15**, 273–89 (2002).
 41. Hipp, J. F. & Siegel, M. BOLD fMRI Correlation Reflects Frequency-Specific Neuronal Correlation. *Current Biology* **25**, 1368–74 (2015).
 42. Nolte, G. *et al.* Identifying true brain interaction from EEG data using the imaginary part of coherency. *Clinical Neurophysiology* **115**, 2292–307 (2004).
 43. Schoffelen, J.-M. & Gross, J. Source connectivity analysis with MEG and EEG. *Hum Brain Mapp* **30**, 1857–1865 (2009).
 44. Palva, J. M. *et al.* Ghost interactions in MEG/EEG source space: A note of caution on inter-areal coupling measures. *Neuroimage* **173**, 632–43 (2018).
 45. Brookes, M. J., Woolrich, M. W. & Barnes, G. R. Measuring functional connectivity in MEG: a multivariate approach insensitive to linear source leakage. *Neuroimage* **63**, 910–20 (2012).
 46. Paatero, P. & Tapper, U. Positive matrix factorization: A non-negative factor model with optimal utilization of error estimates of data values. *Environmetrics* **5**, 111–26 (1994).
 47. Schwarz, G. Estimating the Dimension of a Model. *The Annals of Statistics* **6**, 461–464 (1978).
 48. Murphy, J., Henry, R. & Lomen-Hoerth, C. Establishing Subtypes of the Continuum of Frontal Lobe Impairment in Amyotrophic Lateral Sclerosis. *Arch Neurol* **64**, 330 (2007).
 49. Omer, T. *et al.* Neuroimaging patterns along the ALS-FTD spectrum: a multiparametric imaging study. *Amyotroph Lateral Scler Frontotemporal Degener* **18**, 611–23 (2017).

50. Walhout, R. *et al.* Cortical thickness in ALS: towards a marker for upper motor neuron involvement. *J Neurol Neurosurg Psychiatry* **86**, 288–94 (2015).
51. Schmidt, R. *et al.* Correlation between structural and functional connectivity impairment in amyotrophic lateral sclerosis. *Hum Brain Mapp* **35**, 4386–95 (2014).
52. Kassubek, J. *et al.* Imaging the pathoanatomy of amyotrophic lateral sclerosis in vivo: targeting a propagation-based biological marker. *J Neurol Neurosurg Psychiatry* **89**, 374–381 (2018).
53. Wechsler, D. *Wechsler adult intelligence scale—Fourth Edition (WAIS-IV)*. (Psychological Corporation, 2014).
54. Delis, D. C., Kaplan, E. & Kramer, J. H. *Delis-Kaplan Executive Function System (D-KEFS)*. (Psychological Corporation, 2001).
55. Baron-Cohen, S., Wheelwright, S., Hill, J., Raste, Y. & Plumb, I. The 'Reading the Mind in the Eyes' Test Revised Version: A Study with Normal Adults, and Adults with Asperger Syndrome or High-functioning Autism. *Journal of Child Psychology and Psychiatry* **42**, 241–51 (2001).
56. Bowers, D., Blonder, L. X. & Heilman, K. M. *Florida Affect Battery*. (Center for Neuropsychological Studies, University of Florida, 1991).
57. Kay, J., Lesser, R. & Coltheart, M. *Psycholinguistic Assessments of Language Processing in Aphasia (PALPA)*. (Lawrence Erlbaum Associates, 1992).
58. Graves, R. E., Bezeau, S. C., Fogarty, J. & Blair, R. Boston Naming Test Short Forms: A Comparison of Previous Forms with New Item Response Theory Based Forms. *J Clin Exp Neuropsychol* **26**, 891–902 (2004).
59. Efron, B., Tibshirani, R., Storey, J. D. & Tusher, V. Empirical Bayes Analysis of a Microarray Experiment. *J Am Stat Assoc* **96**, 1151–60 (2001).
60. Efron, B. Size, power and false discovery rates. *The Annals of Statistics* **35**, 1351–77 (2007).
61. Nasserouleslami, B. An Implementation of Empirical Bayesian Inference and Non-Null Bootstrapping for Threshold Selection and Power Estimation in Multiple and Single Statistical Testing. *bioRxiv* 342964 (2018).
62. Zhou, X.-H., McClish, D. & Obuchowski, N. *Statistical Methods in Diagnostic Medicine. Wiley Series in Probability and Statistics*. (Wiley, 2011).
63. Benjamini, Y., Krieger, A. M. & Yekutieli, D. Adaptive linear step-up procedures that control the false discovery rate. *Biometrika* **93**, 491–507 (2006).
64. Beasley, T. M., Erickson, S. & Allison, D. B. Rank-Based Inverse Normal Transformations are Increasingly Used, But are They Merited? *Behav Genet* **39**, 580–95 (2009).
65. Oostenveld, R., Fries, P., Maris, E. & Schoffelen, J.-M. FieldTrip: Open source software for advanced analysis of MEG, EEG, and invasive electrophysiological data. *Comput Intell Neurosci* **2011**, 156869 (2011).
66. Bizovičar, N., Dreo, J., Koritnik, B. & Zidar, J. Decreased movement-related beta desynchronization and impaired post-movement beta rebound in amyotrophic lateral sclerosis. *Clinical Neurophysiology* **125**, 1689–99 (2014).
67. Proudfoot, M. *et al.* Altered cortical beta-band oscillations reflect motor system degeneration in amyotrophic lateral sclerosis. *Hum Brain Mapp* **38**, 237–254 (2017).
68. Riva, N. *et al.* Cortical activation to voluntary movement in amyotrophic lateral sclerosis is related to corticospinal damage: Electrophysiological evidence. *Clinical Neurophysiology* **123**, 1586–92 (2012).
69. Cassim, F. *et al.* Does post-movement beta synchronization reflect an idling motor cortex? *Neuroreport* **12**, 3859–63 (2001).
70. Khanna, P. & Carmena, J. M. Neural oscillations: beta band activity across motor networks. *Curr Opin Neurobiol* **32**, 60–7 (2015).
71. Nihei, K., McKee, A. C. & Kowall, N. W. Patterns of neuronal degeneration in the motor cortex of amyotrophic lateral sclerosis patients. *Acta Neuropathol* **86**, 55–64 (1993).
72. Agosta, F. *et al.* Divergent brain network connectivity in amyotrophic lateral sclerosis. *Neurobiol Aging* **34**, 419–427 (2013).
73. Abrahams, S. *et al.* Word retrieval in amyotrophic lateral sclerosis: A functional magnetic resonance imaging study. *Brain* **127**, 1507–1517 (2004).
74. Heimrath, J. *et al.* Additional resources and the default mode network: Evidence of increased connectivity and decreased white matter integrity in amyotrophic lateral sclerosis. *Amyotroph Lateral Scler Frontotemporal Degener* **15**, 537–545 (2014).
75. Ptak, R. The Frontoparietal Attention Network of the Human Brain. *The Neuroscientist* **18**, 502–15 (2012).

76. Abrahams, S. *et al.* Frontotemporal white matter changes in amyotrophic lateral sclerosis. *J Neurol* **252**, 321–331 (2005).
77. Neary, D. *et al.* Frontotemporal lobar degeneration. *Neurology* **51**, 1546–54 (1998).
78. McMackin, R., Bede, P., Pender, N., Hardiman, O. & Nasserroleslami, B. Neurophysiological markers of network dysfunction in neurodegenerative diseases. *Neuroimage Clin* **22**, 101706 (2019).
79. Vucic, S., Cheah, B. C., Yiannikas, C. & Kiernan, M. C. Cortical excitability distinguishes ALS from mimic disorders. *Clinical Neurophysiology* **122**, 1860–1866 (2011).
80. McMackin, R. *et al.* Measuring network disruption in neurodegenerative diseases: New approaches using signal analysis. *J Neurol Neurosurg Psychiatry* jnnp-2018-319581 (2019).

Supplementary material

Supplementary methods

EEG source localisation

For source analysis, we pursued the following stages for head modelling, as well as projection of data to the source-space in order to obtain time-varying signals, wherein each signal represents a brain region.

Head models

For each subject with an MRI scan, a realistically-shaped volume conduction model was built. A three-layer conduction model, accounting for the brain, skull and scalp, was constructed using the Boundary Element Models (BEM) method,^{1,2} implemented in the open source software OpenMEEG.³ The BEMs were piece-wise approximated with 1000, 2000 and 3000 elements for scalp, skull and brain, respectively. Similarly, for controls and patients who did not undergo MRI, a realistically-shaped BEM based on the ICBM152 template⁴ with the same characteristics was constructed, as template-based BEM and BEM based on individual MRI scans provide comparable localisation accuracy.⁵ For both groups, a 5 mm regular grid was generated in normalised space using the ICBM152 template and, separately for each subject, it was wrapped around the individual's MRI data. Wrapping ensures that each potential source corresponds to the same location in the brain irrespective of individual anatomical differences. In addition, for each individual subject, a template with EEG electrode positions was realigned using the fiducial points, obtained manually from the individual's MRI data. Aligned in the same coordinate system, these structures were used for the calculation of normalised leadfields. The use of normalised leadfield avoids the potential norm artefact of the leadfield, in which the norm of the leadfield changes with location.⁶

Projection to source-space

EEG data were source-reconstructed using the linearly constrained minimum variance (LCMV) beamformer, a time-domain beamforming method.⁷

Covariance matrices, needed for the reconstruction, were computed over a time window spanning the whole recording and using broadband data (1-97 Hz). In order to account for outliers in the data, the orthogonalised Gnanadesikan-Kettenring algorithm was used for the robust estimation of the covariance matrix⁸. Covariance matrices were regularised using the Tikhonov method by μI ,⁹ where the regularisation parameter, μ , is set to 5% of the mean variance of all EEG channels and I is an identity matrix. This was done to avoid reaching an unstable arbitrary solution, caused by reduction in dimensionality due to interpolation of noisy channels. Additionally, it increases temporal signal-to-noise ratio, albeit at the expense of increased spatial smoothness of the beamformed data.

At each grid point we sought to estimate a dipole in the optimal orientation. To achieve this, we estimated the orientation of maximum power of the dipole using the

singular value decomposition (SVD) on the source-level covariance matrix.⁷ Beamformer weights, constructed for the source localisation, spatially filter the scalp recorded data and here were used to reconstruct time-series at each dipole location on the grid. One limitation of the LCMV beamformer is the overestimation of the sources in the centre of the head.^{6,7} To compensate for this, we normalised the weights by their vector norm before reconstructing the time-series.¹⁰ Source localisation was done using the FieldTrip toolbox.¹¹

Estimation of neural time-series at regions of interest

An atlas-based approach was used to evaluate source-space data with respect to the anatomical brain regions.^{12,13} The cortex of each subject was parcelled according to the automated anatomical labelling (AAL) atlas.¹⁴ This was done by using a 5 mm regular grid based on the ICBM152 template and labelling all the cortical sources according to the AAL atlas. In this study we used 90 ROI from AAL atlas, excluding the cerebellum and including all the subcortical regions (olfactory cortex, insula, anterior/middle/posterior cingulate, hippocampus, parahippocampal gyrus, amygdala, caudate, putamen, globus pallidus and thalamus). For each ROI the centre of mass was calculated. To derive a single time-series for each ROI all the time-series within a ROI were weighted using a Gaussian weighting function with the half width at half maximum set to approximately 17 mm,^{13,15} as following:

$$q_{1 \times t} = \sum_i \exp\left(\frac{-r^2(i)}{400}\right) \cdot y_{1 \times t}(i) \quad (1)$$

Where i represents a count of all dipoles within a ROI, r represents a distance in millimetres of each dipole from the centre of mass of the given ROI and t represent the length of the reconstructed signal. This means that signals that are 17 mm far from the centre of the ROI will be attenuated by a factor of 0.5. However, the direction of each estimated dipole is not necessarily the same as the other dipoles in the ROI. In such situations, simple averaging of neighbouring dipoles' time-series would lead to cancellations and incorrect estimation of the effective activity of the ROI. Therefore, before deriving a single time-series of each ROI, we estimated the direction along the maximum power for each region by performing singular value decomposition on the orientations of dipoles within each ROI. Dipoles with the opposite direction (>90 degrees) to the estimated ROI's maximal activity vector were sign-flipped. After completing these steps, we obtained 90 broadband time-series, each representing one ROI from the AAL atlas. This pipeline was applied to each subject individually.

Network definitions for correlation analysis

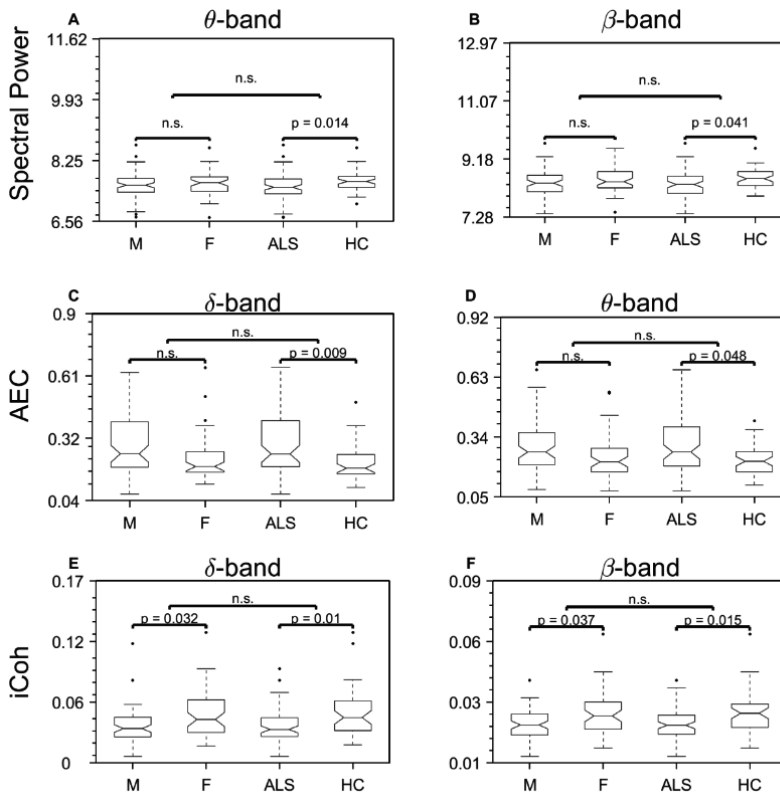
Two different anatomical atlases were used in the correlation analysis: AAL atlas for the connectivity and Destrieux atlas¹⁶ for the structural MRI analysis.

The ROI used to represent the motor network in the connectivity analysis are: L/R supplementary motor area, L/R paracentral lobule, L/R precentral gyrus and L/R rolandic operculum; whereas for the MRI analysis are: L/R paracentral gyrus and

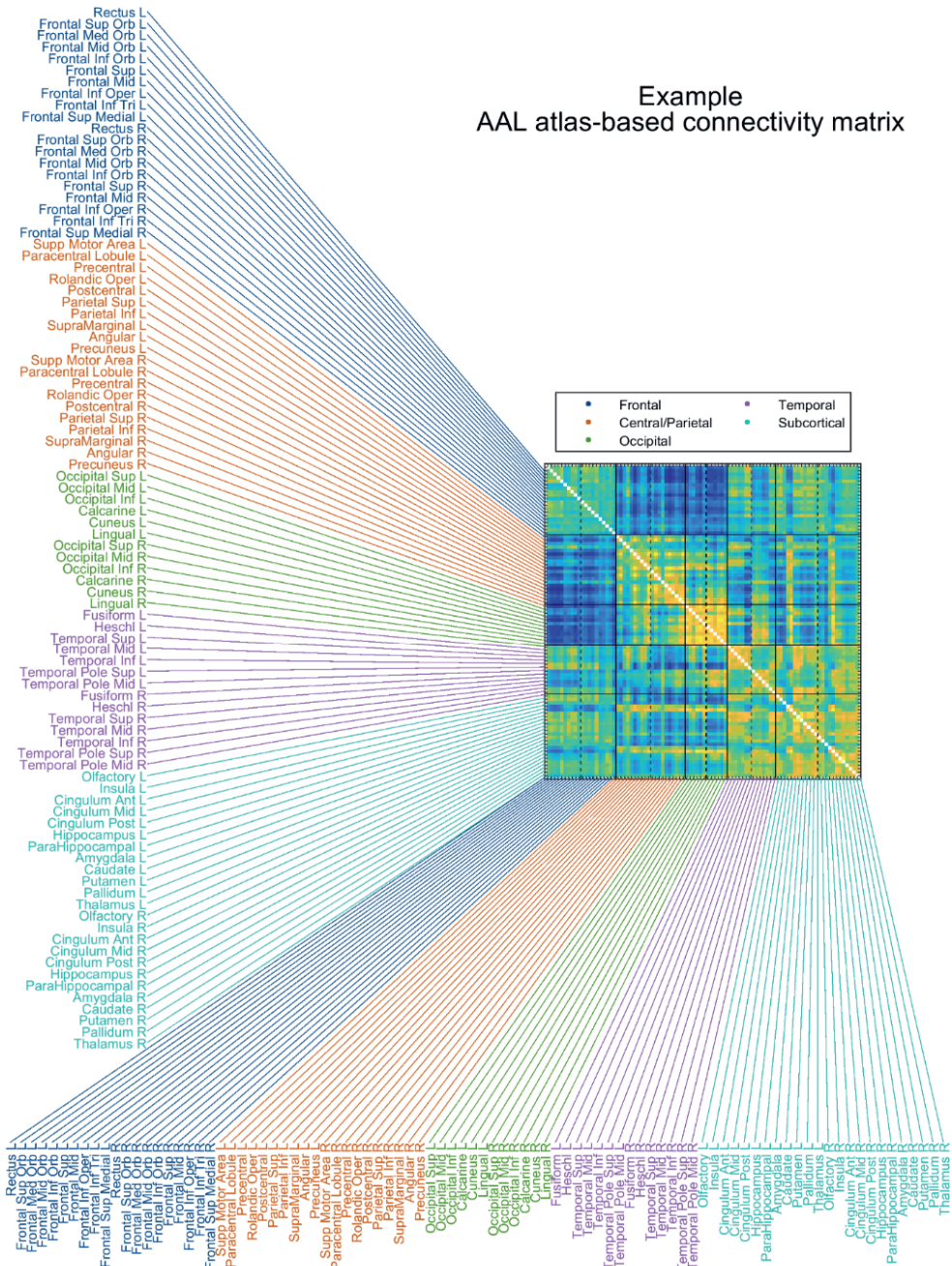
sulcus, L/R subcentral gyrus and sulcus, L/R precentral gyrus, L/R central sulcus, L/R precentral inferior sulcus and L/R precentral superior sulcus.

Similarly, ROI used to represent the frontal network in both connectivity and MRI analyses are the anterior cingulate gyrus and all the frontal regions defined by AAL and Destrieux atlases, respectively. Namely, in the former case the included ROI are: L/R anterior cingulate, L/R rectus, L/R frontal superior orbital, L/R frontal medial orbital, L/R frontal middle orbital, L/R frontal inferior orbital, L/R frontal superior, L/R frontal middle, L/R frontal inferior opercular, L/R frontal inferior triangular and L/R frontal superior medial gyri. In the latter case the included ROI are: L/R anterior cingulate gyrus and sulcus, L/R frontomarginal gyrus and sulcus, L/R transverse frontopolar gyrus and sulcus, L/R frontal inferior opercular gyrus, L/R frontal inferior orbital gyrus, L/R frontal inferior triangular gyrus, L/R frontal middle gyrus, L/R frontal superior gyrus, L/R frontal inferior sulcus, L/R frontal middle sulcus and L/R frontal superior sulcus.

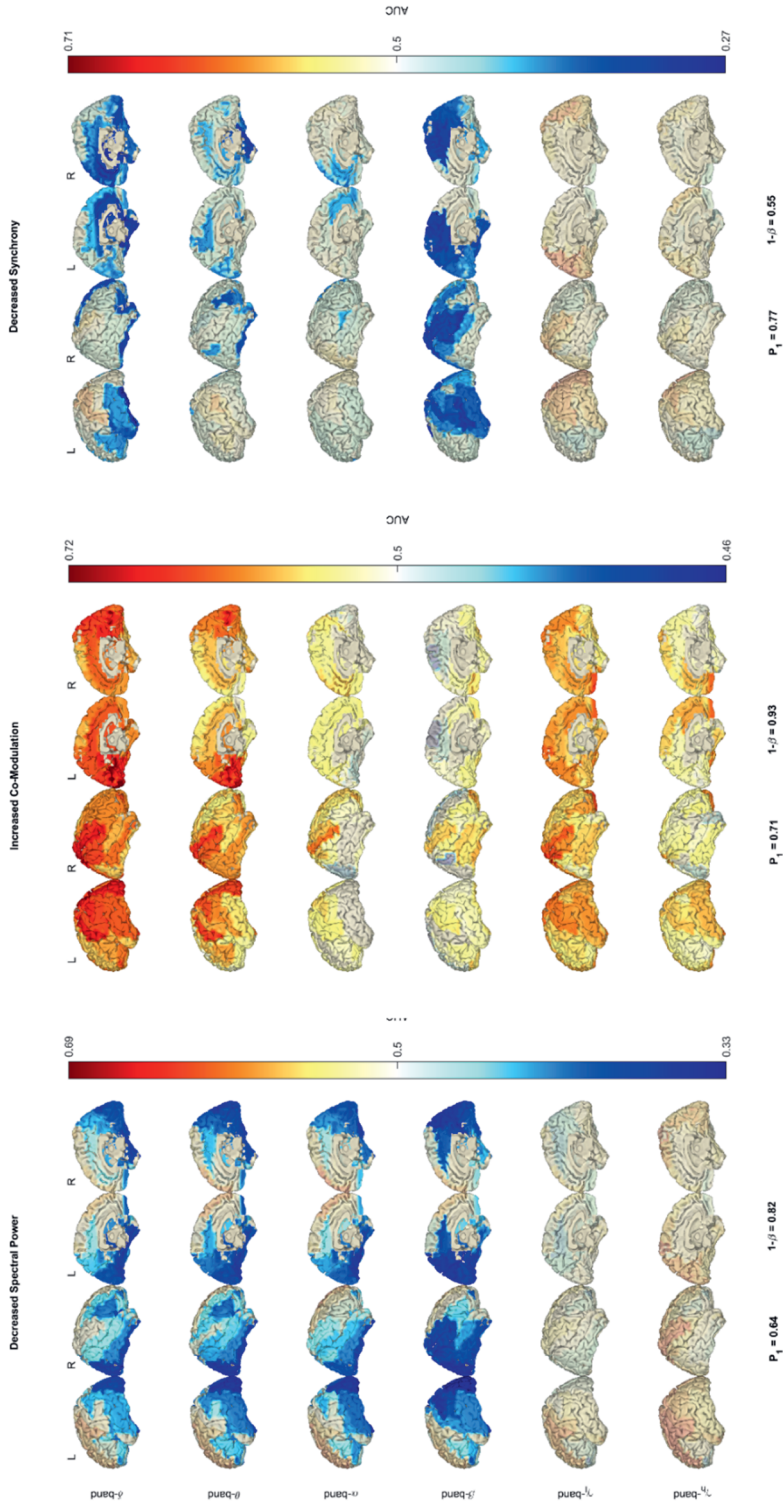
Supplementary figures



Supplementary Figure 1. The effects of gender and ALS disease in all three EEG measures in two frequency bands with the most prominent changes using 2-way ANOVA. Note that the interaction effects are not significant (n.s.) in all cases, eliminating the possibility of the gender-effect on the main findings. The statistical analysis, similar to the analysis of the ALS sub-groups, had two independent variables: gender (M/F) and group (HC/ALS). Prior to the analysis, data were transformed to standard normal distributions using the inverse normal transformation.^{17,18} Spectral power data were log-transformed for plotting purposes. The abbreviations ‘M’, ‘F’, ‘HC’ stand for Male, Female and Healthy controls, respectively.



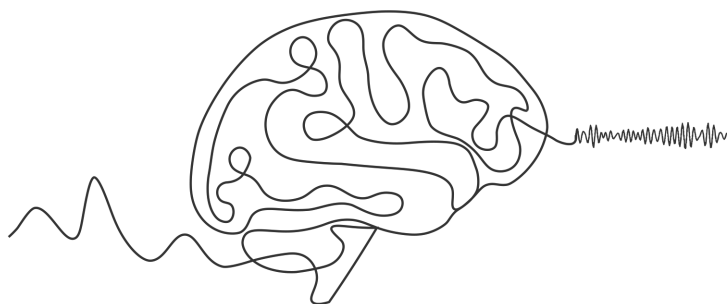
Supplementary Figure 2. An Example of an AAL atlas-based connectivity matrix. From the Automated anatomical labelling (AAL) atlas 90 brain regions (excluding those in cerebellum) were grouped and colour-coded in the following order: frontal (blue), central and parietal (orange), occipital (green), temporal (purple) and subcortical (cyan) regions. Each group has regions from the left (L) hemisphere first and then from the right (R). The same connectivity matrix organisation was used in co-modulation and synchrony figures. The figure corresponds to co-modulation in α frequency band in healthy controls.



Supplementary Figure 3. A side-by-side overview of the results from the statistical analysis of spectral power and average brain connectivity. For each measure, statistical difference between healthy controls ($n = 47$) and ALS patients ($n = 74$) was assessed across six frequency bands using Empirical Bayesian Inference with false discovery rate set to 10%. Spectral power was decreased (δ - β), co-modulation increased (mostly δ , θ and γ) and synchrony was decreased (δ - β) significantly in ALS patients. Nonsignificant findings are presented with lower opacity. AUC: Area under the receiver operating characteristic curve. Frequency bands: δ (2-4 Hz), θ (5-7 Hz), α (8-13 Hz), β (14-30 Hz) and γ (γ l: 31-47 Hz, γ h: 53-97 Hz).

References

1. Fuchs, M., Kastner, J., Wagner, M., Hawes, S. & Ebersole, J. S. A standardized boundary element method volume conductor model. *Clinical neurophysiology: official journal of the International Federation of Clinical Neurophysiology* **113**, 702–12 (2002).
2. Mosher, J. C., Leahy, R. M. & Lewis, P. S. EEG and MEG: forward solutions for inverse methods. *IEEE Transactions on Biomedical Engineering* **46**, 245–59 (1999).
3. Gramfort, A., Papadopoulos, T., Olivi, E. & Clerc, M. OpenMEEG: opensource software for quasistatic bioelectromagnetics. *BioMedical Engineering OnLine* **9**, 45 (2010).
4. Fonov, V., Evans, A., McKinstry, R., Almli, C. & Collins, D. Unbiased nonlinear average age-appropriate brain templates from birth to adulthood. *Neuroimage* **47**, S102 (2009).
5. Douw, L., Nieboer, D., Stam, C. J., Tewarie, P. & Hillebrand, A. Consistency of magnetoencephalographic functional connectivity and network reconstruction using a template versus native MRI for co-registration. *Human Brain Mapping* **39**, 104–119 (2018).
6. Jonmohamadi, Y. *et al.* Comparison of beamformers for EEG source signal reconstruction. *Biomedical Signal Processing and Control* **14**, 175–88 (2014).
7. Van Veen, B. D., Van Drongelen, W., Yuchtman, M. & Suzuki, A. Localization of brain electrical activity via linearly constrained minimum variance spatial filtering. *IEEE Trans Biomed Eng* **44**, 867–80 (1997).
8. Maronna, R. A. & Zamar, R. H. Robust Estimates of Location and Dispersion for High-Dimensional Datasets. *Technometrics* **44**, 307–17 (2002).
9. Tikhonov, A. N. & Arsenin, V. Y. *Solutions of Ill-Posed Problems*. (Halsted Pres, 1977).
10. Cheyne, D., Bostan, A. C., Gaetz, W. & Pang, E. W. Event-related beamforming: a robust method for presurgical functional mapping using MEG. *Clinical neurophysiology: official journal of the International Federation of Clinical Neurophysiology* **118**, 1691–704 (2007).
11. Oostenveld, R., Fries, P., Maris, E. & Schoffelen, J.-M. FieldTrip: Open source software for advanced analysis of MEG, EEG, and invasive electrophysiological data. *Comput Intell Neurosci* **2011**, 156869 (2011).
12. Hillebrand, A., Barnes, G. R., Bosboom, J. L., Berendse, H. W. & Stam, C. J. Frequency-dependent functional connectivity within resting-state networks: An atlas-based MEG beamformer solution. *NeuroImage* **59**, 3909–21 (2012).
13. Tewarie, P. *et al.* Predicting haemodynamic networks using electrophysiology: The role of non-linear and cross-frequency interactions. *NeuroImage* **130**, 273–92 (2016).
14. Tzourio-Mazoyer, N. *et al.* Automated Anatomical Labeling of Activations in SPM Using a Macroscopic Anatomical Parcellation of the MNI MRI Single-Subject Brain. *Neuroimage* **15**, 273–89 (2002).
15. Brookes, M. J. *et al.* A multi-layer network approach to MEG connectivity analysis. *NeuroImage* **132**, 425–38 (2016).
16. Destrieux, C., Fischl, B., Dale, A. & Halgren, E. Automatic parcellation of human cortical gyri and sulci using standard anatomical nomenclature. *NeuroImage* **53**, 1–15 (2010).
17. Beasley, T. M., Erickson, S. & Allison, D. B. Rank-Based Inverse Normal Transformations are Increasingly Used, But are They Merited? *Behav Genet* **39**, 580–95 (2009).
18. Efron, B. Size, power and false discovery rates. *The Annals of Statistics* **35**, 1351–77 (2007).



Chapter 4

EEG β -band oscillations in the sensorimotor network reflect motor symptoms severity in amyotrophic lateral sclerosis

Stefan Dukic[°], Antonio Fasano[°], Amina Coffey, Teresa Buxo, Roisin McMackin, Rangariroyashe Chipika, Mark Heverin, Peter Bede, Muthuraman Muthuraman, Madeleine Lowery, Richard Carson, Orla Hardiman[†], Bahman Nasseroleslami[†]

[°] Joint first authors

[†] Joint senior authors

Abstract

Background: Resting-state electroencephalography (EEG) holds promise for assessing brain networks in amyotrophic lateral sclerosis (ALS). However, its ability to measure motor symptom severity remains unclear. We investigated whether neural oscillations in the sensorimotor network could serve as an objective, quantitative measure of progressive motor impairment and functional disability in ALS patients.

Methods: Resting-state EEG was recorded in 18 ALS patients and 38 age- and gender-matched healthy controls. We estimated source-localised β -band spectral power in the sensorimotor cortex. Clinical evaluation included lower (LMN) and upper (UMN) motor neuron scores, ALSFRS-R score, fine motor function (FMF) subscore, and progression rate. Correlations between clinical scores and β -band power were analysed and corrected using a false discovery rate of $q = 0.05$.

Results: β -band power was significantly lower in patients than controls ($P = 0.004$). It correlated with LMN score ($R = -0.65$, $P = 0.013$), FMF subscore ($R = -0.53$, $P = 0.036$), and FMF progression rate ($R = 0.52$, $P = 0.036$).

Conclusions: β -band spectral power in the sensorimotor cortex reflects clinically evaluated motor impairment in ALS. It merits further investigation as a biomarker for progressive functional disability.

Background

Amyotrophic lateral sclerosis (ALS) is a multi-network neurological disorder with impairment in the upper and lower motor neurons, as well as in the cognitive and behavioural systems.¹ Whereas the diagnosis is primarily based on clinical examination as well as on electromyographic findings, clinical trial outcome measures rely on semi-quantitative tools, such as ALSFRS-R (amyotrophic lateral sclerosis functional rating scale revised). A consensus on ALS clinical trials has emphasised the necessity for easily measured, objective biomarkers,² which quantify the progression of specific aspects of motor or cognitive decline.

The network-based approach using neurophysiological techniques has promise in the development of biomarker candidates in neurodegenerative diseases³ including ALS.^{4,5} Spectral electroencephalographic (EEG) measures have an excellent temporal resolution as they capture electrical activity generated in the brain, whereas the limited spatial resolution can now be ameliorated using high-density EEG and source-localisation techniques.⁶ Consequently, more spatially precise and sensitive network interrogation methods can now be used in clinical settings.⁷ Biomarkers based on resting-state EEG have recently shown promise for interrogating multiple networks and for discovering complex ALS phenotypes.^{4,8}

The utility of these EEG-based measures for specific assessment of progressive motor impairment and functional disability in ALS patients, however, has not been adequately established. We hypothesised that the oscillations in the cortical sensorimotor network can quantify the severity and progression of motor symptoms in ALS. Based on previous studies,^{4,8,9} we chose the source-localised β -band spectral power in the sensorimotor network as the candidate-biomarker. The upper and the lower motor neuron (UMN and LMN) scores as well as the ALSFRS-R were used to measure motor symptoms. Here, we provide evidence that the β -band spectral power differs between ALS patients and healthy controls, and that it correlates with patients' progressive motor impairment and functional disability.

Methods

Participants

The study was approved by the Tallaght University Hospital/St. James's Hospital Joint Research Ethics Committee Dublin [references: 2014 Chairman's Action 7; 2019-05 List 17 (01)] and performed in accordance with the Declaration of Helsinki. All patients provided informed written consent, were prospectively recruited from the multidisciplinary ALS clinic based in Beaumont Hospital (Dublin, Ireland) and were all diagnosed with definite/probable/possible ALS in accordance with the El-Escorial Revised Criteria. Patients diagnosed with ALS restricted phenotypes or suffering from any other neurological condition were excluded.

Clinical assessment and motor symptom scores

Motor impairment was graded by a LMN score representing a sum of the Medical Research Council (MRC) muscle power scores in the following upper limb muscles: deltoid, triceps, biceps, wrist flexors and extensors, fingers flexors and extensors, FDI and APB;¹⁰ it ranged from 0 (severe LMN signs) to 90 (absent LMN signs) corresponding to: $9 \text{ (muscles)} \times 2 \text{ (sides)} \times 5 \text{ (max. MRC score)} = 90$. Clinical examination included deep tendon reflexes and Hoffman's sign. The UMN score was calculated by adding one point for each abnormal reflex observed¹¹ ranging from 0 (absent UMN signs) to 8 (severe UMN signs) corresponding to: $[3 \text{ (brisk reflexes)} + 1 \text{ (positive Hoffmann sign)}] \times 2 \text{ (sides)} = 8$.

Functional disability was assessed with the ALSFRS-R. The fine motor function (FMF) subscore was calculated considering four items from the scale (handwriting, cutting food and handling utensils, dressing and hygiene, turning in bed and adjusting bed clothes). ALSFRS-R progression rate was estimated as $(48 - \text{ALSFRS-R score})/\text{disease duration in months}$, while FMF progression rate was calculated as $(16 - \text{FMF subscore})/\text{disease duration in months}$. All measures were evaluated on the day of EEG recording.

EEG data acquisition and analysis

Six minutes resting-state eyes-open EEG data were acquired using the BioSemi Active Two system (BioSemi B.V., Amsterdam, The Netherlands) at the Clinical Research Facility in St. James's Hospital, Dublin. Participants were seated in a chair and asked to remain relaxed while they fixate their gaze at the letter X printed on a sheet of paper approximately 1 meter away. Source localisation was performed using the linearly-constrained minimum-variance beamformer to obtain time-varying signals originating from the brain. An atlas-based approach, based on the Automated anatomical labelling atlas, was used to estimate β -band (14-30 Hz) spectral power in six regions: left/right precentral, postcentral and paracentral areas. Spectral power was estimated using the Fourier analysis and normalised using the total power of the filtered data (1-97 Hz), and averaged using the six sensorimotor regions. For further details see Dukic et al. 2019.

Statistical analysis

Differences in demographics between groups were calculated using the Mann-Whitney U-test for age and Fisher's exact test for sex distribution differences. The Shapiro-Wilk test was used to assess the normality of the EEG and clinical data distributions. As all variables had a normal distribution, the t-test was used to assess the β -band spectral power difference between the two groups and Pearson's correlation was used to determine the relationship between β -band spectral power and UMN, LMN, FMF subscore and disease progression. In the correlation analysis with UMN scores, only those with observed UMN signs (i.e., UMN score > 0, N = 11) were included. The presented P-values are after correction for multiple comparisons using false discovery rate (FDR, $q = 0.05$). Age did not demonstrate statistical significance as a covariate, thus it was not included in the analysis.

Results

Eighteen ALS patients and 38 healthy controls were prospectively enrolled. Demographics and clinical characteristics are listed in Table 1.

The β -band power in the motor network was significantly lower in ALS patients compared to healthy participants ($P = 0.004$; Fig. 1A). The β -band power significantly correlated with patients' motor impairment as measured by the LMN score ($R = -0.65$, $P = 0.013$; Fig. 1B), where higher β -power being associated with greater muscular weakness. Moreover, the β -band power showed a significant correlation with the FMF subscore ($R = -0.53$, $P = 0.036$; Fig. 1D) and the FMF progression rate ($R = 0.52$, $P = 0.036$; Fig. 1E), where higher β -power was associated with higher functional disability and faster disease progression. Although data suggests that more severe UMN impairment is associated with lower β -power, this correlation was not significant (Fig. 1C). The presented P-values are after FDR correction.

Table 1. Demographics and clinical profiles.

	ALS	Controls	P-value
N	18	38	
Age (years)	65.75 [60.15-72.88]	66.00 [62.00-68.00]	0.60
Sex (male/female)	12 / 6	22 / 16	0.57
Site of onset (spinal/bulbar/respiratory)	14 / 3 / 1		
Disease duration (months)	21.85 [18.6-27.8]		
ALSFRS-R	36 [34-41]		
FMF subscore	12 [11-14]		
ALSFRS-R progression rate (point/month)	0.48 [0.26-0.7]		
FMF progression rate (point/month)	0.2 [0.1-0.25]		
LMN score	78 [70-84]		
UMN score (N = 11)	6 [3.25-8]		

Data are shown as median [interquartile range], except for sex and site of onset, which are shown as counts. Abbreviations: ALS = amyotrophic lateral sclerosis; ALSFRS-R = ALS functional rating scale revised; FMF = fine motor function; LMN = lower motor neuron; UMN = upper motor neuron.

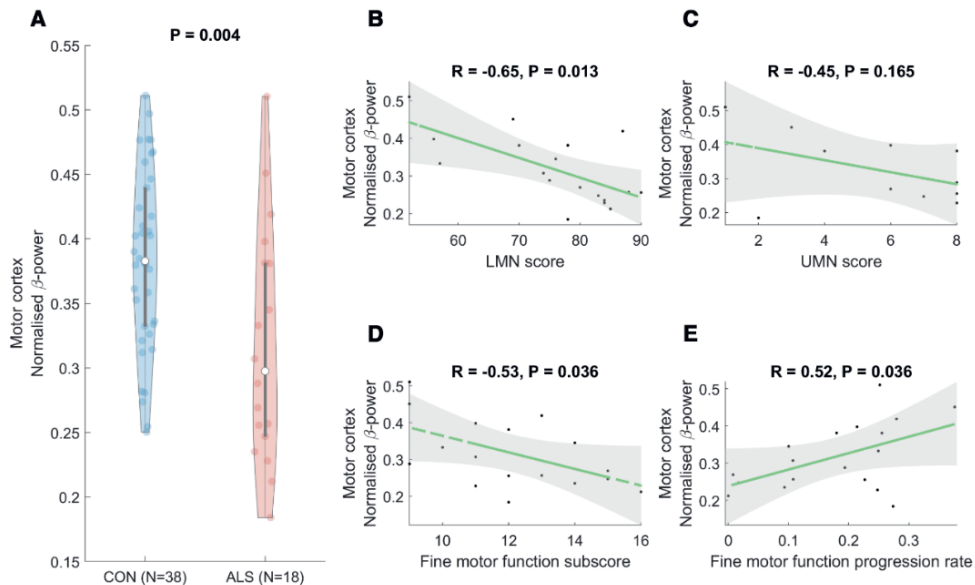


Figure 1. Normalised β -band power in the sensorimotor network is decreased in ALS patients and shows correlation with the clinical measures of motor symptom severity (LMN score), disease burden (FMF subscore) and progression. The presented P-values are after false discovery rate (FDR, $q = 0.05$) correction and the significance is considered as $P < 0.05$. Abbreviations: ALS = Amyotrophic lateral sclerosis; LMN = Lower motor neuron; UMN = Upper motor neuron.

Conclusions

In this cross-sectional study, we show that source-localised β -band power in the sensorimotor network reflects motor impairment and functional disability of ALS patients. These findings expand the previously-described use of resting-state EEG as a multi-dimensional tool for interrogating different networks and phenotyping ALS patients.^{4,8}

Confirming the previous findings^{4,5} ALS patients had a decreased source-localised β -band power in the sensorimotor network, supporting the hypothesis that β -band oscillations are pathologically affected in ALS.^{12,13} Here we have demonstrated a correlation between the β -band power and disability in ALS. These findings suggest that β -band power not only reflects cortical dysfunction but also the state of the entire motor system, encompassing UMNs, the spinal cord, LMNs, and peripheral nerves. This aligns with the notion that neural β -band oscillations are influenced by cortico-spinal projections from the motor system to muscles, indicating the activity of both motor neurons and local interneurons.

ALS patients at the group level showed lower β -band power compared to healthy controls, and we identified a trend towards a progressive increase in patients with higher motor impairment. This result is in keeping with a recent study,⁹ which showed that the median β -band power is higher in ALS patients compared to healthy controls,

when participants with more severe clinical conditions and longer disease duration are considered. As reduction in β activity is associated with an activation of the motor cortex, our findings support the notion that cortical hyperexcitability is an early feature of ALS,¹⁴ which is progressively reduced over time,¹⁵ and could explain the increasing β -band power in our results. Consistent with this, we also showed that β -band power correlates with the ALS-related progressive disability: patients with lower FMF subscore and higher rate of disease progression tended to have a higher β -band power in the sensorimotor network.

This study is limited by the relatively small, heterogeneous dataset recorded, comprising patients in different stages of disease severity and progression.⁹ Larger and longitudinal studies that include patients in wider range of disease stages, could help to better determine the evolving patterns of cortical dysfunction in the course of disease.

In conclusion, our results show that the β -band power in the sensorimotor network has potential as an accessible and quantitative EEG-based candidate biomarker of functional disability in ALS, which can be used along other EEG-based biomarkers of network dysfunction.

References

1. van Es, M. A. *et al.* Amyotrophic lateral sclerosis. *The Lancet* **390**, 2084–2098 (2017).
2. van den Berg, L. H. *et al.* Revised Airlie House consensus guidelines for design and implementation of ALS clinical trials. *Neurology* **92**, e1610–e1623 (2019).
3. McMackin, R., Bede, P., Pender, N., Hardiman, O. & Nasseroleslami, B. Neurophysiological markers of network dysfunction in neurodegenerative diseases. *Neuroimage Clin* **22**, 101706 (2019).
4. Dukic, S. *et al.* Patterned functional network disruption in amyotrophic lateral sclerosis. *Hum Brain Mapp* **40**, (2019).
5. Nasseroleslami, B. *et al.* Characteristic Increases in EEG Connectivity Correlate With Changes of Structural MRI in Amyotrophic Lateral Sclerosis. *Cereb Cortex* **29**, 27–41 (2019).
6. McMackin, R. *et al.* Measuring network disruption in neurodegenerative diseases: New approaches using signal analysis. *J Neurol Neurosurg Psychiatry* **90**, 1011–1020 (2019).
7. Babiloni, C. *et al.* Measures of resting state EEG rhythms for clinical trials in Alzheimer's disease: Recommendations of an expert panel. *Alzheimer's & Dementia* **17**, 1528–1553 (2021).
8. Dukic, S. *et al.* Resting-state EEG reveals four subphenotypes of amyotrophic lateral sclerosis. *Brain* **145**, 621–631 (2022).
9. Notturmo, F., Croce, P., Ornello, R., Sacco, S. & Zappasodi, F. Yield of EEG features as markers of disease severity in amyotrophic lateral sclerosis: a pilot study. *Amyotroph Lateral Scler Frontotemporal Degener.* **24**, 295–303 (2023).
10. de Carvalho, M., Scotto, M., Lopes, A. & Swash, M. Clinical and neurophysiological evaluation of progression in amyotrophic lateral sclerosis. *Muscle Nerve* **28**, 630–633 (2003).
11. Turner, M. R. *et al.* Evidence of widespread cerebral microglial activation in amyotrophic lateral sclerosis: an [¹¹C](R)-PK1195 positron emission tomography study. *Neurobiol Dis* **15**, 601–609 (2004).
12. McMackin, R. *et al.* Sustained attention to response task-related beta oscillations relate to performance and provide a functional biomarker in ALS. *J Neural Eng* **18**, 026006 (2021).
13. Proudfoot, M. *et al.* Altered cortical beta-band oscillations reflect motor system degeneration in amyotrophic lateral sclerosis. *Hum Brain Mapp* **38**, 237–254 (2017).
14. Menon, P. *et al.* Sensitivity and specificity of threshold tracking transcranial magnetic stimulation for diagnosis of amyotrophic lateral sclerosis: a prospective study. *Lancet Neurol* **14**, 478–484 (2015).
15. Shibuya, K. *et al.* The evolution of motor cortical dysfunction in amyotrophic lateral sclerosis. *Clinical Neurophysiology* **128**, 1075–1082 (2017).



Chapter 5

Resting-state EEG reveals four subphenotypes of amyotrophic lateral sclerosis

Stefan Dukic, Roisin McMackin, Emmet Costello, Marjorie Metzger, Teresa Buxo, Antonio Fasano, Rangariroyashe Chipika, Marta Pinto-Grau, Christina Schuster, Michaela Hammond, Mark Heverin, Amina Coffey, Michael Broderick, Parameswaran M. Iyer, Kieran Mohr, Brighid Gavin, Russell McLaughlin, Niall Pender, Peter Bede, Muthuraman Muthuraman, Leonard H. van den Berg, Orla Hardiman[†], Bahman Nasserroleslamii[†]

[†] Joint senior authors



Abstract

Amyotrophic lateral sclerosis (ALS) is a devastating disease characterised primarily by motor system degeneration, with clinical evidence of cognitive and behavioural change in up to 50% of cases. ALS is both clinically and biologically heterogeneous. Subgrouping is currently undertaken using clinical parameters, such as site of symptom onset (bulbar or spinal), burden of disease (based on the modified El Escorial Research Criteria) and genomics in those with familial disease. However, with the exception of genomics, these subcategories do not take into account underlying disease pathobiology, and are not fully predictive of disease course or prognosis.

Recently, we have shown that resting-state EEG can reliably and quantitatively capture abnormal patterns of motor and cognitive network disruption in ALS. These network disruptions have been identified across multiple frequency bands, and using measures of neural activity (spectral power) and connectivity (co-modulation of activity by amplitude envelope correlation and synchrony by imaginary coherence) on source-localised brain oscillations from high-density EEG. Using data-driven methods (similarity network fusion and spectral clustering), we have now undertaken a clustering analysis to identify disease subphenotypes and to determine whether different patterns of disruption are predictive of disease outcome.

We show that ALS patients ($N = 95$) can be subgrouped into four phenotypes with distinct neurophysiological profiles. These clusters are characterised by varying degrees of disruption in the somatomotor (α -band synchrony), frontotemporal (β -band neural activity and γ_1 -band synchrony) and frontoparietal (γ_1 -band co-modulation) networks, which reliably correlate with distinct clinical profiles and different disease trajectories. Using an in-depth stability analysis, we show that these clusters are statistically reproducible and robust, remain stable after re-assessment using a follow-up EEG session, and continue to predict the clinical trajectory and disease outcome.

Our data demonstrate that novel phenotyping using neuroelectric signal analysis can distinguish disease subtypes based exclusively on different patterns of network disturbances. These patterns may reflect underlying disease neurobiology. The identification of ALS subtypes based on profiles of differential impairment in neuronal networks has clear potential in future stratification for clinical trials. Advanced network profiling in ALS can also underpin new therapeutic strategies that are based on principles of neurobiology and designed to modulate network disruption.

Introduction

Amyotrophic lateral sclerosis (ALS) is a heterogeneous neurodegenerative disorder that primarily affects the motor system, causing varying degrees of upper and lower motor neuron dysfunction,¹ with additional involvement of extra-motor regions² presenting as cognitive and/or behavioural impairment that overlaps with frontotemporal dementia (FTD).^{3,4} The ALS population is clinically heterogeneous both in presentation and prognosis, and with variability in underlying disease pathobiology.⁵ Current clinical phenotypes are based on the predominant site of symptom onset (spinal, bulbar and respiratory), family history (sporadic and familial) and relative degree of upper and lower motor neurone involvement (lower and upper motor predominant). In addition, ALS patients are often categorised on the basis of their survival period (short, average and long).⁵ Quantitative measurements that correlate with the clinical subgroups have been sought using structural and functional MRI,⁶ PET^{7,8} and neurophysiological (EEG and EMG) data.^{9–12}

Additional refinements in clinical phenotyping in ALS include the interrogation of behavioural subphenotypes¹³, data from early clinical consultation to determine ranges of survival probability¹⁴ and genomic characterisation. At least 30 identified genes and three main pathophysiological processes (i.e. RNA biology, protein turnover, and axonal transport) have been associated with ALS.¹⁵ Taken together, these observations, along with the absence of a clear correlation between ALS-associated genes, and highly distinctive molecular neuropathological and clinical subtypes,¹⁶ provide evidence that ALS can no longer be considered as a single disease with a singular pathophysiology and clinical course.

Current imaging and neurophysiology evidence suggests that differential disruption of neural networks, underpinned by biological pathology and genetic factors,^{17,18} is likely to reflect heterogeneous clinical presentations. This heterogeneity cannot be fully discerned using existing clinical tools, such as the ALS functional rating scale revised (ALSFRS-R),¹⁹ which measures motor decline, and the Edinburgh cognitive and behavioural ALS screen (ECAS),²⁰ which screens for cognitive and behavioural change.²¹ Though validated as a primary outcome measure in clinical trials, the ALSFRS-R is ordinal, semi-quantitative and the subscales within the instrument are subject to floor and ceiling effects.²²

Technological improvements in neuro-electro-physiological measures, and more specifically EEG, can provide additional insights into functional changes associated with different neurodegenerative diseases at a network level.²¹ Using this approach with task-based paradigms, we have shown changes implicating dysfunction of the frontoparietal network.^{9,23,24} Furthermore, we have shown that resting-state EEG, which can provide distinct measures that reflect different processes in the brain,²⁵ can quantitatively capture both motor and cognitive networks affected in ALS. More specifically, using sensor-space analysis, we have found resting-state EEG changes that are correlated with structural changes in MRI¹⁰ and in line with other EEG studies.^{26–28} In a follow-up study using advanced source-space analysis, we further delineated

dysfunctional networks and corroborated the findings with both structural MRI and clinical data.²⁹

Here, we hypothesise that patient subgroups can be identified based on patterns of network disruption that could be used to reveal potentially different responses to therapy and thus, should be monitored and studied as complementary profiling measures. We show how the EEG measures of activity and connectivity in the brain networks provide the information for forming stable clusters of ALS patients and the distinct neurophysiological profiles associated with these patient clusters.

Methods

Ethical approval

Approval was obtained from the ethics committee of Beaumont Hospital, Dublin, Ireland (reference: 13/102) and the Tallaght Hospital / St. James's Hospital Joint Research Ethics Committee (reference: 2014 Chairman's Action 7) for St James's Hospital, Dublin, Ireland. The experimental procedure conformed to the Declaration of Helsinki. All participants provided written informed consent before taking part in the experiments.

Participants

Patient recruitment

Patients with ALS were recruited from the National ALS clinic in Beaumont Hospital Dublin. Healthy controls included neurologically normal, age-matched individuals recruited from an existing population-based control bank.

Inclusion criteria

All ALS patients were within the first 18 months from diagnosis and fulfilled the revised El Escorial diagnostic criteria for Possible, Probable or Definite ALS.³⁰ All patients underwent cognitive screening and were classified according to the revised Strong Criteria.³¹

Exclusion criteria

Patients diagnosed with primary lateral sclerosis, progressive muscular atrophy, flail arm/leg syndromes, prior transient ischemic attacks, multiple sclerosis, stroke, epilepsy, seizure disorder, brain tumours, structural brain abnormalities, other neurodegenerative conditions and other medical morbidities, such as human immunodeficiency virus, were excluded.

The demographic profiles

A total of 95 ALS patients: 70 with spinal onset (m/f: 52/18; mean \pm standard deviation age: 59 \pm 12 years), 21 patients with bulbar onset (m/f: 14/7; age: 60 \pm 11) and 4 patients with respiratory onset (m/f: 3/1; age: 62 \pm 4) were included, along with 77 healthy

controls (m/f: 29/48; age: 60 ± 11). Five patients (m/f: 2/3; age: 70 ± 9) were diagnosed as ALS-FTD (based on the Strong criteria)³¹ and 11 patients (m/f: 6/5; age: 61 ± 6) had the hexanucleotide repeat expansion in the *C9orf72* gene. Patients and controls were matched for age (Mann-Whitney U-test, $p = 0.73$), but not for gender (Fisher's exact test, $p < 0.001$).

Experiment

Experimental paradigm

The experiment was resting-state with eyes open, divided into three 2-minute recording blocks, allowing for rest between blocks and to ensure patients remained awake. Subjects were seated in a comfortable chair, asked to relax, while they fixated their gaze at the letter X (6 cm × 8 cm) printed on an A4 sheet of paper placed approximately 1 m in front of them.

EEG data

EEG data with 128 channels were collected using the BioSemi Active Two system (BioSemi B.V., Amsterdam, The Netherlands) and sampled at 512 Hz, after a lowpass anti-aliasing filter (0-104 Hz) was applied by the acquisition hardware. Additional filtering was applied during the analysis. Recordings were conducted in a dedicated laboratory with a Faraday cage isolation at St. James's Hospital, Dublin. Besides the initial recording session for 95 ALS and 77 healthy controls, 36 ALS patients had one follow-up EEG session after 4-6 months.

Disease severity and neuropsychology data

The scores from ALSFRS-R ($N = 88$)¹⁹, ECAS ($N = 72$)²⁰ and Beaumont behavioural inventory (BBI, $N = 87$)³² were used to provide clinical profiles of clusters based on neurophysiological patterns. All clinical subscores were either normalised or standardised: ALSFRS-R subscores were normalised by dividing by the maximum possible value in each subscore and subtracting it from one; ECAS subscores were z-score standardised using age and education matched normative data from an Irish population^{33,34} and multiplied by minus one; and BBI score was normalised by dividing by the maximum possible value. This ensured that all subscores had the same direction of change, wherein an increased subscore means an increased impairment in the corresponding function.

In addition to this, King's staging ($N = 84$)³⁵ which assesses the disease burden in patients in stages from one (single region involved) to four (ventilatory support and/or gastrostomy), was used.

Data analysis

EEG data

The preprocessing and processing procedures were identical to those described in our cross-sectional study²⁹. Briefly, we have applied the linearly constrained minimum

variance beamformer³⁶ on the bandpassed (1-97 Hz) EEG data to obtain time-varying signals originating from 90 brain regions (excluding the cerebellum) based on the automated anatomical labelling atlas (see Supplementary Note 1).³⁷ Using the 90 source-reconstructed signals, we estimated normalised spectral power (w.r.t total spectral power), co-modulation (amplitude envelope correlation) and synchrony (imaginary coherence). Spectral power was estimated for each region, while co-modulation and synchrony were estimated between all pairs of brain regions resulting in a 90×90 symmetrical connectivity matrix, wherein 4005 (90×89/2) connectivity features were unique. All three measures were estimated in six frequency bands: δ (2-4 Hz), θ (5-7 Hz), α (8-13 Hz), β (14-30 Hz) and γ (γ_l : 31-47 Hz, γ_h : 53-97 Hz). The analysis resulted in three groups of EEG features: spectral power (90×6 = 540 features), co-modulation (4005×6 = 24030) and synchrony (24030). This analysis was applied on both healthy control and ALS data (see Supplementary Note 1).

Clustering

Without prior knowledge of the EEG features that distinguish one ALS patient from the other, an unsupervised clustering approach was chosen and applied on all available EEG features. First, the similarity network fusion (SNF) method³⁸ was used for combining and preparing the high-dimensional dataset and subsequently the spectral clustering³⁹ was used for inference of the clusters.

For preparation of the data before the clustering, each EEG feature was z-scored. Three patient similarity matrices (one for each group of EEG features) based on the Euclidean distance, were constructed with multiple Gaussian kernels⁴⁰ and fused into one similarity matrix using the SNF method. The SNF method iteratively updates each matrix with the information from the other matrices, thus fusing in the complementary information. To ensure that the irrelevant associations between patients emerging from the accumulated noise over many features are removed, the fused similarity matrix was denoised using the network enhancement method.⁴¹ Finally, subgrouping of patients was undertaken using spectral clustering.³⁹ For additional information, see Supplementary Note 2. This clustering pipeline was selected based on the non-parametric and robust nature of these methods pertinent for clustering, especially in combining the EEG measures, which served to avoid finding clusters that heavily depend on specific mathematical assumptions or individual data values.

Statistical significance of clusters

The optimal number of patient subgroups ($k = 2, \dots, 7$) was chosen using a statistical approach applied on the eigengap and rotation cost indices,⁴² which are based on the eigenvalues and eigenvectors in the spectral clustering method, respectively. The biggest eigen gap and the smallest rotation cost indicate the optimal number of clusters in the dataset (see Supplementary Note 3).

Taking a conservative approach, a statistical procedure that tests whether the two indices are likely to give such high (eigengap) and low (rotation cost) values under null hypothesis of no actual clusters in data (i.e. homogenous data) was applied. In our Monte-Carlo procedure, the null hypothesis was that the data come from the same

dataset but with randomly permuted values within each EEG feature. The clustering was performed on the permuted dataset and the two indices were calculated. This procedure was repeated 5000 times to obtain the empirical null distributions and the p-values.⁴³ In addition to this, bootstrapping was used to estimate the non-null distribution of the indices, statistical power at $\alpha = 0.05$ ($1 - \beta_{0.05}$) and Cliff's delta (a non-parametric measure of effect size).⁴⁴ All the statistical measures were calculated for each clustering solution, $k = 2, \dots, 7$.

Neurophysiological profiles

For each participant, 90 'EEG networks' were defined based on the networks that are known to be activated at rest⁴⁵ and affected in ALS.^{9,29,46,47} Namely, the 90 networks were constructed by separately averaging spectral power, co-modulation and synchrony in five anatomical networks (somatomotor, frontotemporal, frontoparietal, default mode and salience) and in six frequency bands ($3 \times 5 \times 6 = 90$, see Supplementary Note 4). For each combination (i.e. 'EEG network') an AUC (area under the curve of the receiver operating characteristics curve) was used to make the comparison between each ALS cluster and the control data. To further infer statistical significance in the multidimensional space and to control for multiple comparisons ($q = 0.1$, false discovery rate, FDR)²⁹, empirical Bayesian inference (EBI)⁴³ was applied on the AUC test statistics. This statistical tool exploits both the original (non-null) observations and null-permuted data to estimate the probability density function of the data and null, respectively.

The obtained AUC values were then used to determine brain networks that are strongly and exclusively associated with each of the identified clusters. An EEG network was considered as a potential and exclusive characteristic of a cluster if it was statistically significant compared to controls, and unique or directionally opposite in its change compared to other clusters (see Supplementary Note 4). Here, we reported the most characteristic EEG network that is affected for each cluster. Additionally, for each EEG network, the statistical difference between clusters (χ^2 -statistic, Kruskal-Wallis one-way analysis of variance) was tested, while accounting for multiple comparisons ($q = 0.05$, FDR)^{48,49}, and a Monte-Carlo permutation procedure was applied to estimate the associated statistical power ($1 - \beta_{0.05}$).

Additionally, complete brain maps for each EEG measure and frequency band were obtained in a similar manner using AUC and EBI between each cluster and the control data. These maps were then masked using p-values from Kruskal-Wallis one-way analysis of variance to distinguish the EEG abnormalities that are shared by all identified clusters and those specific to each cluster.

Clinical profiles

Clinical profiles of subgroups were compared using the subscores of motor (ALSFRS-R), cognitive (ECAS) and behavioural (BBi) dysfunction. Significant difference of scores across the clusters was tested using Kruskal-Wallis one-way analysis of variance. In addition to this, associations between the identified EEG clusters and known clinical factors (type of initial diagnosis, site of disease onset and *C9orf72* gene status)

that could influence our findings were tested using the Fisher's exact test. Survival probability was analysed using the Kaplan-Meier method, wherein patients that were alive at the time of analysis were right-censored and survival was measured from the time of the reported symptom onset. Logrank test was used for testing of the difference between the survival curves.

Cluster validation

For a reliable interpretation of the derived clusters, we have assessed the accuracy, robustness and stability of clusters mathematically as well as experimentally. Specifically, four validation approaches were implemented using: a different clustering method (the Louvain method for community detection)⁵⁰, a classification approach, and by inspecting the re-assignment of patients under small perturbations of data and when using a single follow-up EEG assessment (after 4-6 months following the initial session, $N = 36$ ALS patients). These validation methods are detailed in Supplementary Note 5.

Clustering using clinical data

To assess whether the derived EEG clusters simply recapitulate the subtypes that can be derived directly from the clinical data, the clustering procedure was applied on $N = 60$ patients with the complete clinical dataset. A fused similarity matrix was constructed from three similarity matrices based on 12 ALSFRS-R, 5 ECAS and 1 BBI subscores ($N = 18$ subscores in total). The optimal number of clusters was determined using the statistical approach as in the main analysis. Furthermore, the accuracy and the robustness of the clustering solution was evaluated using the same procedures that are described above.

Additionally, for comparison with our identified EEG clusters, we inspected the clinical profiles of ALS subgroups that are based on four stages of the King's staging system.

Results

EEG measures identify four clusters of ALS patients

Four distinct clusters were identified based on analysis of spectral EEG patterns of neural activity and connectivity. As assessed by eigengap and rotation cost indices (Fig. 1), the solution of four clusters had high statistical power (0.85 and 0.52, respectively) and a large to medium (0.92 and 0.69, Cliff's d , respectively) effect size, suggesting reproducible findings. The demographics of the identified clusters is shown in Table 1.

Table 1. Breakdown of cluster characteristics.

Group	N	Gender (m/f)	Age (years)	Disease duration (months)	Site of onset (S/B/T)	Diagnosis (ALS/ ALS-FTD)	C9orf72 (+/-)
ALL	95	69/26	59.2±11.6	21.9±17.5	70/21/4	90/5	11/84
Cluster 1	23	14/9	61.0±12.7	21.3±16.8	17/5/1	23/0	0/23
Cluster 2	28	22/6	56.6±13.0	25.7±24.3	23/2/3	28/0	3/25
Cluster 3	19	14/5	58.5±11.5	17.8±8.9	14/5/0	16/3	2/17
Cluster 4	25	19/6	60.7±9.0	22.8±20.2	16/9/0	23/2	6/19

Disease duration: time interval between the estimated symptom onset and the EEG recording; *Site of onset*: Spinal/Bulbar/Thoracic; *C9orf72*: presence (+) or absence (-) of the repeat expansion in the chromosome 9 open reading frame 72; *Age and disease duration*: mean ± standard deviation.

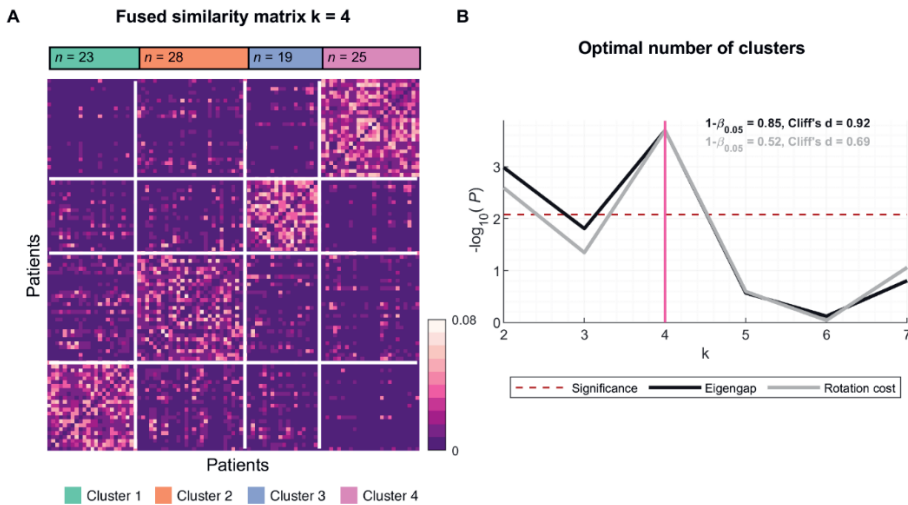


Figure 1. EEG measures identify four ALS clusters: Fused similarity matrix and the optimal number of ALS clusters. (A) Fused similarity matrix of ALS patients is sorted based on the clusters, which were identified using spectral clustering; (B) At $k = 4$, both measures reflecting the optimal number of clusters (eigen gap, black; rotation cost, grey) reach the highest significance ($p < 0.008$, Bonferroni corrected; red dashed line) with statistical power ($1-\beta_{0.05}$) 0.85 and 0.52, and effect size (Cliff's d) 0.92 and 0.69, respectively. The number of patients in cluster 1-4 is $N = 23, 28, 19$ and 25.

EEG clusters show distinct neurophysiological profiles

Analysis of neurophysiological profiles of the four clusters based on EEG measures revealed evidence of distinctly impaired neural networks for each cluster (Fig. 2). For example, cluster 1 shows a characteristic increase in β -band spectral power in the frontotemporal network, whereas the clusters 3 and 4 show decreased power in the same network. Similarly, cluster 2 shows a characteristic increase in α -band synchrony in the somatomotor network, cluster 3 decrease in γ_1 -band synchrony in the frontotemporal network and cluster 4 increase in γ_1 -band co-modulation in the frontoparietal network. The Kruskal-Wallis one-way analysis of variance showed that the four networks vary significantly across clusters ($p < 0.001$, FDR). The EEG abnormalities associated with all four clusters were identified as increased co-modulation (δ - to α -band oscillations) and decreased synchrony (δ - to β -band) in the somatomotor and frontotemporal brain regions (see Supplementary Fig. 1).

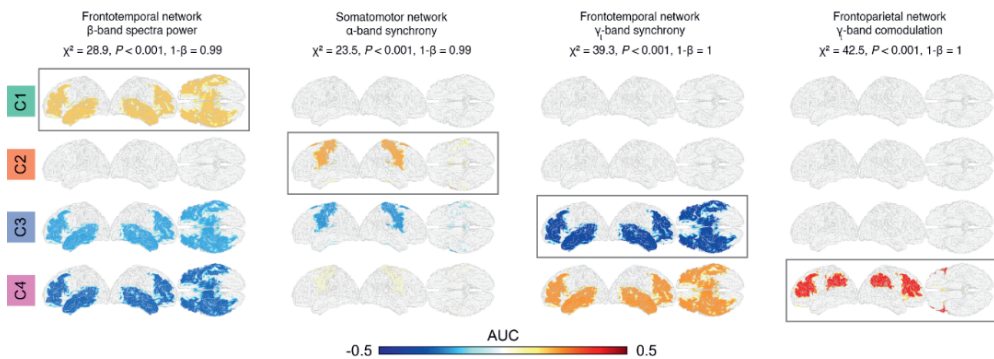


Figure 2. Distinct neurophysiological profiles of ALS clusters. For each cluster, a unique neurophysiological change (brain network, frequency band and EEG measure) was identified using AUC statistics estimated between the ALS clusters and control data (see Supplementary Note 4). The networks vary significantly across clusters in all four cases (Kruskal-Wallis one-way analysis of variance, $p < 0.001$, FDR). The potential effects of age and gender on the identified changes were rejected based on the linear model analysis (see Supplementary Note 6). AUC: Area under the receiver operating characteristic curve centred around zero; positive values indicate an increase, whereas negative values indicate a decrease compared to healthy controls.

EEG clusters have concordant clinical and neurophysiological profiles

The analysis of clinical profiles using the functional scores shows clinical characteristics of each cluster (Fig. 3A-B, see also Supplementary Fig. 2). Although none of the clinical scores vary significantly across the clusters ($p > 0.05$, FDR), the changes are concordant with altered neurophysiological profiles. More specifically, cluster 1 (which has a uniquely increased β -band spectral power in the frontotemporal network) shows moderate limb and mild verbal fluency, executive and memory dysfunction, but no apparent change in the language domain; cluster 2 (which has a uniquely increased α -band spectral power in the somatomotor network) is characterised by mild impairment of limb and verbal fluency, and moderate language and memory impairment, with preservation of executive domain; cluster 3 (which has a uniquely decreased γ_1 -band synchrony in the frontotemporal network) was characterised by

marked impairment of limb, language and verbal fluency; cluster 4 (which has a uniquely increased γ_1 -band co-modulation frontoparietal network) was primarily characterised by impairments in bulbar function, verbal fluency, executive and memory. None of the clusters has notable impairment in the visuospatial domain, whereas all but cluster 2 exhibited mild aspects of behavioural impairment.

In addition to clinical subphenotypes, the clusters were associated with significant differences in overall survival (Logrank $\chi^2 = 13.84$; $p = 0.003$). The survival probability curves (Fig. 3C) show that cluster 4 has the shortest survival (median: ~ 3 years), whereas cluster 2 has the longest survival (~ 6 years).

Although the associations between the clusters and commonly-used clinical stratification parameters (type of initial diagnosis, site of disease onset and *C9orf72* gene status; Fig. 3D-F) are not significant ($p > 0.05$, FDR), the results are consistent with clinical profiles of clusters. Specifically, cluster 3 and 4 (which have the greatest degree of impairment across most cognitive subscores; Fig. 3B) included all patients with the initial diagnosis of ALS-FTD (3/19 and 2/25; ALS-FTD/total). Furthermore, cluster 4 has the highest proportion of *C9orf72*-positive patients (6/25), compared to cluster 2 and 3 (3/28 and 2/19).

There were no significant between-group differences in disease duration, King's staging, age, gender or riluzole usage, which could have affected EEG measures and the reported results (Supplementary Fig. 2). Additionally, we demonstrated that King's staging cannot explain the clusters identified by EEG networks nor how the progression patterns differ in the EEG clusters (Supplementary Fig. 3). The potential effects of age and gender on the identified changes in neurophysiological profiles were tested and rejected based on the linear model analysis (see Supplementary Note 6).

Patient clusters show stability across multiple tests

Further analysis revealed that each cluster has high accuracy, robustness and remained stable at re-assessment. Specifically, the clustering solution based on the Louvain community detection method converged to the same number of clusters ($k = 4$) and had a very high overlap with the spectral clustering solution from the main analysis, wherein only seven patients were assigned differently. Furthermore, the estimated clustering accuracy reached 89%, and the analysis of robustness showed that in the presence of data perturbation 82% of the cluster labels remain stable (both tests are conservatively quantified by the average adjusted Rand index, which controls for chance level). Lastly, using the longitudinal dataset ($N = 36$, with one follow-up EEG measurement 4-6 months after the initial recording session), the overall cluster (re)assignment is 72% ($p < 0.001$, Fisher's exact test; Fig. 4), showing an experimental stability of the discovered clusters.

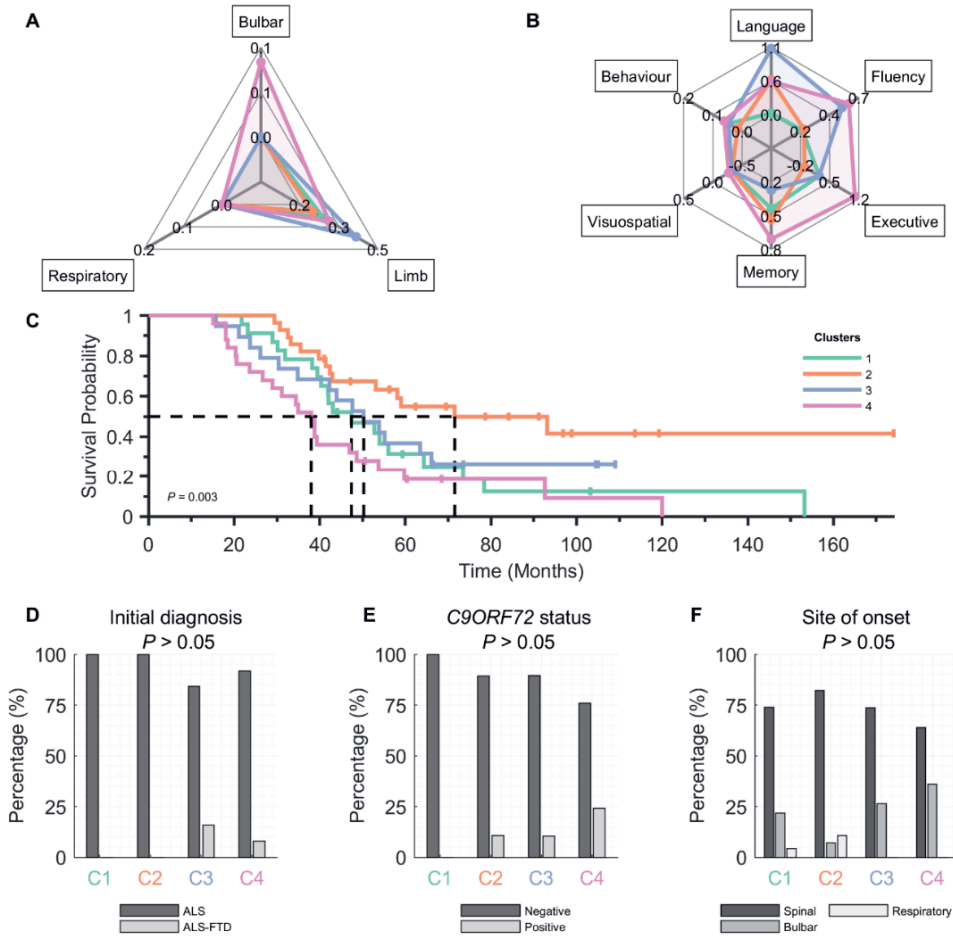


Figure 3. Clinical profiles of ALS clusters derived from EEG measures are concordant with the neurophysiological profiles. The four EEG clusters (colour-coded) suggest different trends in functional/clinical scores in different domains: (A) Normalised ALSFRS-R (bulbar, limb and respiratory) and (B) z-scored ECAS (language, fluency, executive, memory and visuospatial) and normalised BBI (behaviour) score are all non-significant ($p > 0.05$, FDR); (C) Kaplan-Meier survival curves corresponding to the ALS clusters; (D-F) Clinical characteristics. Clinical subscores (A-B) are all normalised or standardised, see Methods section. Note that there are in total: five ALS-FTD, 11 C9orf72-positive and four respiratory-onset patients. Statistical tests: Kruskal-Wallis one-way analysis of variance (A-B), logrank test (C) and Fisher’s exact test (D-F); all FDR corrected.

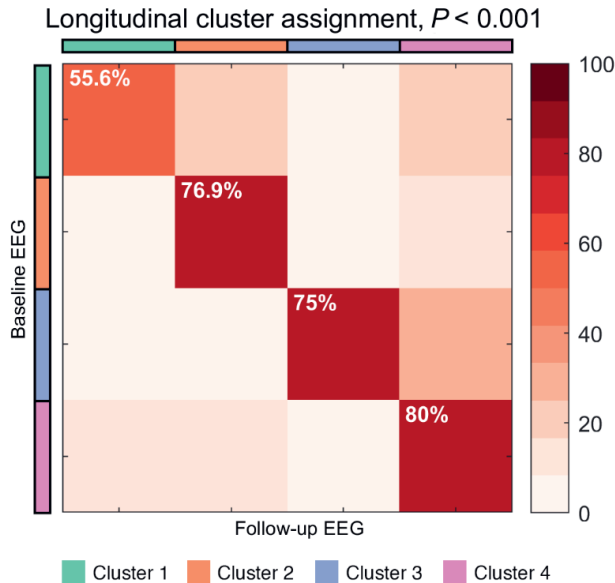


Figure 4. Clusters show high stability at re-assessment. The overall stability is 72% and statistically significant ($p < 0.001$, Fisher's exact test). Total number of patients with a follow-up (mean \pm standard deviation: 5.1 ± 1.8 months after the initial recording session) is $N = 36$, wherein 9, 13, 4 and 10 patients belong to cluster 1-4, respectively.

Clustering based solely on clinical data does not identify stable subgroups

Using the same methodology, all the clinical measures were combined and underwent statistical analysis of the indices that estimate the optimal number of clusters. No significant clusters were identified, demonstrating that commonly-applied clinical determinants were not driving the neurophysiological clustering data (see Supplementary Note 7 and Supplementary Fig. 4).

Discussion

We have shown that analysis of network disturbance using multi-dimensional quantitative EEG can identify subgroups within ALS that are not discoverable using standard clinical assessment tools. Each of the subgroups, identified by data-driven clustering, demonstrates a distinct neurophysiological profile that in turn recapitulates a different combination of clinical attributes. These neurophysiological profiles are stable at re-assessment and are associated with different prognostic outcomes.

Identified EEG clusters characterise distinct brain network impairments

Clinical heterogeneity has emerged as a major obstacle in understanding the pathophysiology of neurodegenerative diseases. This has implications for drug development as clinical stratification parameters remain relatively insensitive as predictors of

disease progression and survival. While it is not surprising that the network disruptions that characterise our identified clusters do not strongly correlate or overlap with the commonly-defined clinical phenotypic subtypes of disease, our results are in alignment with the observations from previous studies. For instance, cluster 4 in this study has the highest proportion of patients with *C9orf72* expansion, which is known to implicate frontotemporal, temporoparietal and subcortical MRI^{6,51} and EEG⁹ changes, and is frequently associated with cognitive and behavioural impairment.⁵² Accordingly, in our study the neurophysiological profile of this cluster is characterised by the distinctive abnormal changes in γ_1 -band co-modulation within the frontoparietal network (also commonly known as central executive network), while the clinical profile of this cluster shows marked dysfunction in the verbal fluency, executive and memory domain. Similarly, this cluster has the highest proportion of bulbar patients, in which MRI studies have shown extensive thinning in frontotemporal, temporoparietal and subcortical brain regions.⁶ Furthermore, while cluster 4 has the highest proportion of patients with *C9orf72* expansion, which is associated with both ALS and FTD, cluster 3 and 4 include all the ALS-FTD patients. Consistent with other studies,⁵³ these two EEG phenotypes show the lowest survival probability in our analysis. Considering the presence of notably increased dysfunction in cognitive and behavioural profile of these two clusters, these ALS patients are likely to have clinical features that align with the FTD-side of the ALS-FTD spectrum.³¹ Interestingly, *C9orf72* patients did not form one separate cluster, suggesting diverging network impairments caused by the same genetic mutation. These findings confirm a complex and heterogeneous nature of the variables (e.g. gene mutation status and presence/absence of FTD) currently used in ALS classification systems. By contrast, subphenotypes derived from EEG measures transcend traditional classification systems of ALS patients and characterise distinct brain networks affected in each subgroup.

Our findings are consistent with previous neuro-electro-magnetic studies in ALS. For example, a recent resting-state magnetoencephalography (MEG) connectivity study reports increased broadband co-modulation in the posterior parts of the brain.⁵⁴ Additionally, studies investigating brain network topology using graph theory, showed diverging MEG γ -synchrony (as assessed by phase lag index)⁵⁵ affecting global brain patterns⁵⁶ and increased EEG γ -synchrony (as assessed by partial directed coherence)⁵⁷ patterns in the frontal networks.⁴⁶ These resting-state findings are in line with the identified connectivity patterns in cluster 3 and 4.

The neurophysiological profiles of cluster 1 and 2 point to the characteristic changes in the β -band frontotemporal and α -band motor network respectively, whilst the corresponding clinical subscores in the language, verbal fluency and motor domains indicate relative preservation of these functions. These abnormal network activations could be attributed either to the topological resilience or active compensation mechanisms that are unique to each cluster,^{58,59} or likely, to subtle impairments to which current clinical tools are not sufficiently sensitive.⁶⁰⁻⁶²

Our work emphasises that not all cluster-specific patterns may be identifiable when ALS patients are compared to controls as a single group. This is due to the difference in the patterns of impairment between different clusters. The identified β -

band power changes suggest two diverging patterns, which could explain the contradictory findings between an MEG study⁶³ that reported an increased cortical β -desynchronisation in ALS patients and EEG studies that reported decreased²⁷⁻²⁹ or no difference.⁶⁴ Additionally, the findings in resting-state studies investigating brain network topology using graph theory, show globally-increased EEG α -synchrony (as assessed by partial directed coherence)⁴⁶ and increased α -band co-modulation mostly in the central brain regions.⁶⁵ Furthermore, our findings support the relevance of γ -oscillations in ALS (see Supplementary Note 8).

Clinical relevance

We have shown that clusters based on patterns of disruption in brain networks are associated with reproducible aggregates of clinical attributes and rate of disease progression, confirming the clinical relevance of our findings. EEG-based subphenotypes with superior statistical power do not recapitulate phenotypes that can be found using clinical data or burden of disease (e.g. King's staging). This indicates that these neurophysiologic patterns provide additional information to that which is discerned by clinical evaluation alone. The EEG-based clusters are statistically robust with distinct patterns, whereas the clinical scores alone could not form meaningful significant clusters. A more in-depth analysis that further explores associations between EEG and clinical observations, would require larger and detailed clinical and genomic datasets.

The identification of such stable subtypes with high statistical power has significant biological and clinical implications. Our findings could contribute to modification of the existing stratification system, which is purely based on the clinical observations. In fact, simulated analysis resulting in high classification accuracy (89%) of new patients – where individual patients are classified to clusters – suggests the potential of our clustering approach to render clinically meaningful findings on an individual patient level. While the underlying neurobiological processes that determine these patterns or network disruption cannot be discerned at this point, the stability of the clusters could reflect pre-morbid patterns of network function and integrity.

Analysis of cluster stability using follow-up data shows that for many patients in our dataset the cluster assignment does not change. This stability further supports that our findings are based on characteristic pathological changes that are reasonably stable over a period spanning several months. Notwithstanding, future studies with more systematic inclusion of the disease stages and the analysis of longitudinal evolution of clusters (over multiple follow-ups) are warranted.

Limitations

This study is limited by its single-site nature. Alternative solutions with more than four clusters are likely to exist, especially if additional more sophisticated neurophysiological measures are included in the clustering analysis. Notwithstanding these limitations, our conservative validation analyses of clustering solutions show that the findings are both robust and reproducible.

Translation of our findings into a clinical setting will require medical-grade equipment with equal or lower number of EEG electrodes (e.g. 32 or 19 from the 10-20

system), which warrants an additional validation study. While this could reduce the preparation time, it should be approached with caution.⁶⁶ Studies showed that electrode arrays with less than 32 sensors lead to severe mislocalisations.⁶⁷ Moreover, our neurophysiological profiles include γ -band findings, and in this context, decreasing the number of electrodes might have a negative effect on our ability to capture these oscillations.^{68,69} Nevertheless, since localisation accuracy starts to plateau from 64 channels,^{67,70} a medical grade 64-channel system could be considered as a candidate for future translational steps.

Conclusion

Our findings have shown for the first time that EEG measures of neural activity and connectivity can be used to reproducibly group ALS patients into subphenotypes with distinct clinical patterns and neurophysiological signatures. Replication of our findings in an independent population with additional clinical and genomic data will be required to further understand the neurobiological factors that underpin these different patterns of network disruption. The demonstration that each cluster is associated with a different disease trajectory and outcome opens a new path towards the discovery of quantitative biomarkers of disease heterogeneity.

Taken together, our results highlight the strengths of using EEG data in identifying ALS subtypes, which have distinct clinical and neurophysiological profiles. The identification of data-driven ALS subtypes based on patterned changes in neuronal networks can facilitate the identification of targeted therapies that are effective across the subtype. The development of reliable biomarkers to identify subtypes will also provide much needed prognostic information for patient stratification.

References

1. Hardiman, O., Van Den Berg, L. H. & Kiernan, M. C. Clinical diagnosis and management of amyotrophic lateral sclerosis. *Nat Rev Neurol* **7**, 639–49 (2011).
2. van Es, M. A. *et al.* Amyotrophic lateral sclerosis. *The Lancet* vol. 390 2084–2098 (2017).
3. Pender, N., Pinto-Grau, M. & Hardiman, O. Cognitive and behavioural impairment in amyotrophic lateral sclerosis. *Current Opinion in Neurology* **33**, 649–654 (2020).
4. Lomen-Hoerth, C., Anderson, T. & Miller, B. The overlap of amyotrophic lateral sclerosis and frontotemporal dementia. *Neurology* **59**, 1077–1079 (2002).
5. Al-Chalabi, A. *et al.* Amyotrophic lateral sclerosis: moving towards a new classification system. *The Lancet. Neurology* **15**, 1182–94 (2016).
6. van der Burgh, H. K. *et al.* Multimodal longitudinal study of structural brain involvement in amyotrophic lateral sclerosis. *Neurology* (2020).
7. Cistaro, A. *et al.* The metabolic signature of C9orf72-related ALS: FDG PET comparison with nonmutated patients. *European Journal of Nuclear Medicine and Molecular Imaging* **41**, 844–852 (2014).
8. Pagani, M. *et al.* Functional pattern of brain FDG-PET in amyotrophic lateral sclerosis. *Neurology* **83**, 1067–1074 (2014).
9. McMackin, R. *et al.* Dysfunction of attention switching networks in amyotrophic lateral sclerosis. *Neuroimage Clin* **22**, 101707 (2019).
10. Nasserroleslami, B. *et al.* Characteristic Increases in EEG Connectivity Correlate With Changes of Structural MRI in Amyotrophic Lateral Sclerosis. *Cereb Cortex* **29**, 27–41 (2019).
11. Baumann, F., Henderson, R. D., Ridall, P. G., Pettitt, A. N. & McCombe, P. A. Use of Bayesian MUNE to show differing rate of loss of motor units in subgroups of ALS. *Clinical Neurophysiology* **123**, 2446–2453 (2012).
12. Geevasinga, N. *et al.* Axonal ion channel dysfunction in C9orf72 familial amyotrophic lateral sclerosis. *JAMA Neurology* **72**, 49–57 (2015).
13. Burke, T. *et al.* A Cross-sectional population-based investigation into behavioral change in amyotrophic lateral sclerosis: subphenotypes, staging, cognitive predictors, and survival. *Annals of Clinical and Translational Neurology* **4**, 305–317 (2017).
14. Ganesalingam, J. *et al.* Latent Cluster Analysis of ALS Phenotypes Identifies Prognostically Differing Groups. *PLoS ONE* **4**, e7107 (2009).
15. Mathis, S., Goizet, C., Soulages, A., Vallat, J. M. & Masson, G. Le. Genetics of amyotrophic lateral sclerosis: A review. *Journal of the Neurological Sciences* vol. 399 217–226 (2019).
16. Ravits, J. *et al.* Deciphering amyotrophic lateral sclerosis: What phenotype, neuropathology and genetics are telling us about pathogenesis. *Amyotrophic Lateral Sclerosis and Frontotemporal Degeneration* **14**, 5–18 (2013).
17. Mendelsohn, A. I., Dasen, J. S. & Jessell, T. M. Divergent Hox Coding and Evasion of Retinoid Signaling Specifies Motor Neurons Innervating Digit Muscles. *Neuron* **93**, 792–805.e4 (2017).
18. Bikoff, J. B. *et al.* Spinal Inhibitory Interneuron Diversity Delineates Variant Motor Microcircuits. *Cell* **165**, 207–219 (2016).
19. Cedarbaum, J. M. *et al.* The ALSFRS-R: a revised ALS functional rating scale that incorporates assessments of respiratory function. *J Neurol Sci* **169**, 13–21 (1999).
20. Abrahams, S., Newton, J., Niven, E., Foley, J. & Bak, T. H. Screening for cognition and behaviour changes in ALS. *Amyotroph Lateral Scler Frontotemporal Degener* **15**, 9–14 (2014).
21. McMackin, R. *et al.* Measuring network disruption in neurodegenerative diseases: New approaches using signal analysis. *J Neurol Neurosurg Psychiatry* jnnp-2018-319581 (2019).
22. Franchignoni, F., Mora, G., Giordano, A., Volanti, P. & Chiò, A. Evidence of multidimensionality in the ALSFRS-R Scale: A critical appraisal on its measurement properties using Rasch analysis. *Journal of Neurology, Neurosurgery and Psychiatry* **84**, 1340–1345 (2013).
23. Iyer, P. M. *et al.* Mismatch Negativity as an Indicator of Cognitive Sub-Domain Dysfunction in Amyotrophic Lateral Sclerosis. *Front Neurol* **8**, 395 (2017).
24. McMackin, R. *et al.* Localization of brain networks engaged by the sustained attention to response task provides quantitative

- markers of executive impairment in amyotrophic lateral sclerosis. *Cerebral Cortex* **30**, 4834–4846 (2020).
25. Engel, A. K., Gerloff, C., Hilgetag, C. C. & Nolte, G. Intrinsic Coupling Modes: Multiscale Interactions in Ongoing Brain Activity. *Neuron* **80**, 867–86 (2013).
 26. Deligani, R. J. *et al.* Electrical and Hemodynamic Neural Functions in People with ALS: An EEG-fNIRS Resting-State Study. *IEEE Transactions on Neural Systems and Rehabilitation Engineering* **28**, 3129–3139 (2020).
 27. Bizovičar, N., Dreo, J., Koritnik, B. & Zidar, J. Decreased movement-related beta desynchronization and impaired post-movement beta rebound in amyotrophic lateral sclerosis. *Clinical Neurophysiology* **125**, 1689–99 (2014).
 28. Riva, N. *et al.* Cortical activation to voluntary movement in amyotrophic lateral sclerosis is related to corticospinal damage: Electrophysiological evidence. *Clinical Neurophysiology* **123**, 1586–92 (2012).
 29. Dukic, S. *et al.* Patterned functional network disruption in amyotrophic lateral sclerosis. *Hum Brain Mapp* hbm.24740 (2019).
 30. Ludolph, A. *et al.* A revision of the El Escorial criteria - 2015. *Amyotroph Lateral Scler Frontotemporal Degener* **16**, 291–2 (2015).
 31. Strong, M. J. *et al.* Amyotrophic lateral sclerosis - frontotemporal spectrum disorder (ALS-FTSD): Revised diagnostic criteria. *Amyotrophic Lateral Sclerosis and Frontotemporal Degeneration* **18**, 153–174 (2017).
 32. Elamin, M. *et al.* Identifying behavioural changes in ALS: Validation of the Beaumont Behavioural Inventory (BBI). *Amyotrophic Lateral Sclerosis and Frontotemporal Degeneration* **18**, 68–73 (2017).
 33. Costello, E. *et al.* Equivalency and practice effects of alternative versions of the Edinburgh Cognitive and Behavioral ALS Screen (ECAS). *Amyotrophic Lateral Sclerosis and Frontotemporal Degeneration* **21**, 86–91 (2020).
 34. Pinto-Grau, M. *et al.* Screening for cognitive dysfunction in ALS: validation of the Edinburgh Cognitive and Behavioural ALS Screen (ECAS) using age and education adjusted normative data. *Amyotroph Lateral Scler Frontotemporal Degener* **18**, 99–106 (2017).
 35. Balendra, R. *et al.* Estimating clinical stage of amyotrophic lateral sclerosis from the ALS Functional Rating Scale. *Amyotrophic Lateral Sclerosis and Frontotemporal Degeneration* **15**, 279–284 (2014).
 36. Van Veen, B. D., Van Dronkelen, W., Yuchtman, M. & Suzuki, A. Localization of brain electrical activity via linearly constrained minimum variance spatial filtering. *IEEE Trans Biomed Eng* **44**, 867–80 (1997).
 37. Tzourio-Mazoyer, N. *et al.* Automated Anatomical Labeling of Activations in SPM Using a Macroscopic Anatomical Parcellation of the MNI MRI Single-Subject Brain. *Neuroimage* **15**, 273–89 (2002).
 38. Wang, B. *et al.* Similarity network fusion for aggregating data types on a genomic scale. *Nature Methods* **11**, 333–337 (2014).
 39. Ng, A., Jordan, M. & Weiss, Y. On Spectral Clustering: Analysis and an algorithm. *Adv. Neural Inf. Process. Syst* **14**, (2002).
 40. Wang, B., Zhu, J., Pierson, E., Ramazzotti, D. & Batzoglou, S. Visualization and analysis of single-cell rna-seq data by kernel-based similarity learning. *Nature Methods* **14**, 414–416 (2017).
 41. Wang, B. *et al.* Network enhancement as a general method to denoise weighted biological networks. *Nature Communications* **9**, 1–8 (2018).
 42. Zelnik-Manor, L. & Perona, P. Self-Tuning Spectral Clustering. in *Proceedings of the 17th International Conference on Neural Information Processing Systems* 1601–1608 (MIT Press, 2004).
 43. Nasserolleslami, B. An Implementation of Empirical Bayesian Inference and Non-Null Bootstrapping for Threshold Selection and Power Estimation in Multiple and Single Statistical Testing. *bioRxiv* 342964 (2018).
 44. Cliff, N. Dominance statistics: Ordinal analyses to answer ordinal questions. *Psychological Bulletin* **114**, 494–509 (1993).
 45. Thomas Yeo, B. T. *et al.* The organization of the human cerebral cortex estimated by intrinsic functional connectivity. *Journal of Neurophysiology* **106**, 1125–1165 (2011).
 46. Iyer, P. M. *et al.* Functional Connectivity Changes in Resting-State EEG as Potential Biomarker for Amyotrophic Lateral Sclerosis. *PLoS One* **10**, e0128682 (2015).
 47. Blain-Moraes, S., Mashour, G. A., Lee, H., Huggins, J. E. & Lee, U. Altered cortical communication in amyotrophic lateral sclerosis. *Neurosci Lett* **543**, 172–6 (2013).
 48. Benjamini, Y. & Hochberg, Y. Controlling the False Discovery Rate: A Practical and Powerful Approach to Multiple Testing. *Journal of the Royal Statistical Society.*

- Series B (Methodological) vol. 57 289–300 (1995).
49. Benjamini, Y., Krieger, A. M. & Yekutieli, D. Adaptive linear step-up procedures that control the false discovery rate. *Biometrika* **93**, 491–507 (2006).
 50. Blondel, V. D., Guillaume, J. L., Lambiotte, R. & Lefebvre, E. Fast unfolding of communities in large networks. *Journal of Statistical Mechanics: Theory and Experiment* **2008**, P10008 (2008).
 51. Bede, P. *et al.* Multiparametric MRI study of ALS stratified for the C9orf72 genotype. *Neurology* **81**, 361–369 (2013).
 52. Byrne, S. *et al.* Cognitive and clinical characteristics of patients with amyotrophic lateral sclerosis carrying a C9orf72 repeat expansion: A population-based cohort study. *The Lancet Neurology* **11**, 232–240 (2012).
 53. Beeldman, E. *et al.* The cognitive profile of ALS: A systematic review and meta-analysis update. *Journal of Neurology, Neurosurgery and Psychiatry* vol. 87 611–619 (2016).
 54. Proudfoot, M. *et al.* Increased cerebral functional connectivity in ALS: A resting-state magnetoencephalography study. *Neurology* **90**, e1418–e1424 (2018).
 55. Stam, C. J., Nolte, G. & Daffertshofer, A. Phase lag index: assessment of functional connectivity from multichannel EEG and MEG with diminished bias from common sources. *Human brain mapping* **28**, 1178–1193 (2007).
 56. Sorrentino, P. *et al.* Brain functional networks become more connected as amyotrophic lateral sclerosis progresses: a source level magnetoencephalographic study. *Neuroimage Clin* **20**, 564–71 (2018).
 57. Baccalá, L. A. & Sameshima, K. Partial directed coherence: A new concept in neural structure determination. *Biological Cybernetics* **84**, 463–474 (2001).
 58. Anthony, M. & Lin, F. A Systematic Review for Functional Neuroimaging Studies of Cognitive Reserve Across the Cognitive Aging Spectrum. *Archives of Clinical Neuropsychology* **33**, 937–948 (2018).
 59. Rittman, T. *et al.* Functional network resilience to pathology in presymptomatic genetic frontotemporal dementia. *Neurobiology of Aging* **77**, 169–177 (2019).
 60. Vucic, S., Nicholson, G. A. & Kiernan, M. C. Cortical hyperexcitability may precede the onset of familial amyotrophic lateral sclerosis. *Brain* **131**, 1540–50 (2008).
 61. Gregory, J. M. *et al.* Executive, language and fluency dysfunction are markers of localised TDP-43 cerebral pathology in nondemented ALS. *Journal of Neurology, Neurosurgery and Psychiatry* **91**, 149–157 (2019).
 62. McMackin, R. *et al.* Cognitive Network Hyperactivation and Motor Cortex Decline Correlate with ALS Prognosis. *Neurobiology of Aging* (2021).
 63. Proudfoot, M. *et al.* Altered cortical beta-band oscillations reflect motor system degeneration in amyotrophic lateral sclerosis. *Hum Brain Mapp* **38**, 237–254 (2017).
 64. Fraschini, M. *et al.* EEG functional network topology is associated with disability in patients with amyotrophic lateral sclerosis. *Scientific Reports* **6**, 1–7 (2016).
 65. Fraschini, M. *et al.* Functional brain connectivity analysis in amyotrophic lateral sclerosis: An EEG source-space study. *Biomed Phys Eng Express* **4**, 037004 (2018).
 66. Michel, C. M. & Brunet, D. EEG source imaging: A practical review of the analysis steps. *Frontiers in Neurology* **10**, 325 (2019).
 67. Michel, C. M. *et al.* EEG source imaging. *Clinical Neurophysiology* vol. 115 2195–2222 (2004).
 68. Zelmann, R., Lina, J. M., Schulze-Bonhage, A., Gotman, J. & Jacobs, J. Scalp EEG is not a blur: It can see high frequency oscillations although their generators are small. *Brain Topography* **27**, 683–704 (2014).
 69. Kuhnke, N. *et al.* High Frequency Oscillations in the Ripple Band (80–250 Hz) in Scalp EEG: Higher Density of Electrodes Allows for Better Localization of the Seizure Onset Zone. *Brain Topography* **31**, 1059–1072 (2018).
 70. Schomer, D. L., Lopes da Silva, F. H., Michel, C. M. & He, B. EEG Mapping and Source Imaging. in (Oxford University Press, 2017).

Supplementary material

Supplementary Note 1: Source localisation

Head models

For each subject with an MRI scan, a realistically-shaped volume conduction model was built. A three-layer conduction model, accounting for the brain, skull and scalp, was constructed using the Boundary Element Method (BEM),^{1,2} implemented in the open source software OpenMEEG.³ Similarly, for controls and patients who did not undergo MRI, a realistically-shaped BEM based on the ICBM152 template⁴ with the same characteristics was constructed, as template-based BEM and BEM based on individual MRI scans provide comparable localisation accuracy.⁵

Beamforming

EEG data were source-reconstructed using the linearly constrained minimum variance (LCMV) beamformer.⁶ Covariance matrices, needed for the reconstruction, were computed over a time window spanning the whole recording and using broadband data (1-97 Hz). In order to account for possible outliers in the data, the orthogonalised Gnanadesikan-Kettenring algorithm was used for the robust estimation of the covariance matrix.⁷ Covariance matrices were regularised using the Tikhonov method by μI ,⁸ where the regularisation parameter, μ , is set to 5% of the mean variance of all EEG channels and I is an identity matrix.

The optimal orientation of each dipole was estimated as the orientation of maximum power of the dipole using the singular value decomposition (SVD) on the dipole's (x-y-z direction) covariance matrix.⁶ The scalar beamformer weights were then used to reconstruct time-series of each dipole. Source localisation was done using the FieldTrip toolbox.⁹

Neural signal estimation

An atlas-based approach was used to evaluate source-space data with respect to the anatomical brain regions.^{10,11} The cortex of each subject was parcellated according to the automated anatomical labelling (AAL) atlas.¹² In this study, we used 90 regions from AAL atlas, excluding the cerebellum. To derive a single time-series for each region, all the time-series within a region were weighted using a Gaussian weighting function (half width at half maximum ~ 17 mm)^{11,13} as following:

$$q_{1 \times t} = \sum_i \exp\left(\frac{-r^2(i)}{400}\right) \cdot y_{1 \times t}(i) \quad (2)$$

Where i represents a count of all dipoles within a region, r represents a distance of each dipole from the centre of mass of the given region and t represent the length of the reconstructed signal. However, before applying the Gaussian formula, we estimated the direction along the maximum power for each region by performing SVD on

the orientations of dipoles within each brain region. Dipoles with the opposite direction (>90 degrees) to the estimated maximal activity vector were sign-flipped.

After completing these steps, we obtained 90 broadband time-series, each representing one brain region from the AAL atlas. This pipeline was applied to each subject individually.

Supplementary Note 2: Similarity matrix construction

Similarity matrix

For each of these three EEG measures, a separate patient similarity (or affinity) matrix was constructed using Gaussian kernels:

$$K(x_i, x_j) = \frac{1}{\varepsilon_{ij}\sqrt{2\pi}} e^{-\frac{\|x_i - x_j\|_2^2}{2\varepsilon_{ij}^2}}$$

Where $\|x_i - x_j\|_2$ is the Euclidean distance (a special case of the p -norm, $\|x\|_p, p = 2$) between patient x_i and x_j in the desired measure. The variance, ε_{ij} , can be locally estimated for the kernel:

$$\mu_i = \frac{\sum_{k \in KNN\{x_i\}} \|x_i - x_k\|_2}{K}, \quad \varepsilon_{ij} = \frac{\sigma \cdot (\mu_i + \mu_j)}{2}$$

Where $x_{k=1, \dots, K} \in KNN\{x_i\}$ is a set of K -nearest-neighbours of the patient i and σ is an adjustable coefficient. In order to improve the performance, we generated 55 different kernels using the combination of the following values $K = 10, 12, \dots, 30$ and $\sigma = 1, 1.25, 1.5, 1.75, 2$, which are suggested in the original study.¹⁴ These 55 kernels resulted in 55 similarity matrices which were then mean averaged to obtain a single similarity matrix per EEG measure.

Fusion of similarity matrices

The three patient similarity matrices (one for each EEG measure) were then combined into one using the similarity network fusion (SNF) method, a non-linear approach which creates a unified view of patients based on multiple data sources that capture different characteristics of patients.¹⁵ Starting with m different patient similarity networks from N patients, SNF iteratively updates each network with the complementary information from the other networks, making them more similar with each step. Once converged, the final fused network of patients represents the average of m non-linearly fused matrices. The method has been proven powerful in finding patterns in large scale data,¹⁶ it does not necessitate a priori selection of features and is robust to different types of noise.¹⁵ In our study, $m = 3$ and $N = 95$.

The fusion was done with K -nearest-neighbours parameter set to $Kn = 13$ (although similar values of Kn resulted in similar clustering solutions). Due to the varying number of patients used in subsequent analyses, Kn parameter was proportionally adjusted in: the analysis of stability under small perturbations ($Kn = 12, N = 90$ patients), the

analysis of stability using longitudinal data ($Kn = 18, N = 131$) and the comparison of clustering solutions based on clinical data only ($Kn = 9, N = 60$).

Similarity matrix enhancement

Further improvement of the fused similarity matrix was done using the network enhancement method.¹⁷ This approach relies on a diffusion-based algorithm for network denoising that does not require any supervision or prior knowledge. The main assumption of the method is that nodes connected through paths with high-weighted edges are more likely to have a direct, high-weighted edge between themselves. The method, therefore, improves the input similarity matrix by strengthening similarities that are either close to other strong similarities in the matrix (according to method's diffusion distance) or are supported by many weak edges. On the other hand, the edges that are not supported by many strong edges are weakened. The network enhancement was applied with K-nearest-neighbours parameter, Kn , set to the same values that were used when constructing the similarity matrices (see above 'Fusion of similarity matrices').

Supplementary Note 3: Optimal number of clusters

In spectral clustering, eigengap and rotation cost are two commonly used indices of the optimal number of clusters. Both indices are based on the eigenvalue decomposition of a similarity matrix.

The eigengap is defined as the difference between the i^{th} and $(i + 1)^{th}$ eigenvalue (previously sorted in an descending order), wherein the number of clusters is indicated by the biggest difference between two successive eigenvalues.¹⁸

The rotation cost exploits the structure of eigenvectors (of a similarity matrix), X , and defines the optimal number of clusters as the case in which the rotational cost of eigenvectors is the lowest.¹⁹ Namely, for each solution of k clusters, the following cost function is minimised by optimising the rotation matrix, R :

$$J = \sum_{i=1}^n \sum_{j=1}^k \frac{Z_{ij}^2}{M_i^2}$$

Where $Z = X \cdot R$ and $M_i = \max_j Z_{ij}$. The function is minimised using the gradient descent method, which applies rotation to the eigenvectors, X , such that the rotated matrix, Z , has a single non-zero entry in each row.¹⁹

Supplementary Note 4: Neurophysiological profiles of the clusters

EEG networks

For the purpose of defining neurophysiological profiles of clusters, co-modulation (amplitude envelope correlation) and synchrony (imaginary coherence) connectivity matrices were separately averaged to reflect median connectivity within each brain

network, whereas spectral power within each brain network was averaged to reflect its median neural activity. Here, we used five brain networks (somatomotor, frontotemporal, frontoparietal/central executive network, default mode and salience) known to be activated during rest²⁰ and to be affected in ALS.²¹⁻²³

Somatomotor: Supplementary motor area L/R, paracentral lobule L/R, precentral L/R, postcentral L/R, putamen L/R, thalamus L/R

Frontotemporal: Frontal middle orbital L/R, frontal inferior orbital L/R, frontal middle L/R, frontal inferior opercularis L/R, frontal inferior triangularis L/R, heschl L/R, temporal superior L/R, temporal middle L/R, temporal inferior L/R, temporal pole superior L/R, temporal pole inferior L/R, hippocampus L/R, parahippocampal L/R, amygdala L/R

Frontoparietal (central executive network): Frontal middle L/R, frontal inferior opercularis L/R, frontal inferior triangularis L/R, parietal inferior L/R, supramarginal L/R, angular L/R

Default mode: Frontal superior L/R, frontal superior medial L/R, cingulum anterior L/R, cingulum posterior L/R, precuneus L/R, supramarginal L/R, angular L/R, temporal pole superior L/R, temporal pole inferior L/R

Salience: Insula L/R, cingulum anterior L/R, amygdala L/R, thalamus L/R

The brain regions were from the automated anatomical labelling (AAL) atlas.¹² Frequency bands were δ (2-4 Hz), θ (5-7 Hz), α (8-13 Hz), β (14-30 Hz) and γ (γ_l : 31-47 Hz, γ_h : 53-97 Hz). Total number of EEG networks in this analysis was, thus, 90 (three measures \times five networks \times six frequency bands).

Determining cluster-characteristic EEG changes

For each of the 90 EEG networks, an AUC (area under the receiver operating characteristic curve) value was calculated for each ALS cluster by comparing with the control data while controlling for the multiple comparisons using empirical Bayesian inference (EBI; FDR at $q = 0.1$)²². The obtained AUC values were then used to determine measures that are strongly and exclusively associated with each of the four clusters. Namely, for each EEG network the four AUC values were ordered ($u \in \{u_1, u_2, u_3, u_4\}$, such that $u_1 < u_2 < u_3 < u_4$) and the clusters associated with extreme values (i.e. u_1 and u_4) were each given a score. The score represents an absolute difference between these two values (u_1 and u_4) and the nearest AUC value (i.e. u_2 and u_3 , respectively): $u_1 - u_2$ and $u_4 - u_3$. The score was calculated only if the extreme AUC value was statistically significant as determined by EBI. Here, we report one characteristic EEG network per cluster, which is determined as the highest score across all 90 EEG networks for the given cluster. For plotting purposes, AUC values were centred around zero, thus ranging between -0.5 and 0.5.

Supplementary Note 5: Cluster validation

First approach

We validated our clusters by employing another clustering method. The Louvain method for community detection is an iterative approach that measures the relative density of edges inside subgroups with respect to edges outside subgroups and merges similar clusters until it converges, thus not requiring a predetermined number of clusters.²⁴ In its original implementation (which is used in this study), the only required input is a similarity matrix. For this purpose, we have reused the same similarity matrix as for the spectral clustering method (which was used in the main analysis). The clusters obtained from the Louvain method were compared to the clusters from the main analysis.

Second approach

We evaluated the accuracy of our cluster assignments using a classifier, with the aim to test how accurate we could classify at individual level, the new, future patients. Here, we used label propagation,²⁵ which makes predictions that are based on the well-defined similarities between the patients from the similarity matrix. The classifier was applied by excluding five randomly selected patients for 5000 times. The excluded patients were treated as test data, while the remaining patients were treated as training samples. The stability was estimated as the agreement between the propagated labels of the test patients and the corresponding labels obtained in the main analysis. Additionally, to control for correct classifications emerging due to chance, the adjusted Rand index²⁶ was used.

Third approach

We evaluated the robustness of our cluster assignments under small perturbations of data. This was achieved by randomly removing five patients and repeating the pipeline from the main analysis 5000 times. The stability was estimated as the agreement between the newly obtained labels and the corresponding labels obtained in the main analysis, using the adjusted Rand index.

Fourth approach

We further validated our clusters by assessing the robustness of cluster assignment over time. The label propagation classifier²⁵ was applied on a subset of patients ($N = 36$) that had a follow-up EEG recording (5.1 ± 1.8 months after the initial recording session). Namely, the follow-up dataset was treated as test data, while the original dataset ($N = 95$) was treated as a training sample. The stability of cluster assignments was reported as a confusion matrix and the Fisher's exact test was used to assess the statistical significance.

Supplementary Note 6: Effects of age and gender

To test whether the main findings (Fig. 2) are underpinned by the potential differences in age and apparent differences in gender between the identified clusters and controls,

we have applied general linear modelling. Namely, for each dysfunctional network, we assessed the differences between each cluster and all controls ($N = 77$), while controlling for gender and age (i.e. $\text{EEG} \sim \text{GROUP} + \text{AGE} + \text{GENDER}$, expressed in Wilkinson notation). Here, EEG data were transformed to a standard normal distribution using the inverse normal transformation.²⁷ The p-values associated with the group effect (and corrected for age and gender) remained significant after multiple comparisons correction ($q = 0.05$, false discovery rate)^{28,29}; thus, showing that the identified differences between ALS clusters and controls are not driven by gender or age.

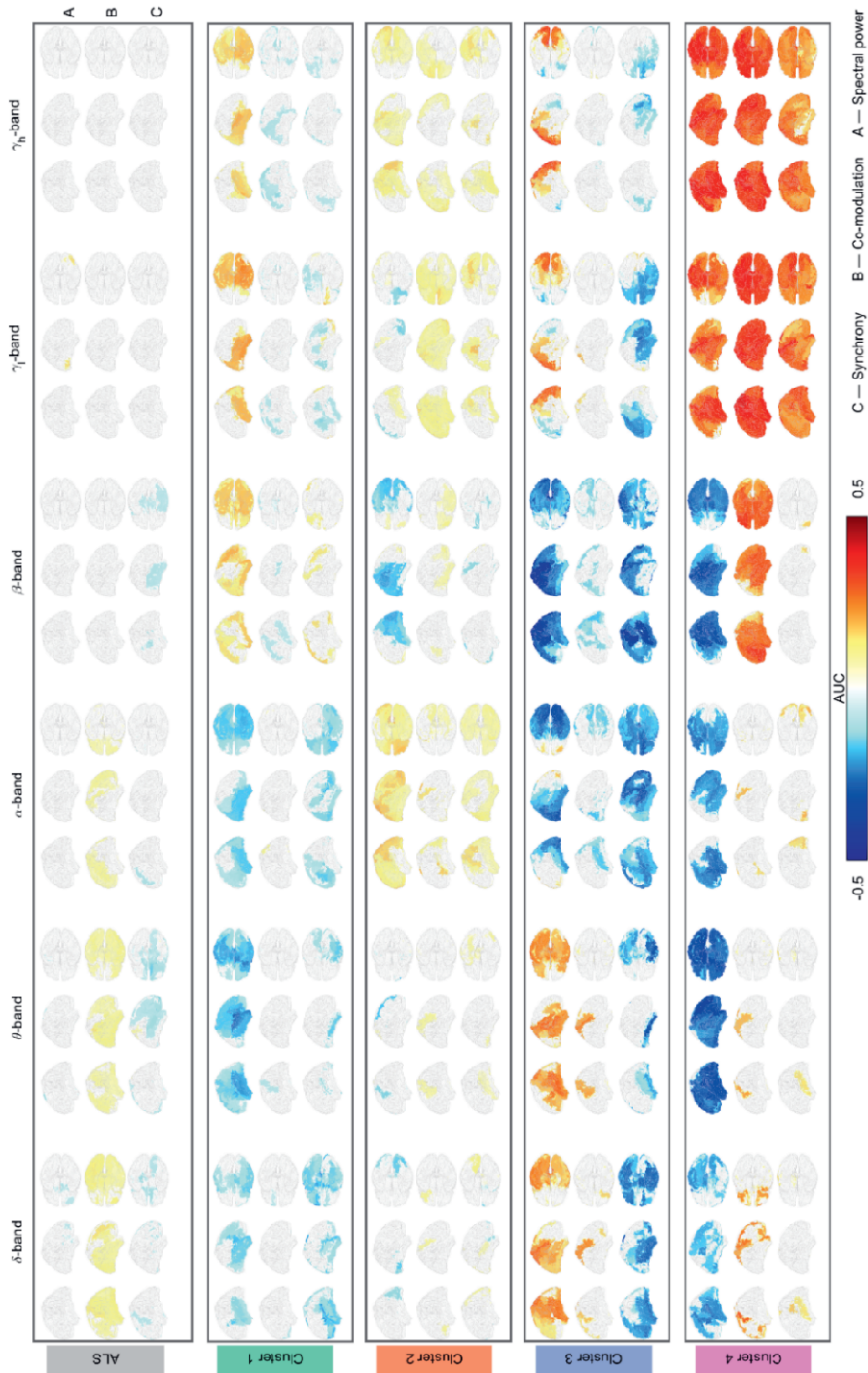
Supplementary Note 7: Clustering based on clinical data

Statistical analysis of clustering solutions ($k = 2, \dots, 6$ subgroups) based only on the clinical data indicate that none of the solutions are statistically significant (Supplementary Fig. 3A). The lack of statistical significance is likely to be due to the low statistical power associated with these clinical data. Furthermore, the stability of the clinical-based clusters was poorer compared to the EEG-based clusters (Supplementary Fig. 3B) across all clustering solutions. For the solution of $k = 4$ clusters, neurophysiological profiles of the clinical-based clusters did not reach statistical significance in any of the 90 EEG networks.

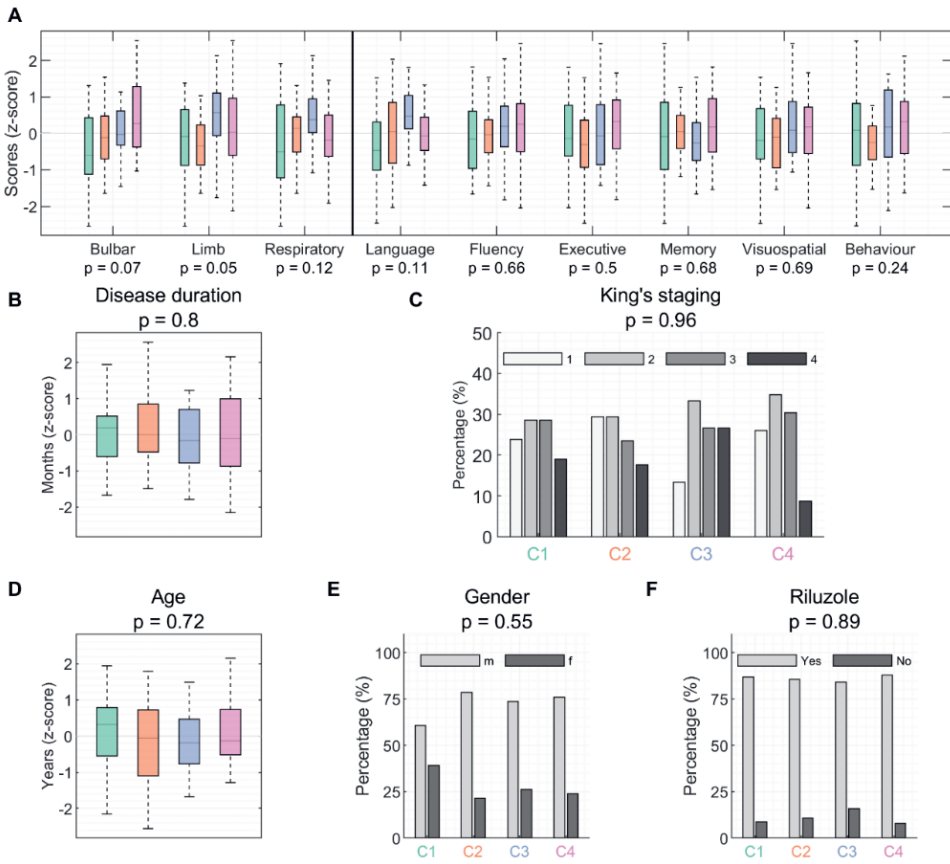
Supplementary Note 8: EEG γ -oscillations

In our study, we have used a high-density EEG system with 128 electrodes, which allows for accurate disentangling of γ -band findings.^{30,31} Since γ -band EEG overlaps with the frequency spectrum of the (scalp) muscle activity, we took a cautious approach and, as part of the preprocessing, we discarded EEG epochs that were marked as noise (eye movements, blinks, muscle activity, etc).³² Further, we have used a robust covariance matrix estimator (needed for source localisation method) to account for potential outliers that are missed in the previous step. Nevertheless, studies have shown that source localisation methods can efficiently account for cranial and ocular muscle artifacts³³ and successfully detect cortical γ -activity.^{34,35} In our previous study,²² from which we use the spectral power and connectivity measures, we have detected γ -band changes (in the frontotemporal network), which were correlated with clinical scores assessing language function. Furthermore, in our sensor-space analysis,³⁶ we have identified γ -band changes that remained even after applying the independent component analysis (ICA) to remove noise (eye movements, blinks and muscle activity). These two studies, together with studies from other groups,³⁷ support the implication and importance of γ -band changes in ALS. Finally, we report changes in the low γ (31–47 Hz), which has a better signal-to-noise ratio (SNR) compared to high γ -band (53–97 Hz).³⁸

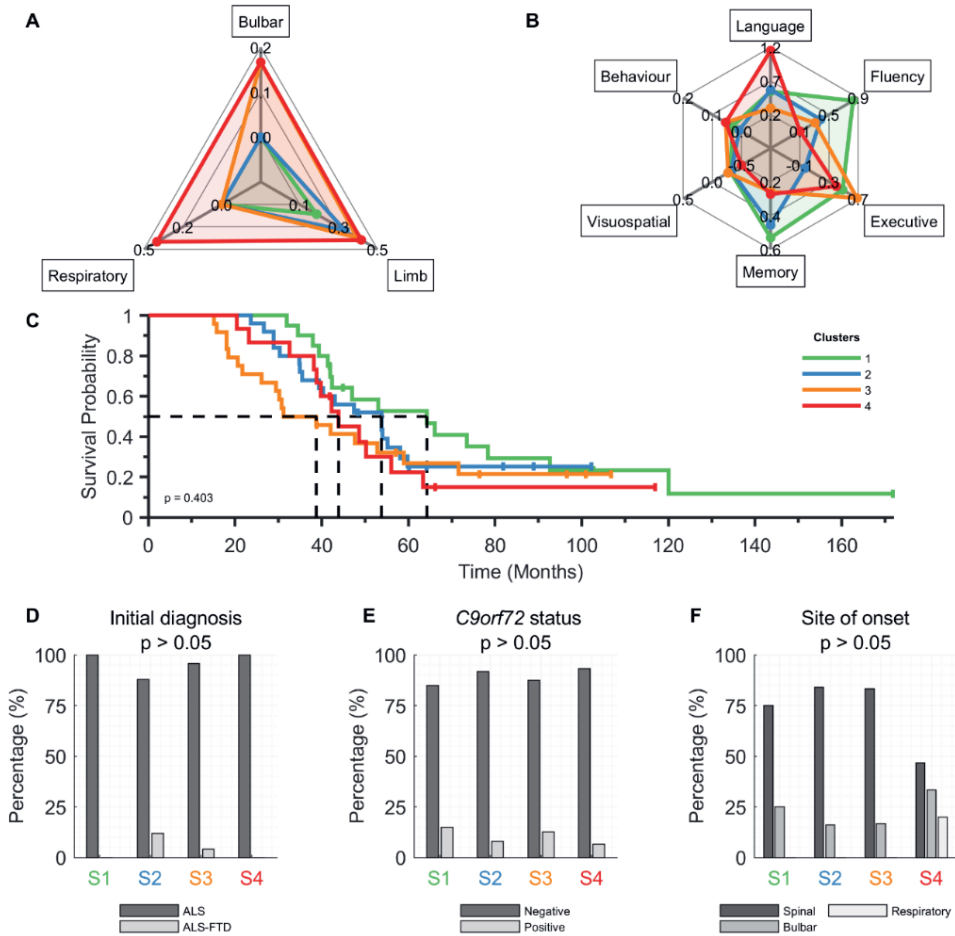
Supplementary figures



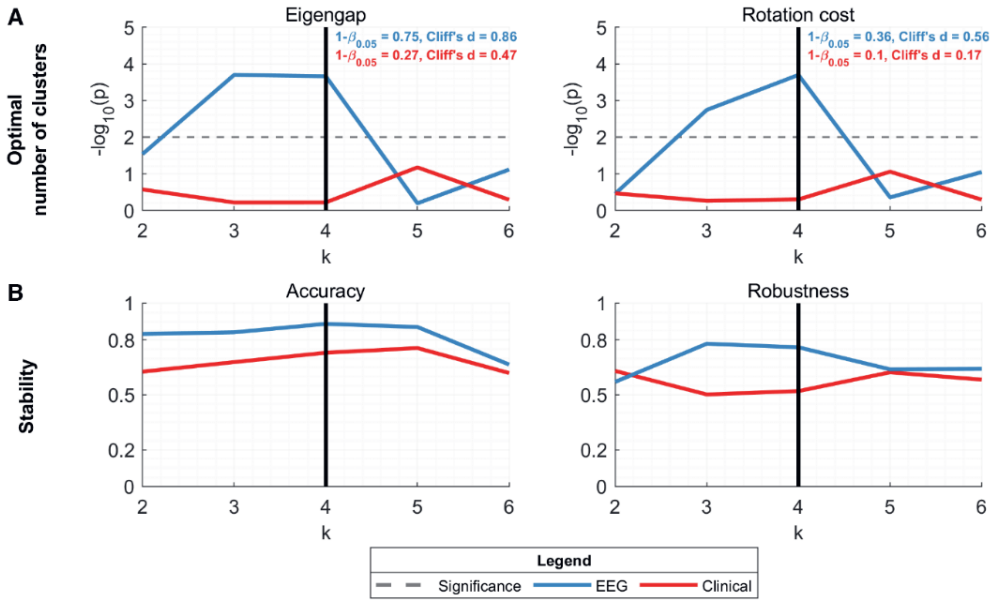
Supplementary Figure 1. Complete neurophysiological profiles of ALS clusters. The brain maps representing the statistical comparison of the spectral measures (A: spectral power, B: co-modulation and C: synchrony) using all ALS patients (first panel) and each cluster separately (panels 2-5) compared to healthy controls. Statistical significance in the high-dimensional space (pooled all three measures across all six frequencies) was carried out using Empirical Bayesian inference with statistical power $(1-\beta_{0.05})$ set to 0.8. Estimated false discovery rate was 0.12, 0.3, 0.33, 0.09 and 0.01, for each panel, respectively. The statistical significance of Kruskal-Wallis one-way analysis of variance was used to further mask the results, such that the first panel reflects EEG changes shared by all four clusters (i.e. those that did not vary significantly across clusters; $p > 0.05$, aFDR), while the other panels reflect EEG abnormalities that varied significantly across clusters ($p < 0.05$, aFDR). The number of patients in each panel was $N = 95, 23, 28, 19$ and 25 . AUC: Area under the receiver operating characteristic curve centred around zero; positive values indicate an increase, whereas negative values indicate a decrease compared to healthy controls.



Supplementary Figure 2. Clinical profiles of ALS clusters and potential factors that may affect the clustering results. Comparison of the four identified clusters (colour-coded) using the (A) functional scores in different domains, including ALSFRS-R (bulbar, limb and respiratory), ECAS (language, fluency, executive, memory and visuospatial) and BBI (behaviour) scores; (B) Disease duration measured from the reported time of disease onset until the date of EEG recording; (C) King's stages (1-4, early-late) reflecting the disease burden; (D-F) Age, gender and Riluzole usage. Data standardisation: data (A, B, D) were transformed to standard normal distributions using the inverse normal transformation²⁷ and then z-scored. Statistical tests: Kruskal-Wallis one-way analysis of variance (A,B,D), Fisher's exact test (C,E,F). ALSFRS-R: ALS functional rating scale revised; ECAS: Edinburgh cognitive and behavioural ALS screen; BBI: Beaumont behavioural inventory.



Supplementary Figure 3. ALS patients subgrouped by King's staging do not have differential survival probabilities. (A) The four King's subgroups (colour-coded) show statistically significant ($p < 0.05$, FDR) differences in normalised ALSFRS-R (bulbar, limb and respiratory), but not in (B) z-scored ECAS (language, fluency, executive, memory and visuospatial) and normalised BBI (behaviour), (C) Kaplan-Meier survival curves and (D-F) clinical characteristics. Clinical subscores (A-B) are all normalised or standardised, see Methods section. Note that there are in total: five ALS-FTD, 11 *C9orf72*-positive and four respiratory-onset patients. Statistical tests: Kruskal-Wallis one-way analysis of variance (A-B), logrank test (C) and Fisher's exact test (D-F); all FDR corrected.



Supplementary Figure 4. The optimal number of ALS clusters and the stability of clustering solutions based on clinical data compared to EEG data. (A) The statistical analysis shows that the optimal number of clusters when using only EEG data (blue) is $k = 4$, since both the eigengap and rotation cost peak at that point. The clustering solutions using only clinical data (red) do not reach significance for any investigated k . **(B)** The two analyses of accuracy and robustness show consistently poorer stability of clinical data-based solutions across all k .

References

1. Fuchs, M., Kastner, J., Wagner, M., Hawes, S. & Ebersole, J. S. A standardized boundary element method volume conductor model. *Clin Neurophysiol* **113**, 702–12 (2002).
2. Mosher, J. C., Leahy, R. M. & Lewis, P. S. EEG and MEG: forward solutions for inverse methods. *IEEE Trans Biomed Eng* **46**, 245–59 (1999).
3. Gramfort, A., Papadopoulos, T., Olivi, E. & Clerc, M. OpenMEEG: opensource software for quasistatic bioelectromagnetics. *Biomed Eng Online* **9**, 45 (2010).
4. Fonov, V., Evans, A., McKinstry, R., Almlí, C. & Collins, D. Unbiased nonlinear average age-appropriate brain templates from birth to adulthood. *Neuroimage* **47**, S102 (2009).
5. Douw, L., Nieboer, D., Stam, C. J., Tewarie, P. & Hillebrand, A. Consistency of magnetoencephalographic functional connectivity and network reconstruction using a template versus native MRI for co-registration. *Hum Brain Mapp* **39**, 104–119 (2018).
6. Van Veen, B. D., Van Drongelen, W., Yuchtman, M. & Suzuki, A. Localization of brain electrical activity via linearly constrained minimum variance spatial filtering. *IEEE Trans Biomed Eng* **44**, 867–80 (1997).
7. Maronna, R. A. & Zamar, R. H. Robust Estimates of Location and Dispersion for High-Dimensional Datasets. *Technometrics* **44**, 307–17 (2002).
8. Tikhonov, A. N. & Arsenin, V. Y. *Solutions of Ill-Posed Problems*. (Halsted Pres, 1977).
9. Oostenveld, R., Fries, P., Maris, E. & Schoffelen, J.-M. FieldTrip: Open source software for advanced analysis of MEG, EEG, and invasive electrophysiological data. *Comput Intell Neurosci* **2011**, 156869 (2011).
10. Hillebrand, A., Barnes, G. R., Bosboom, J. L., Berendse, H. W. & Stam, C. J. Frequency-dependent functional connectivity within resting-state networks: An atlas-based MEG beamformer solution. *Neuroimage* **59**, 3909–21 (2012).
11. Tewarie, P. *et al.* Predicting haemodynamic networks using electrophysiology: The role of non-linear and cross-frequency interactions. *Neuroimage* **130**, 273–92 (2016).
12. Tzourio-Mazoyer, N. *et al.* Automated Anatomical Labeling of Activations in SPM Using a Macroscopic Anatomical Parcellation of the MNI MRI Single-Subject Brain. *Neuroimage* **15**, 273–89 (2002).
13. Brookes, M. J. *et al.* A multi-layer network approach to MEG connectivity analysis. *Neuroimage* **132**, 425–38 (2016).
14. Wang, B., Zhu, J., Pierson, E., Ramazzotti, D. & Batzoglou, S. Visualization and analysis of single-cell rna-seq data by kernel-based similarity learning. *Nat Methods* **14**, 414–416 (2017).
15. Wang, B. *et al.* Similarity network fusion for aggregating data types on a genomic scale. *Nat Methods* **11**, 333–337 (2014).
16. Cavalli, F. M. G. *et al.* Intertumoral Heterogeneity within Medulloblastoma Subgroups. *Cancer Cell* **31**, 737–754.e6 (2017).
17. Wang, B. *et al.* Network enhancement as a general method to denoise weighted biological networks. *Nat Commun* **9**, 1–8 (2018).
18. Ng, A., Jordan, M. & Weiss, Y. On Spectral Clustering: Analysis and an algorithm. *Adv. Neural Inf. Process. Syst* **14**, (2002).
19. Zelnik-Manor, L. & Perona, P. Self-Tuning Spectral Clustering. in *Proceedings of the 17th International Conference on Neural Information Processing Systems* 1601–1608 (MIT Press, 2004).
20. Thomas Yeo, B. T. *et al.* The organization of the human cerebral cortex estimated by intrinsic functional connectivity. *J Neurophysiol* **106**, 1125–1165 (2011).
21. McMackin, R. *et al.* Dysfunction of attention switching networks in amyotrophic lateral sclerosis. *Neuroimage Clin* **22**, 101707 (2019).
22. Dukic, S. *et al.* Patterned functional network disruption in amyotrophic lateral sclerosis. *Hum Brain Mapp* hbm.24740 (2019).
23. Iyer, P. M. *et al.* Functional Connectivity Changes in Resting-State EEG as Potential Biomarker for Amyotrophic Lateral Sclerosis. *PLoS One* **10**, e0128682 (2015).
24. Blondel, V. D., Guillaume, J. L., Lambiotte, R. & Lefebvre, E. Fast unfolding of communities in large networks. *Journal of Statistical Mechanics: Theory and Experiment* **2008**, P10008 (2008).

25. Zhu, X. & Ghahramani, Z. Learning from Labeled and Unlabeled Data with Label Propagation. *CMU-CALD-02-107* (2002).
26. Hubert, L. & Arabie, P. Comparing partitions. *Journal of Classification* **2**, 193–218 (1985).
27. Beasley, T. M., Erickson, S. & Allison, D. B. Rank-Based Inverse Normal Transformations are Increasingly Used, But are They Merited? *Behav Genet* **39**, 580–95 (2009).
28. Benjamini, Y. & Hochberg, Y. Controlling the False Discovery Rate: A Practical and Powerful Approach to Multiple Testing. *Journal of the Royal Statistical Society. Series B (Methodological)* vol. 57 289–300 (1995).
29. Benjamini, Y., Krieger, A. M. & Yekutieli, D. Adaptive linear step-up procedures that control the false discovery rate. *Biometrika* **93**, 491–507 (2006).
30. Zelmann, R., Lina, J. M., Schulze-Bonhage, A., Gotman, J. & Jacobs, J. Scalp EEG is not a blur: It can see high frequency oscillations although their generators are small. *Brain Topogr* **27**, 683–704 (2014).
31. Kuhnke, N. *et al.* High Frequency Oscillations in the Ripple Band (80–250 Hz) in Scalp EEG: Higher Density of Electrodes Allows for Better Localization of the Seizure Onset Zone. *Brain Topogr* **31**, 1059–1072 (2018).
32. Dukic, S. *et al.* Estimation of coherence using the median is robust against EEG artefacts. in *Proceedings of the Annual International Conference of the IEEE Engineering in Medicine and Biology Society, EMBS* (2017).
33. Hipp, J. F. & Siegel, M. Dissociating neuronal gamma-band activity from cranial and ocular muscle activity in EEG. *Frontiers in Human Neuroscience* **7**, 338 (2013).
34. Tamás, G. *et al.* Primary sensorimotor cortex drives the common cortical network for gamma synchronization in voluntary hand movements. *Frontiers in Human Neuroscience* **12**, 130 (2018).
35. Muthuraman, M. *et al.* Cross-frequency coupling between gamma oscillations and deep brain stimulation frequency in Parkinson’s disease. *Brain* **143**, 3393–3407 (2021).
36. Nasseroleslami, B. *et al.* Characteristic Increases in EEG Connectivity Correlate With Changes of Structural MRI in Amyotrophic Lateral Sclerosis. *Cerebral cortex (New York, N.Y. : 1991)* **29**, (2019).
37. Sorrentino, P. *et al.* Brain functional networks become more connected as amyotrophic lateral sclerosis progresses: a source level magnetoencephalographic study. *Neuroimage Clin* **20**, 564–71 (2018).
38. Petroff, O. A., Spencer, D. D., Goncharova, I. I. & Zaveri, H. P. A comparison of the power spectral density of scalp EEG and subjacent electrocorticograms. *Clinical Neurophysiology* **127**, 1108–1112 (2016).



Chapter 6

Localisation of brain networks engaged by the sustained attention to response task provides quantitative markers of executive impairment in amyotrophic lateral sclerosis

Roisin McMackin, Stefan Dukic, Emmet Costello, Marta Pinto-Grau, Antonio Fasano, Teresa Buxo, Mark Heverin, Richard Reilly, Muthuraman Muthuraman, Niall Pender, Orla Hardiman, Bahman Nasserolelami



Abstract

Objective: To identify cortical regions engaged during the sustained attention to response task (SART) and characterise changes in their activity associated with the neurodegenerative condition amyotrophic lateral sclerosis (ALS).

Methods: High-density EEG was recorded from 33 controls and 23 ALS patients during the SART paradigm. Differences in associated event related potential peaks were measured for Go and NoGo trials. Sources active during these peaks were localised and ALS-associated differences were quantified.

Results: Go and NoGo N₂ and P₃ peak sources were localised to the left primary motor cortex, bilateral dorsolateral prefrontal (DLPFC) and lateral posterior parietal cortices (PPC). NoGo trials evoked greater bilateral medial PPC activity during N₂ and lesser left insular, PPC and DLPFC activity during P₃. Widespread cortical hyperactivity was identified in ALS during P₃. Changes in the inferior parietal lobule and insular activity provided very good discrimination (AUROC > 0.75) between patients and controls. Activation of the right precuneus during P₃ related to greater executive function in ALS, indicative of a compensatory role.

Interpretation: The SART engages numerous frontal and parietal cortical structures. SART-EEG measures correlate with specific cognitive impairments that can be localised to specific structures, aiding in differential diagnosis.

Introduction

The sustained attention response task (SART) has been developed to detect clinically relevant lapses in attention. It represents a simple and quantitative task of executive functions that has been used to capture attentional impairments in different neurodegenerative diseases.¹⁻⁴ Drifts in attention are captured by a failure to inhibit motor responses to targets (i.e. commission errors). As the task requires only button press responses it is suitable for performing during EEG recording with little to no electromyographic artefacts. Recently, SART-generated event-related potentials (ERPs) time-locked to Go and NoGo trials have been interrogated in healthy individuals using quantitative EEG. These ERPs have individual peaks which relate to sensory detection ('P1' and 'N1'),⁵ motor control ('N2') and attentional engagement ('P3'). The latter two peaks are typically larger during correct response withholding.⁶ By combining the SART with EEG, distinct indices of the neural network activities required for different aspects of task performance can therefore be determined. This facilitates specific interrogation of the sequentially engaged sensory, motor and cognitive networks on a millisecond-by-millisecond basis in a quantitative, economical manner. Further, by requiring both motor and cognitive performance, the SART is expected to engage networks that bridge cognitive and motor functions, as oppose to tasks that demand only the individual functions. This suggest that the SART has potential as an instrument to assess the neurophysiological substrates underpinning motor and executive decline in conditions such as amyotrophic lateral sclerosis (ALS), Huntington's disease and Parkinson's disease.⁷

Despite these advantages, the cortical regions engaged by the SART remain unclear. Low-resolution sensor-level topographies have indicated frontoparietal engagement during the task^{6,8} and dorsolateral prefrontal and anterior cingulate malfunctioning during the SART has been reported in Huntington's disease.⁹ However, the sources of the SART ERPs in healthy individuals have yet to be reported in high spatial and temporal resolution.

Such source-resolved measures could provide important insights into and biomarkers of different cognitive and/or motor neurodegenerations, such as occurs in the neurodegenerative condition ALS.

ALS is the most common form of motor neurone disease and is characterised by the presence of upper and lower motor neuron degeneration. Clinical,^{10,11} neuroimaging¹² and neuropathological¹³ evidence have demonstrated extensive additional non-motor involvement, however quantitative measurement of this decline in cognition and behaviour in ALS remains challenging.

Detailed neuropsychological assessment with appropriate adjustments for motor impairment has provided information on the nature and frequency of different cognitive domain impairments in ALS.¹⁰ However, these types of assessments are excessively time consuming for clinical trials, in some instances are subject to learning effects, and are insensitive to early, presymptomatic network deterioration. Screening tools, such as the Edinburgh Cognitive and Behavioural Screen (ECAS) for ALS, are useful in

a clinical setting but have limited utility in clinical trials and are not sufficiently sensitive for a detailed assessment of cognitive/behavioural change.¹⁴ Functional magnetic resonance imaging (fMRI) and positron emission tomography (PET) have been used to measure cortical activity during specific tasks, but these technologies are limited by cost,¹⁵ low temporal resolution and variance across different scanners.¹⁶

By contrast, we and others have recently demonstrated how the source localisation of EEG facilitates spatially and temporally precise functional imaging of ALS cortical pathology.¹⁷⁻¹⁹ Therefore, given the motor and cognitive pathology of ALS, measurement of SART-associated ERPs using source-resolved EEG provides an opportunity to simultaneously interrogate motor and cognitive network functions and investigate their relationship to symptomatic impairments.

Here, we have spatially resolved the sources of these cognitive indices in healthy individuals and patients with ALS by linearly constrained minimum variance (LCMV)-based source imaging. We demonstrate how quantifying changes in SART-ERP indices and their relation to cognitive and motor symptoms facilitates investigation of neurophysiological changes associated with cognitive impairment in ALS.

Methods

Ethical approval

Ethical approval was obtained from the ethics committee of St. James's Hospital (REC reference: 2017-02). All participants provided written informed consent before participation. All work was performed in accordance with the Declaration of Helsinki.

Participants

Recruitment

Patients were recruited at the Irish National ALS specialty clinic in Beaumont Hospital. Healthy controls included appropriately consented, neurologically-normal, age-matched individuals recruited from an existing population-based control bank.

Inclusion criteria

Patients were over 18 years of age and diagnosed within the previous 18 months with Possible, Probable or Definite ALS in accordance with the El Escorial Revised Diagnostic Criteria.²⁰

Exclusion criteria

Exclusion criteria included any diagnosed psychological, neurological or muscular disease other than ALS, use of CNS medications (e.g. antidepressants, anti-seizure medication) except riluzole, inability to participate due to ALS-related motor decline (e.g. inability to sit in the chair for the required time or click the mouse to respond), or evidence of significant respiratory insufficiency. Participants were also rescheduled if

they slept two or more hours below normal the night before the session and were asked to abstain from consuming alcohol the night before the recording.

Demographics and characteristics of patients and controls

Patient and control characteristics are summarised in Table 1. None of the participants met the criteria for FTD diagnosis. One patient was using non-invasive ventilation at night time but was clinically asymptomatic with respect to respiratory impairment and had ALS functional rating scale revised (ALSFERS-R) orthopnea and dyspnea scores of 3 (out of 4).

Table 1. Characteristics of ALS patients and controls.

	Patients	Controls
n	23	33
Mean age at EEG [range] (years)	63 [32-78]	63.21 [46-82]
Gender (f/m)	3/20	17/16
Site of onset (spinal/bulbar/thoracic)	17/5/1	N/A
Mean disease duration [range] (months)	20.01 [4-42]	N/A
Handedness (right/left/ambidextrous)	22/0/1	31/2/0
<i>C9orf72</i> +	3	Untested
Mean ALSFRS-R score [range]	38.24 [24-43]	N/A
Mean ECAS total score [n abnormal]	105.33 [3]	Untested
Mean ECAS ALS specific score [n abnormal]	78.47 [3]	Untested
Mean ECAS ALS non-specific score [n abnormal]	26.65 [2]	Untested

Handedness was determined by the Edinburgh Handedness Index. ECAS scores are out of a maximum total score of 136, ALS non-specific score of 36 and ALS specific score of 100. *C9orf72*+ = Carrying a repeat expansion of the *C9orf72* gene. ECAS = Edinburgh Cognitive and Behavioural Assessment Scale; n abnormal = Number of participants scoring below the abnormality cut off score, accounting for years of education.

Experimental paradigm

Task design

EEG was recorded across 128-channels during 4 × 5-minute-long consecutive sessions during which participants undertook the SART. Participants were seated 1 ± 0.1 m from a computer monitor where numbers one to nine in single digit format were appearing in random order for 250ms, using Presentation software (NeuroBehavioural Systems Inc., CA, USA). Digits were presented in light grey (RGB code: 250, 250, 250 from 255) on a black background to reduce discomfort associated with the bright light from purely white numbers, reported during protocol testing. Font size was randomised between 100, 120, 140, 160 and 180 point to avoid participants using a perceptual

template of the number three's features for target recognition, and to encourage cognitive processing of the numerical value.¹ Each stimulus was followed by an interstimulus interval of randomised duration between 1120 and 1220 ms during which time a black screen was presented. Responses were registered by clicking the left button of a computer mouse with the right index finger. Each recording session contained 252 trials of which the number 3 appeared at random in 11% of trials. During these sessions lights were turned off and experimenters were outside the room to avoid visual/auditory distractions. Online performance and EEG measures were monitored by the experimenter in the neighbouring recording room. Appropriate break times were provided to minimise fatigue. Five behavioural measures of performance were captured: NoGo accuracy (percentage of 3-digit stimuli followed by response omission), Go accuracy (percentage of non-3 digit stimuli followed by a response in the permitted time window), total accuracy (combined NoGo and Go accuracy), anticipation (clicking less than 150 ms after a go stimulus) and response time.

Participant instructions

At the beginning of the session the task was explained to participants using the following instructions: Participants were instructed to click the left mouse button every time they saw a number except for the number three. Participants were requested to equally prioritise speed and accuracy as both were used as measures of performance. They were asked to refrain from lifting their finger away from the mouse button between clicks as this would increase response time measures. Instructions to use their finger only to click the mouse, avoiding tension in the arm and shoulder, to reduce noise in the EEG signal, were also given. Participants were then given one practice round to ensure they understood the task, which had up to 45 trials (without performance being measured) and it was performed under supervision of the experimenter.

Data acquisition

EEG data

EEG recordings were conducted in the Clinical Research Facility at St. James's Hospital, Dublin using a BioSemi® ActiveTwo system (BioSemi B.V., Amsterdam, The Netherlands) within a room electromagnetically shielded as a Faraday cage. Subjects were measured with an appropriately-sized 128-channel EEG cap. Data were online filtered to a bandwidth of 0-134 Hz and digitised at 512 Hz. Participant responses and response time were measured and recorded in individual files as well as being marked on the EEG recording to allow for precise time-locking and categorisation of EEG data epochs.

Cognitive- and motor-function tests

Fifteen patients underwent psychological assessment using the ECAS within 4 weeks of the EEG recording. Additionally, ALSFRS-R was collected longitudinally by neurologists at the Irish National ALS specialty clinic in Beaumont Hospital. Total and ALS specific ECAS scores within 30 days of EEG data collection were available for 15

patients, while ALS non-specific scores were available for 17 patients and ALSFRS-R scores were available for 14 patients. Three additional patients had ALSFRS-R data within three months before and after the EEG recording date. Using the data from these two time points, ALSFRS-R scores for these three patients were estimated by interpolation assuming linear decline such that ALSFRS-R scores were available for 17 patients in total. Scores are summarised in Table 1. Of those patient who performed abnormally in the ECAS, two had abnormal ALS non-specific scores but not total or ALS-specific scores, one had an abnormal ALS non-specific score but could not complete the language, fluency and spelling tasks to provide remaining scores and one performed abnormally in total and ALS-specific scores but not in their ALS non-specific score.

Data analysis

Signal preprocessing

Signal pre-processing was performed using custom MATLAB (R2014a and R2016a, Mathworks Inc., Natick, MA, USA) scripts and the EEGLAB²¹ and FieldTrip²² toolboxes. Data were filtered using a 0.3 Hz dual-pass 5th order Butterworth high-pass filter and a 30 Hz dual-pass 117th order equiripple finite impulse response low-pass filter. Highly contaminated and non-stereotyped artefacts were removed by visual inspection before epoching data from 200 before the stimulus to 900 ms post-stimulus. In cases where responses occurred 150 ms or less after stimulus onset, trials were rejected and counted as an ‘anticipation error’. Stereotyped artefacts (e.g. eye blinks, eye movements and noisy single electrodes) were then removed by independent component analysis.²¹ Data were common average referenced and mean baseline amplitude was subtracted. Mean correct Go (clicking upon a non-three digit) and NoGo (not clicking upon a ‘3’ digit) ERPs were calculated for each participant. Due to low error number there were insufficient number of clean epochs for incorrect trial-associated ERP analysis. Mean number of included artefact-free correct Go/NoGo trials was 810.13/82.22 for patients and 815.42/82.79 for controls out of a maximum of 897/111.

Sensor-space analysis

Electrodes of primary interest were chosen based on established topographic maps of the SART N₂ and P₃ peaks.^{6,8} Four characteristics of the N₂ and P₃ peaks of each mean Go and NoGo epoch were measured in Fz, FCz, Cz and Pz electrodes. Namely, the peak (maximal positive amplitude for P₃, maximal negative amplitude for N₂) amplitude and latency, mean amplitude and area of the peak within the 220-350 and 350-550 ms time windows associated with N₂ and P₃, respectively. These time windows were chosen based on visual inspection of group mean ERPs and the existing SART ERP literature.^{6,23-25} Time windows for quantifying peaks of interest were also limited to a maximum of 200 ms to facilitate baseline correction in source analysis (which required matching baseline and peak time windows) while using the same windows for sensor and source analysis.

For assessment of correlations with cognitive performance measures, where similarly significant correlations existed between performance measures and all peak size measures (peak amplitude, mean amplitude and mean area), we report p and ρ values with respect to peak amplitude where describing peak size (e.g. 'smaller' or 'larger') and.

Source-space analysis

Channels with continuously noisy data were excluded (excluded channels mean [range] in controls: 0.18 [0-4], patients: 0.22 [0-4]) and data from these channels were modelled by spline interpolation of neighbouring channels. Source localisation was performed using custom MATLAB scripts and linearly constrained minimum variance (LCMV) beamforming²⁶ as implemented in the FieldTrip toolbox. Boundary element head models²⁷ incorporating geometries for the brain, skull and scalp tissues were generated using the ICBM152 MRI template,²⁸ as template-based and individualised boundary-element head models are found to provide comparable localisation accuracy.^{27,29}

Brain power maps were estimated for the Go and NoGo trials during two time windows, 220-350 and 350-550 ms post-stimulus onset, to localise sources of the N2 and P3 ERPs, respectively. Localisation was performed of Go and NoGo trials, as well as of the corresponding baseline windows of equal duration (N2: -130-0ms, P3: -200-0ms). Source localisations were performed using common spatial filters (estimated separately for Go and NoGo and for N2 and P3) calculated from epoched data spanning the start of the peak's baseline window to the end of that peak's time window. These common spatial filters were then used to source localise baseline and peak time windows separately. Covariance matrices, used by LCMV, were calculated for individual trials and mean averaged. Regularisation of the covariance matrices was implemented at 5% of the average variance of EEG electrodes for each subject separately. Sources within the brain volume were modelled by a grid with 10 mm resolution. The leadfield matrix was normalised to avoid potential norm artefacts.³⁰ Finally, Go and NoGo source activity maps are estimated by incorporating baseline data as $10 \log_{10}(Power_{peak}/Power_{baseline})$, whereas the difference between Go and NoGo source activity maps are estimated as $10 \log_{10}(Power_{NoGo}/Power_{Go})$.

Statistics

Behavioural analysis

Group level comparisons of performance during the SART were implemented with Mann-Whitney U-test. Adaptive false discovery rate (FDR) of 5% was implemented to correct for multiple comparisons, calculated by the Benjamini Hochberg method.³¹ P-values are reported as uncorrected values where significant (determined by a corrected p-value of <0.05).

Sensor-space analysis

A four factor ANOVA was performed for each of the four peak characteristics for both N₂ and P₃, resulting in eight ANOVA. For each ANOVA the variables included were sex (male or female, accounting for non-gender imbalance), trial type (Go or NoGo), electrode (Fz, FCz, Cz or Pz) and group (ALS patient or control). Post-hoc analysis was implemented by Tukey's honestly significant difference.³² Adaptive false discovery rate (FDR) of 5% was implemented to correct post-hoc p-values for multiple comparisons as described for behavioural analysis.

Source-space analysis

A 10 mm grid in the brain volume yields 1726 sources including white matter. To analyse these high-dimensional data, a 10% FDR³³ was used as a frequentist method for determining significant source activity differences. Discrimination ability between patients and controls is quantified by the area under the curve for the receiver operating characteristics curve (AUROC).³⁴ Empirical Bayesian inference (EBI)³⁵ was used to calculate the Bayesian posterior probability and statistical power.

Neuropsychology correlation

Spearman's rank correlation was used to test the association of the changes in EEG measures (peak characteristics or mean power within a cortical region) and cognitive and functional measures based on inter-individual differences. These measures were: Performance in the SART task during EEG collection, performance in the Delis Kaplan Colour Word Interference Task (CWIT),³⁶ ECAS scores and ALSFRS-R scores. Multiple comparison correction was implemented using FDR³¹ set to 5%. For source-space correlation analysis, mean power was calculated for brain regions identified as major sources of peak activity, defined by the Automated Anatomical Labelling atlas.³⁷ Where significant correlations are reported regarding Go and NoGo combination measures, for example total (Go and NoGo) performance accuracy or the difference between NoGo and Go ERP measures, the relationship was verified not to be due to only Go or NoGo trials.

Results

Performance

Patients (N = 23) and controls (N = 33) did not differ significantly in response time or accuracy. However, patients committed significantly more anticipation errors (patient mean [standard deviation]: 8.73% [13.85%], control mean [standard deviation]: 1.01% [3.26%], $p = 0.0031$).

Control characteristics

Sensor-space

Mean patient and control Go and NoGo ERPs in electrodes of interest are shown in Fig. 1. ANOVAs did not reveal any significant gender effects on waveform features.

N₂ in Cz was significantly smaller in Go trials than NoGo trials in controls (peak area $p = 0.018$, peak amplitude $p = 0.006$). This N₂ difference significantly correlated with faster response times ($p = 8.08 \times 10^{-6}$, $r = 0.69$) and poorer NoGo accuracy ($p = 0.0086$, $r = 0.45$) in controls (Fig. 2A).

P₃ was significantly smaller for Go trials compared to NoGo trials in all four electrodes of interest (Fig. 1, Tukey's post-hoc $p = 3.50 \times 10^{-5}$ – 8.15×10^{-7}). P₃ peak latency in the Pz electrodes was also significantly greater in NoGo trials compared to Go trials ($p = 5.12 \times 10^{-7}$). Controls with later responses had later NoGo P₃ peaks in Fz ($p = 0.0020$, $r = 0.52$) while those with better NoGo accuracy had smaller Go P₃ peaks in Cz ($p = 0.011$, $r = -0.43$) and FCz ($p = 0.0034$, $r = -0.50$) and those with better Go accuracy had larger NoGo P₃ peaks in Pz ($p = 0.0070$, $r = 0.46$). Better overall accuracy also correlated significantly with smaller NoGo P₃ peaks in Fz ($p = 1.26 \times 10^{-4}$, $r = -0.62$). Correlations are illustrated in Fig. 3A-D.

Source-space

The left primary motor cortex and bilateral dorsolateral prefrontal cortex (DLPFC) and lateral posterior parietal cortex (PPC) were identified as primary mean sources of both Go and NoGo N₂, with greater bilateral precuneus activation during NoGo trials (Fig. 4).

Mean P₃ sources were similar to those of N₂ for Go and NoGo trials, although controls showed decreased left insular, PPC, and DLPFC activity during NoGo trials relative to Go trials (Fig. 5).

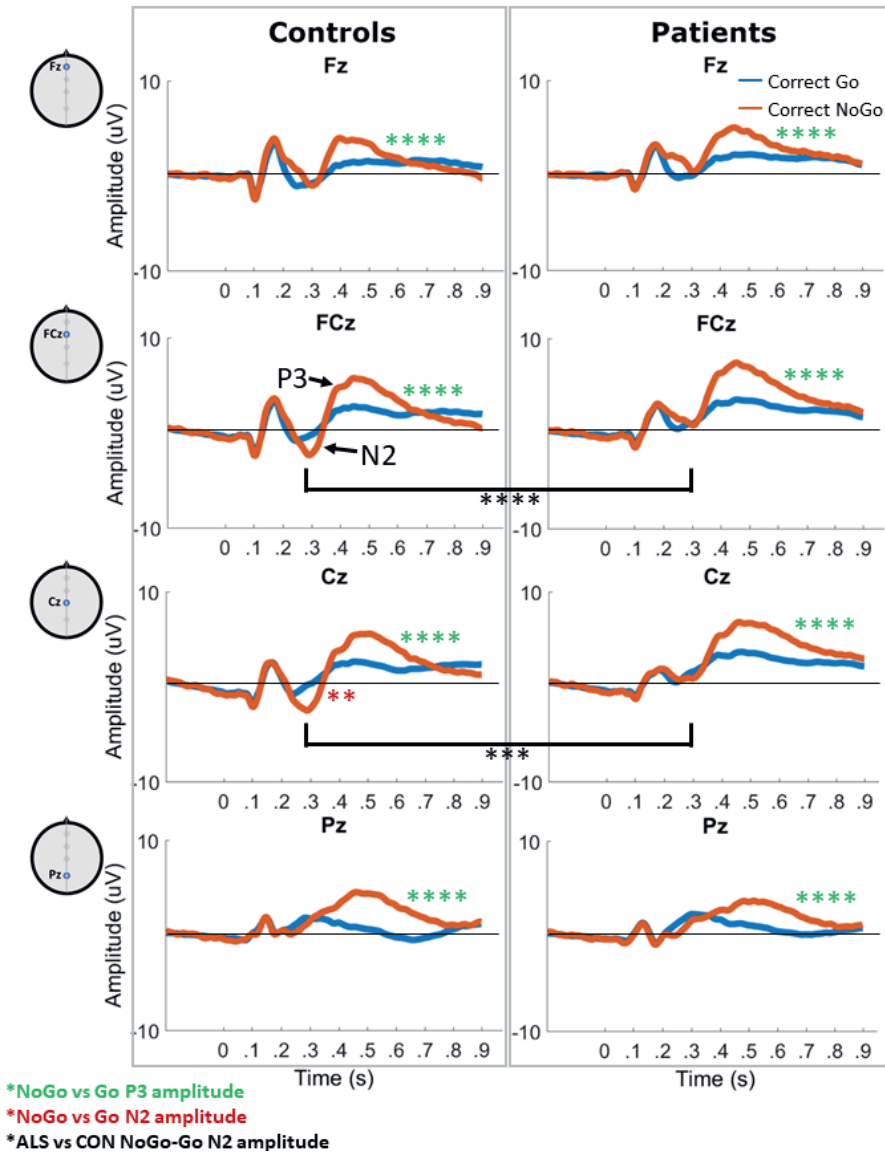


Figure 1. Mean Go (blue) and NoGo (red) trial ERPs in controls ALS patients. N2 peaks are visible in the NoGo trial ERP in Fz and Cz in the 220–350 ms window. P3 peaks are present in the 350–550 ms window in both Go and NoGo trial ERPs in all electrodes. Green asterisks represent significantly larger P3 peak amplitudes in NoGo vs Go trials. Red asterisks represent significantly larger (more negative) N2 peak amplitudes in NoGo vs Go trials. Black asterisks represent significant differences in NoGo-Go N2 peak amplitude between ALS patients and controls. ** $p < 0.01$, **** $p < 0.0001$. CON = Controls.

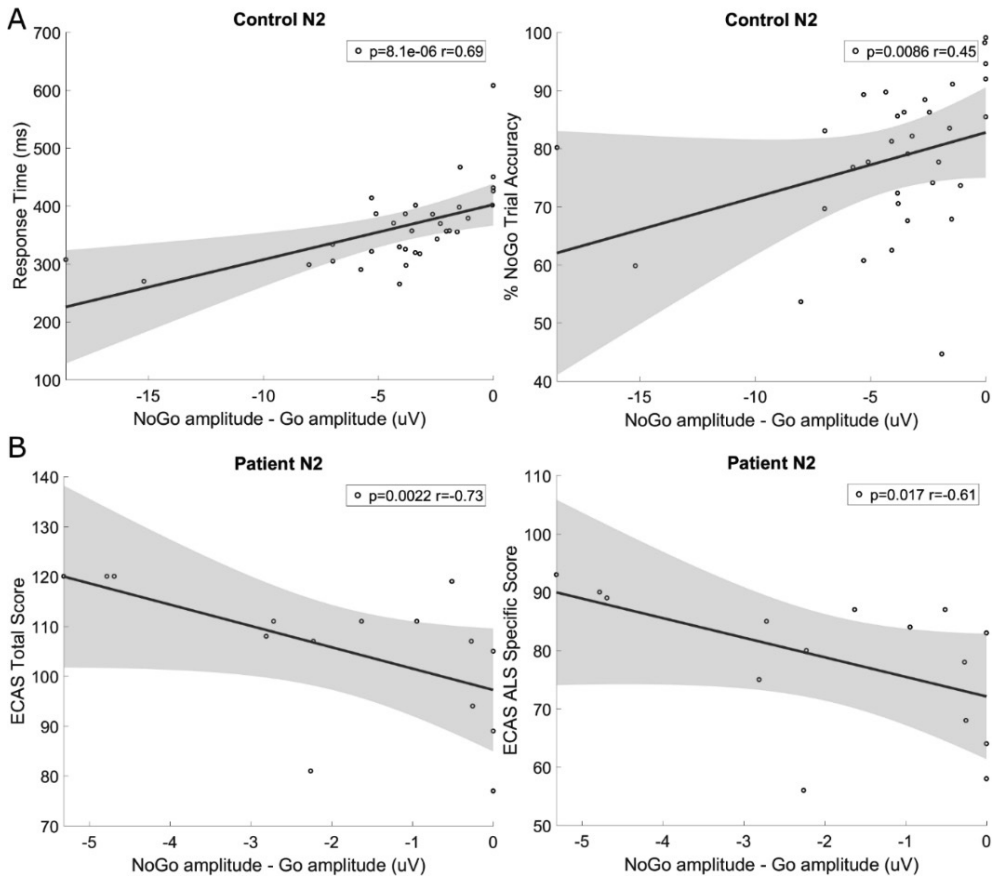


Figure 2. Correlations between NoGo minus Go (NoGo-Go) N2 peak amplitude in Cz and cognitive task performance. (A) Correlation with response time and NoGo trial accuracy in controls demonstrates that those with smaller NoGo versus Go N2 peak differences had significantly faster response times and better NoGo accuracy. (B) Correlation with patient ECAS total and ALS specific score demonstrates that those with smaller (less negative) N2 peak differences had lower ECAS scores.

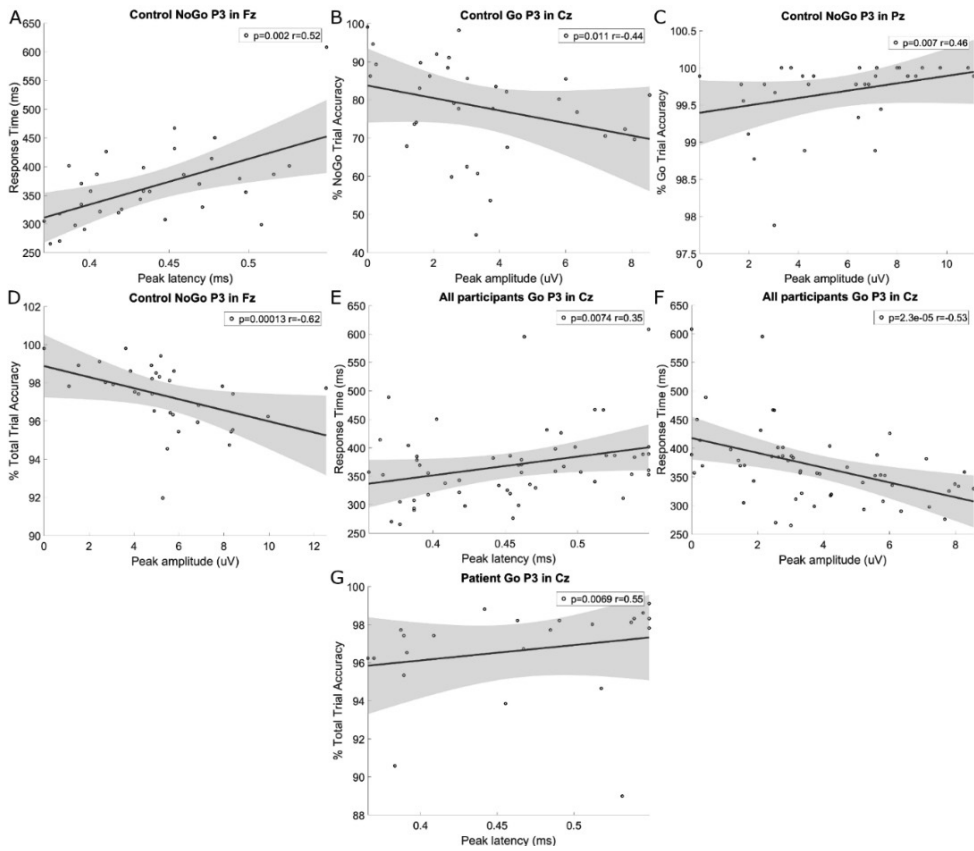


Figure 3. Correlations between P3 peak characteristics and SART performance. In controls, (A) later responses correlate with later P3 peaks in Fz during NoGo trials, (B) better NoGo accuracy inversely correlates with Go P3 peak size in Cz, (C) Go accuracy positively correlates with NoGo P3 peak amplitude in Pz and (D) overall accuracy inversely correlates with NoGo P3 peak amplitude in Fz. In all participants, (E) later response correlate with longer peak latency and (F) smaller peak amplitude during Go trials in Cz. In patients, (G) greater overall accuracy correlates with longer Go P3 peak latency in Cz.

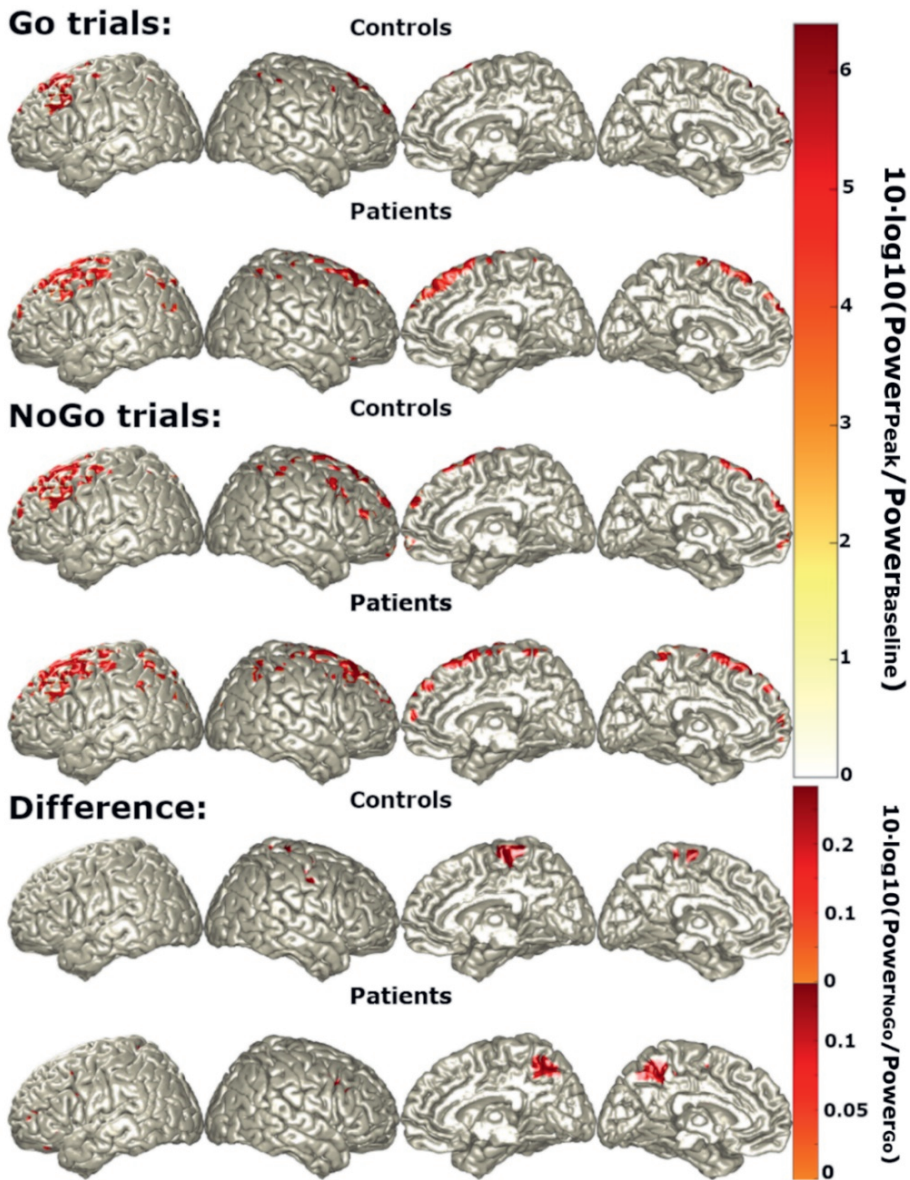


Figure 4. Primary sources (regions with top 5% power) of N₂ during Go trials, NoGo trials and NoGo trials relative to Go trials ('difference') in controls (first rows) and patients (second rows).

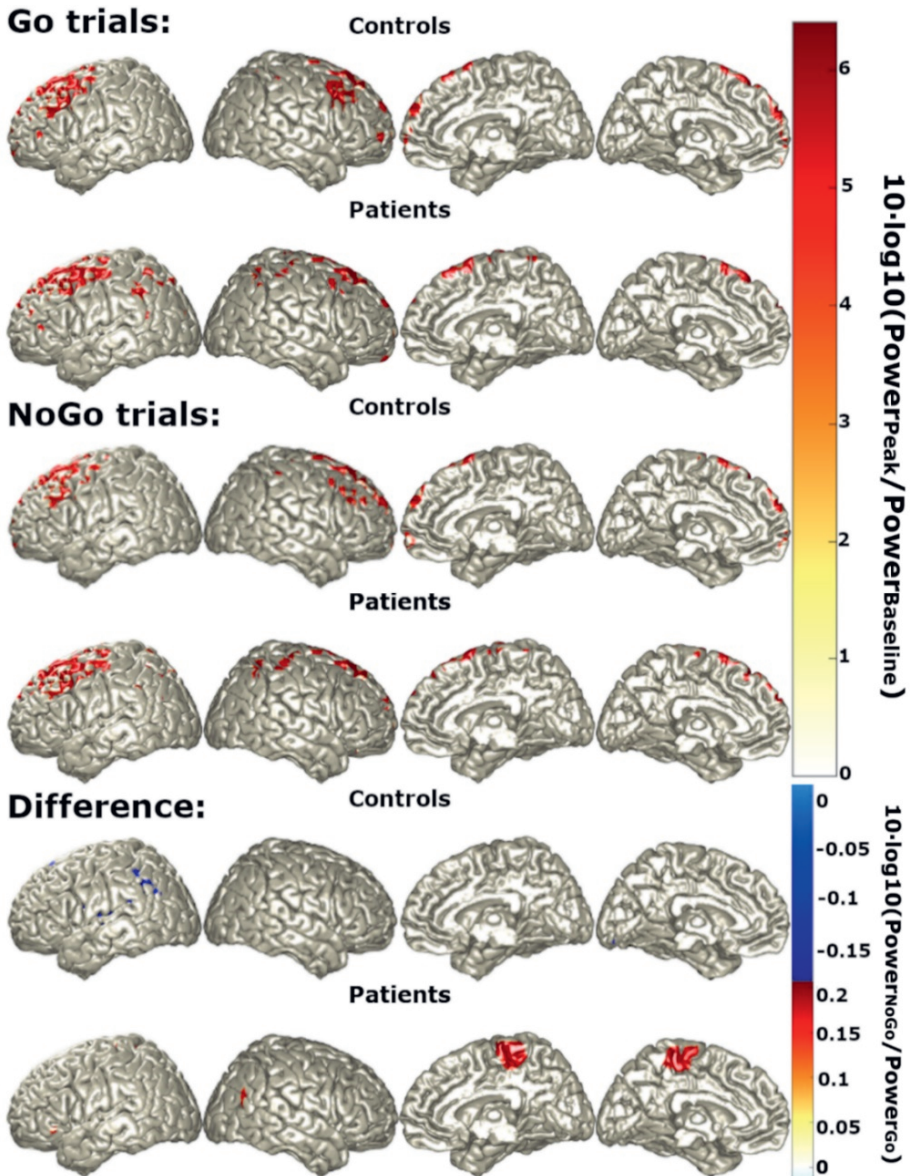


Figure 5. Primary sources (regions with 5% power) of P3 during Go trials, NoGo trials and NoGo trials relative to Go trials in controls (first rows) and patients (second rows).

ALS patient differences

Differences in peak and source measures between patients and controls are summarised in Table 2.

Sensor-space differences

N2: Patients did not show a significant difference in the *N2* peak between Go and NoGo trials. Correspondingly, *N2* was significantly smaller for NoGo trials in ALS patients compared to controls in FCz ($p = 5.08 \times 10^{-4}$) and Cz ($p = 0.001$). Unlike controls, the difference in *N2* between Go and NoGo trials did not correlate with SART performance, however those patients with greater *N2* NoGo-Go differences in Cz had higher ECAS total ($p = 0.0022$, $r = -0.73$, Fig. 2A) and ALS-specific ($p = 0.017$, $r = -0.61$) scores, indicating better cognitive performance, particularly in tasks of executive function and language (Fig. 2B).

P3: The *P3* peak did not differ significantly between patients and controls for any trial type or characteristic. Patients and control with longer response times had later ($p = 0.0074$, $r = 0.35$), smaller ($p = 2.31 \times 10^{-5}$, $r = -0.53$) Go *P3* peaks in Cz (Fig. 3E-F). Otherwise, patients did not display the correlations between their *P3* peak characteristics and task performance that were observed for controls. Overall accuracy was found to significantly correlate with later Go *P3* peaks in Cz in patients ($p = 0.0069$, $r = 0.54$, Fig. 3G).

Source-space differences

Patients showed similar patterns of source activity to controls during *N2* (Fig. 4). While similar locations of source activity were observed in patients and controls during Go and NoGo trials, ALS patients showed similar differences between NoGo and Go source differences to *N2* during *P3* (Fig. 5), unlike controls. Correspondingly, ALS patients displayed widespread, significantly increased activity during NoGo trials relative to Go trials when compared to controls, with the most discriminant differences (AUROC > 0.75) being in the left inferior parietal lobule and left insula (Fig. 6).

Table 2. Significant differences in ALS sensor- and source-level measures compared to controls.

Sensor-space			
Peak	Trial	Electrode	Change in ALS
N ₂	NoGo	Cz	↓ Peak amplitude
		FCz	↓ Peak amplitude
P ₃	NoGo-Go	Cz	No correlation to task performance
	Go	Cz	Later peak positively correlates with greater overall accuracy, no correlation between peak amplitude and accuracy.
	NoGo	Fz, Pz	No correlation between amplitude or latency to performance
Source-space			
Peak	Trial	Source	Change in ALS
P ₃	NoGo-Go	Left posterior parietal and insular cortex	↑ Activation, area under receivership operating curve >0.75

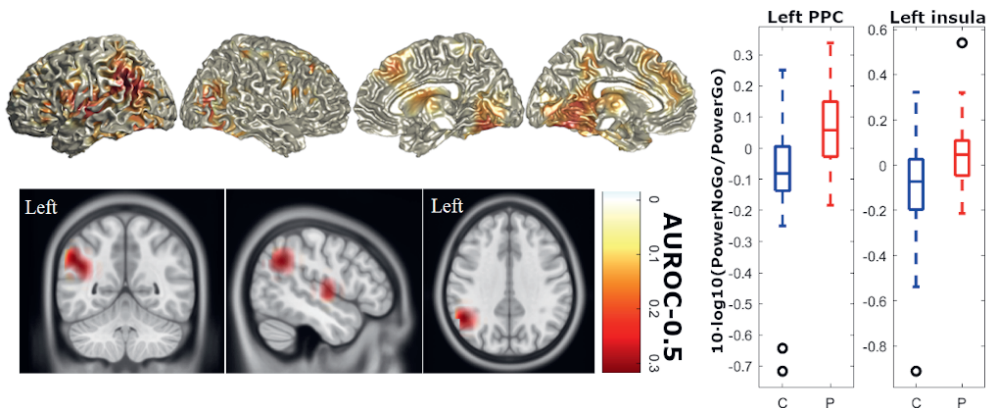


Figure 6. P₃ sources with statistically significant differences in activity in ALS compared to controls. Differences between NoGo and Go trial source activity during the P₃ peak were compared between ALS patients and controls. All highlighted areas represent significant (FDR = 10%, type II error = 0.38, Bayesian posterior probability = 0.87) increases in power with heat map values representing AUROC-0.5 (i.e. perfect discrimination = 0.5). Orthogonal MRI scans show only those differences with an AUROC > 0.75, i.e. very good discriminators. AUROC = Area under the receivership operating curve.

Source-space correlations in ALS patients

Greater right precuneus power during P₃ in NoGo relative to Go trials negatively correlates with CWIT inhibition score ($p = 0.0015$, $r = -0.91$, Fig. 7). As greater scores in this task indicated poorer behavioural inhibition, this relationship demonstrated that the abnormal activation of this area was associated with greater preservation of this executive function.

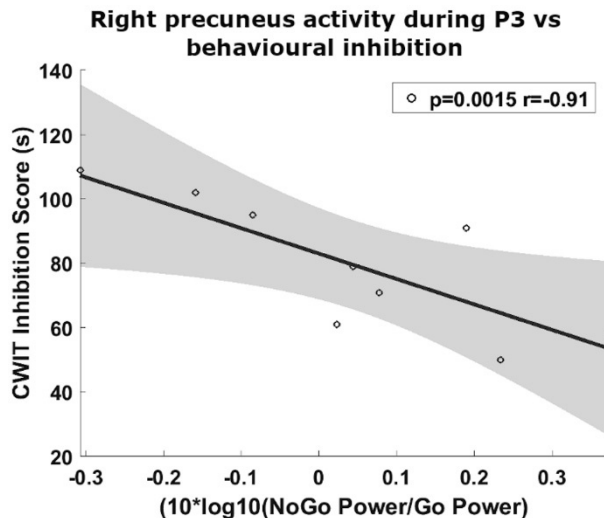


Figure 7. Greater behavioural inhibition in ALS is associated with increased right precuneus activity during NoGo P₃ relative to Go P₃. Higher CWIT inhibition score indicates poorer behavioural inhibition.

Discussion

This study demonstrates for the first time the specific cortical structures that contribute to performance of the SART and quantifies the relationship between SART performance measures and underlying cognitive performance. Furthermore, we have identified abnormalities in cortical function which strongly correlate with executive impairment in ALS.

ERP peak characteristics

At sensor-space, our control findings were consistent with the literature, demonstrating the robustness of SART-associated ERPs. N₂ and P₃ peaks were present in the anticipated time windows and, as expected, larger for healthy individuals during correct response omission.

Central N₂

NoGo N₂ was maximal in Cz, as previously established. We identified that smaller differences in N₂ size between NoGo and Go trials was associated with faster reaction

times. We also identified a correlation between smaller NoGo N2 peaks and better NoGo trial accuracy. As the N2 peak has been associated with automated motor response control,⁶ this may reflect greater ability to withhold and greater response speed where less cortical resources are required to inhibit upper motor neurons.

Notably, these correlations were not present for ALS patients, which may represent the compensatory engagement of alternative cortical resources. Alternatively, the established malfunction of inhibitory cells of the motor system³⁸ in addition to upper motor neurons may lead to reduction in NoGo N2 in combination with slowing reaction times.

Frontal and parietal P₃

The P₃ peak was present across the frontoparietal axis of sensors during NoGo trials in keeping with the SART ERP literature.^{6,8,23} Such spatially distributed P₃ peaks associated with other cognitive tasks have been shown to consist of two distinct entities, namely the frontal and parietal P₃. Frontal P₃ peaks have been associated with orientation to novel stimuli, declining over task duration although remaining elevated in distractible children³⁹ and those with panic disorder.⁴⁰ By contrast, parietal P₃ peaks are associated with working memory and attention to target stimuli.^{39,40}

Here we have identified similarly distinct behaviours in the frontal and parietal SART-associated P₃ peaks. In frontocentral electrodes, P₃ latency related to response timing and is likely to provide an index of orientation speed. Smaller frontocentral P₃ peaks were associated with more accurate performance in the opposite trial type (i.e. better Go performance with smaller NoGo peaks and vice versa). By contrast, larger NoGo parietal P₃ was associated with better Go trial performance. This is in keeping with the cognitive resources required for accurate Go and NoGo SART performance. The engagement of working memory and attentional control was indicated by a large NoGo parietal P₃, and quick orientation to the task was indicated by earlier, smaller frontal P₃ peaks.^{39,40}

The orienting frontal P₃ is typically earlier than the parietal P₃, however it has been hypothesised that frontal P₃ peaks may also encompass compensatory prefrontal engagement due to parietal decline.⁴¹ This may explain why ALS patients, but not in controls, demonstrated greater Cz P₃ peak latencies during Go trials in those with better accuracy.

Cortical source imaging

At source-space both Go and NoGo N2 and P₃ peaks were associated with extensive prefrontal and motor cortex engagement, particularly in the left cortex, in keeping with use of the right hand for task performance. Such widespread cortical engagement is expected, given the numerous cognitive and motor domains required for accurate task performance. The medial PPC (i.e. the precuneus) was additionally engaged during NoGo trials relative to Go trials during N2, in keeping with its role in both voluntary attention shifting and movement control.⁴² By contrast, the left insula and inferior parietal lobule show lower power in NoGo trials relative to Go trials during P₃, in

keeping with role of the left insula in the salience network⁴³ and goal directed behaviour.⁴⁴ The left inferior parietal lobule has been attributed numerous functions, among which are object-directed action⁴⁵ and expectancy violation.⁴⁶ This engagement of numerous cortical structures by different elements of the SART highlights the range of cortical pathologies that could contribute to decline in SART performance measures. While SART ERP analysis can temporally dissect the cause of such performance decline, it is clear from source imaging that a specific peak abnormality could also result from dysfunction in several different cortical structures. Source imaging can therefore not only inform on source contributing to cognitive and motor symptoms but could also discriminate between psychiatric or neurodegenerative syndromes with similar symptoms driven by differing cortical pathologies.

Quantifying cortical pathology driving cognitive impairment in ALS

ALS patients maintained similar Go and NoGo accuracy but were more likely to attempt to complete trials rapidly clicking before cognitively processing the presented digit, resulting in greater anticipation error. Despite sensor-space differences, patients and control activity did not differ significantly at a specific N2 source. This is likely to be a function of spatially distributed differences in activity which summate in signals captured by individual electrodes at source-space. Patients did, however, demonstrate very similar elevation in precuneus activity during NoGo relative to Go trials in both N2 and P3. As this elevation in right precuneus activity during P3 was associated with greater behavioural inhibitory function, this may represent a compensatory recruitment of this region. Indeed, this exemplifies the utility of source localised EEG during task performance for quantifying cognitive pathology during presymptomatic phases of compensatory cortical activity that are more amenable to clinical intervention.

ALS patients demonstrated additional widespread cortical activity elevation during NoGo relative to Go trials during P3, particularly in the left insula and inferior parietal lobule, which showed very good discrimination between patients and controls (AU-ROC > 0.75). Such posterior parietal hyper-engagement has previously been observed during involuntary attention switching¹⁹ and at rest,^{17,47} and may provide additional discriminatory power in the development of cortical diagnostic biomarkers. A previous study in Huntington's disease identified reduced activity in the left DLPFC,⁹ right medial frontal and anterior cingulate cortex during the NoGo P3, while we find hyperactivity in these areas in ALS, highlighting the ability of this task to identify differing underlying cortical pathologies in neurodegenerations with overlapping cognitive and behavioural symptoms.

We acknowledge that while these cross-sectional-data serve well to characterization of ALS disease heterogeneity, these measure demand larger-scale studies for adequately-powered subgroup analysis. Additional larger, longitudinal studies will be required to further evaluate the application of this technology in clinical trials and disease prognostics.

In conclusion, here we have provided a spatially and temporally precise description of the cortical activity which underlies the N₂ and P₃ peaks of the randomised SART-ERP in healthy adults and illustrated the applications of this methodology for interrogating cognitive and motor malfunction in a complex neurodegenerative disease. While larger patient recruitment is required for further investigation of the use of SART as an ALS biomarker, we have established that the SART-ERP and its underlying source activity can provide objective, quantitative, early markers of cognitive and motor pathology. The localisation of EEG recorded during a wider battery of cognitive, motor and sensory tasks has considerable potential to provide patient-specific profiles of cortical network disturbance which could in turn provide biomarkers that improve patient subgrouping, clinical trial stratification and prognostic accuracy.

References

1. Robertson, I. H., Manly, T., Andrade, J., Baddeley, B. T. & Yiend, J. Oops!: performance correlates of everyday attentional failures in traumatic brain injured and normal subjects. *Neuropsychologia* **35**, 747–758 (1997).
2. Bellgrove, M. A., Hawi, Z., Gill, M. & Robertson, I. H. The Cognitive Genetics of Attention Deficit Hyperactivity Disorder (ADHD): Sustained attention as a Candidate Phenotype. *Cortex* **42**, 838–845 (2006).
3. O'Gráda, C. *et al.* Does the ability to sustain attention underlie symptom severity in schizophrenia? *Schizophr Res* **107**, 319–323 (2009).
4. Huntley, J. D., Hampshire, A., Bor, D., Owen, A. M. & Howard, R. J. The importance of sustained attention in early Alzheimer's disease. *Int J Geriatr Psychiatry* **32**, 860–867 (2017).
5. Jin, C. Y., Borst, J. P. & van Vugt, M. K. Predicting task-general mind-wandering with EEG. *Cogn Affect Behav Neurosci* **19**, 1059–1073 (2019).
6. Zordan, L., Sarlo, M. & Stablum, F. ERP components activated by the “GO!” and “WITHHOLD!” conflict in the random Sustained Attention to Response Task. *Brain Cogn* **66**, 57–64 (2008).
7. Gan, L., Cookson, M. R., Petrucelli, L. & La Spada, A. R. Converging pathways in neurodegeneration, from genetics to mechanisms. *Nature Neuroscience* **21**, 1300–1309 (2018).
8. Staub, B., Doignon-Camus, N., Marques-Carneiro, J. E., Bacon, É. & Bonnefond, A. Age-related differences in the use of automatic and controlled processes in a situation of sustained attention. *Neuropsychologia* **75**, 607–616 (2015).
9. Beste, C., Saft, C., Andrich, J., Gold, R. & Falkenstein, M. Response inhibition in Huntington's disease—a study using ERPs and sLORETA. *Neuropsychologia* **46**, 1290–1297 (2008).
10. Phukan, J. *et al.* The syndrome of cognitive impairment in amyotrophic lateral sclerosis: a population-based study. *J Neurol Neurosurg Psychiatry* **83**, 102–108 (2012).
11. Elamin, M. *et al.* Executive dysfunction is a negative prognostic indicator in patients with ALS without dementia. *Neurology* **76**, 1263–1269 (2011).
12. Turner, M. R. *et al.* Neuroimaging in amyotrophic lateral sclerosis. *Biomark Med* **6**, 319–337 (2012).
13. Gregory, J. M. *et al.* Executive, language and fluency dysfunction are markers of localised TDP-43 cerebral pathology in non-demented ALS. *J Neurol Neurosurg Psychiatry* **91**, 149–157 (2019).
14. Pinto-Grau, M. *et al.* Screening for cognitive dysfunction in ALS: validation of the Edinburgh Cognitive and Behavioural ALS Screen (ECAS) using age and education adjusted normative data. *Amyotroph Lateral Scler Frontotemporal Degener* **18**, 99–106 (2017).
15. Lulé, D., Ludolph, A. C. & Kassubek, J. MRI-based functional neuroimaging in ALS: An update. **10**, 258–268 (2009).
16. McMackin, R. *et al.* Measuring network disruption in neurodegenerative diseases: New approaches using signal analysis. *J Neurol Neurosurg Psychiatry* jnnp-2018-319581 (2019).
17. Dukic, S. *et al.* Patterned functional network disruption in amyotrophic lateral sclerosis. *Hum Brain Mapp* hbm.24740 (2019).
18. McMackin, R., Bede, P., Pender, N., Hardiman, O. & Nasserroleslami, B. Neurophysiological markers of network dysfunction in neurodegenerative diseases. *Neuroimage Clin* **22**, 101706 (2019).
19. McMackin, R. *et al.* Dysfunction of attention switching networks in amyotrophic lateral sclerosis. *Neuroimage Clin* **22**, 101707 (2019).
20. Ludolph, A. *et al.* A revision of the El Escorial criteria - 2015. *Amyotroph Lateral Scler Frontotemporal Degener* **16**, 291–2 (2015).
21. Delorme, A. & Makeig, S. EEGLAB: an open source toolbox for analysis of single-trial EEG dynamics including independent component analysis. *J Neurosci Methods* **134**, 9–21 (2004).
22. Oostenveld, R., Fries, P., Maris, E. & Schoffelen, J.-M. FieldTrip: Open source software for advanced analysis of MEG, EEG, and invasive electrophysiological data. *Comput Intell Neurosci* **2011**, 156869 (2011).
23. Hart, E. P. *et al.* Deficient sustained attention to response task and P300 characteristics in early Huntington's disease. *J Neurol* **259**, 1191–1198 (2012).

24. Kam, J. W. Y., Mickleborough, M. J. S., Eades, C. & Handy, T. C. Migraine and attention to visual events during mind wandering. *Exp Brain Res* **233**, 1503–1510 (2015).
25. Jurgens, C. K. *et al.* Basal ganglia volume is strongly related to P3 event-related potential in premanifest Huntington's disease. *Eur J Neurol* **18**, 1105–1108 (2011).
26. Van Veen, B. D., Van Drongelen, W., Yuchtman, M. & Suzuki, A. Localization of brain electrical activity via linearly constrained minimum variance spatial filtering. *IEEE Trans Biomed Eng* **44**, 867–80 (1997).
27. Fuchs, M., Kastner, J., Wagner, M., Hawes, S. & Ebersole, J. S. A standardized boundary element method volume conductor model. *Clin Neurophysiol* **113**, 702–12 (2002).
28. Fonov, V., Evans, A., McKinstry, R., Almlie, C. & Collins, D. Unbiased nonlinear average age-appropriate brain templates from birth to adulthood. *Neuroimage* **47**, S102 (2009).
29. Douw, L., Nieboer, D., Stam, C. J., Tewarie, P. & Hillebrand, A. Consistency of magnetoencephalographic functional connectivity and network reconstruction using a template versus native MRI for co-registration. *Hum Brain Mapp* **39**, 104–119 (2018).
30. Jonmohamadi, Y. *et al.* Comparison of beamformers for EEG source signal reconstruction. *Biomed Signal Process Control* **14**, 175–88 (2014).
31. Benjamini, Y. & Hochberg, Y. Controlling the False Discovery Rate: A Practical and Powerful Approach to Multiple Testing. *Journal of the Royal Statistical Society. Series B (Methodological)* vol. 57 289–300 (1995).
32. Kim, H.-Y. Statistical notes for clinical researchers: post-hoc multiple comparisons. *Restor Dent Endod* **40**, 172–176 (2015).
33. Benjamini, Y. Discovering the false discovery rate. *J R Stat Soc Series B Stat Methodol* **72**, 405–416 (2010).
34. Hajian-Tilaki, K. Receiver Operating Characteristic (ROC) Curve Analysis for Medical Diagnostic Test Evaluation. *Caspian J Intern Med* **4**, 627 (2013).
35. Efron, B. Empirical Bayes Estimates for Large-Scale Prediction Problems. *J Am Stat Assoc* **104**, 1015 (2009).
36. Delis, D. C., Kramer, J. H., Kaplan, E. & Holdnack, J. Reliability and validity of the Delis-Kaplan Executive Function System: An update. *Journal of the International Neuropsychological Society* **10**, 301–303 (2004).
37. Tzourio-Mazoyer, N. *et al.* Automated Anatomical Labeling of Activations in SPM Using a Macroscopic Anatomical Parcellation of the MNI MRI Single-Subject Brain. *Neuroimage* **15**, 273–89 (2002).
38. Menon, P., Yiannikas, C., Kiernan, M. C. & Vucic, S. Regional motor cortex dysfunction in amyotrophic lateral sclerosis. *Ann Clin Transl Neurol* **6**, 1373–1382 (2019).
39. Kilpeläinen, R. *et al.* Persistent frontal P300 brain potential suggests abnormal processing of auditory information in distractible children. *Neuroreport* **10**, 3405–3410 (1999).
40. Clark, C. R., McFarlane, A. C., Weber, D. L. & Battersby, M. Enlarged frontal P300 to stimulus change in panic disorder. *Biol Psychiatry* **39**, 845–856 (1996).
41. van Dinteren, R., Arns, M., Jongasma, M. L. A. & Kessels, R. P. C. Combined frontal and parietal P300 amplitudes indicate compensated cognitive processing across the lifespan. *Front Aging Neurosci* **6**, 294 (2014).
42. Cavanna, A. E. & Trimble, M. R. The precuneus: a review of its functional anatomy and behavioural correlates. *Brain* **129**, 564–583 (2006).
43. Uddin, L. Q., Nomi, J. S., Hébert-Seropian, B., Ghaziri, J. & Boucher, O. Structure and function of the human insula. *J Clin Neurophysiol* **34**, 300 (2017).
44. Varjačić, A. *et al.* The role of left insula in executive set-switching: Lesion evidence from an acute stroke cohort. *Cortex* **107**, 92–101 (2018).
45. Chen, Q., Garcea, F. E., Jacobs, R. A. & Mahon, B. Z. Abstract Representations of Object-Directed Action in the Left Inferior Parietal Lobule. *Cerebral Cortex* **28**, 2162–2174 (2018).
46. O'Connor, A. R., Han, S. & Dobbins, I. G. The inferior parietal lobule and recognition memory: expectancy violation or successful retrieval? *J Neurosci* **30**, 2924–2934 (2010).
47. Proudfoot, M. *et al.* Increased cerebral functional connectivity in ALS: A resting-state magnetoencephalography study. *Neurology* **90**, e1418–e1424 (2018).



Chapter 7

EEG network alterations in asymptomatic *C9orf72* repeat expansion carriers

Stefan Dukic, Roisin McMackin, Kevin van Veenhuijzen, Henk-Jan Westeneng, Ruben P.A. van Eijk, Boudewijn T.H.M. Sleutjes, Bahman Nasserroleslami, Orla Hardiman, Leonard H. van den Berg

In preparation

Abstract

Amyotrophic lateral sclerosis (ALS) is a progressive neurodegenerative disease characterised primarily by the degeneration of motor neurons. While the aetiology of ALS remains complex and multifactorial, a notable subset of approximately 10% of ALS cases in European populations exhibit a discernible genetic inheritance pattern, predominantly associated with the *C9orf72* hexanucleotide repeat expansion. Accurately assessing individuals at risk of developing ALS yields insights into early cerebral changes, promising the identification of biomarkers for timely diagnosis and intervention. We, therefore, aim to evaluate functional alterations in asymptomatic *C9orf72* repeat expansion carriers using electroencephalography (EEG).

A total of 36 family members of 18 patients with familial *C9orf72* hexanucleotide repeat expansion ALS were analysed: 15 with the hexanucleotide repeat expansion in the *C9orf72* gene (C9+) and 21 without it (C9-). High-density EEG data with 128 channels were collected while participants undertook the sustained attention to response task (SART), a variation of a Go/NoGo task entraining frontoparietal and motor networks, known to be affected in ALS. The EEG data were analysed in the sensor- and source-space during N2 (220-350 ms) and P3 (350-750 ms) time windows. Differences between the two cohorts were quantified using linear mixed effects model analysis, incorporating pedigree information to correct for familial relations and lessen effects of other genetic factors.

The results reveal that there is a statistically significant difference between C9- and C9+ family members in the P3 event-related potential. Namely, sensor-space analysis show that the potential is lower across the midline electrodes ($P < 0.01$), while source-space analysis show that the potential is lower in the bilateral sensorimotor cortex ($P < 0.05$), suggesting a lower engagement of the cortical motor system in C9+ family members compared to C9- family members.

These results provide evidence of brain function difference in asymptomatic family members with the *C9orf72* repeat expansion, suggesting a functional impairment of the cortical motor system. These findings could have implications for the development of biomarkers for early detection and intervention, and could be further investigated whether they are predictive of future symptom onset.

Introduction

Amyotrophic lateral sclerosis (ALS) is a progressive neurodegenerative disease characterised by the involvement of upper and lower motor neurons. While the majority of ALS cases occur sporadically, a notable subset of approximately 10% of patients exhibit a discernible genetic inheritance pattern, primarily linked to the hexanucleotide repeat expansion within the *C9orf72* (chromosome 9 open-reading-frame 72) gene.¹ Notably, the *C9orf72* repeat expansion is not fully penetrant and it is also linked to frontotemporal dementia (FTD).² The early diagnosis of ALS presents a significant clinical challenge. Additionally, therapy responses may vary due to disease heterogeneity, highlighting the potential need for phenotype-specific inclusion criteria, ideally in the form of objective and quantitative biomarkers. Better assessment of individuals at risk in their presymptomatic phase can elucidate the brain circuits affected by ALS-associated genetic mutations, thereby potentially uncovering early biomarkers of the disease. Such advancements could help us in the discovery of new therapeutic targets, which could be administered before the irreversible damage occurs.

By the time patients fulfil diagnostic criteria for ALS, considerable disease burden can already be detected. Namely, studies indicate that a significant portion of lower motor neurons, which innervate the muscle, are already lost up to a year before clinical signs appear,³ while centrally, the intracortical motor connectivity becomes significantly impaired, possibly even decades earlier.⁴ Although the presymptomatic stage of ALS is still not fully characterised, several research groups have shown, using structural MRI, that asymptomatic *C9orf72* repeat expansion carriers exhibit widespread (sub)cortical grey and white matter alterations.^{5,6} Besides structural degeneration, a PET study has recently produced evidence of glucose metabolism dysfunction in the frontotemporal regions, precuneus, basal ganglia and thalamus in asymptomatic *C9orf72* repeat expansion carriers.^{7,8}

Although the neurophysiological changes in asymptomatic *C9orf72* repeat expansion carriers have not been elucidated, research using electroencephalography (EEG) and magnetoencephalography (MEG) has shown alterations in the motor cortex and frontoparietal networks in ALS.⁹⁻¹³ A recent EEG study¹⁴ using the sustained attention to response task (SART),¹⁵ a variation of a Go/NoGo task, showed increased engagement in the insula and the parietal cortex in ALS patients. By requiring both motor and cognitive performance, the SART is a highly suitable candidate for interrogating cohorts of those who are at risk of developing motor and cognitive impairments, such as *C9orf72* repeat expansion carriers.

Early detection of ALS is crucial, as the optimal therapeutic window is likely to be in the earliest stages of the disease, prior to observable clinical symptoms. Unlike structural imaging modalities, electrophysiological methods can capture both network dysfunction and compensation, providing sensitive measures of early pathology, which may precede imaging evidence of atrophy. Interestingly, an FTD study of *C9orf72* repeat expansion carriers showed evidence that suggests that the onset of structural and cognitive changes may be preceded by alterations of intracortical connectivity measures.⁴ In recent years, EEG has been proven useful in detecting changes occurring

in ALS patients^{9,10,14} and it has been suggested as a candidate for clinical trials in Alzheimer's disease.¹⁶

The improvement in recording equipment, and the establishment of advanced noise removal tools and signal analysis methods allow more spatially precise and sensitive network interrogation suitable, for use in clinical trials^{17,18} and for early disease detection. As neurophysiological alterations in asymptomatic *C9orf72* repeat expansion carriers have yet to be elucidated, this study aimed to investigate the presence of neurophysiological changes in asymptomatic *C9orf72* repeat expansion carriers by assessing cognitive and motor network differences between *C9orf72*-positive and -negative ALS family members through the analysis of event-related neuroelectric activity from high-density EEG.

Methods

Participants

Between December 2020 and December 2022, we included 36 asymptomatic family members (AFM) of patients with *C9orf72*-associated familial ALS, who were approached by their relatives diagnosed with ALS at the motor neuron disease outpatient clinic of the University Medical Centre Utrecht. All included participants were asymptomatic, defined as absence of signs of upper or lower motor neuron disease, bulbar dysfunction, and cognitive changes. Methods to ascertain asymptomatic status were described previously.⁶ All participants were 18 years or older and gave written informed consent according to the Declaration of Helsinki. The medical research ethics committee of University Medical Centre Utrecht approved this study (NL70373.041.19). Participants with a history of severe head injury, neurodegenerative and neuropsychological conditions and those using psychoactive medication at the time of recording were excluded.

Experimental paradigm

Participants undertook the SART, for which they were instructed to click the left mouse button every time they saw a number on the screen except for the number three. The task was divided into four blocks of 5 minutes, with short break times to minimise fatigue. Participants were seated approximately 1 meter from a computer monitor where numbers from one to nine in single-digit format were appearing in random order for 250 milliseconds (ms), using Presentation software (Version 22.1, Neurobehavioral Systems Inc., Berkeley, CA). Digits were presented in light grey (RGB code: 250, 250, 250 from 255) on a black background to reduce discomfort associated with bright light from purely white numbers. Font size was randomised between 100, 120, 140, 160, and 180 points to avoid participants using a perceptual template for target recognition of the number three and to encourage cognitive processing of the numerical value.¹⁵ Each stimulus was followed by an interstimulus interval of randomised duration, ranging between 1120 and 1220 ms, during which a black screen was

presented. Each recording block contained 252 trials, the number three appearing at random in 11% of trials.

Participants were requested to prioritise speed and accuracy equally since both were used as measures of performance. Under supervision by the experimenter, participants were given one practice round, consisting of up to 45 trials, to ensure they understood the task. During the recording lights were switched off to avoid visual distractions.

Data acquisition

The pedigree of all participants was determined and all were tested for the pathogenic *C9orf72* hexanucleotide repeat expansion using methods described previously.¹⁹ All participants underwent a standardised and comprehensive neurological examination to rule out signs of upper and lower motor neuron involvement, as described previously.²⁰ In addition, to rule out signs of cognitive changes, cognitive status (2.3% cut-off)²¹ of the participants was determined using the Dutch version of the Edinburgh Cognitive and Behavioural ALS Screen (ECAS), a screening tool to determine cognitive and behavioural changes specific for ALS.²¹

Task performance was recorded by Presentation software and six behavioural measures were extracted: NoGo accuracy (percentage of three-digit stimuli followed by response omission), Go accuracy (percentage of nonthree digit stimuli followed by a response in the permitted time window), total accuracy (combined NoGo and Go accuracy), anticipation (clicking less than 200 ms after a Go stimulus), response time and response time variability (standard deviation).

High-density EEG data were collected with 128 channels using the BioSemi Active Two system (BioSemi B.V., Amsterdam, The Netherlands), sampled at 512 Hz and lowpass filtered (0-104 Hz) by the acquisition hardware to prevent aliasing. Trials that were incorrect, containing multiple responses, containing responses within the baseline period or those with response times shorter than 200 ms or longer than 800 ms were excluded from the EEG data analysis.

EEG data analysis

The analysis was performed using custom scripts in MATLAB (Version R2022b, The MathWorks Inc., Natick, Massachusetts) which rely in part on publicly available FieldTrip²² and EEGLAB²³ toolboxes. Data were downsampled to 256 Hz before further processing. Artefacts in the data were identified and removed using the following steps. To improve stationarity of the signals, the data were temporarily highpass (non-causal finite impulse response, Hamming window: 1 Hz passband edge, filter order 1690) and lowpass (non-causal finite impulse response, Hamming window: 40 Hz passband edge, filter order 86) filtered, and then bad channels were automatically detected and removed.²⁴ Independent component analysis (ICA) was applied to common-average referenced signals using CUDAICA (Compute unified device architecture ICA; GPU optimised Infomax-ICA)²⁵ and artefacts representing ocular (probability >0.8) and muscle (probability >0.8) activity were automatically detected using

ICLabel.²⁶ The computed ICA weights were then transferred to EEG data that were highpass (non-causal Butterworth, 0.1 Hz cut-off, 24 dB/oct roll-off) and lowpass (non-causal Butterworth, 30 Hz cut-off, 24 dB/oct roll-off) filtered, and the previously identified artefact ICA components were removed. Bad channels were interpolated using spherical spline interpolation,²⁷ and the cleaned signals were epoched (extending -200 ms to 900 ms relative to the stimulus onset) and baseline corrected. Epochs and channels exceeding $\pm 75 \mu\text{V}$ were interpolated to correct potential high voltage jumps and drifts in the data. If the number of channels exceeding this threshold was above 10, then the epoch was removed. Finally, the epochs were referenced to the common-average and averaged over trials to estimate a Go and a NoGo event-related potential (ERP) for each participant. Breakdown of the preprocessing outcomes and data quality assessments is given in the Supplementary Table 1.

The ERP data were source-reconstructed using the standardised low resolution electromagnetic tomography (sLORETA)²⁸ to obtain time-varying signals originating from the brain. A realistically-shaped finite element model²⁹ was used, based on ICBM152^{30,31} template with anisotropic white matter conductivity.^{32,33} A regular grid with 6,264 locations confined to the grey matter and spaced 5 millimetres apart was used for source estimation. For each participant and task condition, noise regularisation was applied using a diagonal matrix constructed from a diagonal of a covariance matrix of the template leadfield matrix, which was scaled using the estimated signal-to-noise ratios.³⁴

An atlas-based approach was applied to estimate signals from 62 cortical regions, which were defined by the Cerebrum Atlas³⁵ and labelled according to the Desikan-Killiany-Tourville labelling protocol.³⁶ For each task condition, using the singular value decomposition on a source-level covariance matrix (300-750 ms) from dipoles within a given region, we computed an equivalent region dipole in the direction of maximum power.³⁷ Finally, the absolute value of each source-reconstructed ERP was taken to obtain time-varying power changes and to account for arbitrary dipole orientations.

In all our analyses, when comparing the two groups, we assessed both the sensor-space difference wave and the source-space power difference between the two conditions (i.e., NoGo-Go). Group differences were evaluated using the mean of the amplitude and the power during two time windows of interest: N2 (220-350 ms) and P3 (350-750 ms).

Statistical analysis

In this study, we contrasted AFM with the *C9orf72* repeat expansion (C9+) against those without it (C9-), to identify differences in EEG activations.

Differences in demographics between groups were calculated using the Mann-Whitney U-test for continuous variables and Fisher's exact test for categorical variables. Group-level comparisons of performance of the SART and of ECAS scores were implemented with Mann-Whitney U-test, while the differences of the physical examination outcomes used Fisher's exact test. For upper motor neuron functioning, assessed by

physical examination, the signs most deviant from ‘normal’, either left or right, were used.

The difference between the two groups were evaluated using a linear mixed effects model with age, sex and *C9orf72* carriership as fixed effects, and a random term for pedigree ID to incorporate familial effects. The random effect was included as it significantly improved the model fit (Likelihood ratio test: $\Lambda = 14.39$, $P < 0.001$) The mean group differences were evaluated using the mean N2 and P3 ERPs. For sensor-space data, we used the average of central midline electrodes (C21-23 and A1-2; equivalent to the electrodes between Fz and CPz from the 10-10 EEG system), which are typically used in Go/NoGo data analyses³⁸⁻⁴⁰ and previously in the analysis of SART data in ALS.¹⁴ For source-space data, using a hypothesis-free whole-brain analysis, we applied the same linear mixed effects models to each brain region and corrected for multiple comparisons using false discovery rate (FDR, $q = 0.05$).⁴¹ Values of $P < 0.05$ after correction for multiple testing were considered statistically significant.

Data availability

The data that support the findings of this study are available from the corresponding author, upon reasonable request.

Results

The demographic profiles

A total of 36 AFM of patients with familial *C9orf72* hexanucleotide repeat expansion ALS were analysed: 15 with the hexanucleotide repeat expansion in the *C9orf72* gene and 21 without it. Total number of pedigrees was 18, with a median number of AFM per pedigree: 2 (range: 1-5). All participants were up to the third degree of consanguinity with respect to the closest family member with ALS. Demographics of the participants are summarised in Table 1.

Group differences at physical examination and cognitive functioning

No clinical signs of lower motor neuron involvement (i.e., muscle atrophy, weakness, fasciculations, hyporeflexia) were found on physical examination. Signs that can be associated with mild upper motor neuron involvement were observed in both groups without significant differences between them. None of the participants showed cognitive impairments on their ECAS test and there were no significant differences between groups when comparing: ECAS total score, ALS-specific and ALS-nonspecific subscores. The breakdown of physical examination and cognitive screening are presented in Supplementary Table 2.

Task performance results

The two groups did not significantly differ in any of the SART performance measures (Table 2).

Table 1. Demographic and clinical characteristics of asymptomatic family members.

	AFM C9- (N = 21)	AFM C9+ (N = 15)	P-value
Age	41.9 (28.7-47.4)	48.4 (38.7-56.1)	0.15
Sex (M/F)	10/11	5/10	0.50
Education level (low/high)	4/17	8/7	0.07
Handedness (L/R)	2/19	0/15	0.50
Pedigrees	18 (2; 1-5)		

Age data are shown as median (interquartile range), pedigree data as total number pedigrees (median number of AFM per pedigree; range) and other data as count. Education level was assessed using the international standard classification of education (ISCED, 2011 version), which was dichotomised into low (level 0-4) and high (level 5-8) education. Abbreviations: AFM = asymptomatic family member; C9- = carriership of *C9orf72* with normal repeat length; C9+ = carriership of *C9orf72* repeat expansion; M/F = male/female; L/R = left-/right-handed.

Table 2. Performance measures of the SART.

	AFM C9- (N = 21)	AFM C9+ (N = 15)	P-value
Correct NoGo (%)	75 (61-89)	82 (69-87)	0.81
Correct Go (%)	97 (90-99)	96 (93-99)	0.60
Correct total (%)	95 (88-98)	94 (90-98)	0.91
Anticipation error (%)	3 (0-9)	2 (0-5)	0.50
Response time (ms)	306.25 (268.68-331.67)	313.9 (275.22-369.53)	0.40
Response time variability (ms)	70.43 (55.51-99.76)	81.77 (61.78-88.74)	0.59

Data are shown in percentages (%) or milliseconds (ms) and as median (interquartile range). P-values are calculated using Mann-Whitney U-test. Abbreviations: AFM = asymptomatic family member; C9- = carriership of *C9orf72* with normal repeat length; C9+ = carriership of *C9orf72* repeat expansion.

Sensor-space results

For both cohorts, average brain responses (NoGo-Go difference waves; Δ Amplitude) across the average of the midline electrodes reveal the N2 ERP to be within 220-350 ms and the P3 ERP within 350-750 ms (Figure 1A). Linear mixed effects model analysis shows that there is a statistically significant difference between C9- and C9+ AFMs in the average P3 peak (difference [95% confidence interval]: 1.21 [0.35 2.06] μ V; $P = 0.007$), but not in the N2 peak (-0.08 [-1.17 1.00] μ V; $P = 0.876$). Average brain responses across individual channels are shown in Figure 1B.

Source-space results

Based on the findings from the sensor-space analysis, we further analysed the P3 time window only (Figure 2). Average brain activations (NoGo-Go power difference; Δ Power) during the P3 time window indicate frontoparietal activation in both groups. Superior frontal and precentral cortices are primarily activated in C9- AFM, while precuneus, cuneus, inferior parietal and lateral occipital cortices are primarily activated in C9+ AFM. Linear mixed effects model analysis revealed a significant decrease in the average P3 power in C9+ AFM across the bilateral sensorimotor cortex: the pre- and postcentral cortex, and the paracentral lobules (Supplementary Table 3).

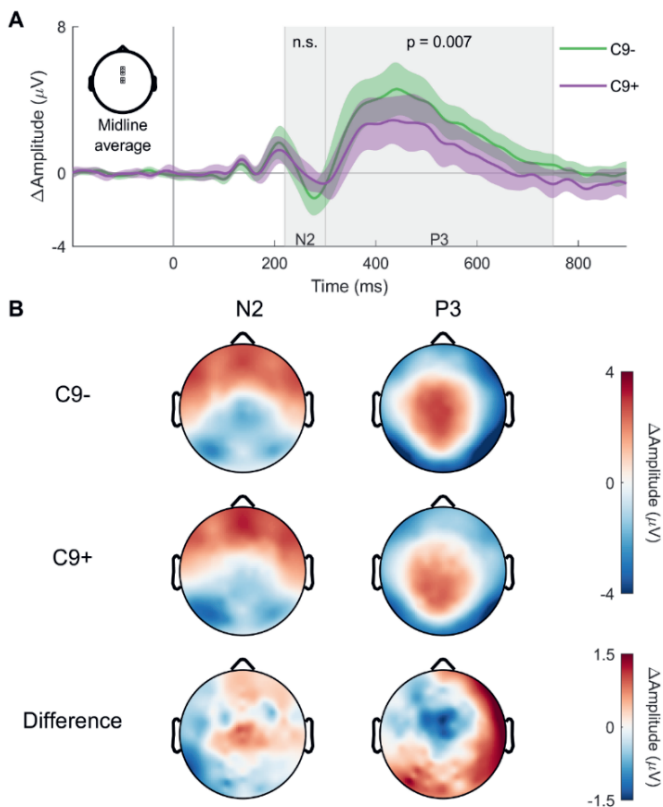


Figure 1. Sensor-space brain responses for C9- and C9+ asymptomatic family members diverge in the central electrodes during the P3 ERP. (A) Linear mixed effects model analysis revealed a significant ($P = 0.007$) decrease in the average P3 in the averaged midline brain response in C9+ AFM (red line) compared to C9- AFM (blue line). The N2 difference between the two groups was not significant (n.s., $P = 0.876$); (B) Topoplot differences between the two groups point to a decreased activation in the frontocentral midline electrodes in C9+ family members. A difference wave of each group was used; vertical bars at 0 ms represent stimulus onset.

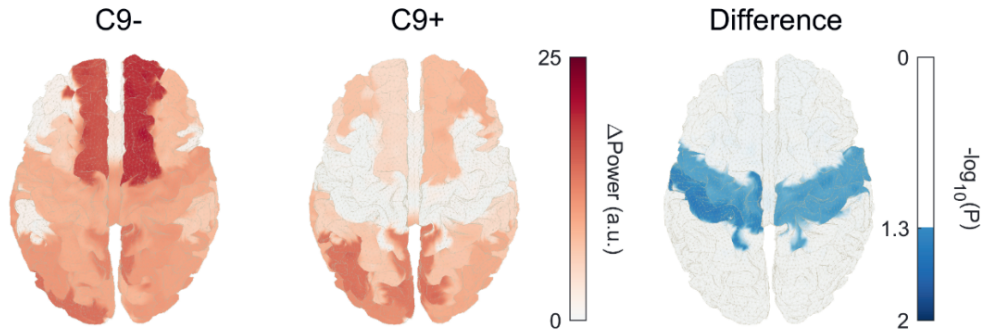


Figure 2. Source-space activation patterns in C9- and C9+ asymptomatic family members diverge in the sensorimotor cortex. Both groups show similar patterns of activation involving the frontoparietal areas, wherein frontocentral areas are primarily activated in C9- AFM, while occipitoparietal areas are primarily activated in C9+ AFM. Linear mixed effects model analysis (correcting for age, sex and pedigree ID) revealed a significant ($P < 0.05$, FDR) decrease in the average P₃ power in the bilateral sensorimotor cortex in C9+ AFM compared to C9- AFM; A power difference (NoGo-Go) of each group was used in all plots.

Discussion

This study demonstrates the ability of EEG to capture subtle abnormalities in cortical functioning in asymptomatic family members with the *C9orf72* hexanucleotide repeat expansion. We compared those with (C9+) to those without the *C9orf72* repeat expansion (C9-) in order to identify EEG differences specific to the mutation during their asymptomatic phase. We found a significant decrease in P₃ ERP activation in the bilateral sensorimotor cortex of AFM with the *C9orf72* hexanucleotide repeat expansion. Our findings indicate that the *C9orf72* repeat expansion affects the function of the sensorimotor network, which may contribute to the development of ALS in conjunction with other factors. These results demonstrate that EEG has the potential to detect functional differences in C9+ AFM, which may aid in the identification of biomarkers for early ALS diagnosis.

Both the N₂ and the P₃ ERP were present across the frontoparietal axis of sensors in keeping with our SART study in ALS⁴⁴ and previous literature.³⁸⁻⁴⁰ The functional role and neural generators of both ERPs are still not well-defined; however, both N₂ and P₃ processes contribute to successful inhibition. The N₂ precedes the response and is often interpreted as an index of conflict monitoring and possibly motor inhibition, and its neural generators are thought to be located within the anterior cingulate, orbitofrontal and dorsolateral prefrontal, and presupplementary motor areas.⁴² In the case of P₃ ERP, research suggests that it is associated with inhibitory processing, as well as performance monitoring.⁴³ In tasks like SART, spatially distributed P₃ activity has been shown to be generated by multiple neural sources.⁴⁴ Our data supports this notion and demonstrates that the P₃ peak is at the group level associated with the engagement of frontoparietal areas and temporoparietal junction, in accordance with prior Go/NoGo literature.^{14,45-48} In addition, our findings are in line with a study showing that the P₃ is partially related to the processing within the motor system.⁴⁹

In our study, the sensor-space N2 ERP was not significantly different between C9- and C9+ AFM. We, however, show that C9+ AFM have decreased activation of the sensorimotor area during P3 ERP. These findings suggest that cognitive processes associated with conflict monitoring and inhibition reflected in N2 are not differential between the two cohorts, while the P3 inhibition processes within the motor system are. This finding is consistent with observations of dysfunctional glucose metabolism⁸ and grey matter aberration^{5,6} in the sensorimotor area in asymptomatic *C9orf72* repeat expansion carriers. Interestingly, M/EEG studies focusing on the movement-related processing in ALS found reduced post-movement cortical activation, which was observed bilaterally to movement execution.^{13,50,51} This impairment, however, was not observed in a heterogeneous group of asymptomatic carriers (N = 12, 10 SOD1 and 2 *C9orf72* repeat expansion).¹³ The post-movement cortical activity is associated with deactivation and inhibition of cortical areas primarily in the hemisphere contralateral to movement execution.⁵² Since it is interpreted as a state of decreased neural excitability or inhibited thalamo-cortical circuitry, our finding could suggest an impaired inhibit/excitatory balance in *C9orf72* pathology, which is hypothesised to underpin ALS.⁵³ Nevertheless, further research is needed to explore this potential relationship. Future research could employ magnetic resonance spectroscopy data to assess the levels of brain metabolites associated with excitatory and inhibitory processes, such as glutamate and GABA, in order to elucidate the neurochemical mechanisms underlying the observed ERP activations.

In our previous SART EEG study, ALS patients demonstrated widespread cortical hyperactivity during P3, particularly in the parietal lobule, which is the area of cortical thinning,⁶ and in left insula, which could be hypometabolic,^{7,8} in asymptomatic *C9orf72* repeat expansion carriers. In the present study, however, we did not observe significant changes in these areas, although the parietal areas, especially bilateral precuneus, are among main observed generators of the P3 ERP in C9+ AFM. While the observation that thinner cortex may not necessarily result in impaired function is intriguing, it is plausible that the finding is influenced by the inadequate statistical power of our study and the relatively low sensitivity of EEG towards deeper sources. Furthermore, our previous study investigating the SART in ALS did not detect any changes in the sensorimotor cortex, which could have been obscured by the identified widespread cortical hyperactivity. Nonetheless, it is worth noting that the P3 ERP window in that study was shorter (350-550 ms) compared to the current study (350-750 ms), and hence, it may have reduced the sensitivity to detect the motor impairment that might be more evident in the later stages of P3 processing. Finally, our previous study primarily included C9- ALS patients, making the findings more representative of general ALS pathology. In addition, it is noteworthy that none of the participants in our AFM cohort exhibited abnormal cognitive functioning, although some demonstrated signs of motor involvement. This may have somewhat restricted our ability to assess alterations within cognitive networks and increased the likelihood of detecting those within motor network.

Despite the observed involvement of the sensorimotor region, none of the participants reported any symptoms, and this was confirmed by a thorough physical examination conducted at our outpatient clinic for neuromuscular disorders. However, some

findings suggestive of mild upper motor neuron involvement (such as pseudobulbar reflexes and brisk tendon reflexes) were equally observed in both groups. Nevertheless, these mild signs of upper motor neuron involvement can also be present in healthy individuals and may not necessarily imply any pathological changes.⁵⁴ Given that the deterioration of the sensorimotor region is considered a key hallmark of ALS, the current observations could indicate early signs of the disease and therefore, require further longitudinal investigations to elucidate their potential significance.

In our study, we have excluded family members (both C₉- and C₉+) who exhibited abnormal cognitive functioning. It is, however, worth noting that a recent study has demonstrated the presence of a cognitive/behavioural endophenotype among certain C₉- family members.⁵⁵ To assess potential EEG differences in family members, irrespective of the repeat expansion length, obtaining a dataset consisting of population-based controls is necessary.

Some limitations of our study merit consideration. Radially-oriented brain sources exhibit greater prominence in EEG as compared to tangentially-oriented sources, resulting in reduced sensitivity to activations in medial and deep brain regions. In our study, we excluded brain dipoles located in the subcortical structures due to their lower signal-to-noise ratio, which precluded the examination of their potential involvement. However, such limitations could potentially be addressed by utilising more sophisticated source modelling that integrates individualised source-localisation models. Additionally, based on our findings, it is not possible to determine whether these changes represent early compensatory mechanisms or early signs of the disease. Indeed, these differences may be neurodevelopmental, given that previous research has demonstrated that C₉+ AFM have lower gyrification than C₉- AFM.⁶ Although our cross-sectional dataset was useful in detecting *C9orf72*-associated brain alterations, larger-scale and longitudinal investigations, perhaps involving multiple centres, are necessary to discern whether these changes precede ALS symptoms.

Conclusion

We have provided evidence of functional changes in the sensorimotor network of asymptomatic *C9orf72* repeat expansion carriers using EEG. The identification and characterisation of such differences could be further studied as biomarkers for early ALS, and consequently help in the early diagnosis and in the development of an early treatment strategy, as well as enhance our understanding of causal (patho)physiological processes.

Acknowledgments

We thank all study participants for their time and effort. This study received funding from the Stichting ALS Nederland.

References

1. Veldink, J. H. ALS genetic epidemiology 'How simplex is the genetic epidemiology of ALS?' *J Neurol Neurosurg Psychiatry* **88**, 537–537 (2017).
2. Diekstra, F. P. *et al.* C9orf72 and UNC13A are shared risk loci for amyotrophic lateral sclerosis and frontotemporal dementia: A genome-wide meta-analysis. *Ann Neurol* **76**, 120–133 (2014).
3. Neuwirth, C. *et al.* Motor Unit Number Index (MUNIX) detects motor neuron loss in pre-symptomatic muscles in Amyotrophic Lateral Sclerosis. *Clinical Neurophysiology* **128**, 495–500 (2017).
4. Benussi, A. *et al.* Clinical and biomarker changes in presymptomatic genetic frontotemporal dementia. *Neurobiol Aging* **76**, 133–140 (2019).
5. Chipika, R. H. *et al.* The presymptomatic phase of amyotrophic lateral sclerosis: are we merely scratching the surface? *Journal of Neurology* **2020** *268*:12 **268**, 4607–4629 (2020).
6. van Veenhuijzen, K. *et al.* Longitudinal Effects of Asymptomatic C9orf72 Carriership on Brain Morphology. *Ann Neurol* **93**, 668–680 (2022).
7. de Vocht, J. *et al.* Use of Multimodal Imaging and Clinical Biomarkers in Presymptomatic Carriers of C9orf72 Repeat Expansion. *JAMA Neurol* **77**, 1008–1017 (2020).
8. Popuri, K. *et al.* FDG-PET in presymptomatic C9orf72 mutation carriers. *Neuroimage Clin* **31**, 102687 (2021).
9. Dukic, S. *et al.* Patterned functional network disruption in amyotrophic lateral sclerosis. *Hum Brain Mapp* **40**, (2019).
10. Nasseroleslami, B. *et al.* Characteristic Increases in EEG Connectivity Correlate With Changes of Structural MRI in Amyotrophic Lateral Sclerosis. *Cereb Cortex* **29**, 27–41 (2019).
11. Proudfoot, M. *et al.* Increased cerebral functional connectivity in ALS: A resting-state magnetoencephalography study. *Neurology* **90**, e1418–e1424 (2018).
12. Proudfoot, M. *et al.* Impaired corticomuscular and interhemispheric cortical beta oscillation coupling in amyotrophic lateral sclerosis. *Clinical Neurophysiology* **129**, 1479–1489 (2018).
13. Proudfoot, M. *et al.* Altered cortical beta-band oscillations reflect motor system degeneration in amyotrophic lateral sclerosis. *Hum Brain Mapp* **38**, 237–254 (2017).
14. McMackin, R. *et al.* Localization of brain networks engaged by the sustained attention to response task provides quantitative markers of executive impairment in amyotrophic lateral sclerosis. *Cerebral Cortex* **30**, 4834–4846 (2020).
15. Robertson, I. H., Manly, T., Andrade, J., Baddeley, B. T. & Yiend, J. Oops!': performance correlates of everyday attentional failures in traumatic brain injured and normal subjects. *Neuropsychologia* **35**, 747–758 (1997).
16. Martínez-Horta, S. *et al.* Impaired face-like object recognition in premanifest Huntington's disease. *Cortex* **123**, 162–172 (2020).
17. Babiloni, C. *et al.* Measures of resting state EEG rhythms for clinical trials in Alzheimer's disease: Recommendations of an expert panel. *Alzheimer's & Dementia* **17**, 1528–1553 (2021).
18. van Straaten, E. C. W., Scheltens, P., Gouw, A. A. & Stam, C. J. Eyes-closed task-free electroencephalography in clinical trials for Alzheimer's disease: an emerging method based upon brain dynamics. *Alzheimers Res Ther* **6**, 1–10 (2014).
19. van Rheezen, W. *et al.* Hexanucleotide repeat expansions in C9ORF72 in the spectrum of motor neuron diseases. *Neurology* **79**, 878–882 (2012).
20. Nitert, A. D. *et al.* Sensitivity of brain MRI and neurological examination for detection of upper motor neurone degeneration in amyotrophic lateral sclerosis. *J Neurol Neurosurg Psychiatry* **93**, 1–11 (2022).
21. Bakker, L. A. *et al.* Derivation of norms for the Dutch version of the Edinburgh cognitive and behavioral ALS screen. *Amyotroph Lateral Scler Frontotemporal Degener* **20**, 19–27 (2019).
22. Oostenveld, R., Fries, P., Maris, E. & Schoffelen, J.-M. FieldTrip: Open source software for advanced analysis of MEG, EEG, and invasive electrophysiological data. *Comput Intell Neurosci* **2011**, 156869 (2011).
23. Delorme, A. & Makeig, S. EEGLAB: an open source toolbox for analysis of single-trial EEG dynamics including independent component analysis. *J Neurosci Methods* **134**, 9–21 (2004).

24. Bigdely-Shamlo, N., Mullen, T., Kothe, C., Su, K. M. & Robbins, K. A. The PREP pipeline: Standardized preprocessing for large-scale EEG analysis. *Front Neuroinform* **9**, 1–19 (2015).
25. Raimondo, F., Kamienskowski, J. E., Sigman, M. & Fernandez Slezak, D. CUDAICA: GPU optimization of infomax-ICA EEG analysis. *Comput Intell Neurosci* **2012**, (2012).
26. Pion-Tonachini, L., Kreutz-Delgado, K. & Makeig, S. ICLabel: An automated electroencephalographic independent component classifier, dataset, and website. *Neuroimage* **198**, 181–197 (2019).
27. Perrin, F., Pernier, J., Bertrand, O. & Echallier, J. F. Spherical splines for scalp potential and current density mapping. *Electroencephalogr Clin Neurophysiol* **72**, 184–7 (1989).
28. Pascual-Marqui, R. D. Standardized low-resolution brain electromagnetic tomography (sLORETA): technical details. *Methods Find Exp Clin Pharmacol* **24**, 5–12 (2002).
29. Vorwerk, J., Oostenveld, R., Piastra, M. C., Magyari, L. & Wolters, C. H. The FieldTrip-SimBio pipeline for EEG forward solutions. *Biomed Eng Online* **17**, 37 (2018).
30. Fonov, V., Evans, A., McKinstry, R., Almlí, C. & Collins, D. Unbiased nonlinear average age-appropriate brain templates from birth to adulthood. *Neuroimage* **47**, S102 (2009).
31. Huang, Y., Datta, A., Bikson, M. & Parra, L. C. Realistic volumetric-approach to simulate transcranial electric stimulation—ROAST—a fully automated open-source pipeline. *J Neural Eng* **16**, 056006 (2019).
32. Mori, S. *et al.* Stereotaxic white matter atlas based on diffusion tensor imaging in an ICBM template. *Neuroimage* **40**, 570–582 (2008).
33. Rullmann, M. *et al.* EEG source analysis of epileptiform activity using a 1 mm anisotropic hexahedra finite element head model. *Neuroimage* **44**, 399–410 (2009).
34. An, N. *et al.* Spatial Accuracy Evaluation of Magnetic Source Imaging Methods on OPM-based MEG. *iScience* 105177 (2022).
35. Manera, A. L., Dadar, M., Fonov, V. & Collins, D. L. CerebrA, registration and manual label correction of Mindboggle-101 atlas for MNI-ICBM152 template. *Scientific Data* 2020 7:1 7, 1–9 (2020).
36. Klein, A. & Tourville, J. 101 labeled brain images and a consistent human cortical labeling protocol. *Front Neurosci* **6**, 171 (2012).
37. Rubega, M. *et al.* Estimating EEG Source Dipole Orientation Based on Singular-value Decomposition for Connectivity Analysis. *Brain Topogr* **32**, 704–719 (2019).
38. Staub, B., Doignon-Camus, N., Marques-Carneiro, J. E., Bacon, É. & Bonnefond, A. Age-related differences in the use of automatic and controlled processes in a situation of sustained attention. *Neuropsychologia* **75**, 607–616 (2015).
39. Hart, E. P. *et al.* Deficient sustained attention to response task and P300 characteristics in early Huntington’s disease. *J Neurol* **259**, 1191–1198 (2012).
40. Zordan, L., Sarlo, M. & Stablum, F. ERP components activated by the “GO!” and “WITHHOLD!” conflict in the random Sustained Attention to Response Task. *Brain Cogn* **66**, 57–64 (2008).
41. Benjamini, Y. & Hochberg, Y. Controlling the False Discovery Rate: A Practical and Powerful Approach to Multiple Testing. *Journal of the Royal Statistical Society. Series B (Methodological)* vol. 57 289–300 (1995).
42. Pires, L., Leitão, J., Guerrini, C. & Simões, M. R. Event-Related Brain Potentials in the Study of Inhibition: Cognitive Control, Source Localization and Age-Related Modulations. *Neuropsychol Rev* **24**, 461–490 (2014).
43. Huster, R. J., Messel, M. S., Thunberg, C. & Raud, L. The P300 as marker of inhibitory control – Fact or fiction? *Cortex* **132**, 334–348 (2020).
44. Polich, J. Updating P300: An integrative theory of P3a and P3b. *Clinical Neurophysiology* **118**, 2128–2148 (2007).
45. Chatroudi, A. H., Rostami, R., Nasrabadi, A. M. & Yotsumoto, Y. Effect of inhibition indexed by auditory P300 on transmission of visual sensory information. *PLoS One* **16**, (2021).
46. Huster, R. J., Westerhausen, R., Pantev, C. & Konrad, C. The role of the cingulate cortex as neural generator of the N200 and P300 in a tactile response inhibition task. *Hum Brain Mapp* **31**, 1260 (2010).
47. Moores, K. A. *et al.* Investigating the generators of the scalp recorded visuo-verbal P300 using cortically constrained source localization. *Hum Brain Mapp* **18**, 53–77 (2003).
48. Bledowski, C. *et al.* Localizing P300 Generators in Visual Target and Distractor Processing: A Combined Event-Related

- Potential and Functional Magnetic Resonance Imaging Study. *Journal of Neuroscience* **24**, 9353–9360 (2004).
49. Smith, J. L., Johnstone, S. J. & Barry, R. J. Movement-related potentials in the Go/NoGo task: The P₃ reflects both cognitive and motor inhibition. *Clinical Neurophysiology* **119**, 704–714 (2008).
50. Bizovičar, N., Dreo, J., Koritnik, B. & Zidar, J. Decreased movement-related beta desynchronization and impaired post-movement beta rebound in amyotrophic lateral sclerosis. *Clinical Neurophysiology* **125**, 1689–99 (2014).
51. Riva, N. *et al.* Cortical activation to voluntary movement in amyotrophic lateral sclerosis is related to corticospinal damage: Electrophysiological evidence. *Clinical Neurophysiology* **123**, 1586–92 (2012).
52. Pfurtscheller, G., Stancák, A. & Neuper, C. Event-related synchronization (ERS) in the alpha band — an electrophysiological correlate of cortical idling: A review. *International Journal of Psychophysiology* **24**, 39–46 (1996).
53. Brunet, A., Stuart-Lopez, G., Burg, T., Scekcic-Zahirovic, J. & Rouaux, C. Cortical Circuit Dysfunction as a Potential Driver of Amyotrophic Lateral Sclerosis. *Front Neurosci* **14**, 363 (2020).
54. Dick, J. P. R. The deep tendon and the abdominal reflexes. *J Neurol Neurosurg Psychiatry* **74**, 150–153 (2003).
55. Costello, E. *et al.* Cognitive and neuropsychiatric endophenotypes in amyotrophic lateral sclerosis. *Brain Commun* **5**, (2023).

Supplementary material

Supplementary Table 1. Preprocessing outcomes and data quality assessments.

	AFM C9- (N = 21)	AFM C9+ (N = 15)	P-value
<u>Preprocessing outcomes</u>			
Removed ICs	11 (8-15)	10 (8-15)	1.000
Interpolated channels	6 (3-9)	4 (1-8)	0.421
Interpolated trials (%)	10.7 (7.1-12.8)	10.9 (9.3-15.1)	0.386
Removed trials (%)	0.1 (0-0.2)	0.1 (0-0.3)	0.684
Total Go trials	824 (738-869)	841 (810-871)	0.564
Total NoGo trials	82 (64-98)	89 (75-97)	0.563
<u>Data quality assessments</u>			
RMS(SME) Go ¹	0.155	0.136	/
RMS(SME) NoGo	0.464	0.415	/
Group-level dependability Go ²	1	0.99	/
Group-level dependability NoGo	0.98	0.98	/

Data are shown as median (interquartile range). Abbreviations: AFM = asymptomatic family member; C9- = carriership of *C9orf72* with normal repeat length; C9+ = carriership of *C9orf72* repeat expansion; IC = independent component; RMS = root mean square; SME = standardised measurement error.

Supplementary Table 2. Outcomes of physical examination and cognitive screening.

	AFM C9- (N = 21)	AFM C9+ (N = 15)	P-value
Physical examination^a			
Dysarthria	0 (0.0)	0 (0.0)	1.00
Impaired tongue movement	0 (0.0)	0 (0.0)	1.00
Sustained glabellar reflex	0 (0.0)	0 (0.0)	1.00
Jaw jerk reflex presence	1 (0.05)	2 (0.12)	0.58
Snout reflex presence	0 (0.0)	1 (0.06)	0.45
Palmomentar reflex presence	3 (0.14)	3 (0.18)	1.00
Hypertonia arm muscles	0 (0)	0 (0)	1.00
Biceps tendon reflex	16 (0.76)	13 (0.76)	1.00
- Low-Normal	5 (0.24)	4 (0.24)	
- Brisk	0 (0.0)	0 (0.0)	
- Very brisk	0 (0.0)	0 (0.0)	
Triceps tendon reflex	16 (0.76)	14 (0.82)	0.71
- Low-Normal	5 (0.24)	3 (0.18)	
- Brisk	0 (0.0)	0 (0.0)	
- Very brisk	0 (0.0)	0 (0.0)	
Deltoid tendon reflex presence	4 (0.19)	5 (0.29)	0.70
Trapezoid tendon reflex presence	3 (0.14)	2 (0.12)	1.00
Pectoral tendon reflex presence	1 (0.05)	2 (0.12)	0.58
Hoffmann's reflex presence	1 (0.05)	3 (0.18)	0.31
Abdominal reflex absence	1 (0.05)	3 (0.18)	0.31
Hypertonia leg muscles	0 (0.0)	0 (0.0)	1.00
Knee jerk reflex	16 (0.76)	12 (0.71)	0.84
- Low-Normal	5 (0.24)	4 (0.24)	
- Brisk	0 (0.0)	1 (0.06)	
- Very brisk	0 (0.0)	0 (0.0)	
Ankle jerk reflex	17 (0.81)	13 (0.76)	1.00
- Low-Normal	4 (0.19)	4 (0.24)	
- Brisk	0 (0.0)	0 (0.0)	
- Very brisk	0 (0.0)	0 (0.0)	

Adductor reflex presence	5 (0.24)	5 (0.29)	1.00
Plantar reflex Babinski response	0 (0.0)	0 (0.0)	1.00
Cognitive screening (ECAS)^b			
Total	119 (110.5-122.3)	116 (112.5-121.8)	0.65
ALS specific	87 (81.8-90.3)	85 (84.0-90.5)	0.96
ALS nonspecific	32 (29.8-32.0)	31 (28.3-31.8)	0.18

Presence of (the highest) reflex or muscle tone either left or right are used per subject. Abbreviations: AFM = asymptomatic family member; C9- = carriership of *C9orf72* with normal repeat length; C9+ = carriership of *C9orf72* repeat expansion; ECAS = Edinburgh Cognitive and Behavioural ALS Screen; ALS = amyotrophic lateral sclerosis.

^a Data are shown in count (%). P values are calculated using Fisher's exact probability test.

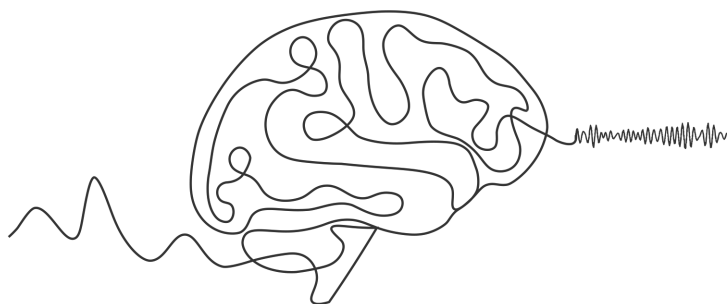
^b Data are shown as median (interquartile range). P values are calculated using Mann-Whitney U-test.

Supplementary Table 3. Linear mixed model outcomes for the significant brain regions.

	Difference [95% confidence interval]	P-value
Paracentral R	10.25 [3.43 17.05]	0.004
Paracentral L	10.73 [4.94 16.54]	0.0007
Postcentral R	8.59 [3.11 14.06]	0.003
Postcentral L	9.74 [4.76 14.71]	0.0004
Precentral R	9.21 [3.34 15.08]	0.003
Precentral L	8.22 [2.85 13.59]	0.004

References

1. Luck, S. J., Stewart, A. X., Simmons, A. M. & Rhemtulla, M. Standardized measurement error: A universal metric of data quality for averaged event-related potentials. *Psychophysiology* **58**, e13793 (2021).
2. Clayson, P. E., Brush, C. J. & Hajcak, G. Data quality and reliability metrics for event-related potentials (ERPs): The utility of subject-level reliability. *International Journal of Psychophysiology* **165**, 121–136 (2021).



Chapter 8

General discussion and future perspectives

This thesis offers insights into the underlying network pathology of ALS and individuals at risk of developing ALS, utilising EEG as a key investigative tool. These findings provide promising directions and guidelines for future research endeavours aimed at finding the cure of ALS.

Multisystem disruption of resting-state networks in ALS

Traditional neuroscience research often employs activation paradigms to selectively target brain functions of clinical interest. However, such paradigms require sustained attention and minimal muscle tension and movement, which are often difficult to achieve due to the motor, cognitive, and behavioural impairments characteristic of ALS. In contrast, the 'resting-state' paradigm, which instructs patients to relax and let their minds wander for several minutes, has emerged as a promising alternative approach to studying the brain in the absence of specific external stimuli. In this thesis, we have utilised the resting-state paradigm in chapters 2-5 to examine the EEG characteristics of ALS patients. Our results demonstrate the advantages of this approach and shed light on the potential of EEG as a clinical tool for the diagnosis and monitoring of ALS.

While there are several resting-state EEG studies in ALS, they are all limited by a small sample size of patients (around $N \leq 20$).¹⁻⁹ Conversely, our study from chapter 2 is the first to analyse EEG data from a larger cohort of ALS patients ($N = 100$). Here, we have shown that in ALS spectral power in the θ -band (but also in the neighbouring frequency bands) over central electrodes is decreased, which is in line with previous findings of decreased spectral power in θ - and α -band.^{1,3,8-10} These findings could be linked with observations of the α -peak frequency shift towards the lower end of the EEG spectrum in locked-in ALS patients.^{3,6,7} In contrast, connectivity patterns in ALS are still understudied and equivocal, mostly due to the different connectivity measures being used. In our study, we observed increased widespread connectivity (as assessed by absolute coherence) in θ - and γ -band, with the strongest changes in the central and frontoparietal electrodes.

Although these results were robust and novel, they were lacking specificity in terms of the exact brain areas that are affected in ALS. Our follow-up study from chapter 3, therefore, expanded the results by source reconstructing resting-state EEG data. Using spectral power and two conceptually different measures of connectivity (amplitude envelope correlation and imaginary coherence), we have demonstrated for the first time neurophysiological evidence of a multisystem disruption of cortical networks in ALS patients. First, we have confirmed our previous findings of decreased spectral power over multiple frequency bands (from δ - to β -band) and associated them with dysfunctions in the specific cortical areas: primarily in the posterior and temporal areas, but also in the frontal and sensorimotor regions. Also, we have evaluated connectivity through the amplitude envelope correlation, which mirrors fMRI connectivity,^{11,12} and showed that it is increased over the whole frequency spectrum, but most notably in θ - and γ -band. These increases were observed in multiple networks (i.e.,

frontotemporal, frontoparietal, motor and visual), thus conforming previous fMRI¹³⁻¹⁶ and MEG findings.^{17,18} Additionally, we have evaluated connectivity through imaginary coherence, showing decreased connectivity in δ - and β -band in the frontal and sensorimotor networks, respectively. Although these findings might seem contradictory to our findings of increased absolute coherence in ALS (chapter 2), note that these two measures reflect somewhat different aspects of connectivity. Namely, imaginary coherence captures nonzero lagged connectivity only, whilst absolute coherence captures both zero and nonzero lagged connectivity; therefore, the results are not directly comparable. In chapter 5, we show that γ -band imaginary coherence can have opposite directions of change in ALS patients, which could also partially explain the diverging results we observed in the results. Notably, both studies point to the role of increased θ - and γ -band connectivity in ALS.

Relationship between EEG and other modalities

Although the observed aberrations in the EEG were consistent with the existing literature, we aimed to augment our findings by exploiting data from other modalities that were available to us, thus allowing us to further validate our results. In chapter 2 of our study, we made a pioneering effort to demonstrate that spectral EEG can be used to quantify the structural degeneration in ALS. Specifically, we identified a significant correlation between a combination of EEG measures and contemporaneous changes in structural MRI, which provided evidence that changes in neural activity are reflective of disease-specific structural changes in ALS. In chapter 3, this relationship was corroborated using δ - and β -band imaginary coherence in the frontal and the motor network, respectively. In the same analysis, we observed that EEG changes also reflect the changes in motor and cognitive functioning. Notably, we found that θ - and γ -band connectivity were associated with cognitive impairments, while β -band connectivity was linked to motor dysfunction.

In these correlation analyses, it was evident that β -band frequency plays an important role in the motor network disruption in ALS. As phase-based connectivity measures (such as coherence) are susceptible to noise, we have explored the β -band spectral power as a prognostic and disease severity biomarker of ALS. In chapter 4, we used a pilot dataset of patients ($N = 18$) with complementary assessments of lower and upper motor neuron (LMN/UMN) function, and ALSFRS-R scores. Here, we show that β -band power is negatively correlated with fine motor function and LMN scores (both likely reflecting the same motor impairment), suggesting the increase in β -band power with disease burden. Furthermore, we show that β -band power is positively correlated with the disease progression rate. These findings confirm results from a recent EEG study¹⁹ and further support the importance of β -band oscillations in assessing disease severity in ALS.⁵ Interestingly, a recent MEG study in frontotemporal dementia (FTD) and early ALS did not show differences in spectral power in ALS patients compared to controls; however, they showed a decrease in β -band power in FTD patients, suggesting that this could be a characteristic of ALS patients with FTD-like symptoms.¹⁸ Finally, we observed no correlation with the UMN scores. While this might be somewhat

surprising, UMN assessment is known to be unreliable²⁰ and subjective,²¹ and it warrants better assessment tools.²²

While this thesis has primarily focused on the association between structural MRI and EEG findings, the combination of EEG with other modalities, such as electromyography (EMG) and magnetic resonance spectroscopy (MRS) can provide a more comprehensive understanding of changes in neural activity in ALS. For instance, combining EMG with EEG allows for the assessment of how changes in neural activity correspond to changes in muscle activity, providing a more detailed picture of the brain-muscle control dysfunction in ALS. Similarly, MRS can measure the levels of different chemicals in the brain, including neurotransmitters (such as glutamate and GABA) and metabolites (such as lactate and N-acetyl-aspartate; NAA), and in combination with EEG, it can provide additional insights into the neurochemical basis of aberrant neural activity in ALS. This multimodal approach has the potential to uncover unique information that may not be revealed by any single modality alone, allowing for a more comprehensive understanding of the underlying mechanisms of brain dysfunction in ALS. However, it is important to note that combining modalities also presents challenges, such as technical considerations, sample size requirements, and data integration issues, which need to be carefully addressed. Despite these challenges, the integration of multiple modalities holds promise in identifying new biomarkers and treatment targets for the diagnosis and progression of ALS, and warrants further investigation in future research.

Differential disruption of resting-state networks in ALS

The absence of clear correlations between genes, molecular neuropathological and clinical subtypes, provides evidence that ALS can no longer be considered as a single disease with a singular pathophysiology and clinical course. This has implications for drug development as clinical stratification parameters remain relatively insensitive as predictors of disease progression and survival. To better understand if EEG can be used for patient stratification with similar network impairments, in chapter 5, we applied a spectral clustering approach on a cohort of ALS patients with resting-state EEG data. Here, we have identified four subgroups with distinct neurophysiological profiles and that are not discoverable using standard clinical assessment tools. While, unsurprisingly, the network disruptions that characterise our clusters do not strongly correlate or overlap with the commonly-defined clinical subtypes of ALS, our results are in alignment with previous observations (see the Discussion section in chapter 5 for more details). Our results from chapters 2 and 3 point to the importance of β -band spectral power in ALS, albeit our clustering results show that this measure is also underpinning heterogeneity in network dysfunction. More specifically, we have shown that ALS patients as a group have decreased β -band spectral power, while one of the ALS subgroups showed a unique increase. Taken into account that the subgroup of patients with increased β -band spectral power showed the lowest stability over time and that the results from chapter 4 suggest that β -band might be correlated with

disease burden, this warrants an in-depth investigation using a bigger dataset. Nevertheless, a recent MRI clustering study²³ revealed three clusters with unique structural changes in the motor, frontotemporal and posterior networks, which is in line with our clustering results implicating the same networks.

Although these findings confirm a complex and heterogeneous nature of clinical observations currently used in ALS classification systems, our results suggest that a modification of the existing stratification system is warranted. In fact, our simulated analysis, in which individual patients are classified to clusters, resulted in high classification accuracy (89%) showing evidence that our clustering approach can render clinically meaningful findings on an individual level, which is pivotal for clinical trial stratification.

Attention networks in ALS and asymptomatic *C9orf72* carriers

The use of resting-state paradigms in assessing patient populations, due to their simplicity, may be suboptimal for assessing specific brain functions and at-risk cohorts such as asymptomatic repeat expansion carriers. A more effective approach is to challenge the brain with paradigms that selectively target brain functions of clinical interest, such as computing event-related potentials (ERPs) to enhance clinically relevant signals while suppressing irrelevant factors. One such paradigm is the sustained attention to response task (SART), which has been used to detect attention lapses and executive impairments in neurodegenerative diseases.²⁴⁻²⁷ As the task requires motor responses as well, it is suitable for characterising both motor and cognitive networks. The SART-generated ERP consists of the N₂ and P₃ peaks, which start around 200 ms and 300 ms post-stimulus, respectively. In this thesis, we used the SART in ALS patients (chapter 6) and asymptomatic *C9orf72* repeat expansion carriers (chapter 7).

In chapter 6, we employed the SART to investigate motor and cognitive network dysfunction in ALS patients. Our findings revealed significantly smaller N₂ ERPs in frontal electrodes, but no differences in N₂ source activity patterns. However, during P₃ ERP, ALS patients showed significantly increased source activity, particularly in the left inferior parietal lobule and left insula. Such posterior parietal hyperactivation has been previously observed during involuntary attention switching²⁸, and in our resting-state EEG (chapters 2 and 3) and in resting-state MEG.¹⁷ Further analysis of ERP characteristics and task performance measures showed some correlations in controls but not in patients, and vice versa, indicating a combination of pathophysiological and compensatory mechanisms contributing to the network disruption in ALS. Such measures of compensatory activity, which sustain the performance of task/functional measures, may serve as potential indicators of presymptomatic ALS pathology.

To achieve timely diagnosis and to disentangle disease-related effects from confounding effects, studying cohorts genetically predisposed to developing ALS is crucial.^{29,30} In chapter 7, we used the SART to investigate asymptomatic family members with *C9orf72* repeat expansion. Similar to the analysis from the previous chapter, by

comparing brain responses during N₂ and P₃ processing between mutation carriers and non-carriers, we found decreased activation in the sensorimotor network, which is consistent with findings of dysfunctional glucose metabolism³¹ and grey matter deterioration.³² Additionally, studies focusing on movement-related processing in ALS using EEG/MEG have reported reduced post-movement cortical activation on both contralateral and ipsilateral sides to movement execution.^{10,33,34} The post-movement cortical activity is associated with deactivation and inhibition of cortical areas primarily in the hemisphere contralateral to movement execution.^{35,36} Since it is interpreted as a state of decreased neural excitability or inhibited thalamo-cortical circuitry, our findings could suggest an impaired excitatory/inhibitory (E/I) balance in *C9orf72* pathology, which is hypothesised to be underpinning ALS.³⁷ These are important early findings calling for more extensive research into the presymptomatic phase of the disease involving different modalities and larger datasets.

While the SART paradigm has been the primary focus of these investigations, it is important to consider other paradigms that may corroborate these findings and provide complementary insights into the pathophysiology of ALS. For example, the mismatch negativity (MMN) paradigm causes involuntary attention shifts and activates frontotemporal networks, which are implicated in ALS pathology. Moreover, this passive paradigm is relatively simple to administer as it involves an administration of standard and deviant tones in a random sequence. Studies in schizophrenia have linked the reduction of MMN amplitude to impaired E/I balance, and EEG-derived measures from this paradigm have shown promise in investigating effects of pharmacological interventions on E/I balance. Additionally, transcranial magnetic stimulation (TMS) studies have shown disrupted E/I balance in ALS patients, with a reduction in short intracortical inhibition (SICI) in the motor cortex, and abnormal SICI in some presymptomatic SOD₁ mutation carriers before symptom onset. Although TMS measurements can be challenging, especially in the case when muscle wasting and fasciculations are present, a novel method that uses resting-state EEG to quantitatively measure the E/I ratio has been developed. This approach can be exploited to further study the hypothesis of impaired E/I balance in the sensorimotor network and help in the development of biomarkers for early detection of ALS that are suitable for clinical trials.

Synergy of sensor- and source-space analysis

As source analysis algorithms are capable of improving the spatial resolution of EEG, the sensor-space approach might be presumed redundant. The findings of this thesis, however, highlight the advantages and disadvantages of both the source- and the sensor-space analysis. In the case of sensor-space measures, spatial resolution is poor due to the conduction of electrical signals to the electrode from both adjacent and distant cortical sources, thus limiting the ability to prescribe detected abnormalities to specific anatomical regions. For instance, in chapter 2, we identified spatially diffuse connectivity changes at sensor-level, and in chapter 3, source analysis was used to determine the underpinning networks. Similarly, using source localisation, we were able to associate the θ -band power changes in central electrodes to the frontotemporal and

mid cingulate areas. Yet, the spatial summation of cortical activity may be advantageous in the investigation. In chapter 6, for example, the sensor-level N2 ERP was significantly reduced in ALS. At source-level, however, a specific region that underpins the abnormality was not discerned, suggesting that a summation of mild cortical disruptions might be present. If sensor-level analysis had been skipped in favour of advanced source-level analysis alone, this diffuse pathophysiology would have remained undetected due to insufficient statistical power. It is, therefore, paramount to investigate EEG at both sensor- and source-level.

The field of EEG is undergoing rapid evolution, with advancements in high-density EEG technology, multimodal integration, and signal processing and machine learning algorithms showing promising results in clinical settings. For instance, source localisation techniques now allow for mapping of brain activity and localisation of abnormalities in conditions like epilepsy.³⁸ However, challenges such as variability in data acquisition and analysis techniques, and lack of standardised protocols still exist and need to be addressed to ensure the reliability and reproducibility of EEG findings. Nonetheless, these limitations are becoming widely recognised,^{39,40} and as EEG continues to mature, it has the potential to significantly impact our understanding of brain disorders.

Future directions

The search for effective targets, treatments, and timing in ALS research remains a formidable challenge, despite significant progress. Finding a cure for this devastating disease requires addressing the low incidence rate and heterogeneity of network dysfunction in ALS, which pose significant challenges in terms of sample size, reproducibility of results, and complexity of analyses. However, several considerations can be pursued in parallel to accelerate the overall research process and advance our understanding of ALS.

One potential solution to the challenges of sample size and heterogeneity in ALS research is through multi-centre collaborations. Collaborative efforts, such as the establishment of partnerships between ALS centres in different locations, can facilitate data sharing, thereby increasing statistical power and external validation of research findings. For example, one such collaboration, between the ALS centres in Dublin and Utrecht, has emerged from this thesis and has demonstrated the value of such partnerships in advancing ALS research.

Increasing sample size is crucial as it will allow for accounting of the observed heterogeneity among ALS patients. EEG and MRI studies have revealed differential subgroups of ALS patients, and it has been observed that some compounds may be effective only in specific subgroups of ALS patients. These findings underscore the importance of adopting a precision medicine approach in ALS, wherein therapies are tailored to individuals or groups of individuals based on their unique characteristics.

In addition to addressing sample size and heterogeneity, the identification of biomarkers that can bridge the gap between preclinical and clinical research is critical for the development of new treatments for ALS. Biomarkers can serve for stratification, allowing for the definition of pathophysiologically homogeneous patient populations, and for target engagement assessment, enabling verification of treatment effects across preclinical and clinical interventions. EEG has shown promise as a tool that can be used at clinical and commercial trial sites for tracking disease progression and treatment effects in other neurodegenerative diseases, such as Alzheimer's disease^{41,42} and schizophrenia.⁴³⁻⁴⁵ Moreover, gene expression atlases⁴⁶ that measure the activity of thousands of genes in multiple brain regions offer opportunities to elucidate the molecular mechanisms underlying ALS-related brain changes.³² By understanding the effects of ALS risk-genes on brain oscillations and identifying new pathologically relevant genes, novel therapeutic targets may be identified.⁴⁷

Although a preventive approach would be ideal, similar to the success seen in spinal muscular atrophy trials,⁴⁸ conducting large prevention trials for late-onset ALS poses significant challenges and may not be feasible due to the prolonged duration of treatment required to achieve a clinical endpoint. Moreover, concerns regarding the cost and safety of treating individuals who may never develop the pathology further compound the challenges. Currently, the only eligibility criterion for treatment therapies is a history of familial ALS or the presence of an ALS-linked genetic mutation. However, the optimal stage for initiating treatment remains unknown. Notably, only patients with established ALS diagnosis are typically included in ALS research,^{23,49,50} which overlooks valuable information on early, presymptomatic changes.⁵¹ Incorporating presymptomatic data into research could not only enhance our understanding of early disease phenotypes but also potentially unveil new disease pathways and therapeutic targets, thereby contributing to improved disease management and treatment strategies.

Nevertheless, ALS research should diversify. Namely, research groups usually focus on one modality (e.g., EEG, MRI, MRS or TMS) only, which is likely to be sensitive to an aberration occurring at a certain stage of the disease and possibly only within different subgroups of patients. This unimodal approach causes a multiverse of findings that is otherwise hard to consolidate into one complete observation – as exemplified by the model of the major biomarkers of Alzheimer's disease, in which different modalities become sensitive at different disease stages.⁵² A more beneficial way, therefore, would be to apply a multimodal approach, in which the same patients are assessed using an array of tests and modalities.

Finally, although high-density EEG recordings are valuable for research purposes, their practicality in clinical trials is limited. Future investigations should prioritise the development and utilisation of more time-efficient data collection methods, such as EEG systems that employ sponge-based or dry electrodes. The optimisation of data collection procedures is expected to yield substantial benefits, including reduced burden on patients and staff, thereby facilitating the implementation of EEG-based assessments in clinical trial settings.

In conclusion, it is imperative that future EEG research in ALS prioritises collaborative efforts to address the challenges of sample size and heterogeneity. One potential avenue for advancement is the identification of biomarkers that can bridge the gap between preclinical and clinical research, which holds promise in enhancing our understanding of the pathophysiology of ALS and identifying novel therapeutic targets. Moreover, a multimodal approach that integrates various assessments within the same patients could provide a more comprehensive and holistic view of the disease. Furthermore, optimising data collection methods, such as the utilisation of EEG systems with electrodes that do not require gelling, could streamline data collection procedures and alleviate burden on patients and staff. Despite the inevitable challenges that lie ahead, sustained research efforts and innovative approaches are essential in the pursuit of effective treatments and ultimately a cure for ALS.

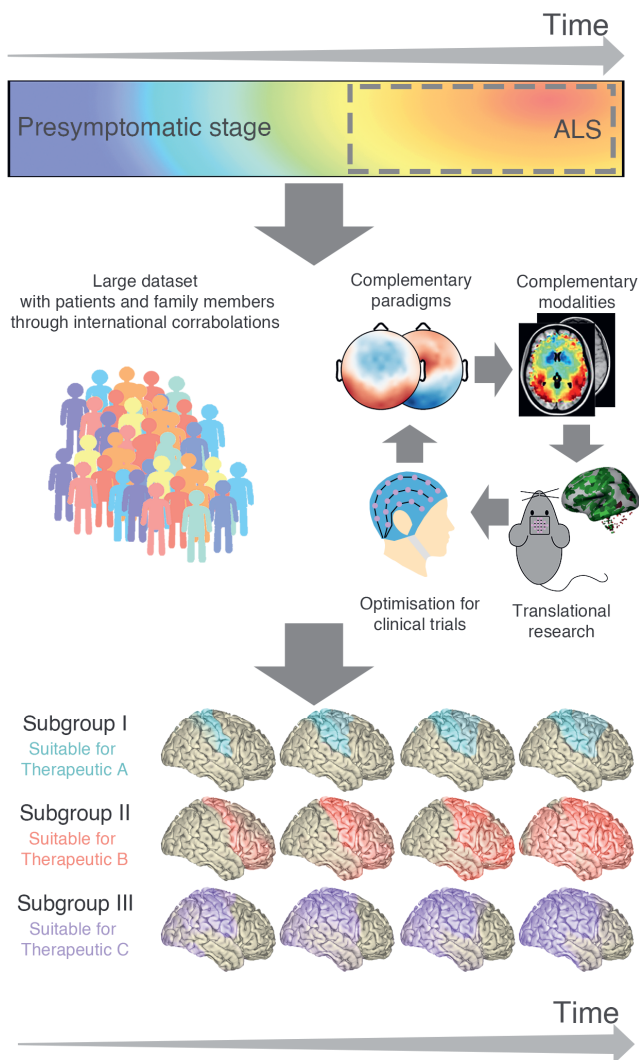


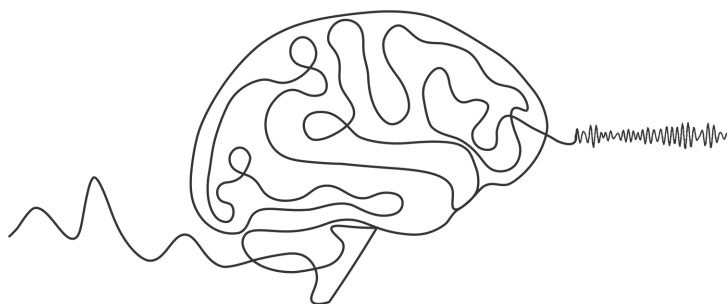
Figure 1. A roadmap for development of translational EEG biomarkers for treatment development in ALS. Future EEG research in ALS should prioritise collaborative efforts to address challenges in sample size and heterogeneity. Additionally, leveraging complementary paradigms and imaging modalities, advancing translational research, and optimising EEG setup for clinical trial use are crucial steps. Despite the inevitable challenges that lie in each of these steps, these research efforts are essential in the pursuit of precision medicine treatments for ALS.

References

1. Mai, R., Facchetti, D., Micheli, A. & Poloni, M. Quantitative electroencephalography in amyotrophic lateral sclerosis. *Electroencephalogr Clin Neurophysiol* **106**, 383–386 (1998).
2. Iyer, P. M. *et al.* Functional Connectivity Changes in Resting-State EEG as Potential Biomarker for Amyotrophic Lateral Sclerosis. *PLoS One* **10**, e0128682 (2015).
3. Maruyama, Y. *et al.* Electroencephalography of completely locked-in state patients with amyotrophic lateral sclerosis. *Neurosci Res* **162**, 45–51 (2021).
4. Frasnini, M. *et al.* Functional brain connectivity analysis in amyotrophic lateral sclerosis: An EEG source-space study. *Bio-med Phys Eng Express* **4**, 037004 (2018).
5. Frasnini, M. *et al.* EEG functional network topology is associated with disability in patients with amyotrophic lateral sclerosis. *Sci Rep* **6**, 1–7 (2016).
6. Khalili-Ardali, M., Wu, S., Tonin, A., Birbaumer, N. & Chaudhary, U. Neurophysiological aspects of the completely locked-in syndrome in patients with advanced amyotrophic lateral sclerosis. *Clinical Neurophysiology* **132**, 1064–1076 (2021).
7. Hohmann, M. R. *et al.* Case series: Slowing alpha rhythm in late-stage ALS patients. *Clinical Neurophysiology* **129**, 406–408 (2018).
8. Jayaram, V. *et al.* Brain-computer interfacing in amyotrophic lateral sclerosis: Implications of a resting-state EEG analysis. in *2015 37th Annual International Conference of the IEEE Engineering in Medicine and Biology Society (EMBC)* 6979–82 (IEEE, 2015).
9. Santhosh, J., Bhatia, M., Sahu, S. & Anand, S. Decreased electroencephalogram alpha band [8–13 Hz] power in amyotrophic lateral sclerosis patients: A study of alpha activity in an awake relaxed state. *Neurol India* **53**, 99 (2005).
10. Bizovičar, N., Dreo, J., Koritnik, B. & Zidar, J. Decreased movement-related beta desynchronization and impaired post-movement beta rebound in amyotrophic lateral sclerosis. *Clinical Neurophysiology* **125**, 1689–99 (2014).
11. Brookes, M. J. *et al.* Measuring functional connectivity using MEG: Methodology and comparison with fMRI. *Neuroimage* **56**, 1082–1104 (2011).
12. Siegel, M., Donner, T. H. & Engel, A. K. Spectral fingerprints of large-scale neuronal interactions. *Nat Rev Neurosci* **13**, 121–34 (2012).
13. Douaud, G., Filippini, N., Knight, S., Talbot, K. & Turner, M. R. Integration of structural and functional magnetic resonance imaging in amyotrophic lateral sclerosis. *Brain* **134**, 3470–9 (2011).
14. Agosta, F. *et al.* Sensorimotor Functional Connectivity Changes in Amyotrophic Lateral Sclerosis. *Cerebral Cortex* **21**, 2291–2298 (2011).
15. Schulthess, I. *et al.* Functional connectivity changes resemble patterns of pTDP-43 pathology in amyotrophic lateral sclerosis. *Sci Rep* **6**, (2016).
16. Proudfoot, M., Bede, P. & Turner, M. R. Imaging cerebral activity in amyotrophic lateral sclerosis. *Front Neurol* **10**, 1148 (2019).
17. Proudfoot, M. *et al.* Increased cerebral functional connectivity in ALS: A resting-state magnetoencephalography study. *Neurology* **90**, e1418–e1424 (2018).
18. Govaarts, R. *et al.* Cortical and subcortical changes in resting-state neuronal activity and connectivity in early symptomatic ALS and advanced frontotemporal dementia. *Neuroimage Clin* **34**, 102965 (2022).
19. Notturmo, F., Croce, P., Ornello, R., Sacco, S. & Zappasodi, F. Yield of EEG features as markers of disease severity in amyotrophic lateral sclerosis: a pilot study. *Amyotroph Lateral Scler Frontotemporal Degener.* **24**, 295–303 (2023).
20. Swash, M. Why are upper motor neuron signs difficult to elicit in amyotrophic lateral sclerosis? *J Neurol Neurosurg Psychiatry* **83**, 659–662 (2012).
21. Thaller, M. & Hughes, T. Inter-rater agreement of observable and elicitable neurological signs. *Clinical Medicine* **14**, 264–267 (2014).
22. Nitert, A. D. *et al.* Sensitivity of brain MRI and neurological examination for detection of upper motor neurone degeneration in amyotrophic lateral sclerosis. *J Neurol Neurosurg Psychiatry* **93**, 1–11 (2022).
23. Tan, H. H. G. *et al.* MRI Clustering Reveals Three ALS Subtypes With Unique Neurodegeneration Patterns. *Ann Neurol* (2022).
24. Robertson, I. H., Manly, T., Andrade, J., Baddeley, B. T. & Yiend, J. Oops!': performance correlates of everyday attentional

- failures in traumatic brain injured and normal subjects. *Neuropsychologia* **35**, 747–758 (1997).
25. Huntley, J. D., Hampshire, A., Bor, D., Owen, A. M. & Howard, R. J. The importance of sustained attention in early Alzheimer's disease. *Int J Geriatr Psychiatry* **32**, 860–867 (2017).
 26. O'Grada, C. *et al.* Does the ability to sustain attention underlie symptom severity in schizophrenia? *Schizophr Res* **107**, 319–323 (2009).
 27. Bellgrove, M. A., Hawi, Z., Gill, M. & Robertson, I. H. The Cognitive Genetics of Attention Deficit Hyperactivity Disorder (ADHD): Sustained attention as a Candidate Phenotype. *Cortex* **42**, 838–845 (2006).
 28. McMackin, R. *et al.* Dysfunction of attention switching networks in amyotrophic lateral sclerosis. *Neuroimage Clin* **22**, 101707 (2019).
 29. Benatar, M. & Wu, J. Presymptomatic studies in ALS. *Neurology* **79**, 1732–1739 (2012).
 30. Chipika, R. H. *et al.* The presymptomatic phase of amyotrophic lateral sclerosis: are we merely scratching the surface? *Journal of Neurology* **2020** 268:12 **268**, 4607–4629 (2020).
 31. de Vocht, J. *et al.* Use of Multimodal Imaging and Clinical Biomarkers in Presymptomatic Carriers of C9orf72 Repeat Expansion. *JAMA Neurol* **77**, 1008–1017 (2020).
 32. van Veenhuijzen, K. *et al.* Longitudinal Effects of Asymptomatic C9orf72 Carriership on Brain Morphology. *Ann Neurol* (2022).
 33. Riva, N. *et al.* Cortical activation to voluntary movement in amyotrophic lateral sclerosis is related to corticospinal damage: Electrophysiological evidence. *Clinical Neurophysiology* **123**, 1586–92 (2012).
 34. Proudfoot, M. *et al.* Altered cortical beta-band oscillations reflect motor system degeneration in amyotrophic lateral sclerosis. *Hum Brain Mapp* **38**, 237–254 (2017).
 35. Pfurtscheller, G. Event-related synchronization (ERS): an electrophysiological correlate of cortical areas at rest. *Electroencephalogr Clin Neurophysiol* **83**, 62–9 (1992).
 36. Pfurtscheller, G., Stancák, A. & Neuper, C. Event-related synchronization (ERS) in the alpha band — an electrophysiological correlate of cortical idling: A review. *International Journal of Psychophysiology* **24**, 39–46 (1996).
 37. Brunet, A., Stuart-Lopez, G., Burg, T., Scekcic-Zahirovic, J. & Rouaux, C. Cortical Circuit Dysfunction as a Potential Driver of Amyotrophic Lateral Sclerosis. *Front Neurosci* **14**, 363 (2020).
 38. van Mierlo, P., Vorderwülbecke, B. J., Staljanssens, W., Seeck, M. & Vulliémot, S. Ictal EEG source localization in focal epilepsy: Review and future perspectives. *Clinical Neurophysiology* **131**, 2600–2616 (2020).
 39. Niso, G. *et al.* Good scientific practice in EEG and MEG research: Progress and perspectives. *Neuroimage* **257**, 119056 (2022).
 40. Pernet, C. R. *et al.* EEG-BIDS, an extension to the brain imaging data structure for electroencephalography. *Scientific Data* **2019** 6:1 **6**, 1–5 (2019).
 41. Van Straaten, E. C. W., Scheltens, P., Gouw, A. A. & Stam, C. J. Eyes-closed task-free electroencephalography in clinical trials for Alzheimer's disease: an emerging method based upon brain dynamics. *Alzheimers Res Ther* **6**, 1–10 (2014).
 42. Babiloni, C. *et al.* Measures of resting state EEG rhythms for clinical trials in Alzheimer's disease: Recommendations of an expert panel. *Alzheimer's & Dementia* **17**, 1528–1553 (2021).
 43. Joshi, Y. B. & Light, G. A. Using EEG-Guided Basket and Umbrella Trials in Psychiatry: A Precision Medicine Approach for Cognitive Impairment in Schizophrenia. *Front Psychiatry* **9**, 554 (2018).
 44. Javitt, D. C. *et al.* A roadmap for development of neuro-oscillations as translational biomarkers for treatment development in neuropsychopharmacology. *Neuropsychopharmacology* **2020** 45:9 **45**, 1411–1422 (2020).
 45. Cecchi, M. *et al.* Validation of a suite of ERP and QEEG biomarkers in a pre-competitive, industry-led study in subjects with schizophrenia and healthy volunteers. *Schizophr Res* **254**, 178–189 (2023).
 46. Fornito, A., Arnatkevičiūtė, A. & Fulcher, B. D. Bridging the Gap between Connectome and Transcriptome. *Trends Cogn Sci* **23**, 34–50 (2019).
 47. Korobeynikov, V. A., Lyashchenko, A. K., Blanco-Redondo, B., Jafar-Nejad, P. & Schneider, N. A. Antisense oligonucleotide silencing of FUS expression as a therapeutic approach in amyotrophic lateral sclerosis. *Nature Medicine* **2022** 28:1 **28**, 104–116 (2022).
 48. Motyl, A. A. L. & Gillingwater, T. H. Timing is everything: Clinical evidence

- supports pre-symptomatic treatment for spinal muscular atrophy. *Cell Rep Med* **3**, 100725 (2022).
49. Dukic, S. *et al.* Resting-state EEG reveals four subphenotypes of amyotrophic lateral sclerosis. *Brain* **145**, 621–631 (2022).
50. Drysdale, A. T. *et al.* Resting-state connectivity biomarkers define neurophysiological subtypes of depression. *Nat Med* **23**, 28–38 (2017).
51. Benatar, M. *et al.* Mild motor impairment as prodromal state in amyotrophic lateral sclerosis: a new diagnostic entity. *Brain* **145**, 3500–3508 (2022).
52. Jack, C. R. *et al.* Tracking pathophysiological processes in Alzheimer’s disease: an updated hypothetical model of dynamic biomarkers. *Lancet Neurol* **12**, 207–216 (2013).



Addenda

Summary

Summary in Dutch (Nederlandse samenvatting)

List of publications

Acknowledgements

Curriculum vitae

Summary

Amyotrophic lateral sclerosis (ALS) is a progressive neurodegenerative disease that affects both upper and lower motor neurons, leading to motor dysfunction. It has an estimated annual incidence rate of 2-3 new cases per 100,000 individuals, typically affecting those between the ages of 55 and 65. The most common cause of death in ALS is respiratory failure, which typically occurs 2-5 years after the onset of symptoms. It also affects nonmotor functions, resulting in cognitive and behavioural impairments. Although the precise cause of ALS remains largely unknown, genetic and environmental risk factors are known to contribute to its development. The most prevalent and well-established genetic mutation associated with ALS is the repeat expansion in the *C9orf72* gene. Despite notable advancements in ALS research, many crucial questions remain unanswered, including understanding the relationship between risk genes, the manifestation of diverse phenotypes, and the early detection and prognosis of the disease. Addressing these questions can facilitate the identification of therapeutic targets, the development of earlier treatment strategies, and the enhancement of clinical trial designs.

Biomarkers are measurable biological changes that are utilised for diagnosing and predicting the prognosis of diseases. In the context of ALS, the current diagnosis heavily relies on clinical examinations conducted by experienced neurologists, often resulting in diagnostic delays. Furthermore, patient prognosis remains unpredictable, and existing outcome measures in clinical trials have limitations in accurately assessing disease progression. Consequently, there is an urgent need to develop objective and quantifiable biomarkers that can capture dysfunction in upper motor neurons (UMNs) as well as changes in nonmotor aspects of the disease. Electrophysiology, specifically electroencephalography (EEG), holds promise in fulfilling this requirement. EEG provides real-time information transmission throughout the entire brain at a millisecond timescale and is relatively cost-effective and portable. By surpassing the limitations of other neuroimaging techniques, EEG emerges as a promising tool for the development of biomarkers in ALS.

Findings

In chapter 2, we aimed to investigate the altered cortical activity and connectivity patterns in ALS using resting-state EEG data. Prior investigations in EEG and ALS were constrained by limited sample sizes, whereas our study analysed a larger cohort of ALS patients ($N = 100$). Our findings revealed a significant decrease in spectral power in the θ -band (and extending to neighbouring bands) over central electrodes, corroborating previous research outcomes. Furthermore, we observed enhanced widespread connectivity in both θ - and γ -bands, with the most pronounced changes occurring in the central and frontoparietal electrodes. Importantly, the correlation analysis between the EEG data and structural magnetic resonance imaging (MRI) scans demonstrated a concurrence between disease-specific structural degeneration in motor areas and corticospinal tracts, and the observed alterations in neural activity. These results contribute to our understanding of the progressive network decline in ALS and lay the

groundwork for the development of validated and cost-effective spectral EEG-based biomarkers.

In chapter 3, we extended the previous findings by reconstructing resting-state EEG data and examining spectral power and two measures of connectivity: co-modulation and synchrony. Our analysis confirmed the presence of reduced spectral power across multiple frequency bands, ranging from δ to β , indicating dysfunction in specific cortical areas, particularly in the posterior and temporal regions, as well as the frontal and sensorimotor regions. Moreover, we observed increased co-modulation across the entire frequency spectrum, with notable enhancements in θ - and γ -bands, within multiple networks including the frontotemporal, frontoparietal, motor, and visual networks. Additionally, we identified decreased synchrony in the δ - and β -bands within the frontal and sensorimotor networks. These findings shed light on the role of heightened θ - and γ -band connectivity in ALS. Importantly, the observed changes in connectivity exhibited correlations with alterations in structural MRI, functional motor scores, and cognitive scores. Overall, our results underscore the extensive disruption of disease-associated networks in ALS, indicating widespread dysfunction in both motor and cognitive networks.

In chapter 4, we examined the role of β -band motor network disruption in ALS. Our findings suggest that an increase in β -band power is associated with the increase in the disease burden and the progression rate. The study also observed a negative correlation between β -band power and fine motor function, as well as with lower motor neuron (LMN) scores, which are likely reflective of the same motor impairment. We, however, did not observe any correlation with upper motor neuron (UMN) scores, which may warrant higher sample size and further research into better assessment tools. The study provides preliminary evidence for further research in β -band oscillations in assessing disease severity in ALS.

In chapter 5, we demonstrate the ability of EEG to identify four distinct subgroups among ALS patients, each characterised by unique neurophysiological profiles that cannot be detected through conventional clinical assessment tools. Our findings align with a recent MRI clustering study, which identified three clusters displaying distinct structural changes in the motor, frontotemporal, and posterior brain networks, thus implicating the same networks as observed in our study. The identification of ALS subtypes based on profiles of differential impairment in neuronal networks holds promise for future stratification in clinical trials. Furthermore, it lays the foundation for the development of novel therapeutic strategies grounded in neurobiological principles that aim to modulate network disruption.

In chapter 6, our objective was to examine the dysfunction of motor and cognitive networks in individuals with ALS, employing the sustained attention to response task (SART). We found that ALS patients exhibited significantly reduced N2 event-related potential (ERP) amplitudes in frontal electrodes, indicating diminished neural responses during the 220-350 ms time window. However, we did not observe any differences in the patterns of N2 source activity. Furthermore, our findings revealed a significant increase in source activity during the P3 ERP component (350-550 ms),

particularly within the left inferior parietal lobule and left insula, suggesting compensatory mechanisms at play. Taken together, our results point towards a combination of pathophysiological processes (reflected by diminished N₂) and compensatory mechanisms (reflected by overactivated P₃), contributing to the disruption of networks along the frontoparietal axis in ALS.

In chapter 7, our focus shifted to a cohort with a genetic predisposition to developing ALS, as early diagnosis is critical in managing the condition effectively. Specifically, we employed the SART to investigate asymptomatic family members with the *C9orf72* repeat expansion, a known genetic risk factor for ALS. While we did not observe any discernible alterations in N₂ ERP processing, we identified reduced activation during the P₃ ERP component within the sensorimotor network among repeat expansion carriers, in comparison to noncarriers. This finding aligns with observations of dysfunctional glucose metabolism and grey matter deterioration within the same network. Our results could suggest a potential disruption in the excitatory/inhibitory balance associated with *C9orf72* pathology, which is hypothesised to underlie the development of ALS. These preliminary yet promising findings warrant further investigation into the presymptomatic phase of the disease, using diverse modalities and larger datasets, to enhance our understanding of its pathophysiology.

Taken together, this thesis provides compelling evidence that EEG is useful in gaining deeper understanding of ALS as a multinetwork disorder. Our results showed that the spectral power in lower frequency bands is decreased in ALS patients; however, there is some evidence that β -band power has a nonlinear effect, and it is increasing with the disease burden. The brain communication is overall increased (as per co-modulation) but with low efficiency (as per synchrony). ALS patients can be clustered into four stable subgroups with differential EEG profiles, corroborating that ALS is a heterogeneous disease affecting multiple brain networks and that frontotemporal and frontoparietal networks play a role in ALS. Finally, we showed that EEG could be sensitive enough to detect differences in the motor network function between ALS family members.

However, challenges persist in the pursuit of effective targets, treatments, and timing in ALS research. To address these challenges, potential strategies can be considered. Multicentre collaborations have the potential to tackle issues related to sample size and heterogeneity by enabling data sharing and enhancing statistical power. Precision medicine approaches that account for differential subgroups of ALS patients, coupled with the utilisation of biomarkers, hold promise in developing tailored treatments. Furthermore, a multimodal research approach encompassing various assessment modalities, along with the optimisation of data collection methods such as time-efficient EEG systems, holds promise for advancing ALS research and improving the conduct of clinical trials. These strategies, in conjunction with the findings presented in this thesis, provide promising avenues for future investigations in ALS research aimed at developing effective treatments and ultimately finding a cure.

Summary in Dutch (Nederlandse samenvatting)

Amyotrofische laterale sclerose (ALS) is een progressieve neurodegeneratieve ziekte die zowel de bovenste als de onderste motorneuronen aantast, wat leidt tot motorische disfunctie. Het heeft een geschatte jaarlijkse incidentie van 2-3 nieuwe gevallen per 100.000 individuen en treft doorgaans mensen tussen de leeftijden van 55 en 65 jaar. De meest voorkomende doodsoorzaak bij ALS is respiratoir falen, dat meestal 2-5 jaar na het begin van de symptomen optreedt. Het beïnvloedt ook niet-motorische functies, wat resulteert in cognitieve en gedragsstoornissen. Hoewel de exacte oorzaak van ALS grotendeels onbekend blijft, zijn genetische en omgevingsfactoren bekend die bijdragen aan de ontwikkeling ervan. De meest voorkomende en bekende genetische mutatie die verband houdt met ALS is de herhaling van het gen *C9orf72*. Ondanks opmerkelijke vooruitgang in ALS-onderzoek blijven veel cruciale vragen onbeantwoord, waaronder het begrijpen van de relatie tussen risicogenen, de manifestatie van diverse fenotypen en de vroege detectie en prognose van de ziekte. Het aanpakken van deze vragen kan de identificatie van therapeutische doelen vergemakkelijken, de ontwikkeling van vroegere behandelingsstrategieën mogelijk maken en de verbetering van klinische onderzoeksontwerpen bevorderen.

Biomarkers zijn meetbare biologische veranderingen die worden gebruikt voor de diagnose van ziekten en het voorspellen van het beloop ervan. In het geval van ALS steunt de huidige diagnostische aanpak sterk op klinisch onderzoek van ervaren neurologen, wat leidt tot vertragingen in de diagnose. Bovendien kan de prognose van de patiënt onvoorspelbaar zijn en hebben bestaande uitkomstmaatregelen in klinische onderzoeken beperkingen bij het nauwkeurig beoordelen van de ziekteprogressie. Daarom is er een dringende behoefte aan de ontwikkeling van objectieve en meetbare biomarkers die motorneuron-dysfunctie kunnen vastleggen, samen met veranderingen in niet-motorische aspecten van de ziekte. Elektrofysiologie, met name elektroencefalografie (EEG), lijkt veelbelovend om aan deze eis te voldoen. EEG biedt real-time informatie over de hele hersenen op een tijdschaal van milliseconden en is relatief kosteneffectief en draagbaar. Door de beperkingen van andere neurobeeldvormingstechnieken te overtreffen, komt EEG naar voren als een veelbelovend hulpmiddel voor de ontwikkeling van biomarkers bij ALS.

Resultaten

In hoofdstuk 2 hebben we getracht de veranderde corticale activiteit en connectiviteitspatronen bij ALS te onderzoeken met behulp van het EEG in rusttoestand. Eerdere onderzoeken naar EEG en ALS werden beperkt door kleine steekproefgroottes, terwijl onze studie een groter cohort van ALS-patiënten analyseerde (N = 100). Onze bevindingen toonden een significante afname van de spectrale kracht in de θ -band (en aangrenzende banden) over de centrale elektroden, wat eerdere onderzoeksresultaten bevestigde. Bovendien observeerden we een versterkte uitgebreide connectiviteit in zowel θ - als γ -band, waarbij de meest uitgesproken veranderingen plaatsvonden in de centrale en frontopariëtale elektroden. Belangrijk is dat de correlatieanalyse tussen de EEG-gegevens en structurele *magnetic resonance imaging* (MRI) scans een overeenkomst aantoonde tussen ziekte-specifieke structurele degeneratie in motor-

ische gebieden en corticospinale banen en de waargenomen veranderingen in neurale activiteit. Deze resultaten dragen bij aan ons begrip van de progressieve netwerknafname bij ALS en leggen de basis voor de ontwikkeling van gevalideerde en kosteneffectieve spectrale EEG-gebaseerde biomarkers.

In hoofdstuk 3 breidden we de eerdere bevindingen uit door bronreconstructie uit te voeren op het EEG in rusttoestand en de spectrale kracht en twee maten van connectiviteit te onderzoeken: co-modulatie en synchronie. Onze analyse bevestigde de aanwezigheid van verminderde spectrale kracht over meerdere frequentiebanden, variërend van δ tot β , wat wijst op disfunctie in specifieke corticale gebieden, met name in de posterieure en temporale regio's, evenals de frontale en sensorimotorische regio's. Daarnaast observeerden we een toename van co-modulatie over het gehele frequentiespectrum, met opmerkelijke verhogingen in de θ - en γ -band, binnen meerdere netwerken, waaronder de frontotemporale, frontopariëtale, motorische en visuele netwerken. Bovendien identificeerden we verminderde synchronie in de δ - en β -band binnen de frontale en sensorimotorische netwerken. De waargenomen veranderingen in connectiviteit vertoonden correlaties met veranderingen in structurele MRI, functionele motorscores en cognitieve scores. Dit hoofdstuk benadrukt de implicatie van verbeterde connectiviteit binnen de θ - en γ -band, evenals uitgebreide stoornissen in netwerken die verantwoordelijk zijn voor motorische en cognitieve functies.

In hoofdstuk 4 onderzochten we de rol van β -band motorische netwerkverstoring bij ALS. Onze bevindingen suggereren dat een toename van het vermogen van de β -band gekoppeld kan worden aan een toename van de ziektebelasting en de progressiesnelheid. De studie observeerde ook een negatieve correlatie tussen het vermogen van de β -band en fijne motorische functie, evenals met scores voor lagere motorneuronen, die waarschijnlijk dezelfde motorische beperking weerspiegelen. We observeerden echter geen correlatie met scores voor bovenste motorneuronen, wat mogelijk vraagt om een grotere steekproefomvang en verder onderzoek naar betere beoordelingsinstrumenten. De studie levert voorlopig bewijs voor verder onderzoek naar β -band oscillaties bij het beoordelen van de ernst van ALS.

In hoofdstuk 5 laten we zien dat EEG in staat is om vier verschillende subgroepen bij ALS-patiënten te identificeren, elk gekarakteriseerd door unieke neurofysiologische profielen die niet kunnen worden gedetecteerd via conventionele klinische beoordelingsinstrumenten. Onze bevindingen komen overeen met een recente MRI-clusterstudie, die drie clusters identificeerde met verschillende structurele veranderingen in de motorische, frontotemporale en posterieure hersennetwerken, wat wijst op dezelfde netwerken zoals waargenomen in onze studie. Het identificeren van ALS-subgroepen op basis van profielen van verschillende stoornissen in neuronale netwerken is veelbelovend voor toekomstige stratificatie in klinische onderzoeken. Bovendien legt het de basis voor de ontwikkeling van nieuwe therapeutische strategieën gebaseerd op neurobiologische principes die tot doel hebben netwerkverstoring te moduleren.

In hoofdstuk 6 was ons doel om de disfunctie van motorische en cognitieve netwerken bij mensen met ALS te onderzoeken, met behulp van de *sustained attention to re-*

sponse task (SART). We ontdekten dat ALS-patiënten significant verminderde N2 *event-related potential* (ERP) vertoonden in frontale elektroden, wat wijst op verminderde neurale responsen binnen het tijdvenster van 220-350 ms. We observeerden echter geen verschillen in de N2-bronactiviteit. Tijdens de P3 ERP (350-550 ms) werd een significante toename van bron- (maar niet sensor-) activiteit waargenomen, met name binnen de linker inferieure pariëtale kwab en linker insula, wat wijst op de betrokkenheid van compensatiemechanismen. Samen wijzen onze resultaten op een combinatie van pathofysiologische processen (weerspiegeld door verminderde N2) en compensatiemechanismen (weerspiegeld door overactieve P3), die bijdragen aan de verstoring van netwerken langs de frontopariëtale as bij ALS.

In hoofdstuk 7 richtten we ons op een cohort met een genetische aanleg voor ALS, waarbij we het belang van een vroege diagnose voor een effectieve behandeling van de aandoening erkenden. Specifiek gebruikten we de SART om asymptomatische familieleden te onderzoeken met de herhaling in het gen *C9orf72*, een bekende genetische risicofactor voor ALS. Hoewel we geen waarneembare veranderingen in N2 ERP-verwerking waarnamen, identificeerden we verminderde activatie tijdens de P3 ERP binnen het sensorimotorische netwerk bij dragers van de mutatie, in vergelijking met niet-dragers. Deze bevinding komt overeen met waarnemingen van disfunctioneel glucosemetabolisme en achteruitgang van grijze stof binnen hetzelfde netwerk. Onze resultaten zouden kunnen wijzen op een mogelijke verstoring in het excitatoire/inhibitoire evenwicht dat geassocieerd wordt met de *C9orf72*-pathologie, die wordt verondersteld grondslag te liggen aan de ontwikkeling van ALS. Deze voorlopige maar veelbelovende bevindingen vereisen verder onderzoek naar de presymptomatische fase van de ziekte, met het gebruik van diverse modaliteiten en grotere datasets, om ons begrip van de onderliggende pathofysiologie te verbeteren.

Samengevoegd biedt deze scriptie overtuigend bewijs dat EEG waarde heeft bij het bevorderen van een dieper begrip van ALS als een stoornis van meerdere netwerken. Onze resultaten toonden aan dat de spectrale kracht in de lagere frequentiebanden verminderd is bij ALS-patiënten; er is echter enig bewijs dat het vermogen van de β -band een niet-lineair effect heeft en toeneemt met de ziektebelasting. De hersencommunicatie is over het algemeen verhoogd (zoals blijkt uit co-modulatie), maar met lage efficiëntie (zoals blijkt uit synchronie). ALS-patiënten kunnen worden ingedeeld in vier stabiele subgroepen met verschillende EEG-profielen, wat bevestigt dat ALS een heterogene ziekte is die meerdere hersennetwerken aantast en dat de frontotemporale en frontopariëtale netwerken een rol spelen bij ALS. Ten slotte hebben we aangetoond dat EEG gevoelig genoeg kan zijn om verschillen in de functie van het motorische netwerk tussen familieleden met ALS te detecteren.

Er blijven echter uitdagingen bestaan in de zoektocht naar effectieve behandelingen voor ALS, wat aanzet tot de overweging van verschillende potentiële strategieën om ze te vinden. Samenwerkingen met meerdere centra hebben de potentie om problemen met betrekking tot steekproefomvang en heterogeniteit aan te pakken door het eenvoudiger uitwisselen van gegevens. Benaderingen voor precisie-geneeskunde die rekening houden met verschillende subgroepen van ALS-patiënten, in combinatie met het gebruik van biomarkers, doen verwachten tot de ontwikkeling van geperson-

aliseerde behandelingen. Bovendien geven multimodale studies die complementaire technieken integreren, samen met geoptimaliseerde gegevensverzameling, de mogelijkheid tot vooruitgang binnen het ALS-onderzoek en zijn ze in staat de uitvoering van klinische onderzoeken te verbeteren. Deze strategieën, in combinatie met de bevindingen gepresenteerd in deze scriptie, bieden veelbelovende wegen voor toekomstig onderzoek naar ALS met als doel effectieve behandelingen te ontwikkelen en uiteindelijk een remedie te vinden.

List of publications

Dukic S, Iyer PM, Mohr K, Hardiman O, Lalor EC, Nasseroleslami B. Estimation of coherence using the median is robust against EEG artefacts. In: Proceedings of the Annual International Conference of the IEEE Engineering in Medicine and Biology Society, EMBS 2017;3949-3952.

Nasseroleslami B, Dukic S, Broderick M, et al. Characteristic Increases in EEG Connectivity Correlate With Changes of Structural MRI in Amyotrophic Lateral Sclerosis. *Cerebral Cortex*. 2019;29(1):27-41.

Dukic S, McMackin R, Buxo T, et al. Patterned functional network disruption in amyotrophic lateral sclerosis. *Human Brain Mapping*. 2019;40(16):4827-4842.

McMackin R, Dukic S, Broderick M, et al. Dysfunction of attention switching networks in amyotrophic lateral sclerosis. *Neuroimage: Clinical*. 2019;22:101707.

McMackin R, Dukic S, Costello E, et al. Localization of brain networks engaged by the sustained attention to response task provides quantitative markers of executive impairment in amyotrophic lateral sclerosis. *Cerebral Cortex*. 2020;30(9):4834-4846.

McMackin R, Dukic S, Costello E, et al. Cognitive Network Hyperactivation and Motor Cortex Decline Correlate with ALS Prognosis. *Neurobiology of Aging*. 2021;102:57-70.

McMackin R, Dukic S, Costello E, et al. Sustained attention to response task-related beta oscillations relate to performance and provide a functional biomarker in ALS. *J Journal of Neural Engineering*. 2021;18(2):026006.

Coffey A, Bista S, Fasano A, Buxo T, Mitchell M, Giglia E R, Dukic S, et al. Altered supraspinal motor networks in survivors of poliomyelitis: A cortico-muscular coherence study. *Clinical Neurophysiology*. 2021;132(1):106-113.

Dukic S, McMackin R, Costello E, et al. Resting-state EEG reveals four subphenotypes of amyotrophic lateral sclerosis. *Brain*. 2022;145(2):621-631.

Acknowledgments

This thesis has been a lengthy endeavour, certainly longer than I anticipated, and further challenged by the COVID-19 pandemic. However, I shall not complain. It has unfolded across two charming cities—Dublin and Utrecht—and brought me into contact with many wonderful people. I take this opportunity to express my gratitude to those who have made direct or indirect contributions to this thesis, my career, and my overall well-being.

Dear Leonard, my supervisor, I am grateful for your trust and support. It allowed me to pursue my own research questions and I could not have asked for more. Consequently, I am excited to continue my work within your research group. Furthermore, I want to extend my heartfelt appreciation for your thoughtful check-ins regarding my well-being, particularly during the initial stages of my work and throughout the challenging times brought about by the pandemic. Your concern and care have made me feel valued, and I am truly thankful for it. And, I know, I must be *pushier*.

Dear Orla, my supervisor, I wish to thank you for believing in me and for offering me the research assistant position back in 2016. I am also grateful for your mentorship, support and enthusiastic promotion of my work. Collaborating with you has been a pleasure, and I deeply appreciate your dedication to providing swift e-mail replies. Despite my current affiliation with the ALS Centre Utrecht, which I owe to you, I genuinely hope that our close collaboration will continue to thrive.

Dear Boudewijn, my co-supervisor, thank you for being a supportive and dedicated daily supervisor. Your guidance during those first months of my work in 2019 meant a great deal to me, and I deeply appreciate your commitment to offering timely feedback. It has been an pleasure working with you, and I am looking forward to our future collaborations.

Dear Bahman, my co-supervisor, I am grateful for your patience and willingness to generously answer my numerous questions. Sitting next to you in the office was undoubtedly convenient for me – I hope you think so, too. I appreciate your belief in my potential and your efforts to facilitate my personal development through relevant workshops and conferences. I wish you the best of luck in managing your research team and look forward to continued collaboration with you.

Dear Kevin, my Dutch paronymph, thank you for our stimulating scientific discussions and the countless other conversations we have shared. Thank you for your willingness to exchange ideas and your patience in responding to my all *Keveiiiiiiin*'s. Your presence in the office will be greatly missed – consider coming back to us. Anyway, I kindly implore you to exercise mercy and stop creating 'inspirational tiles' featuring my quotes – our future colleagues might perceive me as entirely immature.

Dear Roisin, my Irish paronymph, to you too I am thankful for our engaging scientific and, at times, less scientific discussions. Our times together at conferences, sharing a glass of wine, and chats in the office kitchen have been truly enjoyable. I am so proud

of your accomplishments and I know that you will continue to achieve great things. While we may no longer share an office, I eagerly look forward to our scientific collaborations and reunions.

I would like to acknowledge the members of the Assessment Committee: Prof. M.J.N.L. Benders, Prof. K.P.J. Braun, Prof. R.J. Pasterkamp, Prof. N.F. Ramsey, and Prof. C.J. Stam. Your time and attention in reviewing my thesis are greatly appreciated.

To my dear colleagues in the office, thank you for all the *gezellig* moments, noon-time-sharp lunches, and coffee breaks. I have learned a lot about Dutch culture through our conversations, and the constant exposure has helped me pick up some Dutch. Rest assured, I am committed to enrolling in a Dutch course to master the language properly now that the demanding thesis phase is behind me. Even though I was the only international, thank you for making me feel like I am part of the group.

Dear Malu and Robin, I extend a special thanks to you two for being exceptional teammates and persons. I am very glad you both joined the EEG project, and I am excited to continue working with you. I want you to know that you are both doing an excellent job, even if I might not express it as often.

Dear Henk-Jan, despite not being my daily supervisor, it frequently felt as if you were. Thus, I take this moment to express my gratitude for your invaluable assistance and constructive feedback on my 'rough diamonds.' Additionally, thank you for enlightening me on Dutch expressions and sayings; perhaps, I will manage to memorise them one day.

Dear Annemarie, I greatly appreciate your patience and your role in ensuring the smooth flow of things in the team. Most importantly, thank you for your invaluable assistance, particularly for your remarkable ability to find a place for me in Leonard's busy schedule.

Dear Ivana and Kristina, I want to take a moment here to express my heartfelt gratitude to both of you. Our enduring friendship, even though we have lived in different countries for the majority of it, is something I hold dear to my heart. Thank you for the countless wonderful moments, unwavering support, and for patiently enduring my self-reflections. It truly is a pleasure to have friends with whom you can effortlessly pick up where you left off, even after several months have passed. The memories we have created together throughout the early 2010s are some of my dearest, and I sincerely wish we lived closer to one another so that we can continue making new ones.

Dear Dario and Dominik, the Irish afterparty where we first crossed paths was undeniably a blast, but our friendship has certainly grown into something far more meaningful since that time. I am genuinely delighted that we have met, that we had great *cráic* in our lively twenties, and that our bond has remained strong despite the fact that we now reside in three different countries. I miss having you around.

Dear Jorrit, thank you for being such a generous person and a million thanks for letting me stay at yours when I returned to the Netherlands. Your efforts to introduce me to

new people have been very kind, and our discussions about academic life have always been amusing. I wish you the best of luck in your new endeavours in Brussels!

Dear Neil and Rene, thank you for being open to meet me in the pandemic times when I truly needed new friends in a city where I did not know anyone. I am very grateful for all the nice chats and for listening to my sanity-checks, for nice dinners and movie nights and for taking care of my plants in my absence. Thank you for all your help in organising my own events, as well as for encouraging me to step outside of my comfort zone. Thank you for being so kind and easy-going.

Dear CEMACUBE family – Beshoy, Eva and Nicole – thank you for being such an incredible blend of individuals. I love the diversity of our personalities and cultural backgrounds, our shared adventures, and our inside jokes. Even though the years have flown by, it is wonderful to see that we have kept in touch. I hope that we can continue embarking on great adventures together.

Dear Etienne, thank you for all the nice moments we shared during our pandemic walks around Utrecht and our trips. I am very grateful for your help in making my 30th birthday happen despite the challenges of the pandemic. And, of course, you deserve extra credit for allowing me to spend time with your adorable dog, Zsa Zsa.

Dear Davide, having a friend with whom I can relish a wide range of experiences, from attending science talks to partying until the early hours, is truly a pleasure. I very much appreciate your warm Italian hospitality and willingness to be a good listener. And... let's keep our little secret about my occasional cappuccinos after 11 AM between us. Ciao, Ciao.

Драги родитељи и тетка, желим да вам упутим дубоку захвалност за вашу безграничну подршку. Хвала вам што и даље гајите веру у мене, и што ме, иако то можда није увек било лако, подржавате да останем у далекој Холандији. Ваше лепе речи, лепа тренуци, неуморна пажња и безусловна љубав које сте ми пружили су неприкосновени. Непрестани труд који сте уложили током протекле три деценије како бисте ми помогли да остварим своје циљеве није прошао непримећено. То је био труд испуњен љубављу и посвећеношћу, и за то сам вам дубоко захванан. Завршетак ове тезе означава крај једног дугог, али и подједнако драгоценог раздобља, док истовремено означава почетак нечега новог. Уз вашу непроцењиву подршку, уверен сам да ћу успешно корачати кроз све изазове који долазе. Хвала вам. С нестрпљењем ишчекујем наше будуће сусрете и путовања. Заувек ваше мало дете.

Finally, this thesis would not have been possible without the enormous contribution of patients and their relatives. I am deeply grateful for their participation in our research. Their contributions are essential to the search for a cure for ALS.

Curriculum vitae

Stefan Dukic (Serbian: Stefan Đukić, Стефан Ђукић) was born on the 14th of December 1991 in Subotica, Yugoslavia (Serbia). After completing secondary technical school 'Ivan Sarić' in his hometown, he relocated to Novi Sad to pursue a bachelor's degree with honours in Electrical and Computer Engineering at the University of Novi Sad. During his academic journey, he discovered his passion for biomedical engineering under the guidance of professors Dragana Bajić and Tatjana Lončar-Turukalo. This newfound interest galvanised him to apply for the Erasmus Mundus dual-degree programme in Biomedical Engineering with specialisation in Neural Engineering (CEMA-CUBE) in 2014. As he was granted a scholarship, he embarked on a year of study at the University of Groningen in The Netherlands, followed by another year at Trinity College Dublin in Ireland. After completing his master's degree with distinction, he got a research assistant position at the ALS Centre in Dublin. Within a year, this role segued into a PhD position bridging the ALS centres in Dublin and Utrecht, under the mentorship of Prof. Leonard H. van den Berg and Prof. Orla Hardiman. In 2022, he secured a three-year postdoctoral fellowship titled '*A Neurophysiological Approach to Successful Clinical Trials*' and a project grant titled '*Mapping ALS: Paving the Way Towards Improved Early Network Dysfunction Trajectories using EEG*' both generously awarded by Stichting ALS Nederland. He plans to settle down and continue his work in the Netherlands.



UMC Utrecht



Universiteit Utrecht

ISBN 978-90-393-7599-0